IMPINGEMENT HEAT TRANSFER INVESTIGATIONS USING LIQUID CRYSTALS FOR SINGLE UNCONFINED AND SEMI-CONFINED JETS

DONALD EASTWOOD

A thesis submitted in partial fulfilment of the requirements of The Nottingham Trent University for the degree of the Master of Philosophy

August 1994

Copyright

ABSTRACT

Impingement heat transfer investigations using liquid crystals for single unconfined and semi-confined jets.

Donald Eastwood

Experimental results are presented for a single unconfined and semi-confined air jet impinging normally onto a heated flat plate. The nozzle to plate distances, expressed as a ratio of the nozzle diameter are 2, 4 and 6 and the Reynolds number range is 31 000 to 145 000. Heat transfer rates were determined from measured values of temperature difference across the plate and the thermal properties of the plate. The radial variation of the plate surface temperature was obtained by using liquid crystals. These measurements provided the data for the determination of local values of Nusselt number for radius to nozzle diameter ratios of 1 to 10.

Correlations are presented for the two jets relating Nusselt number to Reynolds number, the nozzle distance ratio and the radius distance ratio for radius ratio values in excess of 2.5. For both modes the jets show a dependence of the Nusselt number on Reynolds number, this being stronger in the case of the semi-confined jet. The dependence on the radius ratio is characteristic of a wall jet. For radius ratios greater than 5 and for both jets the thermal energy transfer rates are almost independent of the nozzle distance. The transfer of thermal energy for the unconfined jet is greater because of the increased entrainment of surrounding air into the jet as it develops. For radius ratios greater than 2.5 the difference between the jets increases with increasing radius but decreases with increasing Reynolds number and increasing nozzle distance ratio. Over the range of geometric and flow conditions the Nusselt number for the unconfined jet is from 5 to 50 per cent greater than for the semi-confined jet.

ACKNOWLEDGEMENTS

The author is grateful to my Director of Studies Eur Ing Professor Emeritus Bryan L Button for all the encouragement and advice freely given during the compilation of this work. My thanks are also due to my colleague Dr R J Munton who alas retired before I completed the thesis. To the technical staff of the Mechanical Engineering Department of The Nottingham Trent University I express my gratitude for the construction of the experimental rig. My special appreciation is due to my wife Penny for her patience and support.

CONTENTS

LIST OF FIGURES

LIST OF TABLES

LIST OF PLATES

LIST OF APPENDICES

NOTATION

English symbols

A	surface area /m^2
c	velocity /m s^{-1}
C	orifice coefficient of discharge
d	nozzle diameter /mm
D	pipe diameter /mm
e	orifice expansibility factor
E	orifice velocity of approach factor
h	surface film heat transfer coefficient /[W m^{-2} K^{-1}]
k	thermal conductivity /[W m^{-1} K^{-1}]
L	length /mm
$\dot{m}$	mass flow rate /[kg s^{-1}]
Nu	Nusselt number for the jet with air properties determined at the mean value of the nozzle air temperature and the plate surface temperature
p	pressure /bar
Pr	Prandtl number
$\dot{Q}$	thermal energy transfer rate /W
$\dot{q}$	specific thermal energy transfer rate /[W m^{-2}]
r	radial distance from jet centre line /mm
Re	Reynolds number for the jet with air properties determined at the (nozzle air temperature plus the plate temperature)/2

t temperature /°C

T temperature /K

x,y general variables

z distance from nozzle exit plane to impingement plate /mm

Greek symbols

α angle/°

β ratio of orifice to pipe diameters

Δ difference values

ε radiation emissivity

μ dynamic viscosity /[kg m^{-1} s^{-1}]

σ Stefan Boltzmann constant /[W m^{-2} K^{-4}]

Subscripts

1,2...m sections or values

a air

b black body

g glass

n nozzle

o orifice

s surface

w water

∞ surroundings

Statistics

α	significance level
$\beta_{o\text{-}n}$	predictor coefficients
ψ	residual value
σ^2	variance
ν	degrees of freedom
∇	result value
Ω	uncertainty value
$b_{o\text{-}n}$	regression coefficients
$j_{o\text{-}n}$	sets of values
$u_{o\text{-}n}$	observations
R^2	degree of correlation between measured and fitted values

CHAPTER 1

Introduction

The chapter lists the applications of jet impingement to thermal energy transfer processes and describes the development of the associated flow regions for a single circular jet impinging normally onto a flat surface. Extensive literature surveys are included for turbulent jet impingement and for the application of liquid crystals to temperature measurement. The need for further work is justified and the aims and objectives of the work are listed.

1.1 Applications of jet impingement

The impingement of jets on to a surface is frequently used in industry to enhance heat and mass transfer rates. Compared with normal convection cooling or heating processes, these rates are substantially increased by the technique. Applications for which jet impingement is of benefit are the annealing of ferrous sheets, the tempering of glass, anti-icing devices for the protection of aircraft surfaces, the drying of surfaces, the cooling of turbine blades and the rapid melting of metals. The geometric and hydrodynamic arrangements of the jets are various, ranging from a single round jet to multiple arrays of two-dimensional jets with impingement angle acting as a further variant. The jet is generated by a nozzle which according to the application provides varying degrees of entrainment and turbulence. The extreme limits of design can be defined on the one hand as the tube type from which the jet issues freely into the surroundings and on the other as the orifice in the plate design where the plate runs parallel

to the target surface. The first extreme, the unconfined jet, provides for large entrainment of the surrounding atmosphere, whilst the second design or the semi-confined jet, receives restricted entrainment. In the context of this work, semi-confinement refers to the use of a square plate fitted axi-symmetrically in the exit plane of the nozzle and running parallel to a target plate of similar size. The term 'confined' as opposed to 'semi-confined' is generally applicable to a design in which the constraining surfaces run parallel to the jet axis. Such an application is typical of gas burners.

1.2 Flow regions for a jet issuing from a nozzle

Figure 1.1 is a diagrammatic representation of the flow of a jet impinging normally onto a surface. The free jet region is one of developing flow and is characterised by an increase of jet width resulting from an intensive exchange of momentum with the surroundings at the jet boundary. The surrounding fluid is entrained into the jet thereby reducing its velocity. Extending from the nozzle is the potential core where the centre-line velocity remains almost constant at the nozzle outlet plane value. Gautner et al, 1970 put the length of the core at about 6 nozzle diameters whilst accepting that its absolute value depends upon the jet Reynolds number. A contrary view as expressed by Abromavich 1963 is that the velocity profile at the nozzle outlet is of greater significance. Downstream of the potential core the axial velocity reduces with increasing distance and Schlichting 1968 showed the reduction to be proportional to the displacement from the end of the potential core. A similar relationship exists for the increase in the jet half width defined as the radial section where the velocity is one half of the velocity

at the jet centre-line. When the length of the free jet is sufficiently large then the velocity profile in this region approaches a bell shape and the flow is fully developed. The onset of stagnation flow which according to Schrader 1961 occurs at 1.2 nozzle diameters from the impingement surface is when the axial component of jet velocity is converted into an accelerating radial component. This radial component reaches a maximum under the action of momentum exchange with the surroundings and then decreases as the wall jet becomes fully developed. The boundary layer transition to turbulence is generally considered to occur at the onset of the deceleration of the radial velocity.

1.3.1 Literature survey for jet impingement

The subject area has created a good deal of interest amongst researchers over the past 25 years and the extent of the bibliography substantiates this point. The requirement to optimise heat transfer rates in such specialised processes as the cooling of gas turbine blades has prompted an increased activity in recent years and publications have accelerated. In 1970 Gautner et al surveyed literature on the flow characteristics of a single jet impinging on a flat plate and a bibliography of jet impingement was presented by Button and Wilcock in 1978. A literature review on heat transfer from impinging jets by Hrycak in 1981 was followed by a literature survey on jet impingement heat transfer by Downs and James in 1987. This summarises forty seven papers and serves to illustrate the wide range of parameters and techniques employed and the divergence of results obtained. A further survey followed in 1989 by Button and Jambunathan

covering the period 1976-1985. In 1992, Jambunathan et al reviewed heat transfer data for single circular jet impingement. The applications of jet impingement to engineering situations is covered in detail by Martin (1977) and these are supported by useful correlations for Nu. These relate to single round and slot jets and to jet arrays.

It is to Gardon and Cobonpue 1961 that the early experimental studies are attributed. The work involved unconfined single and multi-jets impinging normally on a heated plate with a transducer being used to measure the local values of heat flux. Data relates to conditions at the stagnation point and to a Reynolds number range of 7 000 to 56 000. For a single round jet, the correlation of local values of Nusselt number with radial position was limited to nozzle to plate distances greater than 10 nozzle diameters. Gardon and Akfirat 1965 investigated local and average heat transfer conditions between an isothermal plate and impinging two-dimensional jets. Hrycak 1983 used a single unconfined jet operating within a Reynolds number range of 14 000 to 67 000 with conditions at the stagnation point being given particular attention. Calorimetric methods were used for the measurement of heat fluxes but no attempt was made at correlating local values of Nusselt number with radius.

The liquid crystal method of temperature measurement was first exploited by den Ouden 1974. A glass plate, forming the side of a water bath acted as the impingement plate and results for an unconfined jet were reported for five Reynolds numbers between 37 750 and 264 250. den Ouden's results compare

favourably with those of Schlunder and Gnielinsky 1967 and Petzold 1963 who also concentrated on relationships for $0<r/d<7.5$ and $2<z/d<12$. More detailed experiments and analyses were carried out by den Ouden and Hoogendoorn 1974 in which the variation of Nusselt number at the stagnation point was further investigated. Hoogendoorn 1977 furthered the understanding of the thermal energy transfer process at low values of z/d by investigating turbulence intensity and velocity profiles in the boundary layer. The transition from the laminar to the turbulent boundary was clearly identified at $r/d \approx 2$ when operating at z/d=2. Overall the measurements were limited to a radius ratio of 3 and a high Reynolds number of 66 000. In addition, Hoogendoorn compared the results for a jet issuing from a long pipe with those for a convergent-divergent nozzle. For $r/d>1$ and z/d=2 similar heat transfer profiles were reported but at the stagnation point the pipe values were higher. Gundappa et al 1989 compared thermal energy transfer profiles for jets issuing from orifices and long pipes and found that for z/d=7.8 similar trends resulted although pipe values were higher for all radii. Amano and Sugiyama 1985 obtained generally good agreement between experimental and predicted values of heat transfer characteristics using the Boussinesq viscosity model to solve the two-dimensional Navier-Stokes equations. The comparison was limited to a single Reynolds number of 20 000 and to z/d=4,7 and 10.

Vlachopoulos and Tamich 1971 used a heated jet with nozzle exit Mach numbers up to 0.84. The range of nozzle distance ratios was from 3 to 31. A more comprehensive range for the variables r/d and z/d was employed by Huang

1963 in his investigations using a heated jet at Reynolds numbers from 3 500 to 25 000. The data correlation was in marked contrast to the results obtained by Perry 1954 who had previously operated with a heated jet over a similar Reynolds number. The work of Baughn et al 1991 into the effect of heated jets concluded that if local heat transfer coefficients are defined in terms of the local adiabatic wall temperature then values for an unheated jet can be used for a heated jet. Effects of jet turbulence were investigated by Obot et al 1979 who found that the replacement of a contoured nozzle with a nozzle of sharp edged inlet increased stagnation point Nusselt numbers by approximately 25 per cent at z/d=4. Similar increases were reported by Popiel and Boguslawski 1986. Ali Khan et al 1982 investigated the operation of a semi-confined single nozzle for z/d values up to 15 but limited their investigations to a Reynolds number of 52 000. Obot et al 1982 compared the unconfined jet with a semi-confined jet for 18 000<Re<59 000 and found that confinement reduced the thermal energy transfer. This reduction was more pronounced at low values of z/d. Bedii Ozdemir and Whitelaw 1992 used flow visualisation and liquid crystal techniques to investigate velocity and temperature profiles using a variable impingement angle and fixed values of Reynolds number at 13 000 and a nozzle distance to diameter ratio of 22. Other investigations in which impingement angle was included as a variable were carried out by Beltaos 1976, Sparrow and Lovell 1980 and Lovell 1978.

The usual way of reporting experimental data has been to correlate the Nusselt number with the Reynolds number, the non-dimensional values for the nozzle

position and the radial displacement and where practicable, the Prandtl number. Such considerations have lead to correlations of the form Nu = f(Re,r/d,z/d,Pr). Recent work by Jambunathan et al 1992 has recognised that within this functional relationship the Re variable itself is dependent upon r/d and z/d. When correlations are quoted the limited operating ranges are generally acknowledged and it is accepted that insufficient reliable data exists to cover all eventualities.The earlier measurement techniques relied upon strategically placed thermocouples for temperature measurement or small thermal flux meters embedded into the impingement surfaces. The introduction of liquid crystals as a temperature measurement medium provided opportunities for full field investigation with enhanced resolution.

1.3.2 Literature survey for the application of liquid crystals to thermal energy transfer and in particular to jet impingement

For most substances the transition from the solid phase to the isotropic liquid phase is well defined and specific. The substance either exhibits the properties of a solid or those of the liquid. However, some organic compounds, the so called "liquid crystals", show an intermediate behaviour when subject to temperatures in this transition region. Their molecules are subject to a certain ordering where an intermediate or a mesophase exists in which flow occurs and a crystalline state is also present. Historically the existence of liquid crystals was first observed in 1888 by the Austrian botanist Friedrick Reinitzer. His observations revealed the formation of an intermediate cloudy liquid as

cholesteryl benzoate underwent the transition from a solid to a clear liquid. It was left to O Lehmann to show that this cloudy liquid had a crystal like molecular structure. It was a further 70 years or so before this particular behaviour was practically exploited. It was notably in digital electro-optical type display devices that their usefulness became apparent.

Liquid crystals are classified into two main types- thermotropic in which phase changes are temperature induced and lyotropic in which phase changes are effected by changes in solvent concentration. It is the first type which provides for the greater opportunities in temperature and heat transfer measurements. Liquid crystals based upon non-sterol organic compounds give rise to the classification chiral nematic in which layers of molecules exist. Within each of the layers the molecules themselves are orientated such that their axes lie parallel to the plane of the layers. It is the loosening of the bonds between these layers at certain applied temperatures that provides the crystal with the optical properties of a solid and the mechanical properties of a liquid. The chiral nematic type of liquid crystal has been used in this work.

Fergason 1968 provided a review of the history, understanding and early developments in applications of liquid crystals whilst a more up to date review of the various applications is to found in the paper by Gray 1985. Yet it is only within the last 20 years that the unique properties have been fully researched and exploited for the purpose of temperature measurement.

The earlier disadvantages of liquid crystals in operation, namely the rapid deterioration with age, the contaminating effects of the surroundings and the

influence of viewing angle were greatly overcome by encapsulation in which the crystals were coated with gelatin in an alcoholic binder. The process enabled the liquid crystal to be used in the form of either pre-coated black substrate on mylar or as a slurry. Cooper et al 1975 employed encapsulated cholesteric liquid crystals for investigations into Nusselt number variations on right circular cylinders placed in a cross-flow of air. One of the first applications of liquid crystals to jet impingement was perfected by den Ouden 1973 who again used a cholesteric crystal encapsulated in a polyacrylate resin. The surface coating was applied by a spraying technique. Hoogendoorn 1977 repeated the application for his work on single jet impingement. The use of encapsulated versions of cholesterol crystals continued with extensive work in various thermal field measurements by Giannini et al 1979 using a monochromatic light source, Brown and Saluja 1978 who provided good evidence of the colour displays at changing temperatures and Simonich and Moffat 1984. They reported on the use of cholesterol liquid crystals in transient situations and its application to concave surfaces. Further applications and classifications are to found in the book by Kasagi et al 1989 and in which there is considerable detail on the liquid crystal properties relevant to flow visualisation. Hippensteele et al 1983 investigated heat transfer coefficients in turbine blade cooling configurations using a composite of a heater element and liquid crystal sheet. Goldstein and Franchett 1988 also used a composite sheet for their investigations into thermal energy transfer from oblique jets.

The recent development and use of chiral nematic liquid crystals has prompted

investigations into their response times to changing temperatures. Ireland and Jones 1987 reported delay times in the occurrence of the colour display of no more than few milliseconds for temperature gradients of 2 000 K s^{-1} whilst Baughn and Yan 1991 investigated transient methods of determining heat transfer coefficients for jet impingement. Jones et al 1992 describe the structures of liquid crystals and relate these to measurements of temperature and shear stress. The technique of colour image processing, a requirement in the analysis of transient systems, is also given coverage. The transient liquid crystal technique has been further used by Martinez-Botas et al 1993 in the measurement of surface heat transfer coefficients over turbine blade passages. Mee et al 1991 have compared temperature sensitive and shear sensitive liquid crystals in the detection of boundary layer transitions. They conclude that both methods are suitable for transition indications and for the determination of quantitative measurements although the reliability of the shear sensitive crystals is limited to lower levels of measurement. The application of liquid crystals in liquid environments is illustrated by the work of Davenport 1989 in which a surface of encapsulated chiral nematic crystals was subjected to impingement by a water jet. Refinements to the manufacturing process of liquid crystals have led to enhanced properties and they are now accepted as a proven reliable method of temperature measurement.

1.4 Scope for further investigations into jet impingement and thermal energy transfer

The literature review reveals how data tends to be either specific to a particular

set of conditions or to cover a spectrum of such width that detail is sacrificed. It was felt that for the single jet configuration an area of study could be chosen which in conjunction with an appropriate range of independent variables, would enlarge the existing data and thereby provide for more coherent empirical relationships. The relative absence of information on jets operating in the semi-confined mode is apparent from the tabled summary of authors contained within the review by Jambunathan et al 1992. In addition the simple industrial application of a long pipe as the source of the jet has received relatively little treatment and here it was decided was the basis for a good comparative study. Finally the versatility of liquid crystals as a means of temperature measurement had to be further demonstrated and exploited.

1.5 Aims and objectives of the study

As a consequence of the literature survey and to enhance the field of research in jet impingement currently being undertaken in the Mechanical Engineering Department of The Nottingham Trent University, the following aims and objectives formed the basis for the study.

1.5.1 Aims

(a) (i) To carry out an experimental investigation to determine the thermal energy transfer data for a turbulent unconfined and semi-confined air jet impinging normally onto a surface.

(ii) To provide an understanding of the jet impingement process and to correlate the thermal energy transfer rate with the jet

Reynolds number and the nozzle and radial displacements from the impingement point.

(b) To compare the thermal energy transfer process for an unconfined jet with that of a semi-confined jet operating under identical conditions.

1.5.2 Objectives

The above aims were to be achieved by

(a) The building of a rig to a design which would allow for the formulation of correlation equations for unconfined and semi-confined jets.

(b) The use of an isothermal impingement surface of such a size as to allow radial displacement investigations up to r/d=10.

(c) The use of a nozzle arrangement which would allow for a Reynolds number range of approximately 25 000 to 150 000 and a z/d range of 1 to 6. Airflow rates to be measured and determined according to an appropriate British Standard.

(d) Thermal energy transfer rates to be obtained from temperature measurements across the plate and from measured thermal properties for the plate. Impingement surface temperatures to be

determined by the use of encapsulated liquid crystals.

(e) The experimental approach is to be based upon a common sense approach to replication and randomisation in which allowance would be made for the steady state constraint of thermal equilibrium. The acceptable uncertainty level in measuring equipment is to be determined by its relative contribution towards the estimated uncertainty in the associated calculated value. This procedure will assist in establishing an appropriate calibration method.

(f) The statistical approach used to analyze the derived data to be the same for the two jets. It would provide with a confidence level of 95 per cent, prediction equations in which Nu is expressed as a functional relationship of Re, r/d and z/d. These equations to form the basis for a comparison between the two jets.

CHAPTER 2

Design criteria for the experimental rig

The chapter contains a review of the appropriate theory as a preliminary to the description of the experimental rig. The approach and the reasons for the final design are explained. The thermal and airflow measurements receive detailed treatments and a section is included for the determination of a value for the thermal conductivity of glass.

2.1 Introduction

Any design for a thermal energy transfer system relies fundamentally on the laws of thermodynamics for the equivalence of energy and the science of "heat transfer" for the rate at which the energy is transferred. These principles formed the basis from which the design for the experimental rig developed. The purpose of the rig was to enable investigations into the thermal energy transfer rate between a hot plate and a semi-confined or unconfined air jet impinging normally upon it. The original specifications were to provide a design solution for a Reynolds number range of 25 000 - 150 000, with full ability to measure the associated Nusselt numbers at varying radii from the jet centre for nozzle distance to diameter ratios of 2, 4 and 6.

2.2 Theory for the evaluation of the surface heat transfer coefficient

Considering a solid-fluid boundary as shown in figure 2.1 where the fluid is air, then the laws of thermal energy transfer lead to the following equation for the

non-transient one dimensional case.

$$-k\left(\frac{\partial T}{\partial x}\right) + h(T_a - T_s) + \sigma\epsilon(T_\infty^4 - T_s^4) = 0 \quad \ldots Eq\ 2.1$$

For a system of finite thickness of solid material and for an inner surface temperature T_w then

$$\frac{k}{x}(T_w - T_s) = h(T_s - T_a) + \sigma\epsilon(T_s^4 - T_\infty^4) \quad \ldots\ldots\ldots Eq\ 2.2$$

This is the fundamental working equation for the evaluation of h and for the design of the apparatus. Estimates of the radial conduction along the glass plate showed this to be insignificant at less than 0.5 per cent of the normally transmitted energy.

2.3 Design criteria

A successful apparatus design must meet the following requirements.

(a) At operating conditions the surface temperature must be uniform. Thermal resistances in the y and z planes must be large compared with those in the x direction - a condition honoured by insulation at the boundary edges and by the use of a 'large' plate.

(b) Equilibrium status must exist at operating conditions. Thermal masses and energy inputs must be sufficiently highly rated to guarantee this status.

(c) Commensurate with the conditions mentioned in (b) the apparatus response time to step changes must provide for realistic time intervals.

(d) Design parameters must be such as to provide acceptable uncertainty levels.

(e) The apparatus must be capable of exploiting to the full the operating properties of primary measurement elements. In particular, the response

characteristics of liquid crystals must be catered for.

(f) The apparatus must give coverage to the desired operating range.

(g) Simplicity of operation and control must be considered as a desirable feature.

(h) Correct material selection must provide for robustness and reproducibility.

(i) The design must be such that other workers can reproduce identical experimental conditions. In particular the nozzle form must be easily reproducible.

(j) The constraints imposed by (a) - (i) must be considered within a realistic scale of material and manufacturing costs.

2.4 The experimental rig

2.4.1 The water bath

The above criteria are met to a large extent by the rig shown in plates 1.1 and 1.2 and figures 2.2 and 2.3. Simplicity is the keyword in that the impingement plate formed one side of a specially designed water bath. The overall dimensions provided a water volume of 0.125 m^3 and the unit was insulated on all non-working surfaces with 100 mm of polystyrene. The main frame of the bath was made from 15 mm polyethylene sheet with the construction being by means of screws together with internal welding for the production of water tight joints. Figures 2.2 and 2.3 show that the impingement plate was in toughened glass and the reasons for the choice of this material are discussed towards the end of this section. The dimensions are provided in figure 2.3 and its attachment to the bath was by means of recessed strips forming an exterior frame. The

water-tight integrity of the attachment was assured by rubber seals. The opposite side of the bath contained the copper plate used in the calibration of the liquid crystals. The calibration procedure is described in detail in chapter 3 but the principle adopted was the replication of conditions encountered by the impingement plate during test conditions. The known very low thermal resistance of copper meant that a surface of known uniform temperature was available and if an appropriate liquid crystal application had been applied to this surface then a calibration procedure was possible. Figures 2.2 and 2.3 show the installation of the plate and the provision for a sealed optical perspex cover is also apparent. This was used to minimise convection and radiation thermal losses and to assist in the calibration. Rubber seals around the copper again ensured the integrity of the joints. Heating and temperature control of the water together with provision for its internal circulation, was provided by a Tu-16D Techne water bath unit rated at 1 800 W. A mercury-in-glass thermometer previously calibrated against a National Physics Laboratory standard thermometer provided the "true" temperature but this was supported by four calibrated Ni/Cr thermocouples, spatially distributed to be representative of the bulk water temperature. The output from these provided evidence of uniform and steady conditions.

In deciding the correct choice of material for the impingement plate, consideration was given to three main requirements. These were (a) the requisite thermal resistance, (b) the physical stability of the material under operating conditions and (c) the degree of certainty associated with the material

property values. It was clear that thermal resistance values had to be as large as possible to provide temperature differences which were measurable to a high degree of certainty. In this respect the value and uniformity of the material thickness and its thermal conductivity assumed importance. Metals were excluded on account of their high thermal conductivities and the choice lay between polymer materials and glass. An approximate value of thermal conductivity for glass is 1.1 W m^{-1} K^{-1} whilst a value for most polymers is around 0.3 W m^{-1} K^{-1}. On these grounds, glass was less favourable in providing for a realistic thermal resistance. However, when considering physical stability over the expected operating temperature of 30 °C to 85 °C, then glass in its annealed form provided the answer. At the higher temperatures, a considerable risk of distortion or even softening of most polymers exists. Industrial information existed on thermal conductivity values for the two classes of materials but this was in need of verification. The available method for the determination of the thermal conductivity required that the specimen be subjected to temperatures in excess of the softening temperatures of polymers. This provided further support for the use of glass as the material for the impingement plate.

2.4.2 The nozzle

The nozzle design was as shown in figure 2.4. In order to cover a possible extension to the Re range two versions were manufactured. In subsequent trials and under the prevailing conditions of supply air pressure nozzle A proved suitable for a Re range of 70 000 to 185 000 whilst the range for nozzle B was

30 000 to 145 000. Restrictions were imposed upon the use of the smaller nozzle at Re < 60 000 by the orifice design specification as given in BS 1042 in which lower limits are placed on the orifice pipe Reynolds number. These limits were exceeded when nozzle A was in use at the smaller mass flow rates. In addition the smaller diameter of nozzle A demanded greater precision in the measurement of nozzle and radial distances at small values of z/d and r/d and as a consequence virtually all the experimental work was carried out using nozzle B. In order to provide a uniform design and a standard jet exit velocity profile at a given Re the nozzle outlet section was machined to a taper as given in figure 2.4. The angle was of arbitrary value and was chosen as being as small as precision machining would allow. Its inclusion had the additional advantage of removing any unwanted burrs.

The same nozzle B was used for semi-confined and unconfined operation and figure 2.2 is the arrangement for the semi-confined jet in which the nozzle exit plane formed a flush fit with the confinement plate surface. The plate was 300 mm by 300 mm, made from perspex and it was attached to the bath at four points. Variable distances from the impingement plate were achieved by the use of variable length spacers. Radial distances from the jet centre line were measured by means of a linear scale etched onto the inside surface of the confinement plate. Figure 2.3 and plate 1.1 show the arrangement for the unconfined jet where the nozzle was simply supported from above and radial measurements were obtained through a suitably inscribed pointer. Flow interference was minimised by slim design of the supporting attachments.

2.4.3 Jet temperature

The temperature difference between the jet and the impingement plate surface at the point of measurement was expected to be between 10 K and 20 K. It was therefore important to ensure that any measurement of the jet temperature was to a known level of uncertainty. To this end, certain precautions were taken in locating the measuring thermocouple and these are shown in figure 2.5. The main purpose of the design was to provide increased area of flow and hence reduced air velocity and to further reduce stagnation effects by recessing the tip of the thermocouple into the sheath. The arrangement as shown reduces the air velocity to approximately 15 per cent of its inlet value which for the higher Re values represents a temperature equivalent of 0.02 K. Further assurance of a true static temperature was gained by the protection afforded by the sheath as shown in figure 2.5.

2.4.4 Performance of the rig

During service, the bath design proved to be highly satisfactory and met all the criteria listed in section 2.3. The one design fault lay in failure to allow for the thermal expansion difference between the copper and the polyethylene at the higher water temperatures of 60-70 °C. This resulted in the failure of the sealed joints with consequent spoiling of the copper face. However, this did not affect the calibration potential of the apparatus as this took place at around 30°C where the joints were effective. At the design stage, designing out of this potential fault had been considered as an over-elaboration. In general operation, the apparatus provided a high thermal capacity source with a resulting uniform

temperature field. Evidence for this is provided by plates 2.1 and 2.6. These are referred to in more detail in chapter 3 but at this stage they serve to illustrate a high degree of uniformity in the liquid crystal response which means a uniform temperature field. Further support for the satisfactory operation of the rig is to be found in plates 2.7,3.1 and 3.2 where the clarity and definition of the liquid crystal outputs is very acceptable.

2.4.5 Computation of the surface heat transfer coefficient and the Nusselt number

The surface heat transfer coefficient was obtained through equation 2.2 and this provided a Nusselt number value defined in terms of the internal diameter of the nozzle. Uncertainty analysis was used to determine the significance of the surface emissivity as a contributor to the value of h and this is explained in greater detail in paragraph 3.4. The conclusion is that for the levels of temperature experienced during experimentation the rate of energy transfer by radiation is small when compared with the energy transfer by convection and that the significance of its contribution decreases with increasing values of h. A value of $\varepsilon=0.9$ was used in the computation as being representative of a glass surface coated with black paint. A highly unlikely value of $\varepsilon=0.4$ would have altered h by no more than 1 per cent for the high range and 3 per cent for the low range. The contribution of the thermal conductivity value for the glass plate was highly significant and details of its measurement are included in paragraph 2.6. Allowance was made for the variation of the thermal conductivity with temperature. The computational steps for the determination of h and Nu are

contained within the programme "jetprog2" and are to be found in appendix A1.4, lines 560 - 980.

2.5 Air supply and measurement

2.5.1 Air supply

An air supply at a maximum pressure of 5 bar was available. Control of the supply to the rig was provided by a standard pressure control valve suitable for supply pressures up to 10 bar. Incorporated into the unit was a filter and moisture trap, thereby ensuring a clean dry supply to the nozzle. The valve operated on a limiting turn down ratio of 100.

2.5.2 Measurement of the airflow

In deciding the type of device to be used for the measurement of the airflow, consideration was given to the aspects of uncertainties, reliability, costs, operating conditions, availability and calibration difficulties. The object was to determine the mass flow rate of air for a given condition and subsequently to convert this value to a Reynolds number based upon the nozzle diameter. Precision had to be a feature and a correct knowledge of the uncertainty associated with a particular device was considered to be a prerequisite. Costs which are a function of precision and reliability were to be kept within reasonable limits whilst providing for measurements within a designated specification. The prescribed conditions were a flow rate range from 1 l s^{-1} to 20 l s^{-1} with a nozzle inlet gauge pressure range up to 4.5 bar. Calibration procedures for externally supplied equipment are expensive in time and money

and supplier's quoted uncertainty values are often misleading and unreliable. For these reasons it was decided to opt for a pressure differential device in which the primary element would be a standard orifice plate. The whole unit could be manufactured in-house to specifications which were well within those stated by BS1042. Most importantly measurements would be available to known degrees of uncertainty.

2.5.3 Design specifications for the orifice plate arrangement

To comply with the requisite British Standards, certain limitations on size and operating conditions have to be imposed. Given these limitations then the working formula for the determination of flow rate, as given in BS1042, can be used. The uncertainties quoted for the values of coefficient of discharge and expansibility factor will then be applicable.

The specification is a square edged orifice plate installed in pipes of diameter 25 mm $\leq D <$ 50 mm, as per BS1042: Section 1.2:1984 which is to be read in conjunction with BS1042: Section 1.2:1981. The installed pipe diameter was 28.00 mm as measured according to section 6.1.5 of the 1981 standard and the orifice diameter was 15.045 mm as measured according to section 7.1.7.2 of the same standard. A comparison between the orifice plate installation and the British standard specification is shown in appendix A2.1. The specifications cover the operation of the 10.28 mm diameter nozzle working within the range 25 000 $< Re_n <$ 180 000.

2.5.4 Component details

The seamless cold drawn steel pipe of nominal internal diameter 28 mm and which carried the orifice plate had straight length measurements of 3 m upstream and 1 m downstream from the plate. These were well within the requirements of the British Standard, the quoted values being 44 and 7 when expressed as multiples of the pipe diameter. The upstream air supply pipe was required to expand its diameter through a ratio of 2 and this was completed over a distance of 50 mm as per BS1042, section 6.2. The pipe internal diameter used in the evaluation of the meter coefficient of discharge was determined as the mean value of the diameters measured at sections 28 mm, 35 mm and 42 mm upstream of the orifice plate. At each section, measurements were made at four diameters. The data so obtained is shown in appendix A2.2 The surface roughness of the inside of the pipe was measured using the Tallyrand testing machine. Defining the surface roughness as the mean value of the difference "valley to peak" then its value was 0.03 mm, based upon the five highest and five lowest readings. The relative roughness was then given by the quotient 0.03/28, which at 10. 7 x 10^{-4} is just within the accepted value for cold drawn tubes as given by BS1042.

The orifice plate was designed and manufactured with strict adherence to the standard specifications. The 15.045 mm diameter plate, together with installation details are shown in Appendix A2.4. The bore diameter was measured using shadow graph techniques and a mean value was determined from the measurements at four diameters. These values are shown in Appendix A2.3 from

which it is to be observed that no diameter differs by more than 0. 05 per cent from the mean diameter value - a criteria for circularity. The plate was judged by visual inspection for surface finish, flatness and burred edges.

The upstream and downstream pressure tapping points were located at distances of 28 mm and 14 mm from the upstream face of the plate, ensuring conformity to the standards for D and D/2 orifice plates. The upstream static pressure tapping point was also at 28 mm whilst a shrouded thermocouple was located 200 mm downstream from the plate.

For an orifice plate installation conforming to BS1042, then the uncertainties associated with its use are well documented. For a plate installed in a pipe line of internal diameter between 25 mm and 50 mm then additional uncertainties have to be included but again these are known. It was therefore with confidence that flow rates of air and hence Reynolds numbers were determined.

2.5.5 Computation of the airflow rate

Computational steps for the evaluation of the mass flow rate and hence the Reynolds number are contained within the main computer programme "jetprog2" a listing of which is to be found in Appendix A1.4. Essentially the procedure is iterative around an initial value assumed for the coefficient of discharge which in itself is dependent upon the Reynolds number. Perturbations in the value of the coefficient finally equate to a value as determined by the Stolz equation (section 7.2.2.1 of BS1042: Section 1.1:1981). In this equation the coefficient is

expressed as a function of Reynolds number and ß, the orifice to pipe diameter ratio. A flow diagram for the determination of the nozzle Reynolds number is contained in Appendix A1.5.

2.6 Measurement of the thermal conductivity of glass

The application of equation 2.2 to the situation of a jet impinging on a glass plate requires information on the plate thickness, the plate thermal conductivity and the inside and outside plate surface temperatures. The plate thickness is a simple linear measurement and can be determined to a high degree of certainty. The two surface temperatures are dealt with comprehensively in chapter 3. It is to the thermal conductivity of glass that this section is devoted.

The contribution of the glass thermal conductivity to the degree of uncertainty in the Nusselt number was determined by allocating an approximate value of 1.1 W m^{-1} K^{-1}. Table 1.2 illustrates the role of thermal conductivity where at low levels of Nusselt number, typically 50, a 3 per cent uncertainty in its value produces an uncertainty in the Nusselt number of 5.2 per cent. For the higher values of Nusselt number then the influence of thermal conductivity is less but it was clear that a high degree of confidence in a value was a definite requirement. Discussions with the scientific services of Pilkingtons manufactures and the National Physics Laboratory revealed expected values for borosilicate glass of between 1 and 1.2 W m^{-2} K^{-1} and of course there exists a temperature dependency. Confirmation of the thermal conductivity value for the glass used in the rig was required and experimental measurements were made.

2.6.1 Experimental procedure for the determination of the glass thermal conductivity

The apparatus used was a standard piece of laboratory equipment as supplied by Cussins Ltd and it is shown in plate 1.3. The principle is that an electric heater source and a cold water "sink" generate a measurable temperature difference across a carefully machined and ground thin sample of the glass. The thermal flux through the glass is measured from the mass flow rate of water and its associated temperature rise. Figure 2.6 is a diagrammatic representation of the principle. The glass is sandwiched between two axially spring loaded copper cylinders each of which contains thermocouples at the specified locations. For the assumption that zero contact resistance exists between the glass and copper then linear temperature extrapolation leads to the values t_{g1} and t_{g2} for the surface temperatures of the glass. The applied contact pressure and the use of high conductivity surface paint between the surfaces minimises the contact resistance. The water flow rate is determined by collection and timing and its temperature change is measured by mercury-in-glass thermometers.

2.6.2 Estimation of errors

The determination of thermal conductivity using the apparatus described in the above previous section assumes that all thermal energy transfer through the glass is transferred to the cold water. The process is considered to be one-dimensional with no losses to the surroundings from the lower copper cylinder. In order to achieve this idealised condition the system is isolated from the surroundings by a Dewer flask radiation shield the inside lining of which is

highly polished. The presence of the shield is symbolically represented in figure 2.7. Estimates were made of the net radiation losses by applying a surface thermocouple to the shield and by using estimates of the emissivity values for the copper and glass surfaces. The system was treated as being analogous to an enclosed body with the lower copper cylinder being the body and the radiation shield its enclosure. For such an arrangement in which end radiation transfer is considered as being negligible then use of the following equation was justified on the grounds that it served to illustrate the magnitude and significance of the thermal radiation losses.

$$\dot{Q}_R = \frac{A_c(\dot{q}_{bc}-\dot{q}_{bf})}{\frac{1}{\epsilon_c}+\frac{A_c}{A_f}(\frac{1}{\epsilon_f}-1)} \quad \ldots . Eq\ 2.3$$

where suffixes c and f refer to the copper cylinder and the radiation shield respectively. $\dot{q}_b$ is the black body thermal radiation transfer as given by the Stefan Boltzmann law.

Appendix A3.1 contains the data and principles for the determination of the radiation losses. As the copper was in the polished condition then an estimate for its emissivity as being less than 0.1 was considered as realistic. The influence of the shield was that being highly polished its emissivity was low. Even if its emissivity was between 0.6 and 1.0 then the errors in the estimates had little effect on the overall radiation losses when these were expressed as percentage values of the energy transfer by conduction. Table 1.3 shows these percentages for the case of copper emissivity = 0.1 and shield emissivity = 0.2.

The values shown in parenthesis are the corresponding figures for the case where the shield emissivity is 0.9. It is clear that the radiation losses are negligible and that specifically they account for between 0.04 and 0.06 per cent of the energy transfer by conduction.

As mentioned in section 2.6.1 the method assumes that contact resistance between the copper and glass are zero. This was not necessarily the case and some evidence of the degree of error associated with the assumption was required. The contact resistance is a function of the surface texture, the contact pressure and the parallel alignment of opposing faces. It was not possible to determine the copper-glass relationship and the nearest equivalent was determined by the measurement of the temperature difference across the two contacting copper surfaces. This approximated to a copper-glass system for similar surface finishes. By reference to figure 2.6 it is clear that, with the glass removed the linear extrapolation of t_4 through t_3 to the contact surface provides a surface temperature t_{s1}. A similar exercise applied to the lower copper cylinders provides an equivalent temperature t_{s2} and with zero contact resistance these two temperatures are equal. Any difference between the two is a measure of the contact resistance present. Appendix A3.2 shows the measurements and results of such an exercise. A mean value of 4.6 K existed and because of the relative lack of discrimination in the temperature measurements, the value was subjected to a high degree of uncertainty at ± 1.5 K or ± 33 per cent. This is apparently a high figure although its contribution to the uncertainty in the thermal conductivity at ±0.025 W m^{-1} K^{-1} is surprisingly small.

2.6.3 Experimental results for the determination of the thermal conductivity of glass

Appendix A3.3 contains the experimental measurements and the calculated results for the determination of the glass thermal conductivity. Corrections for the radiation loss and the contact resistance are included in the evaluation. An uncertainty analysis reveals the high significance of the water temperature uncertainties and careful calibration of the thermometers was carried out. The calibration procedure is described in chapter 3, and the calibration curves are to be found in appendix A4.2. It was possible to carry out the measurements at three mean values of glass temperature. At each value, five sets of data were obtained thereby providing for a degree of statistical credibility. Figure 2.8 is a comparison of the three experimental results with data as supplied by Pilkington glass. There is confirmatory agreement and the quoted equation was accepted for use in the main stream calculation of Nusselt number. The uncertainty associated with each of the water temperatures was ±0.1 K and these contributed separately 40 per cent to the total uncertainty in the thermal conductivity. The other major contributor was the water volume measurement at ±1 ml or 12 per cent. The overall contribution of each of the measured variables to the uncertainty in the thermal conductivity value was ±0.04 W m^{-1} K^{-1} and its variation with temperature was taken to be represented by the equation

$$k_g/[W\,m^{-1}\,K^{-1}] = 1.047 + 1.21x10^{-3}t/[K] - 2.6x10^{-6}t^2/[K^2] \quad \ldots Eq\ 2.4$$

CHAPTER 3

Calibration procedures for the measured variables

This chapter details the calibration methods adopted for each of the measured variables. The three primary variables were length, used to express aspect ratios, pressure to evaluate flow rates and temperature to determine fluid properties and thermal energy transfer rates. Considerable coverage has been given to the calibration of the liquid crystal and the chapter concludes with details of the uncertainty analysis used in assessing the significance levels for the measured variables. Table 1.1 summarises the order of uncertainties for each of these variables.

3.1 Length measurements

These provided nozzle and radius diameter ratios and were taken as read on a graticule or linear scales. The more significant uncertainty was associated with the measurements of radial distribution from the jet centre line. In particular for the smaller radii, errors of 10 per cent were estimated as a consequence of parallax problems and the relatively poor definition in the visual image. The nozzle distances were more exact in that carefully machined spacers were used to provide the required variation. An uncertainty of ±1 mm was easily achieved.

3.2 Pressure measurements

(a) The static pressure upstream of the orifice plate was measured by means of a

Bourdon pressure gauge, range 0-10 bar. The gauge was calibrated against a standard dead weight tester and the resulting calibration curve is presented in Appendix A4.3. The scale graduation and pointer thickness were such that readings were recorded with a uncertainty level of ± 0.05 bar.

(b) A high specification U tube manometer was used to measure the pressure difference across the orifice plate. This, being a length measurement, was treated as a primary standard with operating conditions as per the manufacturer's specifications. Measurements were possible to within ±1 mm which at the lower ranges represented 1 per cent of the reading.

3.3 Temperature measurements

The laboratory standard used for the calibration of all temperature sensing elements was a calibrated mercury-in-glass thermometer of range -5 °C to 105 °C and with a scale interval of 0.1 K. This in turn had been compared with a platinum resistance thermometer calibrated at the National Physics Laboratory. The registered calibration service was the Regional Calibration Centre of the then Central Electricity Generating Board and the calibration serial number was 00131.

3.3.1 Thermocouples and mercury-in-glass thermometers

Temperature sensing elements in the form of Ni/Cr thermocouples, manufactured according to BS 4937K and additional mercury-in-glass thermometers were calibrated against the laboratory standard. The method was immersion in a temperature controlled water bath sensitive to temperature

changes of 0.02 K. The calibration range was 25 °C to 80 °C and the output curves are to be found in Appendices A4.1 and A4.2. Readings were generally taken as having uncertainties of ±0.1 K

3.3.2 Liquid crystals

Before justifying the adopted calibration procedure for liquid crystals it is timely to collate the experience gained in the use of liquid crystals as a temperature sensing element. By so doing then the conditions under which they were used to provide assessments of surface temperature are revealed and their practical limitations exposed.

3.3.3 Experience gained in the use of liquid crystals

The liquid crystal type was chiral nematic and was supplied in the micro-encapsulated form. It was suitable for spray application, with or without a black sub-strata. An adopted standard of three coatings was chosen with each application being by means of an air brush at a supply pressure of approximately 2 bar. Optimum response sensitivity was achieved by choosing a manufacturer's specification of temperature band width equal to 1 K.

In establishing a suitable operating procedure it is important to recognise the behaviour pattern and characteristics of liquid crystals. Figure 3.1 shows the variation of output wavelength with observation angle. The measurements formed a part of a student thesis investigating the properties of liquid crystals Davies (1989). A monochromometer selected discrete wavelength ranges

produced by a heated liquid crystal surface at 33.6 °C and passed these to a photomultiplier tube. Output from the tube was measured by means of an oscilloscope. It is very apparent that a large shift in apparent colour occurs with variations in viewing angle. This is further substantiated by plate 2.1 in which at a water temperature of 38.4 °C a colour transformation from green to blue is seen as the viewing angle moves through 45°. For the particular liquid crystal, this represented an apparent temperature increase of approximately 0.5 K.

Intense sources of illumination are to be avoided whenever possible although these provide for superior and brighter colours. Plate 2.2 shows the temperature effect of a floodlighting system at 1 m distance from the surface. This is purely a heating effect, it is temporary and its effect is minimised by the use of intervening perspex and of course by shortened exposure times. The "strip effect" shown on plate 2.2 is a by-product of the photographic copying process. A more significant and unknown effect of light on the response characteristics of liquid crystals is shown in plate 2.3. Here the protective effect of perspex is apparent in the "ghost" outline of its shape. In this particular case the shielded area beneath the measuring pointer represents the true temperature, whilst unprotected corrupted areas have experienced a permanent shift in their output characteristics. This leads to higher interpretations of the surface temperature.

It was appreciated at the initial stages that superior liquid crystal displays would result from the inclusion of a black painted sub-strata applied to the outside of the impingement plate. However this introduced an unknown quantity into the

measurements and subsequent calculations in the form of an extra thermal resistance. Hence trials were initiated into the use of liquid crystals where the required background was provided by painting the inside surfaces of the bath with black paint. Greater care had to be taken in the preparation of a clean surface, prior to the spray application of the liquid crystal, otherwise adhesion properties were impaired. It was considered prudent to compare any differences which resulted from the two techniques, the one in which the liquid crystal was applied directly onto the glass and the other in which the outside of the glass had received an initial coating of black paint. Plate 2.4 shows the comparisons for the two operating conditions where the right hand half of the surface had received a sub-strata of recommended black paint. Explicitly shown are the colour transformations as the water temperature was gradually raised from 36.5 °C to 37.0 °C. It is to be noted that the painted surface leads the non-painted surface, that is a given colour appeared at a lower water temperature. Plate 2.5 shows the effect of paint on the rings of colour produced when a jet of air impinged upon the plate. Here again a definite shift occurred and as the temperature was increasing from the centre outwards, it is clear that for a black painted surface any given colour occurred at a lower temperature. Conversely a given value of Nu apparently occurred at a smaller radius.

To explain the difference let the null hypothesis be that it arose not from a property change of the crystals but rather as a consequence of the thermal energy transfer process. In this case, the most likely event was that the application of a painted surface increased the thermal resistance to conduction and because of an increased surface emissivity, it decreased the thermal

resistance to radiation. Hence for unchanged boundary temperatures for the water and the surroundings, the external surface temperature as given by the liquid crystal transformation should have decreased on both counts. This assumes that the application of the paint did not lead to any significant change in the convection thermal resistance between the liquid crystal surface and the surroundings. However the evidence of plate 2.4 is that a painted surface was at a higher temperature - at least according to colour. If the differences were to be explained purely by thermal energy transfer reasons then the appearance of a given colour would be at a greater radius for the painted surface. The conclusion is that the null hypothesis does not hold and it was incorrect to ascribe the difference to a purely thermal energy phenomenon. The visual outputs for the two surfaces were in directions contrary to that expected and it was apparent that the application of a black painted sub-strata shifted the colour-temperature display of the liquid crystal. The above supports the idea that the output response of liquid crystals is sensitive to surface coatings. This presented no problem when the procedures for calibration and actual measurement were identical and so the deciding factor determining whether or not paint had to be used depended upon the chosen calibration procedure. As shown in figures 2.2 and 2.3 this involved the use of a copper plate, heated to a known temperature on the inside with visual observation of a liquid crystal application being made on the external surface. For the colour display to be visual, such an arrangement required the use of black paint applied to the external copper surface, thereby providing a suitable reflecting background for the liquid crystal.

In section 3.4 the application of uncertainty analysis is presented and a particular consequence is that a contribution of 0.95 per cent to an overall uncertainty of 4.5 per cent in the Nusselt number was due to the surface temperature. It was evident therefore that rigorous calibration of the colour changes of liquid crystals with temperature was a definite requirement.

3.3.4 Calibration of the liquid crystal

Figure 2.3 shows the inclusion of the copper plate into the general arrangement of the apparatus. Identical applications of the liquid crystal could be made to the impingement and the calibration surfaces since both surfaces were geometrically and thermally similar. They were of the same size and formed a part of the same heating system. Additionally viewing arrangements were similar thereby reducing errors due to the subjective nature of colour interpretation. For the method to be reproducible and dependable then the following points had to be addressed.

a) Steady state conditions had to be guaranteed. In designing the apparatus, attention had been paid to the thermal mass of the unit and to its thermal response characteristics. The correct operating balance was considered to be one providing simultaneously for thermal stability and for realistic experimental times with step changes being reached over acceptable intervals. The good insulation standards, together with a sufficiently high rated heating unit contributed towards satisfying these conditions. In addition the temperature control was precise at ± 0.1 K and the apparatus was situated in surroundings which exhibited a high degree of temperature stability over reasonable operating

periods.

b) The thermal resistance of the water/copper system had to be either negligible or if not, then quantifiable to some extent. The design objective was to reduce the thermal flux at the calibrating temperature to a minimum by the inclusion of a sealed air gap between the copper plate and its surroundings. Reference to figure 2.2 shows the shielding of the copper plate by an optical perspex cover, thereby providing an air gap of approximately 10 mm. This minimised thermal losses by convection and to a lesser extent by radiation. Measurements of the thermal fluxes for the calibration plate were made from readings of an electricity meter coupled across the input to the water bath heater. Two sets of values were obtained. The first was for the case where the complete bath including the calibration cover plate was fully insulated. This provided at the calibration temperature an apparatus specific power loss of 5.2 W per degree of temperature difference between the water and the surroundings. The second case was where only the calibration cover plate was without insulation and the net flux for the plate was determined from the difference figure between the two sets of readings. The experimental data showing the results for a sequence of six runs are presented in Appendix A.5.

The result was a power loss through the painted calibration plate of 118 W m^{-2} at a calibration temperature of 30.10 °C. Using a thermal conductivity value for copper of approximately 380 W m^{-1} K^{-1} then the specific thermal resistance of the plate was 2.5 x 10^{-5} K m^2 W^{-1}, the plate thickness being 9.6 mm. For a thermal flux value of 118 W m^{-2} then the temperature difference across the

copper was of the order of 3×10^{-3} K - a negligible amount.

c) Information had to be available on the thermal properties of the black paint. Unfortunately the suppliers had not responded to requests and it was a requirement that at least an estimate be obtained of the paint's contribution to any uncertainties in the calibration temperature.

The paint was applied by means of an air brush and a thin film with an even matt surface was easily produced. Consider a uniformly thick film of surface area equal to 1 m^2. Table 1.4 shows the expected temperature difference across such a film for three values of thermal resistance when the thermal energy transfer rate is 118 W. It was clear that if reasonably reliable values for the thermal resistance of the black paint could be determined then some degree of validity could be attached to the liquid crystal calibration data by making the appropriate corrections. This was achieved in the following manner.

Repeated spraying of a specimen surface provided a film thickness which could be measured. The remaining problem was one of obtaining a reasonable estimate or measurement of the film's thermal conductivity. The situation was firstly investigated by inspecting a dried film under the electron-microscope. Figure 3.2 is the output, from which it is apparent that the bulk of the paint composition is carbon, with some oxygen and sulphur. The physical nature of the film provided further justification for the assumption that the paint was of the carbon black type and that if this were the case then its thermal conductivity could possibly equate to that of amorphous carbon at 1.5 W m^{-1} K^{-1}.

Further evidence on the value of the film thermal conductivity was sought by direct measurement. A carefully machined copper disc of nominal thickness 3 mm and diameter 25 mm was prepared. The measured variation in thickness at any point was no greater than 0.005 mm. Conductivity measurements were taken as prescribed for a glass specimen in section 2.6.1. One face of the disk was then sprayed with the paint as in the preparation of the calibration plate except that the application was judged to be twice the calibration thickness. This provided a film, easily measured at a thickness of 0.05 ± 0.01 mm. The conductivity measurements were repeated for the painted specimen and any increase in thermal resistance resulted directly from the application of the paint. As the method used a difference figure in the determination of the thermal resistance then any errors due to contact resistances were eliminated.

The measurements and derived values are to be found in appendix A.6. These show that for an area of 1 m^2 the thermal resistance of the applied film is 1.13 x 10^{-4} K W^{-1} and its thermal conductivity is 0.44 W m^{-1} K^{-1}. This of course compares unfavourably with the original proposal to use a value appropriate to amorphous carbon with a thermal conductivity of 1.5 W m^{-1} K^{-1}. However the direct measurements provided stronger evidence and since they represented the worst case scenario the value of the thermal conductivity at 0.44 W m^{-1} K^{-1} was used in assessing the effect of the paint. A reason for the difference was possibly due to the physical nature of the film as a consequence of the spraying and drying processes. With this value of thermal conductivity and for an applied thickness of between 0.02 mm and 0.04 mm and an area of 1 m^2 then the range

of thermal resistance to be allowed for in the calibration process was 5 x 10^{-5} K W^{-1} to 1 x 10^{-4} K W^{-1}. Referring to table 1.4 it is to be concluded that for the measured calibration flux of 118 W m^{-2}, the painted surface contributes an error in calibration temperature of approximately 0.01 K. This value, being of such small magnitude was considered as being of secondary significance to the uncertainty associated with the visual interpretation of colour in the liquid crystal calibration process and was therefore neglected.

The calibration procedure itself was a straight forward process in which visual observation of the coated copper surface was recorded against water temperature. Preliminary trials of the effect of layer thickness on image brightness and colour quality had optimised a spray application at three coats, each of which was allowed to dry before further coverage. Viewing was through the optical perspex cover and short term floodlighting was identical to that used during the main experimental programme. Spacial variations in water temperature were detected by thermocouples and the reference temperature was as indicated by the calibrated mercury in glass thermometer, details of which are given in section 3.3.1. The two liquid crystal specifications used during the experimentation were R(31)C(0.5)W and R(35)C(1)W, both of which were microencapsulated mixtures of the chiral nematic type. The sensitivity of such crystals can be judged from plate 2.6 in which a given application of the crystal was subjected to a succession of temperatures. It is to be noted that the photographs relate to colour changes for the impingement plate. Previous trials of a jet impinging on a plate containing a liquid crystal application suggested

that the best colour for visual interpretation would be bright green. Tables 1.5.1 and 1.5.2 contain the details of the temperature colour transformations for the two liquid crystals used during the experiments. It is to be noted that the manufacturer's specification for R35C1W gave slightly higher temperature changes than those produced during the adopted calibration procedure. At the chosen calibration colour of bright green this difference amounted to +0.2 K. As the calibration method was designed to reproduce the actual experimental conditions then the values obtained were judged as being more appropriate. There was consistency in the measured and quoted band widths as defined from the start of red to the start of blue and it was reassuring to note the small tendencies to hysteresis effects in the middle of the calibration ranges. At the outer limits of the colour transformations the gradual changes in colour intensity provided difficulties in discrimination. This was particular true for the blue end of the spectrum where the sensitivity of the colour change with temperature was poor and detection was correspondingly less certain.

As the planned programme involved the use of an air jet impinging onto the liquid crystals a trial was undertaken to assess their durability under the prevailing conditions. A jet, having a Reynolds number of 70 000 impinged continuously on the liquid crystal surface for two hours. Plate 2.7 shows the initial and final displays to be identical, thereby verifying the stable and non - degrading nature of the surface. The same surface was allowed to cool and it was then subjected to repeat conditions. There was again no identifiable alteration to the output characteristics and it was therefore with confidence that

a programme of multiple readings, using the one application of liquid crystal could be planned. In practice, the cyclic nature of the experimental procedure accelerated the deterioration in image quality and brightness and this resulted in more frequent re-newals of the liquid crystal surface than expected.

3.4 Uncertainty analysis for the measured and derived variables

Appendix A.1 contains the objectives and method for the determination of the uncertainty of a derived value. Extensive reference has been made to the work of Moffat,1985 and the working equations used in determining the uncertainties for the derived variables are presented in appendix A1.2. Appendix A1.3 lists the computer program used in their evaluations. The estimates for the uncertainties of the primary or measured variables are presented in table 1.1 and the calculated values of uncertainty for Nu, Re, z/d and r/d using these estimates are to be found in table 1.6.

The uncertainty associated with the evaluation of Nu was ±4.50 per cent. The glass thermal conductivity uncertainty contributed ±3.15 per cent towards this value and the surface temperature's contribution was ±0.95 per cent. The balance was divided amongst the glass thickness, the water and air temperatures, the nozzle diameter and the calculated values of radiation losses from the plate surface. The latter were allowed for by the application of the Stefan Boltzmann equation using estimated values for the surface emissivity and by considering the surroundings as being large and black. For an allocated surface emissivity of 0.9 and an uncertainty value of -0.5 the latter being a possible lower extremity

then its contribution to the overall per cent uncertainty in Nu was no more than 0.1 per cent. This was a consequence of the relatively low contribution by radiation to the total thermal energy transfer. In conclusion the uncertainties in the Nusselt number were dominated firstly by the glass thermal conductivity and secondly and to a lesser extent, by the impingement plate surface temperature as determined by the liquid crystal. These were the reasons for the particular attention paid to the measurement and calibration processes associated with these variables.

In the determination of the Reynolds number the uncertainty was approximately 3.5 per cent to which the most significant contribution was the uncertainty associated with the air mass flow rate. The orifice plate method used for its determination was appropriate to small pipe bore installations for which increased uncertainty values exist. As a consequence the meter coefficient of discharge uncertainty was the most significant and accounted for 2.7 per cent. The static pressure and orifice plate differential pressure were the remaining significant contributors to the overall uncertainty in Re.

As for the uncertainty associated with r/d which at low values was high at 7.5 per cent, the most significant errors were in the measurement of radial distances from the jet centre line. These arose from the combined causes of less than perfect colour discrimination for the liquid crystal display and eye parallax problems in reading radius scales in particular when operating as a confined jet. The uncertainty in the radius measurement was estimated at ±1.5 mm. The

maximum uncertainty in z/d was ±4.8 per cent with the nozzle distance itself being the main contributor.

CHAPTER 4

Presentation of results

The chapter contains information on the experimental results and on their conversion to derived values. A concluding section concentrates on the quality and interpretation of the data.

4.1 General arrangements

The experimental data formed the input to the main computer program "jetprog2" (appendix A1.4). The output containing the derived variables Nusselt number, Reynolds number (range 31 000-145 000), nozzle distance ratio (range 2,4 and 6) and radius ratio (1.5-9.5) was transferred to a suitable spreadsheet from which the format as contained in appendices A7 and A8 was obtained. The presentation has been arranged into primary sets of Reynolds numbers and secondary sets of nozzle distance ratios. The graphical representations are to be found in figures 4.1-4.30. For each mode of operation the graphs have been arranged into two major sets- the one showing the effect of Reynolds number, the other the effect of nozzle distance ratio.

4.2 Unconfined jet

The results for the unconfined jet are to be found in appendix A7. There are 247 separate entries of which test numbers 216 to 247 demonstrate the repeatability of the results. Typical visual examples of the liquid crystal display for the unconfined jet are shown in plates 3.1 and 3.2. In plate 3.1 the effect of nozzle distance ratio is clearly seen. At z/d=2 the inner ring display has ventured into

the blue zone before returning via green to the start of a further continuum of colour spectrum. Hence a given temperature, say the calibration temperature, is identified at 3 radially distributed points. A similar occurrence is featured with a value of z/d=4, although in this case the first and second displays of green are almost coincidental. The resolution at r/d < 2 is somewhat limited and would have been improved by the use of a larger diameter nozzle. However for a given Reynolds number, this would have required larger mass flow rates and these were limited by the system capacity. In addition, at the lower ranges of Nusselt number the temperature difference across the glass plate would have been so small as to introduce significant errors. At z/d=6, the interpretation is straight forward in that a single ring only is present. In each case there is evidence of the existence of more widely dispersed colour rings. These green rings tended to exist in isolation and did not form a part of the normal colour spectrum. Such a phenomenum is difficult to interpret as the suggestion is that there is no continuous temperature distribution either side of the ring and that a step change in temperature is occurring. The most likely explanation is that the feature arises as a consequence of the particular response characteristics of the chosen liquid crystal. There is insufficient discrimination in the visual output and only the green part of the spectrum is being activated. Even so a non-sequential temperature change is being detected by the liquid crystal although the quality of the response does not allow for assured interpretation. Such cases have therefore been excluded from the presented results whilst acknowledging the need for further investigation possibly with a crystal having a wider response range.

Plate 3.2 shows the effect of the Reynolds number on the output display for constant z/d=2. It is clear that a single ring exists and that the radius of such rings increases with increasing Re. Once again there are vague appearances of green outer circles.

Figures 4.1-4.6 are graphical representations of the effect of increasing Re values and figures 4.7-4.13 show the influence of nozzle distance ratio. The graphical presentations of the repeat programme are shown in figures 4.14 and 4.15. The first of these figures is for two different sets of Reynolds number and the second for a change in nozzle distance ratio. In both cases the degree of reproducibility is good. Figures 4.2, 4.4 and 4.6 also include experimental data according to den Ouden 1973. For values of $r/d \geq 3$ the same trend exists and within the quoted experimental uncertainties of section 3.4, namely Nu ±4.5 per cent the agreement is good for all values of z/d. For $r/d < 3$ and $z/d = 2$ and 4 a considerable difference is to be observed although figure 4.6 shows that for $z/d = 6$ then good agreement again exists for all r/d values. The differences are further discussed in chapter 6 where the variable nature of jet turbulence is put forward as a reason for the differences.

4.3 Semi-confined jet

The range of test values for this mode of operation is represented by test numbers 1 - 332, contained within appendices A8. The data is slightly more comprehensive than for the unconfined mode of operation and there is an extra input of Reynolds number at 90 000. The graphical presentations are shown in

figures 4.16 to 4.29. It is to be noticed that data plots are included for r/d less than approximately 1.9. However there was a considerable degree of uncertainty in the quality and definition of the image produced within this range. There was a suggestion of a "double ring" but its location was uncertain. For the sake of completion the interpreted values are shown but in any statistical analysis as in chapter 5 these values have been excluded. A repeat programme for the semi-confined mode is represented in figure 4.30 in which there is again good agreement between the two sets of data.

It is noteworthy that in general the semi-confined nozzle programme was carried out with a liquid crystal transformation temperature of 31.2 °C whilst for the unconfined programme the corresponding temperature was 35.3 °C. The use of the two different crystals was not a deliberate policy but more a question of supply and availability. The purpose was to compare the two jets under identical conditions but the small difference in surface temperature was considered as having no significant effect on the comparison. The working equations were common and of course the derived results were obtained using the appropriate values.

CHAPTER 5

Statistical analysis of the results

This chapter contains an overview of the regression analysis and its application to the collected data. Testing procedures for model adequacy and significance levels together with estimates of confidence limits are presented for the unconfined and semi-confined readings. The analysis makes extensive use of the text by Draper and Smith 1981.

5.1 Regressional Analysis

Regressional analysis has been used throughout the study to draw meaningful conclusions to any dependency relationships that exist between the response variable, in this case Nu and the predictor variables, z/d, r/d and Re. The method of least squares is used to investigate the random variations associated with the response variable. Any random variations in the predicted variables are considered as being small compared with their range of observed value. The extent to which this is true depends upon the control and planning of the experimental programme and the care taken in the limitation of measurement errors.

The statistical approach is to assume a mathematical model and the regression process is then carried out around the model. Such a model may be represented by the equation

$$Y = \beta_0 + \beta_1 X + \psi$$

where the parameters β_0 and β_1 determine whether or not a model is linear. ψ is the error or residual by which any individual value of the response variable differs from the regression or predicted value. Of course the correctness of the assumed model is more likely to be assured if knowledge is to hand of models used in similar circumstances. For the situation of jet impingement then the literature survey as detailed in chapter 1 points to a an appropriate model which is of the form

$$Nu = \phi (Re)^a (r/d)^b (z/d)^c \quad \ldots\ldots Eq\ 5.1$$

Logarithmic transformation of this equation produces a linear first order equation of the form

$$Y = \beta_0 + \beta_1 X_1 + \beta_2 X_2 + \beta_3 X_3 + \psi \ldots . Eq\ 5.2$$

The corresponding predictive or regression equation is

$$\hat{Y} = b_0 + b_1 X_1 + b_2 X_2 + b_3 X_3 \ldots\ldots Eq\ 5.3$$

where $b_{0 \rightarrow 3}$ are regression coefficients or estimates of the parameters $\beta_{0 \rightarrow 3}$. Their values are determined by the method of least squares.

5.1.1 Analysis of variance

The regression coefficients determined by the method of least squares are supported by an analysis of variance table. These provide the evidence for the precision of the regression equation. The data is standard in that the total sum of the squares of the deviation is split into an explained sum of squares due to

regression $\Sigma(\hat{Y}_i - \bar{Y})^2$ and an unexplained sum of squares about regression given by $\Sigma(Y_i - \hat{Y}_i)^2$. The correlation between the measured value Y_i and the fitted value $\hat{Y}$ or the proportion of total variation about the mean $\bar{Y}$ is given by the coefficient R^2. Its value is determined by the quotient of $SS_{(regression)}$ and SS_{error}. Good correlation exists when $R^2 \rightarrow 1$.

5.1.2 Conditions for inference

In estimating confidence limits or carrying out tests of significance then a prerequisite is that the regression is based upon an adequate postulated model. This aspect is dealt with in para 5.1.4. In addition certain assumptions are made concerning the distribution of the Y_i and error values. These assumptions are

(i) the variance in Y_i is constant = σ^2

(ii) the errors ψ_i are normally distributed variables with mean zero

Deviations from these assumptions have been investigated by means of residual plots and residual cumulative frequency plots.

5.1.3 Significance tests

Significance tests for individual coefficients are referred to the t statistic and rejection or acceptance of the null hypothesis H_0: $\beta = 0$ with its alternative H_1: $\beta \neq 0$ is decided by the 2 tail test at the significance level α.

Overall regression significance is tested by use of the F statistic which is represented by the quotient of mean square regression and mean square error. The appropriate null hypothesis is H_0: all coefficients equal zero with the alternative H_1: not all coefficients equal zero.

In a similar manner, confidence intervals for an individual parameter are determined using the Student t statistic(t_c) which is appropriate to the degrees of freedom and the desired confidence level.

Confidence interval = parameter ± t_c(estimated standard deviation)

Prediction interval = parameter ± $t_c\sqrt{}$[(estimated standard deviation)^2 + s^2].

5.1.4 Adequacy of the chosen model

The importance of examining the residuals in regressional analysis has been referred to in para 5.1.2. Such evidence can often be used to identify a wrong choice of postulated model. As additional support the lack of fit test can be used.

The theory and proof are well documented by Draper and Smith 1981 and only the working equations are quoted here. The test depends upon the existence of a genuine set of repeat experimental values, which for a multiple regression situation means repeat sets of the predictor variables (X_1,X_2,X_3,....X_p). For j=1...m different sets of predictor variables, each of which has observations u = 1...n_j then the pure error sum of squares is given by

$$SS_{pure} = \sum_{j=1}^{m}\sum_{u=1}^{\bar{\gamma}}(Y_{ju}-\bar{Y})^2 \text{.....} Eq\ 5.4$$

The degrees of freedom for pure error is given by

$$\nu = \sum_{j=1}^{m}(n_j-1) \text{.....} Eq\ 5.5$$

The total error sum of squares for the regression consists of two parts - one due

to the pure error as given by equation 5.4 and the other due to a lack of fit resulting from the original choice of the model. An appropriate F statistic is defined as the quotient of the mean square due to lack of fit and the mean square due to pure error. For a given significance level the statistical decision can then be made whether or not to reject the null hypothesis H_0: the model is adequate. Assuming the value of the F statistic to be insignificant then at the chosen confidence level there is no reason to doubt the adequacy of the model and the mean square error can be used as a reliable estimate of the variance in Y_i. Hence an F test for the overall regression can be carried out as mentioned in paragraph 5.1.3.

Practically it was difficult to obtain exact replicas in the predictor variable sets and a tolerance of ±0.1 in the radius ratio was allowed when forming the sets.

5.2 Statistical analysis of the results for the unconfined jet.

It is clear from the graphical outputs shown in figures 4.1-4.13 that a single regression equation claiming to cover all values of radius ratio is not justified. This is particularly the case for, nozzle distance ratios equal to 2 and 4 when with radius ratios less than approximately 3 the thermal flux distribution becomes distinctly complex. As mentioned in section 4.3 the characteristics for the semi-confined jet at r/d values less than approximately 2.0 were somewhat unreliable. Hence for a comparison between the two modes, the statistical analysis has been limited to those r/d values for which a good degree of confidence existed.

5.2.1 Analysis for $3.0 \leq r/d \leq 9.0$

For this range of the radius ratio the regression equation is

$$\ln(Nu) = 0.357 + 0.538\ln(Re) - 1.024\ln(r/d) - 0.0239\ln(z/d) \ldots Eq\ 5.6$$

The analysis of variance for the above regression is given in Table 2.1.

5.2.1 Adequacy of the model

The procedure adopted for the lack of fit test is as given in section 5.1.4 and the appropriate derived results are recorded in appendix A9. The repeat measurements numbered 216 to 247 of appendix A7, provided the basis for the test. Table 2.1 contains the results of the test and it is to be seen that the F statistic =0.95. For an F distribution with percentage points (113,16,0.95) the critical value is 2.07 and for any level of significance the value is greater than unity. Therefore the test statistic F=0.95 is not significant and there is no reason to doubt the adequacy of the model. Hence it is reasonable to take the mean square error at .0021 as being a fair estimate of σ^2, the variance in Y. Additional evidence for the variation in Y is provided by R^2. This shows that approximately 99 per cent of the variation in Y is explained by the regression on (X_1, X_2, X_3).

5.2.3 Statistical significance of the regression

Figure 5.1 is a plot of standard residuals against fitted values from which is it apparent that the distribution tends to a horizontal band with no obvious

abnormality. This is confirmatory evidence that the variance is constant. Figure 5.4 is a cumulative frequency plot against residuals, using normal probability paper. Although the line is not exactly straight, the number of deviations is small and they occur at the extremities of the distribution. There is no reason to suspect that the residuals are not normally distributed and their mean is shown to be zero. The conditions for inference as laid down in section 5.1.3 have been met and significance tests of the regression are justified.

5.2.4 F significance tests for the unconfined jet

Referring to Table 2.1 the F test statistic for regression is 3459 with regression and residual degrees of freedom equal to 3 and 129 respectively. The upper percentage point F(3,129,0.95)) for the F distribution is 2.68 and the regression equation is highly significant. This is true even at the 99 per cent level. It is therefore only with minimal risk that the null hypothesis H_o : all coefficients = 0 is to be rejected. This is further substantiated by t ratio values for the predictor coefficients. For b_0, b_1, b_2 and b_3 these values are 3.91, 67.8, -75.49 and -2.73 respectively and certainly at a confidence level of 95 per cent coefficients b_1 and b_2 are statistically very significant. For b_0 there is a less than 1 per cent chance of being in error when claiming significance. However the value for b_3 at -2.73 is less convincing and shows that z/d is not a useful predictor of Nusselt number values. This is of course confirmed by reference to figures 4.7 - 4.13 where the limited effect of z/d is apparent.

5.2.5 Confidence limits for the predictor coefficients

The 95 per cent confidence intervals for the predictor coefficients β_0, β_1, β_2, and β_3 have been calculated in accordance with section 5.1.3 and are shown in table 2.2. Confidence in the regression equation is again illustrated by the close intervals for the β_1 and β_2 coefficients whilst z/d is again shown as not being a useful estimator of Nu.

5.2.6 Conclusions on the analysis for the unconfined jet with $3.0 \leq r/d \leq 9.0$

The regression equation as described by Eq 5.6 explains 99 per cent of the total variation in the response variable ln(Nu) about the mean value. There is no reason to suspect the model as being inadequate and there is strong support for the Reynolds number and the radius ratio as being useful estimators of the Nusselt number. An indication of the confidence with which a single "future" value may be predicted is contained in figure 5.2. At the 95 per cent confidence level the difference between limiting values and the corresponding fitted value equates to a Nusselt number variation of ±10. This varies slightly according to the level of fitted values. Confidence intervals for the prediction of "future" average values produce smaller ranges in the Nusselt number.

The regression equation for the range $31\,000 \leq Re \leq 145\,000$, $3 \leq r/d \leq 9$ and $2 \leq z/d \leq 6$ is

$$Nu = 1.43(Re)^{0.538}(r/d)^{-1.02}(z/d)^{-0.0239} \quad \text{.....Eq 5.7}$$

The relationship between fitted and measured values for this equation is illustrated in figure 5.3 where good agreement is seen to exist.

5.3 Statistical analysis of the results for the semi-confined jet.

The statistical analysis is restricted to a limited range of r/d - in this case to between 2.5 and 9.0. The regression model for the Nusselt number is again considered as being a continuous function of the three other non-dimensional numbers as decreed by equation 5.1. The support for this assumption lies in the similarity in the outputs of the two modes.

5.3.1 Analysis for $2.5 \leq (r/d) \leq 9.0$

For these limiting values of the radius ratio and for a range of Reynolds number from 31000 to 145000 the regression equation is

$$\ln Nu = -1.950 + 0.731\ln(Re) - 1.130\ln(r/d) + 0.039\ln(z/d) \ldots Eq\ 5.8$$

For this regression the analysis of variance is shown in table 2.3.

5.3.2 Statistical significance of the regression

Inspection of figure 5.5 shows how the residuals tend to a horizontal which is centred around zero - again illustrating the constancy of variance. Hence the mean square error at .006 can be taken as a good estimate of the variance in Y. The comparable figure for the unconfined jet was .0021 showing the regression line to be a somewhat better representation of the measured data. Even so the semi-confined mode of operation leads to a very acceptable value of R^2 at .978. The statistical conditions for inference are met and tests of significance are in order.

5.3.3 F Significance tests for the semi-confined jet

At a value of the F test statistic at 3938 the regression is highly significant, the upper percentage point F(3,256,0.95) being 2.64. As for the predictor coefficients, the respective t ratio values are 17.4, 73.4, -89.5 and 3.64. As in the case of the unconfined mode and for a 95 per cent level of confidence the predictors b_1 and b_2 are statistically significant whilst b_3, again gives little confidence for the use of z/d as a predictor variable. The above arguments are supported by table 2.4 which contains the 95 per cent confidence intervals for the predictor coefficients.

5.3.4 Conclusions on the analysis for the semi-confined jet with 2.5<(r/d)<9.0

The regression equation Eq 5.8 explains 98 per cent of the total variation in the response variable ln(Nu) about the mean value. Transformed values for the Reynolds number and radius ratio serve as useful estimators for the Nusselt number. However the relatively wide confidence limits for the transformed nozzle distance ratio variable as shown in table 2.4 together with the small value of its predictor coefficient confirm the conclusion that this variable is as an unreliable estimator. The 95 per cent prediction values for the regression are given in figure 5.6 from which the limiting range equates to a ±17 variation in Nusselt number about the fitted value. This compares with a corresponding value of ±10 for the unconfined operating mode thereby illustrating a reduction in prediction confidence for the semi-confined mode of operation.

The regression equation for the operating range 31 000≤Re≤145 000, 2.5≤r/d≤9.0 and 2≤z/d≤6 is

$$Nu = 0.142(Re)^{.731}(r/d)^{-1.13}(z/d)^{.0400} \quad .....Eq\ 5.9$$

This regression line is illustrated graphically in figure 5.7. It is evident that at higher Nusselt numbers the regression equation becomes less reliable and that errors are of greater significance. It is also interesting to compare the output with that of figure 5.3 where for the unconfined mode of operation a greater degree of confidence in the regression equation exists over the whole range of Nusselt number.

CHAPTER 6

Discussion of the results

The chapter firstly discusses the separate results for the unconfined and semi-confined jets. The adopted methods of comparing the two jets are then presented and the chapter concludes with a detailed discussion of the output differences.

6.1 Unconfined jets

It is suggested in section 4.2 that the variable turbulence levels of an impinging jet could significantly affect the thermal energy transfer characteristics. den Ouden 1974 deliberately increased the turbulence levels at the exit from nozzles and reported up to 50 per cent increases in the Nusselt number within the stagnation region although these differences rapidly disappeared for $r/d > 2.5$. The amount of turbulence and hence the level of Nusselt number within the stagnation region is a feature of the nozzle design and the nozzle distance ratio. The experimental work of Hrycak 1983, Gardon and Cobonpue 1962 and den Ouden and Hoogendoorn 1974 suggested slight decreases in the Nusselt number up to $z/d = 4$ followed by a rather rapid increase up to $z/d = 6$ or 7. Schlunder 1967 showed that mass transfer rates within the stagnation region are not only increased by free jet turbulence levels but also by turbulence levels artificially introduced at radii just outside the immediate vicinity of the stagnation point. Such inclusions could increase local mass transfer rates by 70 per cent. Schlunder also concluded that turbulence levels for a given value of Reynolds number were higher for larger diameter nozzles than smaller ones. It is therefore

suggested that for the region around the stagnation point differences will exist between this work and that of others and that the extent of the differences is a consequence of variations in nozzle design. With this in mind the discussion on unconfined jets concentrates on two regions of radial displacement, namely r/d < 2.5 and r/d > 2.5.

6.1.1 r/d < 2.5

Within this range peak values in Nusselt numbers reveal the nature of the heat transfer process. These are more prominent at the higher Reynolds numbers and their magnitude and position are determined by the jet characteristics and turbulence levels. According to the nozzle design and geometric arrangement various values for the potential core length have been quoted. Hrycak et al 1970 carried out velocity profile measurements at the jet centre line and concluded that a maximum value was found at Re = 1 000 and that beyond Re = 10 000 the length is essentially independent of Reynolds number. Importantly at high Reynolds numbers the effect of the nozzle diameter was considered to be insignificant. Vlachopoulos 1971 suggested a value of core length to diameter ratio of 5 and den Ouden 1973 ascribed the transitional zone to a ratio range of 5 to 10. Referring to figures 4.7 to 4.13 then for z/d = 6 no maximum in the heat transfer coefficient is present - a feature quite opposed to the characteristics for z/d = 2 and 4. For the lower values of z/d jet velocity dominates over turbulence levels in determining the heat transfer process. For z/d = 6 the turbulence levels have increased and the increased heat transfer coefficient at the stagnation point is reflected in the manner of responses at increasing values of

r/d. The effect of increasing Reynolds number is not only to increase the peak values but to move its radial position slightly away from the stagnation region. This is explained by the widening of the jet with increasing Reynolds number and subsequently a radial displacement of the onset of the wall jet region. These observations are in agreement with published data in particular den Ouden 1973 and Schlunder 1970. Hrycak 1970 showed that the radial position of the onset of the wall jet as determined by the position of the maximum radial velocity profiles increased from r/d = 1 to 2.5 as z/d increased from 2 to 20. This trend was substantiated by boundary layer thickness measurements which at particular values of r/d < 2.5, showed increasing values as z/d increased. The onset of the wall jet as witnessed by the growth in the boundary layer thickness was radially delayed for the larger values of z/d. This is not fully supported by figures 4.11 to 4.13 in which comparisons for z/d = 2 and 4 show that the decrease in Nusselt number starts at a distance nearer to the stagnation region when z/d = 4.

6.1.2 r/d > 2.5

The general trends of decreasing Nu values with distance from the stagnation point, together with the dependence of Nu on Re are clearly shown in figures 4.1 to 4.6. The regression equation Eq 5.7 for the experimental range $31000 \leq Re \leq 145\,000$, $3 \leq r/d \leq 9$ and $2 \leq z/d \leq 6$ is

$$Nu = 1.43(Re)^{0.538}(r/d)^{-1.02}(z/d)^{-0.0239}$$

The R^2 value for the equation is .988 and a high degree of correlation exists. The correlation is presented in figure 6.1 together with the data of den Ouden 1973 and Schlunder 1966. The comparison is favourable and the value for the

Re exponent as given by den Ouden is almost identical. However a significant difference exists when a comparison is made with Schlunder's value at approximately 0.75. It is to be expected that for turbulent flow conditions the dependence of Nu on Re would be defined by an exponent value of around 0.6. The survey as conducted by Downs and James 1987 suggests a range from 0.5 to 0.9 according to geometric configurations, operating ranges, nozzle type and on the precise definition of Reynolds number. Trabold et al 1987 reports that for convergent nozzles producing uniform velocity profiles and relatively low turbulence levels there is general agreement on the amount of entrainment. However for tubes as used during this work, the suggestion is that entrainment depends not only on the tube length but also on the nozzle exit configuration. In particular at a distance of z/d=4 then for tubes extending into the atmosphere an entrainment increase of 60 per cent is quite possible. Trabold also concludes that entrainment is independent of Reynolds number at values in excess of 30 000. Although the mass of entrained air continues to rise with increasing Reynolds number its influence on the Reynolds number when defined in terms of the total air impinging on the plate declines. Such arguments in terms of definitions lead to the range of quoted values in the literature. It is interesting to note that den Ouden's experiments involved the use of a long tube type 'nozzle'. A further interesting feature is that for the semi-confined arrangement of this work for which restricted entrainment applies, the value of the Re exponent is 0.731.

The review of heat transfer data for a single jet as presented by Jambunathan et al (1992) suggests that the Re exponent depends upon the distance from the

stagnation point and on the nozzle to distance ratio. The information was retrieved from publications spanning the years 1962 to 1988 and was processed by means of enlarged photography and digitisation techniques. The data relates to ASME elliptical and orifice type nozzles. The review highlights the influence of nozzle geometry, confinement, jet temperature, and turbulence intensity and concludes that there is a requirement for further information on the effects of these variables if comparisons between experimental data are to be meaningful. Statistical interpretation of the relationship between the Re exponent a and r/d for the present work and for the range $3 \leq r/d \leq 8$ was found to be of the form

$$a \propto (r/d)^{-b}$$

where b depends upon the nozzle distance. For z/d = 2,4,6 b = 0.151, 0.136, and 0.12 respectively. It is firstly to be concluded that the Re exponent increases with increasing nozzle distances. This confirms the trend as given by the correlation of Jambunathan et al (1992) in which a is expressed explicitly as a function of r/d and z/d. The second conclusion is that the Re exponent decreases with increasing distance from the stagnation point. This is an unexpected feature as turbulence intensity and its penetration of the boundary layer within the wall jet is generally accepted as increasing with increasing distance. A possible explanation for the contrary trend is the range of r/d values over which this and other investigations have concentrated. The review data of Jambunathan et al (1992) is concerned very much with the transformation from the laminar flow conditions within the stagnation region and the onset of the wall jet zones where there is strong evidence for increasing values in the Re exponent. However for

values of r/d in excess of 4, the exponent tends towards a fixed value with no conclusive evidence as to its trend within the higher regions of r/d. A contrary argument, based upon the findings of Hrycak (1970) is that boundary layer thickness increases as r/d increases although this trend does not continue indefinitely. The variation of the Re exponent with r/d for the unconfined and semi-confined jets is illustrated in figure 6.19. The trend of decreasing values of the exponent with increasing values of r/d is clearly illustrated and it is interesting to note how the trend tends towards a constant value at the higher ranges of r/d.

The near independence of Nu on z/d is illustrated in figures 4.7 to 4.13 and is quantitatively confirmed in the regression equation with a z/d exponent of -0.0239. This corroborates the findings of Hrycak 1970 who found that for r/d>4 boundary layer thicknesses became independent of z/d. For nozzle to plate distance ratios up to 6, Gardon and Akfirat found little change in local heat transfer coefficients at a particular radius.

As for the influence of radius ratio on local values of Nu then the relationship is as to be expected and reflects the flow properties of a wall jet. den Ouden reports a functional relationship between Nu and r/d as having an exponent value of -1.1. Martin 1977 describes how maximum values of wall jet velocity tend to zero with $(r/d)^{-n}$ where n is about 1 for the axisymmetric turbulent wall jet. Hrycak 1970 presents an analytical analysis for the maximum velocity decay along an impingement plate. Expressing the maximum wall jet velocity as a

ratio of the nozzle outlet velocity then for values of r/d>4 and for nozzle spacings up to 10 the ratio varies as $(r/d)^{-1.12}$.

Figure 6.2 is a comparison of average Nu values, obtained by integration of the regression equation over $2.5 \leq r/d \leq 6.5$, with those obtained by Schlunder 1967. In presenting the data use has been made of the empirical formula suggested by Schlunder, namely

$$\frac{Nu(av)}{Pr^{0.42}} . F\left(\frac{r}{d}, \frac{z}{d}\right) = f(Re)$$

where

$$F\left(\frac{r}{d}, \frac{z}{d}\right) = \frac{r}{d} . \frac{1+0.1\left(\frac{z}{d}-6\right)/\frac{r}{d}}{1-1.1/\frac{r}{d}}$$

The value of Prandtl number is taken as 0.71. The two sets of data show the same trend although it is acknowledged that the present values are somewhat higher.

6.2 Semi-confined jet

The experimental data for the semi-confined operation are reproduced in figures 4.16 to 4.29 and figures 6.3 and 6.4 are comparisons of the present work with that of Obot et al 1981. Their experimental work was based upon the heating of copper rings forming the impingement plate and temperature measurement was by thermocouples. As a consequence the output data was at discrete intervals of radial displacement and as such possibly lacked the continuous field

measurement afforded by the use of liquid crystals. This could account for the discontinuity in the Obot curves as shown at r/d=5. Both sets of data show similar trends at the higher values of r/d and indicate the presence of peak values in heat transfer coefficients in the region close to the stagnation region. Many of the features raised in sections 6.1 to 6.1.2 for the unconfined jet are relevant to the semi-confined operation but certain aspects of the latter are worthy of further attention.

6.2.1 r/d ≤ 2.5

Generally observation and data acquisition for the region r/d < 2.5 were more difficult and less certain than in the case of unconfined operation. Certainly the visual definition was less exact and the visual identification of rings was difficult. As in the case for unconfined flow, peak values for the present work are comparatively high and this is again suggested as being a consequence of the nozzle characteristics. Referring to figure 4.20 and 4.21 it is clear that for z/d=6 and for all Re values used during the experiments, peak values of heat transfer coefficients do not exist. As commented on in section 6.1, entrainment for an unconfined jet starts as the jet leaves the nozzle and the increased volume flow rate can be of the order of 30 per cent (Crow and Champagne,1971). For semi- confined situations and in particular for nozzle spacings which are very much less than confinement plate widths then entrainment is limited to the outer regions of the plate. Under such circumstances there is a strong possibility that re-circulation zones are set up adjacent to the issuing jet and that these interfere with the local surface temperatures. The combination of this together with the

narrow active band width of the liquid crystals is suggested as a reason for the lack of discrimination of semi-confined data at r/d<2.5. Even so the different output characteristics for z/d=6 and z/d<6 are demonstrated through figures 4.22 to 4.29.

6.2.2 r/d > 2.5

The general trends in local Nusselt number are decreasing with increasing distance from the stagnation point and increasing with increasing Reynolds number. There is certainly no tendency to a minimum value at around r/d=5 as suggested by Obot (see figures 6.3 and 6.4). The dependence of Nu on z/d is minimal, in particular at the higher range of r/d. For r/d values decreasing below approximately 5 a stronger dependence is present as the heat transfer characteristics come under the influence of the flow regime within the stagnation zone. The regression equation for 31 000≤Re≤145000, 2.5≤r/d≤9.0 and 2≤z/d≤6 as determined in chapter 5 is

$$Nu = 0.142(Re)^{0.731}(r/d)^{-1.13}(z/d)^{0.0400}$$

The R^2 value for the regression is .978 which although slightly inferior to the value for the unconfined jet nevertheless still shows a high degree of correlation. The weak dependence on z/d is illustrated and turbulent flow conditions are confirmed by the Reynolds number exponent. As in the case of unconfined flow the exponent was found to decrease with radial displacement for z/d=4 and 6 but as is revealed in figure 6.19 it is approximately constant at 0.72 for z/d=2. The r/d exponent is applicable to a wall jet in which flow velocity decreases as

radius increases.

6.3 Comparisons between the unconfined and the semi-confined jets

Figures 6.5 - 6.9 are direct comparisons of the experimental data for the unconfined and semi-confined jets. Comparisons using the correlation equations for the two jets are contained within the figures 6.11 - 6.18. Figure 6.10 compares the variation in the mean value of Nu with Re, the mean value being determined by integration of the correlation equations over the range $2.5 \leq r/d \leq 9$. Figures 6.11 - 6.14 show how the difference values in Nu for the two jets vary with Re whilst figures 6.15 - 6.17 show the variations with r/d. The influence of z/d on the ratio of Nu for the semi-confined and unconfined jets is shown in figure 6.18.

6.3.1 Comparisons at various Reynolds numbers

Figure 6.10 illustrates the reduced values of the mean values of Nu for semi-confined operation. Further illustrations are contained within figures 6.11 to 6.14 where for given values of radial displacement and nozzle distance from the impingement plate the difference between the two jets, expressed as a fraction of the unconfined flow is plotted against Reynolds number.The positive difference in favour of unconfined flow confirms the work of Obot et al,1982 who attributed the lower values for semi-confined flow to the significant restriction to interaction between the surface jet and the surrounding fluid. The corresponding reduction in mean velocity adjacent to the impingement surface

was reported as being 40 per cent with confinement. It is to be noted that in particular at the outer limits of the impingement plate, the reduction in the heat transfer is of this order for the lower Reynolds numbers. Referring to figures 6.11 to 6.14 it is clear that the difference between the two jets decreases with increasing Reynolds number and the suggestion is that for values of Re in excess of those used during the experiments then the Nusselt numbers for the two jets approach each other. This tendency is related to the flow conditions within the confinement space where entrainment for the semi-confined jet is dependent on air being induced through the impingement space in a direction contrary to the main stream flow. The resulting viscous forces are overcome by the pressure difference existing between the surroundings outside the plate and the jet itself. This will vary as the square of the jet velocity and at very low Reynolds numbers it is quite possible that the magnitude of the pressure difference is such as to provide very little entrainment. Successive increases in jet velocity however will produce progressively more entrainment- a situation that will improve as Reynolds numbers rise. This, coupled with the findings of Trabold 1987 that entrainment for unconfined jets at Reynolds numbers in excess of 30 000 reaches a finite amount, provide reasons for the trends as shown in figures 6.11 to 6.14. The specific value of Reynolds number at which possible equalisation of the Nusselt number occurs depends upon the radius ratio under consideration and on the nozzle distance. In general the value increases with increasing r/d but decreases with increasing z/d. The indications from figure 6.11 are that at r/d = 3 and for z/d = 6 equal Nusselt numbers for the two jets will exist when the Reynolds number is approximately 160 000.

6.3.2 Comparisons at various radius ratios

A further trend revealed in figures 6.10 to 6.14 and emphasised in figures 6.15 to 6.17 is the role of confinement as radial distances increase. For example at a Reynolds number of 40 000 and z/d=2, the fractional difference between the two jets increases from 0.29 to 0.36, as r/d increases from 3 to 9. When expressed as a ratio of the unconfined value of Nusselt number the semi confined value is 71 percent at r/d =3 and 64 per cent at r/d = 9. As distance away from the stagnation region increases the action of confinement is to further reduce the heat transfer process - other factors being equal. This is explained again by reference to the differences between the two entrainment processes. For the semi-confined situation interaction between the two opposing streams decelerates the radial flow velocity and so at a given radius, heat transfer coefficients tend to be lower. This tendency will become increasingly pronounced towards the edge of the confinement plate. Comparison of the two r/d exponents in the regression equations confirms the larger rate of decrease of Nu with r/d for the semi-confined situation.

6.3.3 Comparisons at various nozzle distance ratios

Figures 6.11 to 6.14 show how for the larger values of nozzle distance from the impingement plate the influence of semi-confinement is less dominant. For example at a radial position of r/d=3, increasing z/d from 2 to 6 at a Reynolds number of 40 000 decreases the fractional difference between the two jets from 0.29 to 0.24 - a change of 17 per cent. Similar reductions occur at other radii whilst the effects at larger Reynolds numbers are more pronounced. For an Re

value of 140 000 and r/d = 3 the effect of the same increase in z/d is to decrease the fractional difference by 0.07 or by 70 per cent. Such changes are summarised in figure 6.18 where the influence of confinement is expressed by the Nusselt number ratio for the two jets. At r/d = 3 and Re = 140 000 the effect of increasing the nozzle distance is to increase the ratio of semi-confined to unconfined Nu from 90 to 97 per cent. It is accepted that entrainment levels increase with increasing z/d levels- a feature reported by Trabold et al 1986. However they also showed that the relationship between entrainment and z/d was linear for unconfined and non-linear for semi-confined long tubes respectively. For values of z/d>8, entrainment levels for the two jets approached equality as the nozzle distance ratio increased. For z/d > 12 Obot et al 1982 reported heat transfer coefficients to be unaffected by confinement. Certainly this work supports these trends with the suggestion that semi-confinement ceases to have an affect at z/d values not much in excess of 6.

The physical interpretation of these findings can be simply stated in terms of the ease of access of the surrounding air to the impingement surface. For a given Reynolds number the pressure difference motivating the induced reversed flow of air is approximately independent of the distance between the confinement and impingement plates. However the viscous forces opposing this flow decrease with increased separation of the two plates. There is a resultant increase in induced flow with consequent increases in entrainment levels. This increase will not continue indefinitely and there is an optimum value for z/d after which no further increases in entrainment take place. Changes in z/d, certainly at values

less than 6 are considered to have a greater influence on the heat transfer process for the semi-confined jet than for the unconfined jet. Hence increases in z/d favour the semi-confined jet and when expressed as a ratio of the unconfined jet its Nusselt number increases. Extrapolation to higher values of z/d would confirm the findings of Trabold and Obot. The argument is applicable to higher levels of Reynolds number where the square relationship of jet velocity with pressure difference reduces further the influence of semi-confinement.

CHAPTER 7

Conclusions

The overall aim of the work was to compare the thermal energy transfer process for the unconfined and semi-confined jet when operating under identical conditions. To achieve this aim an experimental rig was designed and built and this provided the data for the formulation of correlation equations for the two jets. Liquid crystals were used to determine the surface temperatures. The aims and objectives were met and the conclusions on the rig, its operation and the comparison of the experimental data for the unconfined and semi-confined jet are presented. The chapter concludes with suggestions for further work.

7.1 The rig and its operation

The rig provided a highly satisfactory steady state technique for the measurement of local surface heat transfer coefficients for a single jet impinging normally onto a surface. The ranges of Reynolds numbers, radius and nozzle ratios as specified in the original objectives were fully covered and the apparatus thermal capacity together with the high insulation standards guaranteed the provision of an isothermal surface. The use of an encapsulated liquid crystal in surface temperature measurement required standardisation and consistency in its spray application and calibration. For visual interpretation which is normal to the surface and with protection of the surface from the transient and permanent effects of external light sources then temperature measurements were possible to an uncertainty of ±0.15 K. In the evaluation of

the Nusselt number the most likely source of error arose from the uncertainty in the value for the glass plate thermal conductivity. The significance of the latter was such that it accounted for 90 per cent of the uncertainty in the Nusselt number value. It was therefore important to account for and to eliminate wherever possible, any errors in the thermal conductivity measurement as this parameter was the controlling element in minimising the estimated uncertainties in Nu. The thermal conductivity values were estimated as having uncertainties of ±4 per cent after corrections had been made for losses associated with its measurement. The total contribution from each of the measured variables to the Nusselt number uncertainty was estimated at between 4 and 5 per cent.

The orifice plate provided a reproducible method for the measurement of mass flow rates and uncertainties were controlled by the coefficient of discharge uncertainty which for small bore pipes is relatively significant. Even so Reynolds number values were determined to an uncertainty of ±3.5 per cent. The uncertainties associated with the radius and nozzle diameter ratios were estimated at between 2 and 7 per cent and 2 and 5 per cent respectively.

7.2 Experience gained from the use of liquid crystals in the measurement of surface temperatures

Standardisation on a given technique for the application and calibration of the liquid crystal was considered as being fundamental to securing reproducible results to a known uncertainty. The variation in output wave length with viewing angle for a given temperature was appreciated at an early stage and all

readings were taken normal to the surface. The wavelength decreased with increasing viewing angle, the exact relationship being a feature of the particular liquid crystal. In an extreme situation of a 60 ° viewing angle the order of error in temperature measurement was estimated at 1 K. The effect of a sub-strata of black paint on the liquid crystal output display was contrary to expectations. Normally the introduction of an extra thermal resistance between the hot source and the crystal surface would be expected to decrease the temperature of that surface and the liquid crystal colour to change accordingly. In fact the colour change of the liquid crystal was in the opposite direction and it is suggested that the black paint is influential in making a fundamental change to the response characteristics of the liquid crystal. The life expectancy of a given application of liquid crystal was investigated from two viewpoints. Firstly the physical influence of a jet playing onto the liquid crystal surface was investigated by the continuous application of the jet for two hours. There was no detectable change either in the quality of the image nor in the temperature response characteristics. The second feature investigated concerned the change in output response characteristics as a result of exposure to light - in particular light sourced by discharge tubes. The conclusion is that there is permanent shift in the output characteristics with exposure and that protection, to some extent by the use of an intervening perspex sheet is a definite requirement. For values of r/d less than approximately 2.5 the visual discrimination in the output of the liquid crystals was poor - a situation which would be improved by the use of a larger diameter nozzle.

7.3 The correlation equations for the unconfined and semi-confined jets

For a single air jet impinging normally onto a flat surface the following correlation equations were found to be appropriate.

Unconfined jet: 30 000 ≤ Re ≤ 145 000, 2 ≤ z/d ≤ 6 and 3 ≤ r/d ≤ 9

$$Nu = 1.43(Re)^{0.538}(r/d)^{-1.02}(z/d)^{-0.0239}$$

The degree of correlation R^2 = .988.

Semi-confined jet: 31 000 ≤ Re ≤ 145 000, 2 ≤ r/d ≤ 6 and 2.5 ≤ r/d ≤ 9.0

$$Nu = 0.142(Re)^{0.731}(r/d)^{-1.13}(z/d)^{0.0400}$$

The degree of correlation R^2 = .978.

These equations are overall correlations on a macro scale and the variation of Nusselt number with Reynolds number is represented by a single exponent value. On a micro scale, for both jets and for the stated ranges, the Reynolds number exponent was found to decrease with increasing radius ratio. As for variations in the exponent with increasing nozzle distance a pronounced increase occurred for the semi-confined jet, in particular at the lower values of radius ratio. This tendency to increase was less certain for the unconfined jet with the magnitude of any changes being considerably reduced. In both cases the variation in the Reynolds number exponent with nozzle distance ratio tended to zero as the radius ratio increased.

7.4 Comparisons between the two jets

For otherwise identical conditions and for 3≤r/d≤9 thermal energy transfers for

the semi-confined operating mode were found to be generally lower than those for the unconfined mode. The extent of the difference between the two jets was variable and depended upon the level of Re, z/d and r/d. For Re = 40 000 the average Nusselt number over the range $3 \leq r/d \leq 9$ for the unconfined flow was 50 per cent in excess of the semi-confined flow. The corresponding figure for Re = 140 000 was 16 per cent.

The data for the range $r/d < 2.5$ suffered from a lack of discrimination arising from the use of a relatively small diameter nozzle. Hence the scope for meaningful comparisons between the two jets was minimal although there was a strong suggestion that the semi-confined data followed a similar profile to that for the unconfined flow. Certainly the transition to turbulent flow and the onset of radial flow as characterised in unconfined flow was also a feature for the semi-confined jet.

7.4.1 The effect of semi-confinement

(i) Expressing the effect of semi-confinement as the ratio of local Nusselt numbers then

$$\frac{Nu_{semi-confined}}{Nu_{unconfined}} = \phi_1 Re^{m_1}$$

where ϕ_1 is a function of r/d. For $39\,000 \leq Re \leq 145\,000$ the Reynolds exponent m_1 determined as a mean value for $3 \leq r/d \leq 9$ equals 0.15, 0.17 and 0.19 for z/d = 2,4 and 6 respectively. For a given value of z/d the positive

values for the exponent illustrate the declining influence of semi-confinement on local heat transfer coefficients as Reynolds number increases. This is as a direct consequence of the relatively stronger dependence of Nusselt numbers on Reynolds numbers for the semi-confined flow. As z/d approaches 6 then so the influence of semi-confinement decreases and the Nusselt numbers approach those for unconfined flow. At the higher range of Re the difference in Nu values for the two operating modes is reduced by 70 per cent as z/d is increased from 2 to 6.

(ii) The effect of semi-confinement on local Nu values is more pronounced as distance from the stagnation point increases. For 39 000 ≤ Re ≤ 145 000 and 3 ≤r/d ≤ 9 the effect can be expressed by the empirical equation

$$\frac{Nu_{semi-confined}}{Nu_{unconfined}} = \phi_2 (r/d)^{m_2}$$

where ϕ_2 is a function of Re and m_2 equals -0.19, -0.11 and -0.082 for z/d = 2, 4 and 6 respectively. The negative exponent illustrates the declining values of the Nusselt number ratio and hence an increasing influence of semi-confinement as r/d increases. At a given value of r/d the declining influence of semi-confinement as z/d approaches 6 is again confirmed.

As a consequence of the conclusions in paragraphs 7.4 and 7.4.1 it is inappropriate to recommend the use of semi-confinement for cooling purposes in single jet operation. Of course enhanced cooling results from multi jet

impingement where the physical application calls for some kind of confinement and where cross flow conditions often apply. Heating applications in which local high temperature regions are a requirement will benefit from the use of a semi-confined jet.

7.5 Suggestions for further work

Based upon this work for a single normal air jet and excluding all other geometric and flow conditions, the following suggestions for further work are put forward.

(i) During the discussion, paragraph 6.3.1, the suggestion was made that at some higher values of Reynolds number, semi-confined and unconfined profiles become equal. Confirmation of this suggestion, especially in view of accompanying high Mach numbers, would be of interest. The jet Mach number and the dimensionless temperature T_w/T_a should be included in the correlation equations to ascertain their effect on the thermal energy transfer processes. Variations in the statistical treatment of the existing data could be made to determine different functional relationships having improved degrees of correlation.

(ii) Many of the reasons given for the different heat transfer characteristics have been explained in terms of flow velocity profiles and turbulence levels. Corroboration of the heat transfer data for the semi-confined flow in terms of such arguments is a definite requirement. This is particularly the case for the

measurement of entrainment and the application of flow visualisation techniques to the space between the confinement and impingement plate will lead to a fuller understanding of the phenomenon. There is a need to quantify the turbulence intensity of the two jets not only because of its role in the thermal energy transfer process but also because of its design importance in allowing for accompanying pressure drops. As a contribution to a general database on jet impingement there is a need for a theoretical and experimental programme into a nozzle design based upon the principle of optimisation between reproducible thermal energy transfer rates and operating pumping power costs.

(iii) The experimental data for this work was for the one size of confinement plate. Entrainment is a function of plate size and including this as an extra variable will provide useful information. In addition an investigation into the effect of surface roughness on the thermal energy transfer process and the pumping power costs would form a valuable contribution to a statement on operating standards. No such data is presently available.

(iv) For a fuller understanding and comparison of the thermal energy transfer process within and around the stagnation region then further experimental data is required. The discrimination in this region of small radii can be improved by the use of a larger diameter nozzle and the subjectivity associated with the visual interpretation of the liquid crystal output eliminated by the use of image processing techniques.

(v) There is possibly a need to extend the z/d range of investigation although little new information is to be expected from values greater than about 10. However experimental data for the range 6 to 10 would support the basis for some of the arguments used in this work although the practical value of data at such values of z/d is questionable.

(vi) Meaningful comparisons on the effect of confinement will possibly result from the use of a hot jet as opposed to a cold jet as was the case in this work. Similarly comparisons of the steady state method with transient data will lead to improved techniques for the two methods and to a greater confidence in the results and their interpretation.

REFERENCES

Abromavich, G.N., 1963. The theory of turbulent jets.

Amano, R.S. and Sugiyama, S. 1985. An investigation on turbulent heat transfer of an axisymmetric jet impinging on a flat plate. *Bulletin of JSME* **28** No 235, 74-79.

Baughn, J.W and Shimizu, S. 1989. Heat transfer measurements from a surface with uniform heat flux and an impinging jet. *Journal Heat Transfer. ASME,* **111**, 1096-1098.

Baughn, J.W. and Yan, X. 1991. Liquid crystal methods in experimental heat transfer. *Proceedings 32nd Heat Transfer Fluid Mechanics Institute.* California State University, 15-40.

Baughn, J.W., Hechanova, A.E. and Yan, X. 1991. An experimental study of entrainment effects on the heat transfer from a flat surface to a heated circular impinging jet. *Proceedings ASME/JSME Thermal Engineering Joint Conference,* Reno, Nevada, **3**, 143-149.

Bedii Ozdemir, I. and Whitelaw, J.H. 1992. Impingement of an axisymmetric jet on unheated and heated flat plates. *Journal Fluid Mechanics*, **240**, 503-532.

Beltaos, S. 1976. Oblique impingement of circular turbulent jets. *Journal Hydraulic Research*, **14(1),** 17-36.

Brown, A. and Saluja, C.L. 1978. The use of cholesteric liquid crystals for surface temperature visualisation of film cooling processes. *Journal Physics Science and Instrumentation*, **11** 1068-1072.

Button, B.L. and Wilcock, D. 1978. Impingement heat transfer- a bibliography 1890 - 1975. *Previews Heat Mass Transfer,* **4**, 83-89.

Button, B.L. and Jambunathan, K. 1989. Jet impingement heat transfer: a bibliography 1976-1985. *Previews Heat Mass Transfer*, **15**, 149-178.

Cooper, T.E. et al 1975. Liquid crystal thermography and its applications to the study of convective heat transfer. *ASME Journal of Heat Transfer*, **97** 442-450.

Davenport, C.J. 1989. A technique for measuring local heat transfer due to an impinging liquid spray. *ASME Proceedings National Heat Transfer Conference*, Philadelphia, **106**, 531-536.

Davies, G. 1989. A study of jet impingement using liquid crystals. BSc project report. Department of Mechanical Engineering, The Nottingham Trent University.

den Ouden, C. 1973. Determination of local heat transfer coefficients by use of liquid crystals. Delft Progress Report, Delft University of Technology, 33-38.

den Ouden, C. and Hoogendoorn, C.J. 1974. Local convective heat transfer coefficients for jets impinging on a plate; experiments using a liquid crystal technique. *Proceedings of the Fifth International Heat Transfer Conference*, **5**, 293-297.

Downs, S.J. and James, E.H. 1987. Jet impingement heat transfer - a literature survey. *ASME*. Paper 87-HT-35.

Draper, N.R. and Smith, H. 1981. Applied regression analysis.

Fergason, J.L. 1980. New instrumentation for temperature measurement. Liquid Crystal Chemical Corporation Kent, Ohio. NSF/RA-8000037.

Gardon, R. and Cobonpue, J. 1961. Heat transfer between a flat plate and jets of air impinging on it. *International Developments in Heat Transfer; International*

Heat Transfer Conference, University of Colorado. CO, USA, August 28 to September 1, **2**, 454-460.

Gardon, R. and Akfirat, J.C. 1966. Heat transfer characterstics of impinging two dimensional air jets. *Journal Heat Transfer*, **88**, 101-108.

Gautner, J.W., Livingood, J.N.B. and Hrycak P. 1970. Survey of literature on flow characteristics of a single turbulent jet impinging on a flat plate. NASA TN D-5652 NTIS N70-18963.

Giannini, F. and Maltese, P. and Sorrentino,R. 1979. Liquid crystal improved techniques for thermal field measurements. *Applied Optics*, **18**, 3048-3052.

Goldstein, R.J. and Franchett, M.E. 1988. Heat transfer from a flat surface to an oblique impinging jet. *ASME Journal Heat Transfer*, **110(1)**, 84-90.

Goldstein, R.J. and Timmers, J.F.1982. Visualisation of heat transfer from arrays of impinging jets. *International Journal Heat and Mass Transfer*, **25**, 1857-1868.

Goldstein, R.J., Sobolik, K.A. and Seol, W.S 1990. Effect of entrainment on the heat transfer to a heated circular air jet impinging on a flat surface. *ASME J. Heat Transfer*, **112**, 608-611.

Gundappa, M., Hudson, J.F. and Diller, T.E. 1989. Jet impingement heat transfer from jet tubes and orifices. *National Heat Transfer Conference*, Philadelphia, PA, USA, August 6-9, **107**, 43-50.

Gray, G.W. 1985. Liquid Crystals; an arena for research and industrial collaboration among chemists, physicists and engineers. *Proceedings Royal Society*, **402**, 1-36.

Hippensteele, S.A. Russell, L.M. and Stepka, F.S. 1983. Evaluation of a method for heat transfer measurements and thermal visualisation using a composite of a heater element and liquid crystals. *ASME Journal of Heat Transfer*, **105** 184-189.

Hollingsworth, D.K., Boehman, A.L., Smith, E.G. and Moffat, R.J. 1989. Measurement of temperature and heat transfer coefficient distributions in a complex flow using liquid crystal thermography and true colour image processing. *Collected Papers in Heat Transfer,* San Francisco, California, 10-15 December, **123,** 35-42.

Hollworth, B.R, and Gero, L.R. 1985. Entrainment effects on impingement heat transfer. Part2. Local heat transfer measurements. *Journal Heat Transfer Transactions. ASME,* **107**, 910-915.

Hoogendoorn, C.J. 1977. The effect of turbulence on heat transfer at a stagnation point. *International Journal Heat and Mass Transfer,* **20,** 1333-1338.

Hrycak, P. Lee, D.T., Gauntner, J.W. and Livingood, J.N.B. 1970. Experimental flow characteristics of a single turbulent jet impinging on a flat plate. NASA TN D-5690.

Hrycak, P. 1983. Heat transfer from round impinging jets to a flat plate. *International Journal of Heat and Mass Transfer,* **26** 1857-1865.

Huang, G.C. 1963. Investigations of heat transfer coefficients for air flow through round jets impinging normal to a heat transfer surface. *ASME Journal of Heat Transfer,* **85**, 237-245.

Ireland, P.T. and Jones, T.V. 1987. The response time of a surface thermometer employing encapsulated thermochromic liquid crystals. *Journal Phys.E: Sci. Instrumentation,* **20** 1159-1199.

Jambunathan, K., Lai, E., Moss, M.A. and Button, B.L. 1992. A review of heat transfer data for single circular jet impingement. *International Journal Heat and Fluid Flow,* **13(2)**, 106-115.

Jones, T.V., Wang, Z. and Ireland, P.T. 1992. Liquid crystal techniques. *International Symposium on Heat Transfer in Turbomachinery, ICHMT,* Athens.

Kasagi, N. Moffat, R.J. and Hirata, M. 1989. Liquid Crystals. *Hand book of flow visualisation, Chapter 8. New York Hemisphere.*

Kline, S.J. and McClintock, F.A. 1953. Describing uncertainties in single-sample experiments. Mechanical Engineering.

Lovell, B.J. 1978. Local transfer coefficients for impingement of an axisymmetric jet on an inclined surface. Department of Mechanical Engineering, University of Minnesota, MN, USA.

Martin, H. 1977. Heat and mass transfer between impinging gas jets and solid surfaces. *Advances in Heat Transfer,* 13, 1-60.

Moffat, R.J. 1985. Using uncertainty analysis in the planning of an experiment. *Journal of Fluids Engineering*, **107,** 173.

Moreno, O.A. et al 1993. Mass transfer of an impinging jet confined between parallel plates. *IBM Journal Research Development*, **37, No 2** 143-155.

Obot, N.T., Douglas, W.J.M. and Mujumdar, A.S. 1982. Effect of semi-confinement on impingement heat transfer. *Seventh International Heat Transfer Conference,* Munchen, Germany, September 6-10, **3**, 395-400.

Obot, N.T., Mujumdar, A.S. and Douglas, W.J.M. 1979. Effect of nozzle

geometry on impingement heat transfer under a round turbulent jet. *ASME Paper No.79-WA/HT-53*.

Perry, K.P. 1954. Heat transfer by convection from a hot gas jet to a plane surface. *Proceedings Institute Mechanical Engineering,* **168**, 775-780.

Popiel, C.O. and Boguslawski, L.(1986). Mass or heat transfer in impinging single round jets emitted by a bell-shaped nozzle and sharp ended orifice. *Proc. 8th International Heat Transfer Conference,* San Francisco, CA, 17-22 August, 1187-1192.

Rhine, J.M. and Tucker, R.J. Modelling of gas-fired furnaces and boilers. Chap 4.

Rogers,G.F.C. and Mayhew, Y.R. 1988 Thermodynamic and Transport Properties of Fluids.

Ryan, T. and Joiner, B. 1976. Minitab student handbook.

Schlichting, H. 1968. Boundary-Layer Theory.

Schlunder, E.U. and Gnielinski, V. 1967. Heat and mass transfer between a surface and an impinging jet. *Chem. Ing. Tech.,* **39**, 578-584.

Simonich, J.C. and Moffat, R.J.(1982). New techniques for mapping heat transfer coefficient contours. *Review Science Instrumentation,* **53**, No.5, 678-683.

Simonich, J.C. and Moffat, R.J.(1984).Liquid crystal visualisation of surface heat transfer on a concavely curved turbulent boundary layer. *ASME Journal of Engineering for Gas Turbines and Power,* **106**, 619-627.

Sparrow, E.M., Goldstein, R.J. and Rouf, M.A. 1975. Effect of nozzle surface separation distance on impingement heat transfer for a jet in a cross-flow *ASME Journal of Heat Transfer*, **97**, 528-533.

Sparrow, E.M. and Lovell, B.J. 1980. Heat transfer characteristics of an obliquely impinging circular jet. *ASME Journal of Heat Transfer*, **102,** 202-209.

Trabold, T.A., Esen, E.B. and Obot, N.T. 1987. Entrainment by turbulent jets issuing from sharp-edged inlet round nozzles. *Journal of Fluids Engineering ASME,* **109,** 248-254.

Vlachopoulos, J. and Tamich, J.F. 1971. Heat transfer from a turbulent hot air jet impinging normally on a flat plate. *Canadian Journal of Chemical Engineering, 49*, 462-466.

Yan, X., Baughn, J.W., and Mesbah, M. 1992. The effect of Reynolds number on the heat transfer distribution from a flat plate to an impinging jet. *ASME Heat Transfer Division: Fundamental and Applied Heat Transfer Research for Gas Turbine Engines HTD*, **226,** 1-7.

BIBLIOGRAPHY

Beltaos, S. and Rajaratnam, N. 1974. Impinging circular turbulent jets. *ASCE, Journal of the Hydraulics Division,* **100**, 1313-1328.

Davies, R.M., Rhines, J.M. and Sidhu, B.S. 1984. The application of the liquid crystal technique to the experimental modelling of forced convective heat transfer in industrial heating processes. British Gas Research and Development Report. **MRS E 420.**

Florschuetz, L.W.1982. Jet array impingement flow distribution and heat transfer characteristics. *NASA* **CR 3630.**

Goldstein, R.J.1985 Heat transfer to impinging air jets. *Proceedings Third Symposium on Energy Engineering Science.* Pennsylvania State University, 8-10 October, 256-265.

Hollworth, B.R. and Berry, R.D. 1978. Heat transfer from arrays of impinging jets with large jet to jet spacing. *ASME* **78-GT-117.**

Hrycak, P 1981. Heat transfer from impinging jets:a literature review. *New Jersey Institute of Technology.* **AFWAL-Tr-81-3054.**

Ireland, P.T and Jones, T.V. 1985. The measurement of local heat transfer coefficients in blade cooling geometries. *Heat Transfer and Cooling in Gas*

Turbines, AGARD Conference Proceedings, **No 390 Paper 28.**

Jones, T.V. 1991. The use of liquid crystals in aerodynamic and heat transfer testing. *Proceedings of the Fourth International Symposium on Transport Phenomena in Heat and Mass Transfer,* Sydney, 14-19 July, **2**, 1242-1273.

Jones, T.V. and Hippensteele, S.A 1987. High resolution heat transfer coefficient maps applicable to compound curve surfaces using liquid crystals in a transient wind tunnel. *Proceedings 24th National Heat Transfer Conference and Exhibition,* Pittsburgh,PA, 9-12 August **97** 1-9.

Katoaka, K., 1985. Optimal nozzle to plate spacing for convective heat transfer in nonisothermal, variable density impinging jets. *Drying Technology,* **3**, 235.

Lucas, M.G., Ireland, P.T., Wang, Z., Jones, T.V. and Pearce, W.J. Fundamental studies of impingement cooling thermal boundary conditions. *AGARD Conference Proceedings,* **527** 14.1-14.10.

Martinez-Botas, R.F., Spencer, M.C., Lock, G.D. and Jones, T.V. 1993. The measurement of full surface heat transfer coefficients over turbine blade passages using a cold heated transfer tunnel. Department of Engineering Science, Oxford University.

Popiel, C.O., van der Meer, T.H. and Hoogendoorrn, C.J. 1980. Convective

heat transfer on a plate in an impinging round hot gas jet of low Reynolds number. *International Journal of Heat and Mass Transfer*. **23** 1055-1068.

Popiel, C.O. and Boguslawski, L. 1988. Effect of flow structure on the heat or mass transfer on a flat plate in impinging round jet. *Second United Kingdom National Conference on Heat Transfer*, University of Strathclyde 14-16 September, **1**, 663-685.

Popiel, C.O. and Trass, O. 1982. The effect of ordered structure of turbulence on momentum, heat and mass transfer of impinging round jets. *Proceedings Seventh International Heat Transfer Conference*, Munchen, Germany 6-10 September, **6**, 141-146.

Popiel, C.O. and Trass, O. 1991. *Visualisation of a free and impinging round jet. Experimental Thermal Fluid Science*, **4**, 253-264.

Rojas, J. and Yianneskis M. 1984. The development of liquid crystal techniques for the measurement of wall heat transfer coefficients in ducts. Imperial College of Science and Technology, Mechanical Engineering Department, **FS/84/27**.

Roson, H.N. 1978. Evaluation of drying times, drying rates, and evaporation fluxes when drying wood with impinging jets. *Proceedings First International Symposium on Drying*. Montreal, **192**.

Simonich, J.C. and Moffat,R.J. 1984. Liquid crystal visualization of surface heat transfer on a concavely curved turbulent boundary layer. *J. Eng. Gas Turbines Power. Transactions ASME,* **106(3)**, 619-627.

Simonich, J.C. and Moffat, R.J. 1982. New technique for mapping heat transfer coefficient contours. *Review Science Instrumentation.* **53(5)** 678-683.

Kasagi, N. 1980. Liquid crystal application in heat transfer experiments. Mechanical Engineering Department Stanford University.

Van Treuren, K.W, Wang,Z., Ireland, P.T. and Jones, T.V. 1993. Application of the transient liquid crystal technique to measure heat transfer and adiabatic wall temperature beneath an array of impinging jets. *Proceedings Eurotherm 32,* Oxford University, UK, 5-7 July, 82-86.

Van Treuren, K.W., Wang, Z. Ireland, P.T and Jones, T.V. 1993. Detailed measurements of local heat transfer coefficient and adiabatic wall tempertaure beneath an array of impinging jets. *International Gas Turbine and Aeroengine Congress and Exposition,* Cincinnati.

Fig 1.1 Flow zones for a circular jet impinging onto a flat surface

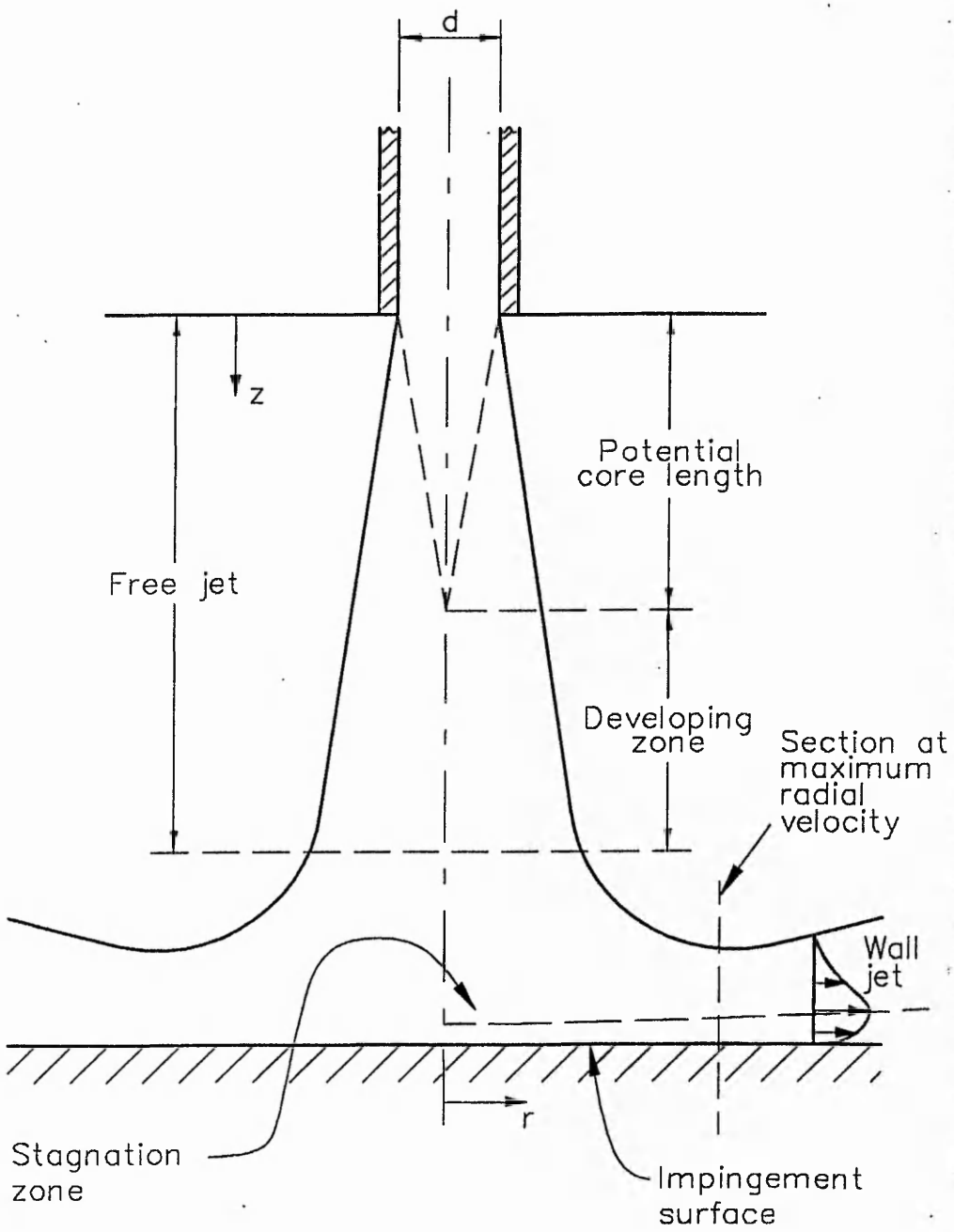

Fig 2.1 Thermal energy transfer at a boundary

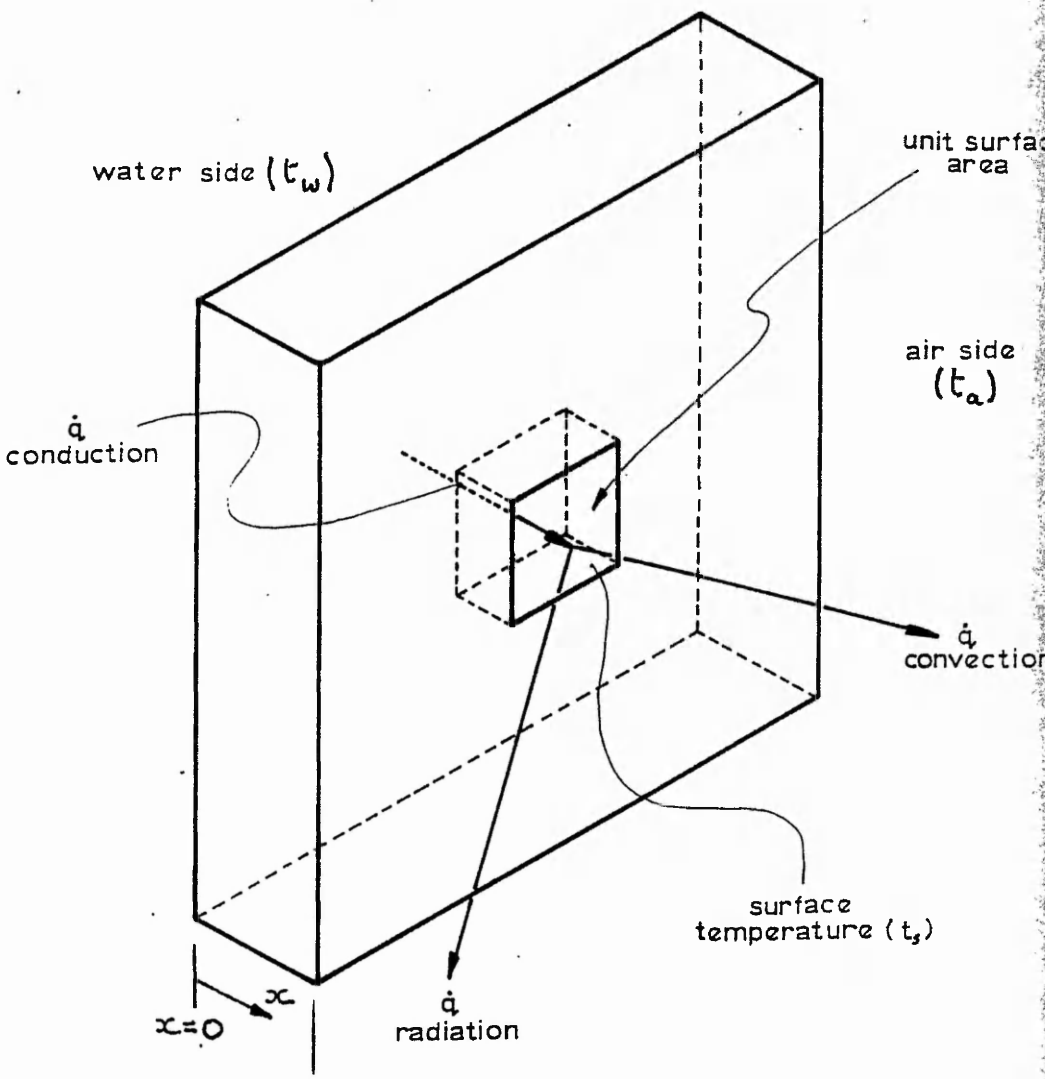

Fig 2.2 General assembly of the water bath for the semi-confined jet

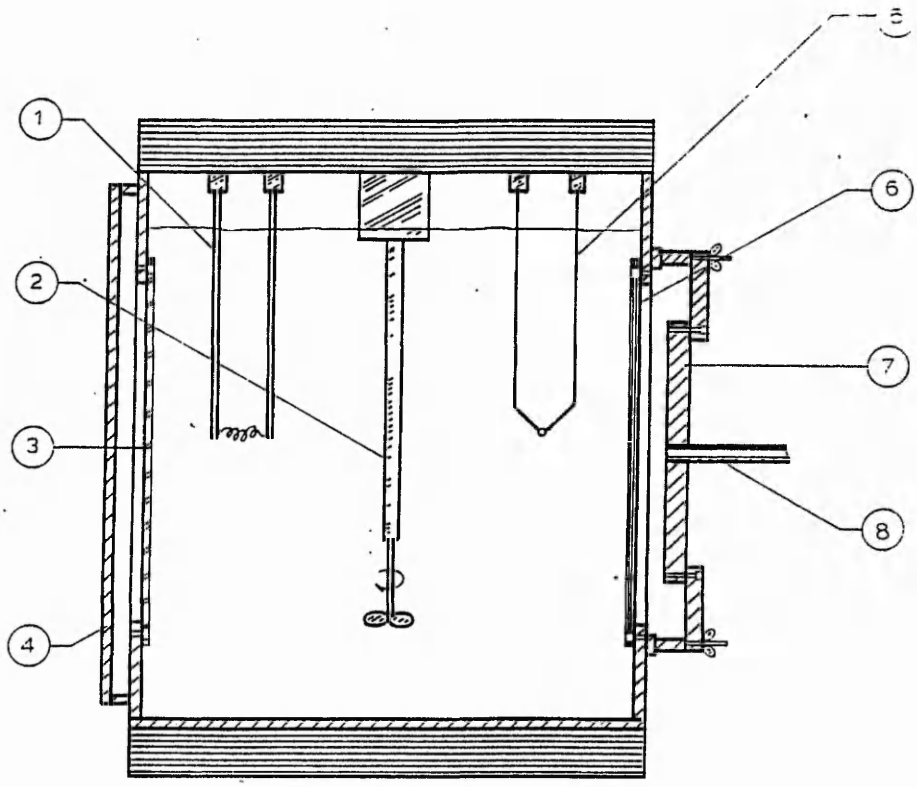

1. HEATER
2. STIRRER
3. COPPER CALIBRATION PLATE
4. OPTICAL PERSPEX COVER
5. THERMOCOUPLES - various depths
6. TOUGHENED GLASS IMPINGEMENT PLATE
7. CONFINEMENT PLATE
8. IMPINGEMENT NOZZLE

Fig 2.3 Arrangement showing unconfined jet and copper calibration plate

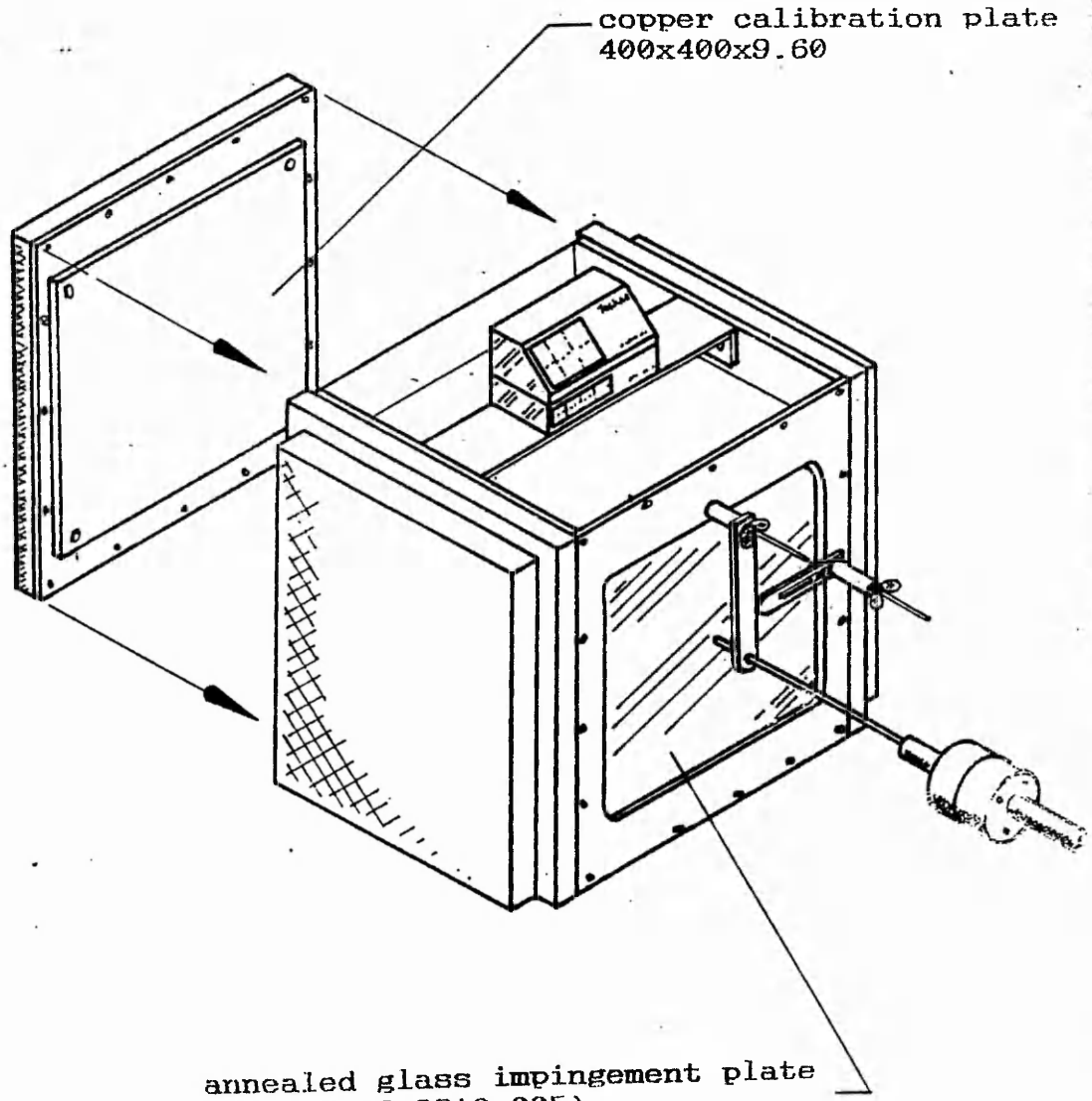

all dimensions in millimetres

Fig 2.4 Nozzle details

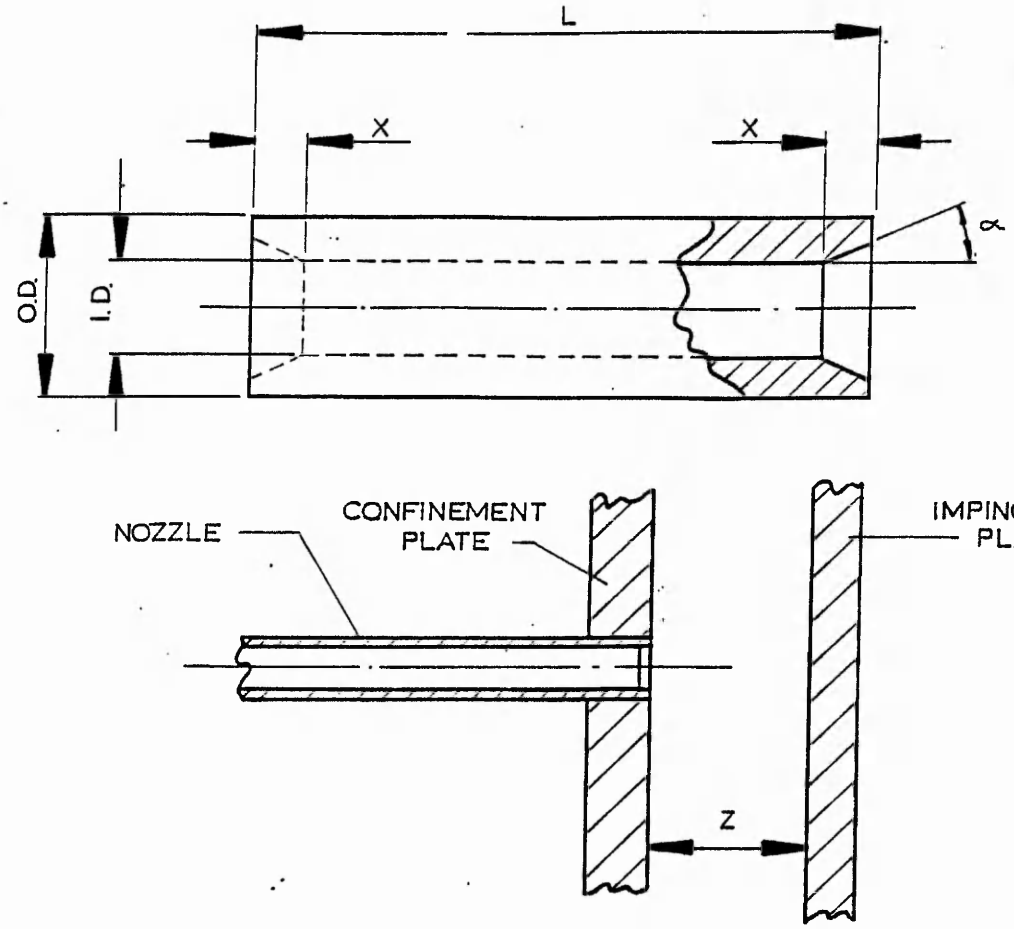

	I.D./ mm	O.D./ mm	X/ mm	α/ deg	L/ mm
NOZZLE 'A'	4.93	6.35	3	5	300
NOZZLE 'B'	10.28	12.70	5	5	300

Fig 2.5 Measurement of nozzle air temperature

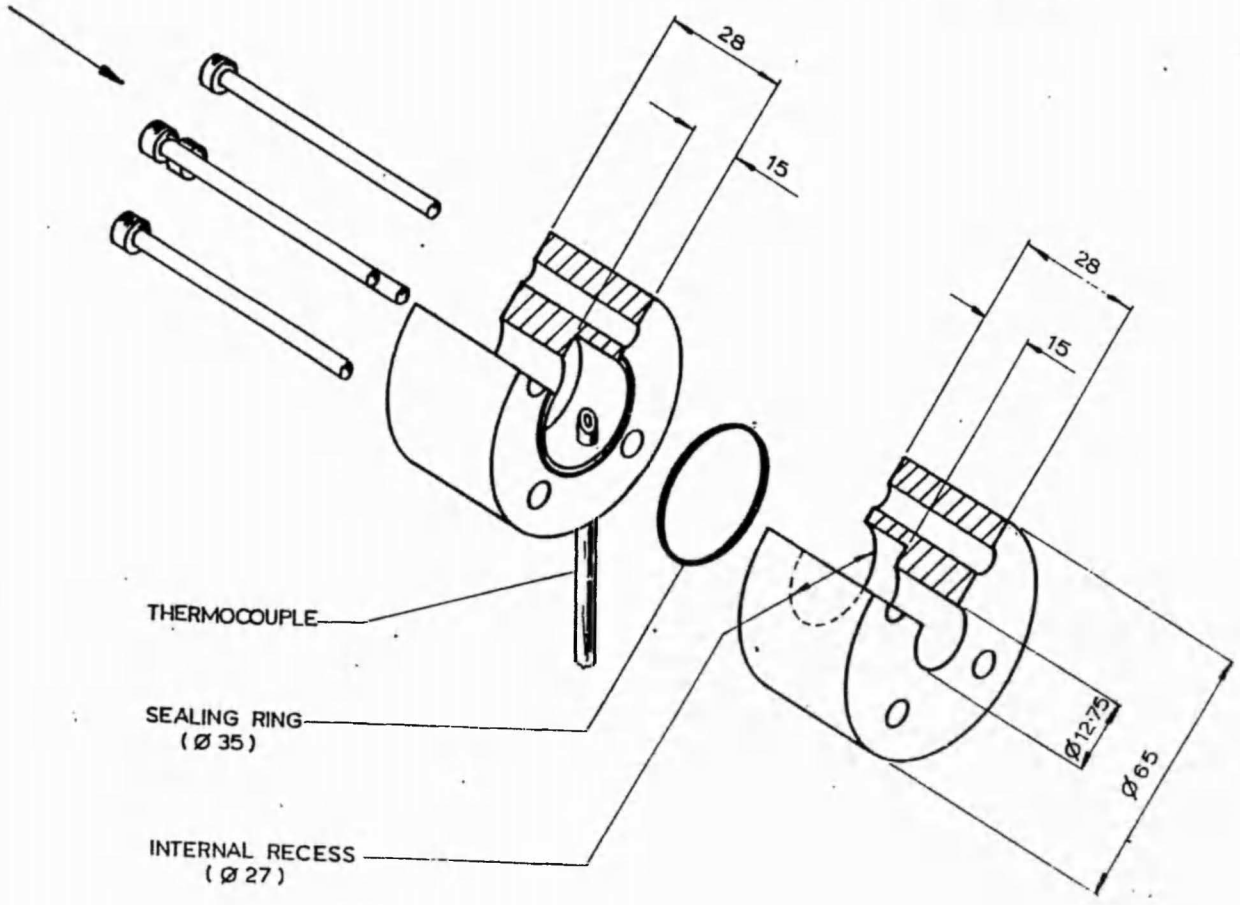

Fig 2.6 Thermal conductivity measurement

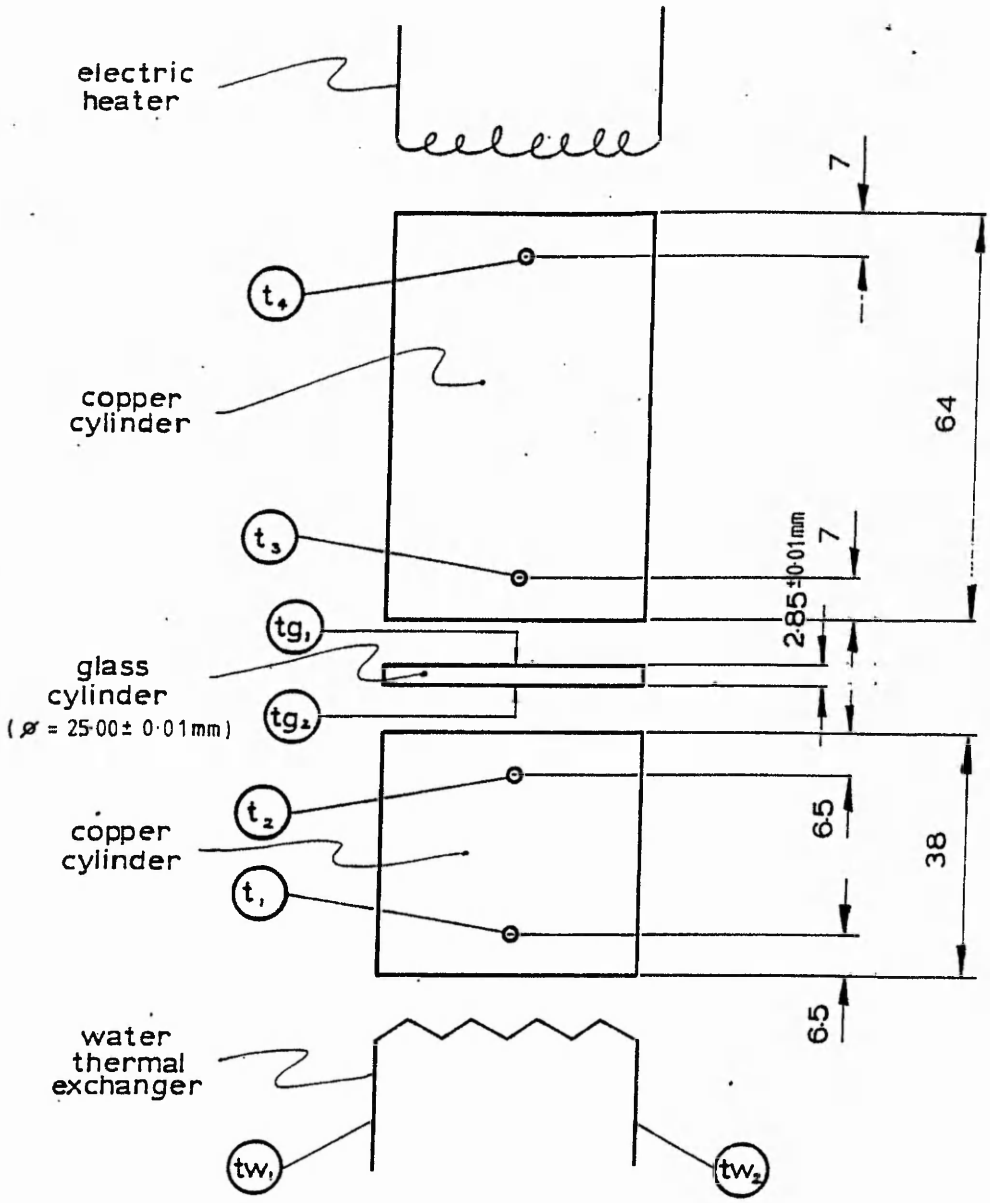

t_1 t_2 t_3 t_4	-	thermocouples
tw_1 tw_2	-	mercury-in-glass thermometers

Fig 2.7 Measurement of glass thermal conductivity: radiation losses

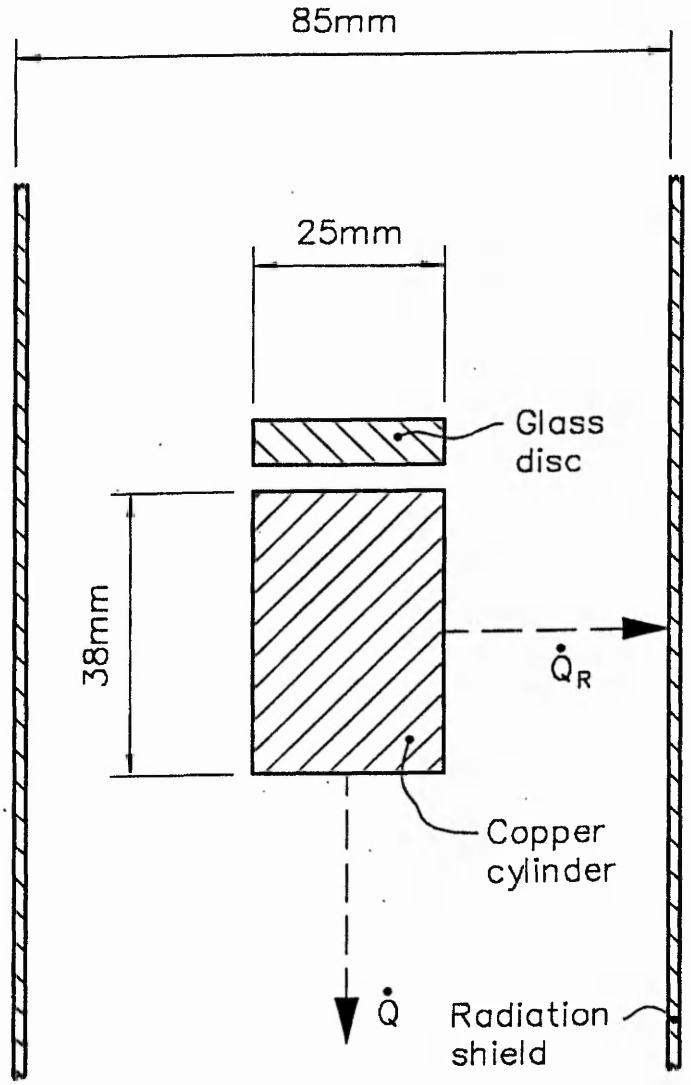

Fig 2.8 Glass thermal conductivity values

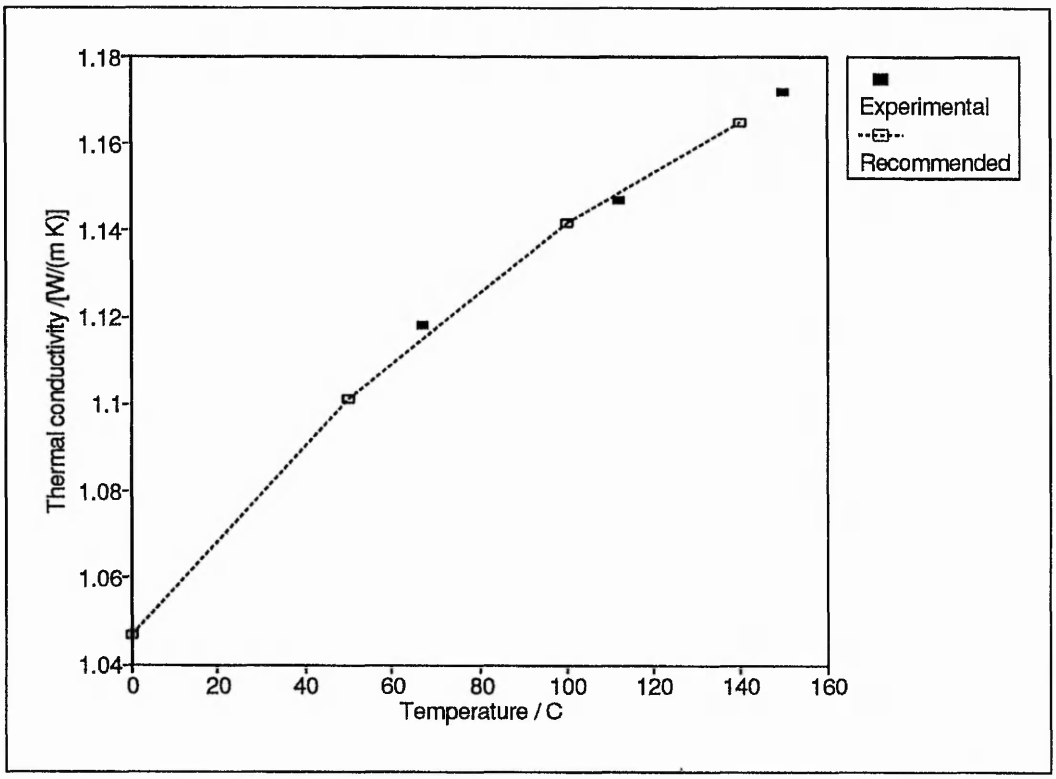

Fig 3.1 Variation of output wavelength with viewing angle for a liquid crystal

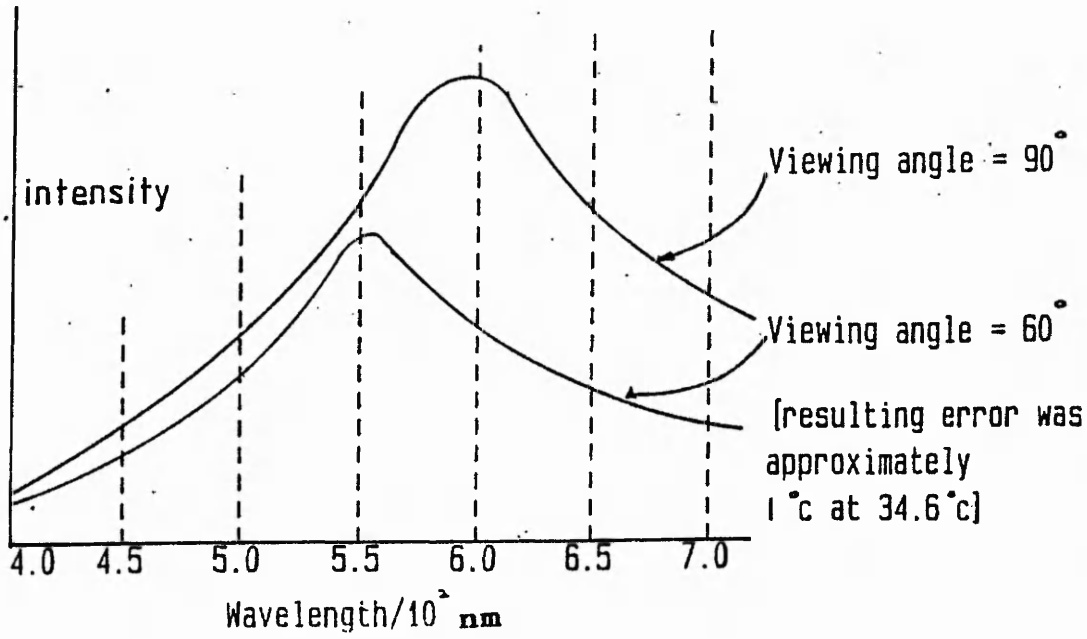

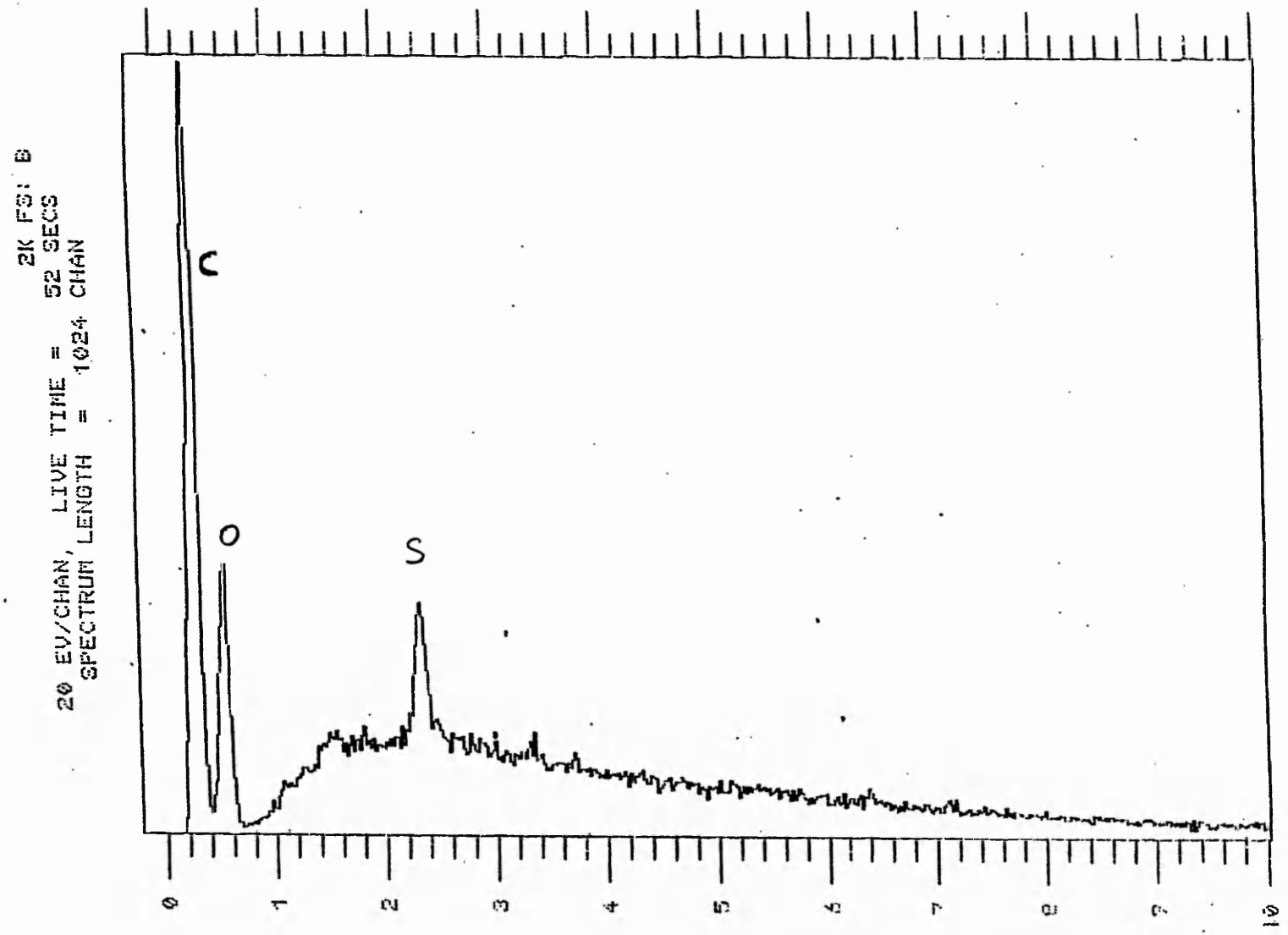

Fig 3.2 Constituents of black paint- electron microscope output

Fig 4.1 Nu versus r/d for Re=31 000→70 000 and z/d=2 for unconfined jet

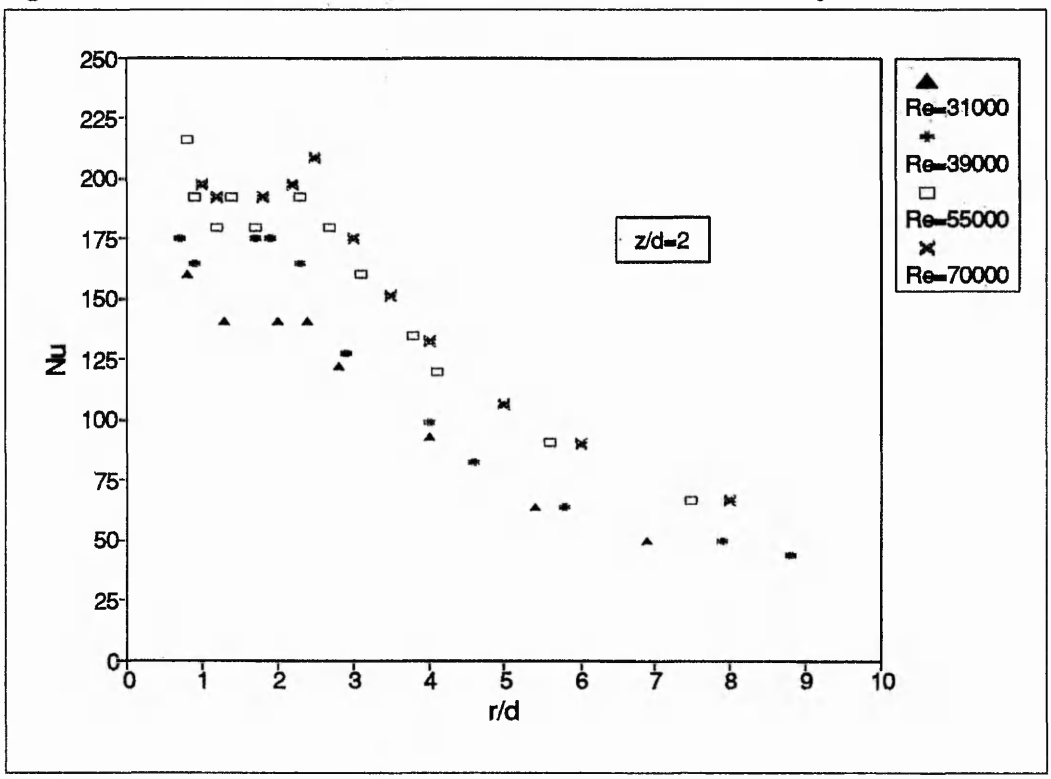

Fig 4.2 Nu versus r/d for Re=112 000→145 000 and z/d=2 for unconfined jet

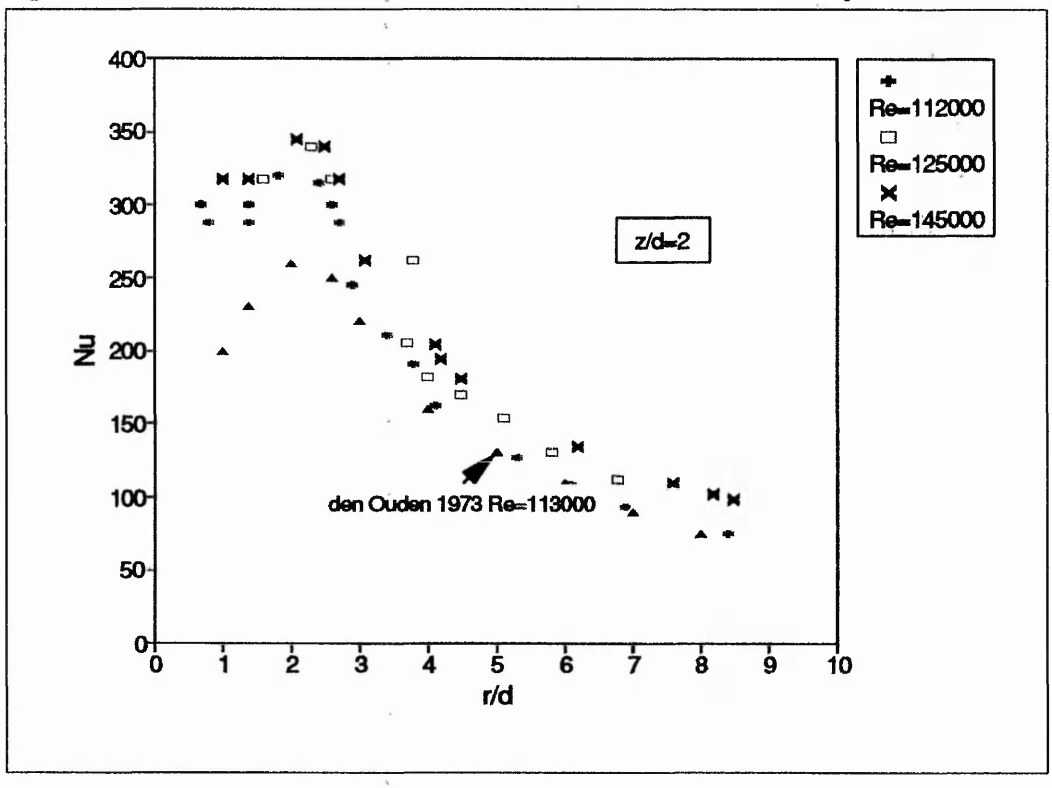

Fig 4.3 Nu versus r/d for Re=31 000→70 000 and z/d=4 for unconfined jet

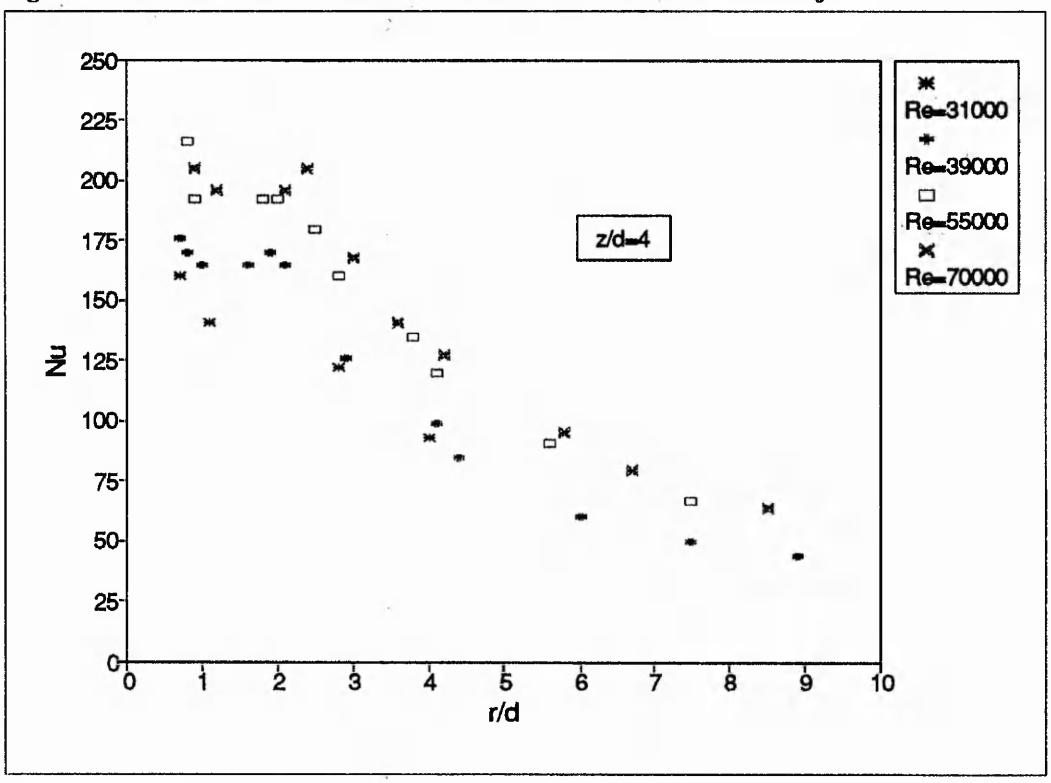

Fig 4.4 Nu versus r/d for Re=112 000→145 000 and z/d=4 for unconfined jet

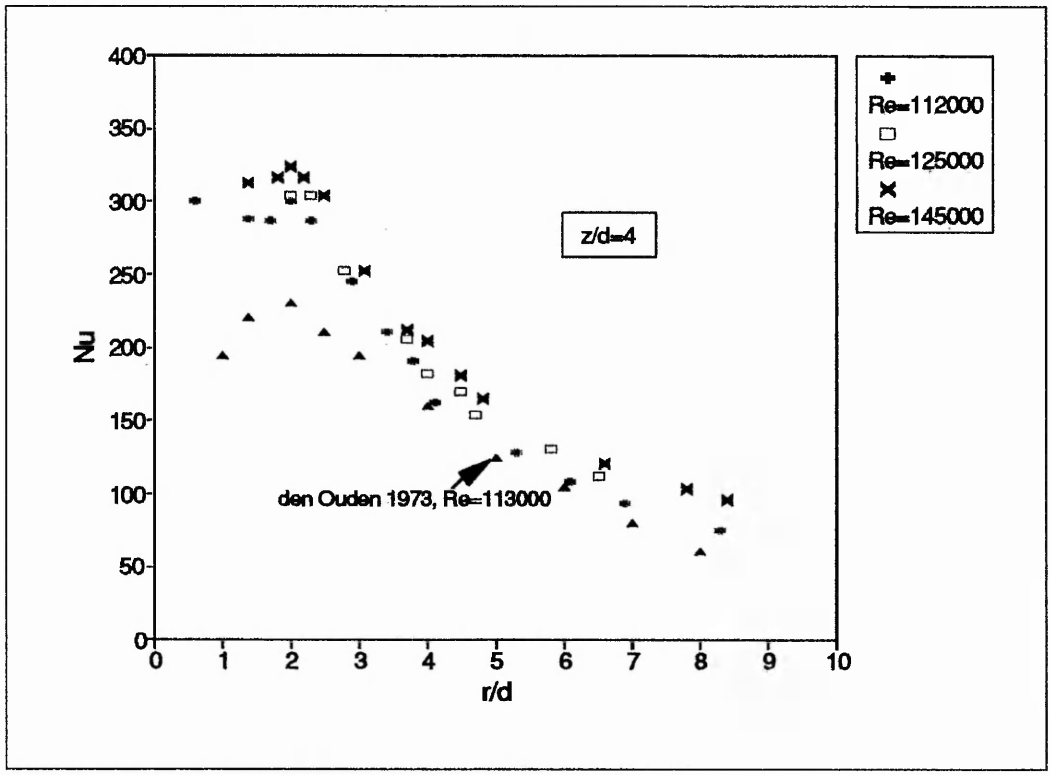

Fig 4.5 Nu versus r/d for Re=31 000→70 000 and z/d=6 for unconfined jet

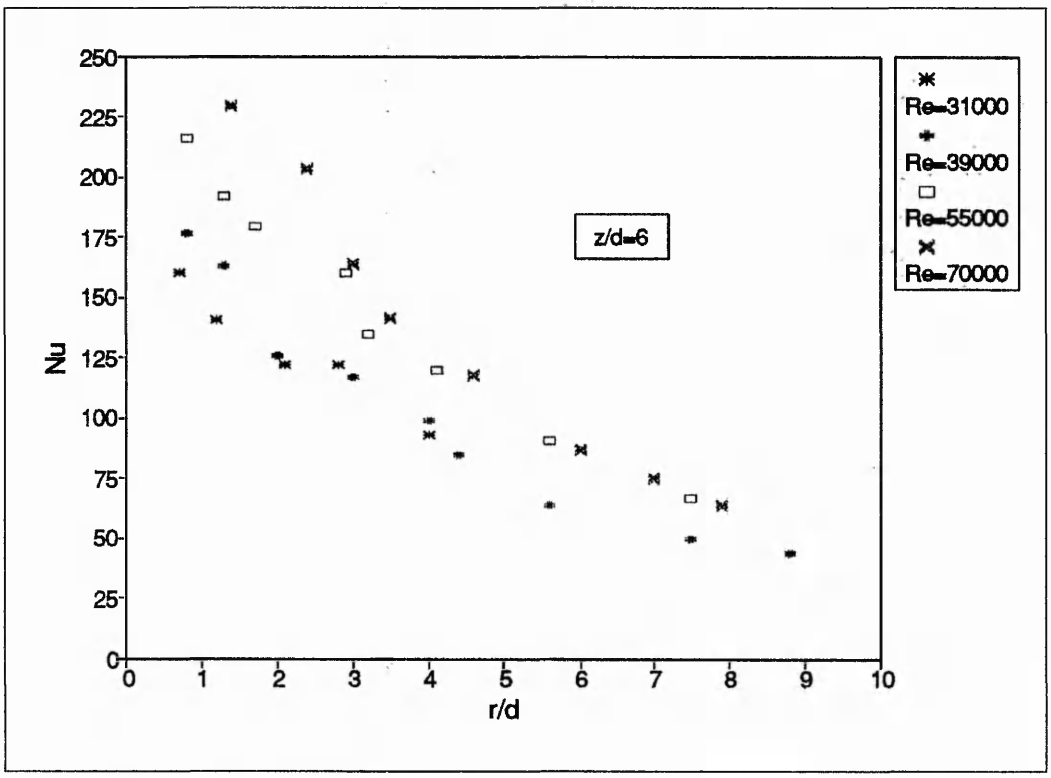

Fig 4.6 Nu versus r/d for Re=112 000→145 000 and z/d=6 for unconfined jet

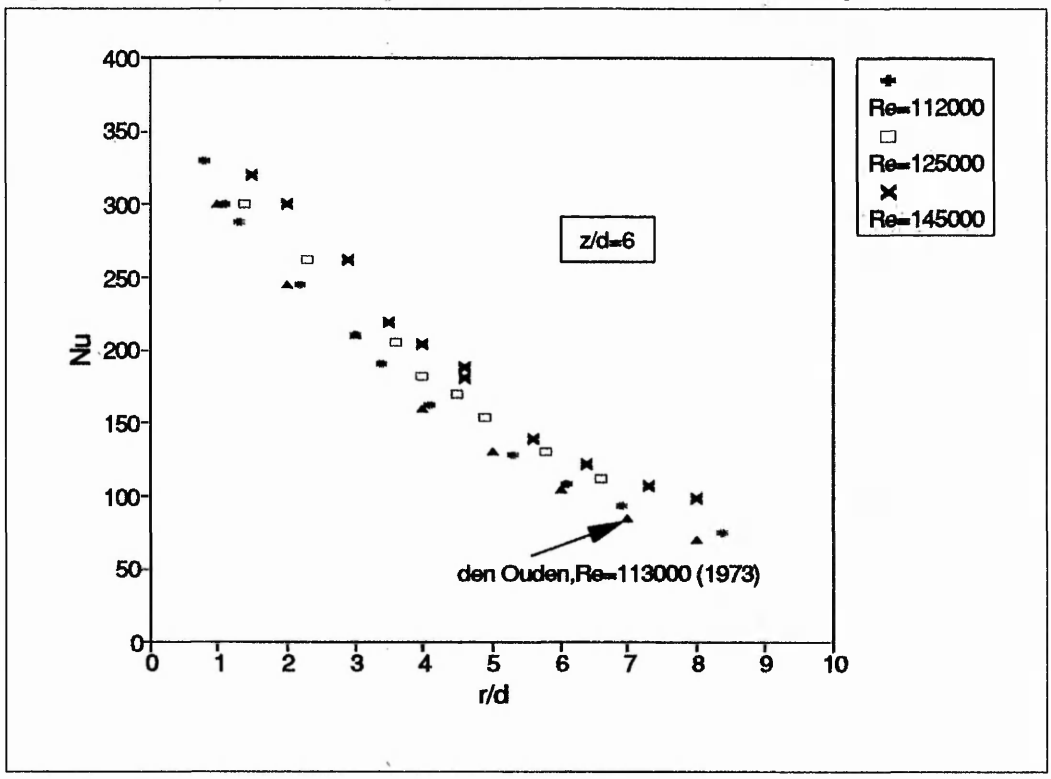

Fig 4.7 Nu versus r/d for z/d=2,4 and 6 and Re=31 000 for unconfined jet

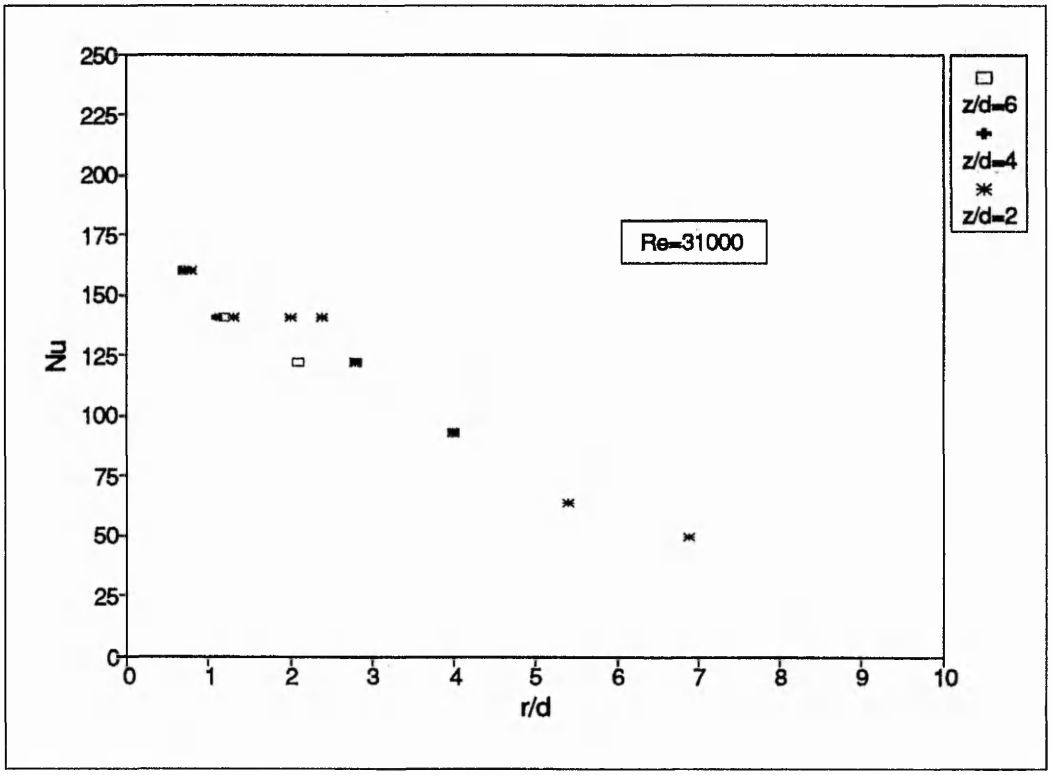

Fig 4.8 Nu versus r/d for z/d=2,4 and 6 and Re=39 000 for unconfined jet

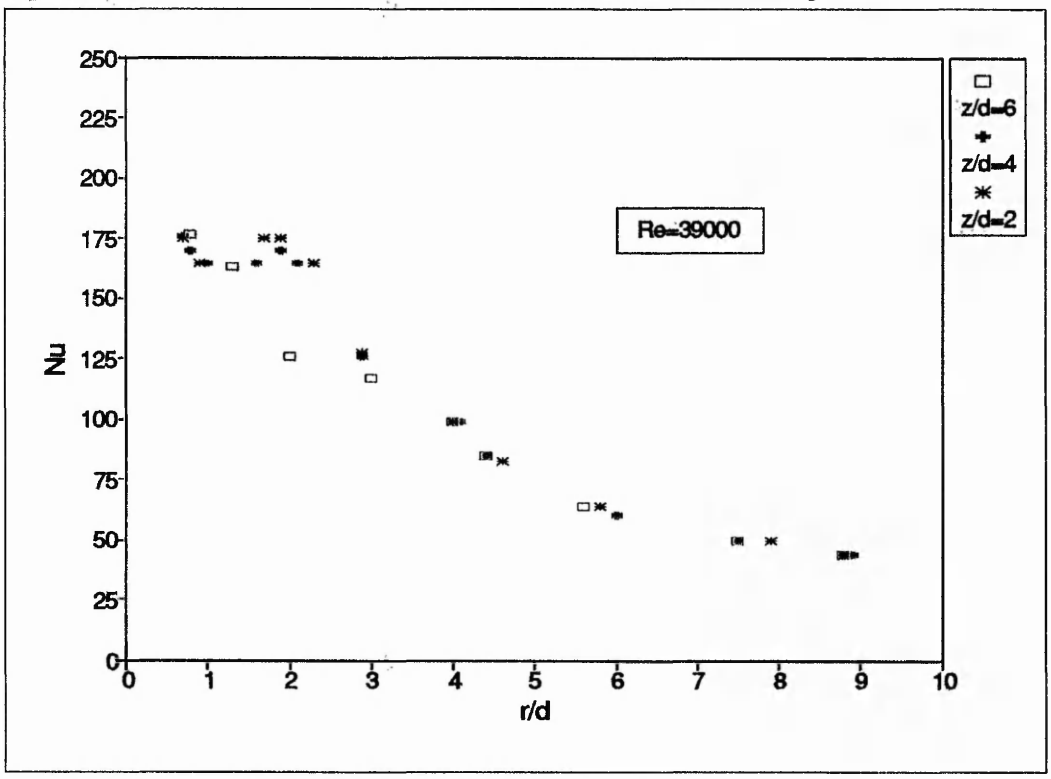

Fig 4.9 Nu versus r/d for z/d=2,4 and 6 and Re=55 000 for unconfined jet

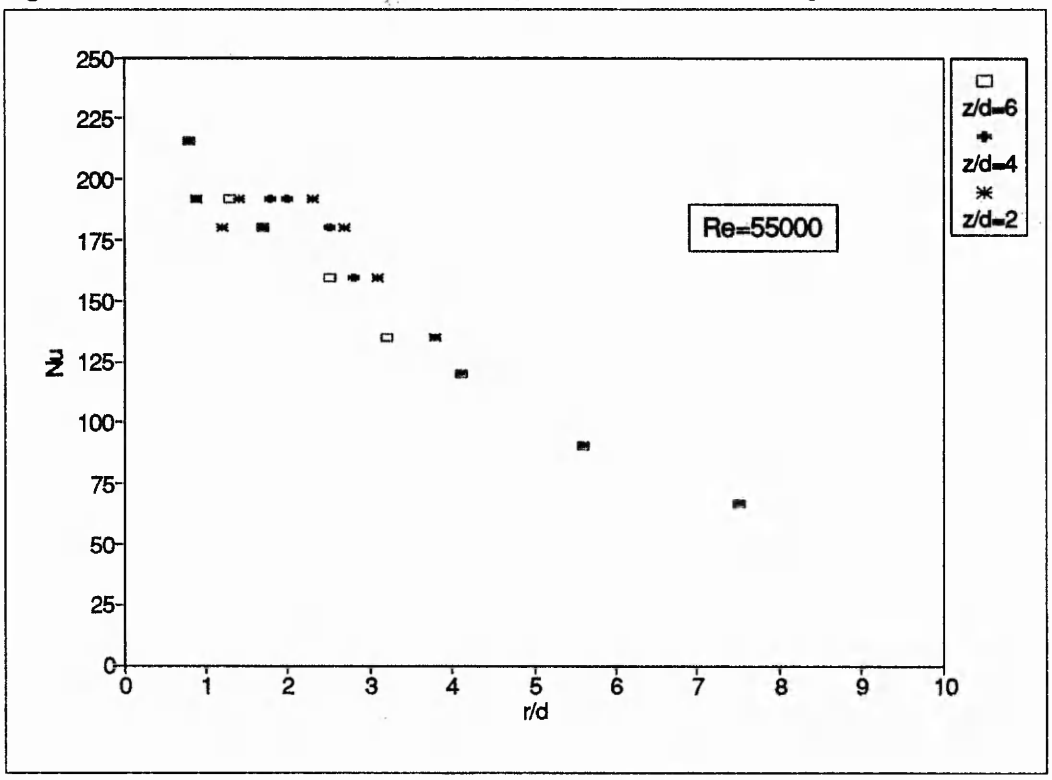

Fig 4.10 Nu versus r/d for z/d=2,4 and 6 and Re=70 000 for unconfined jet

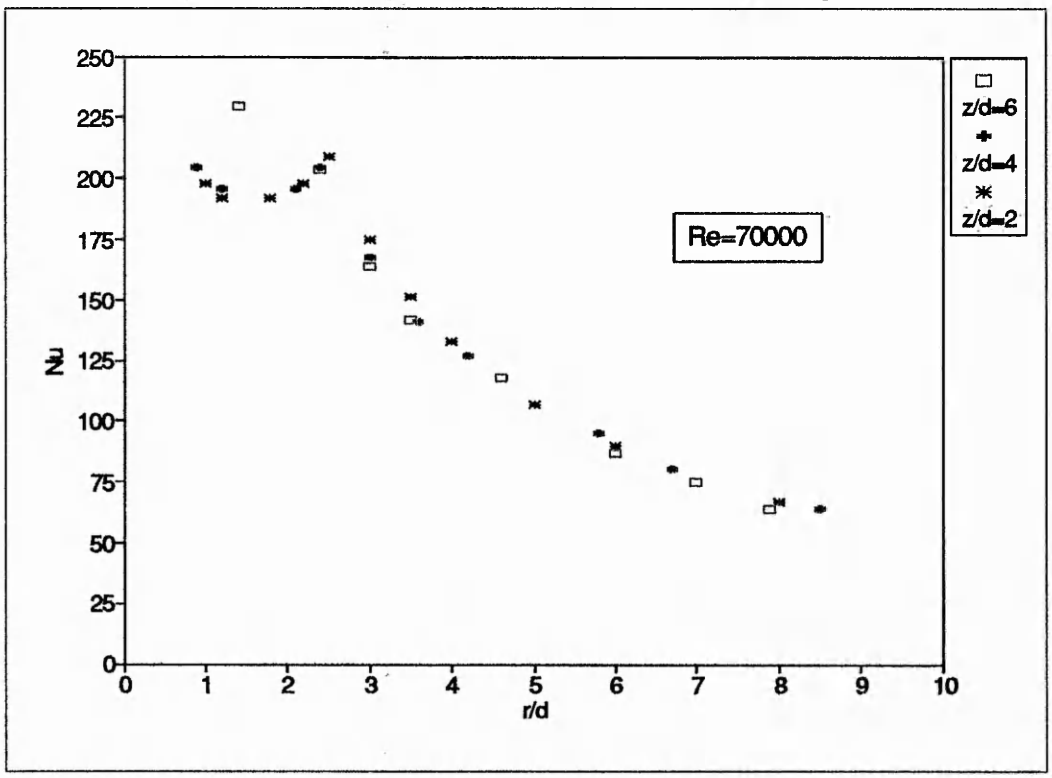

Fig 4.11 Nu versus r/d for z/d=2,4 and 6 and Re=112 000 for unconfined jet

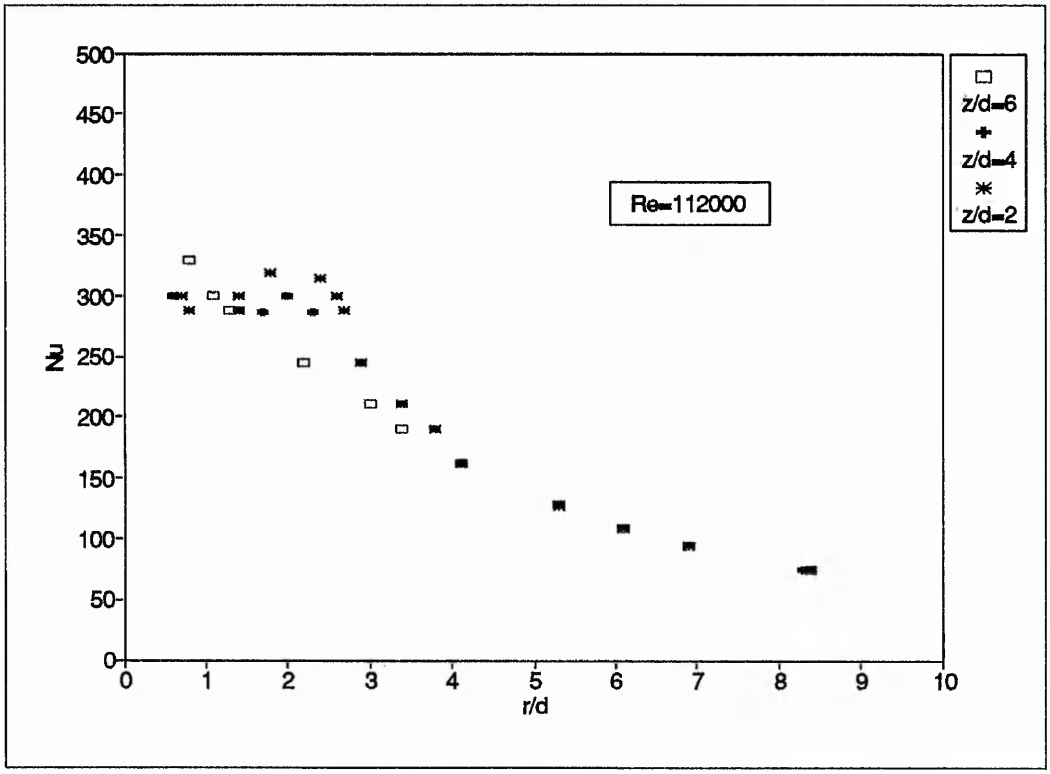

Fig 4.12 Nu versus r/d for z/d=2,4 and 6 and Re=125 000 for unconfined jet

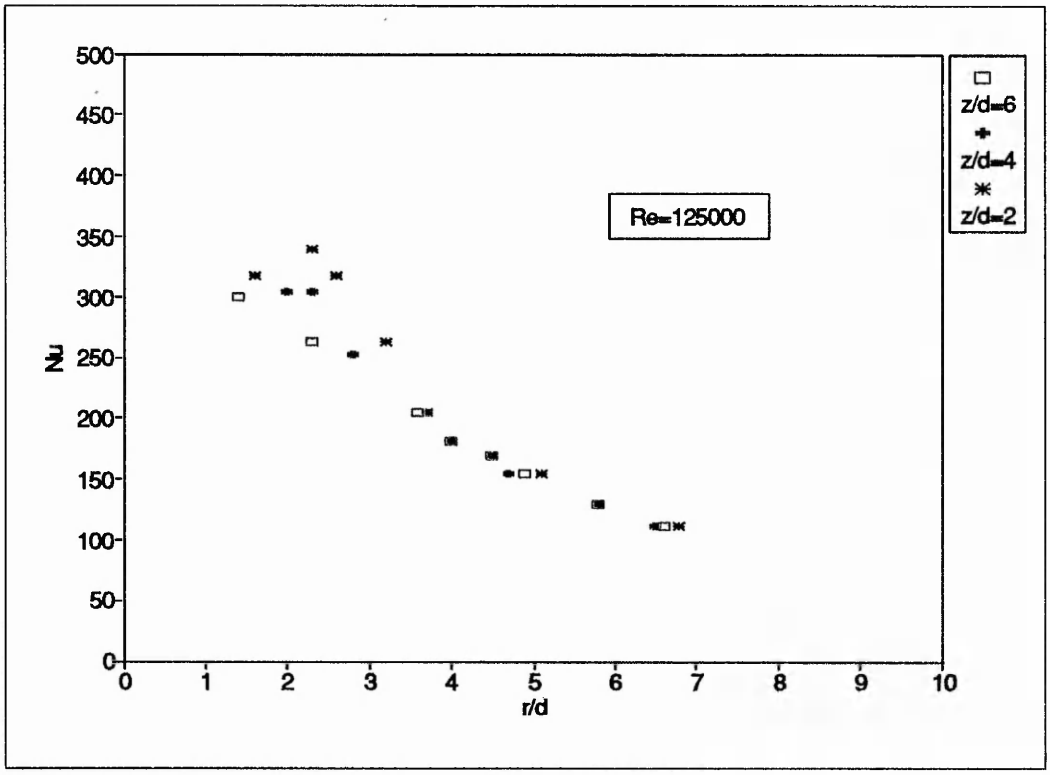

Fig 4.13 Nu versus r/d for z/d=2,4 and 6 and Re=145 000 for unconfined jet

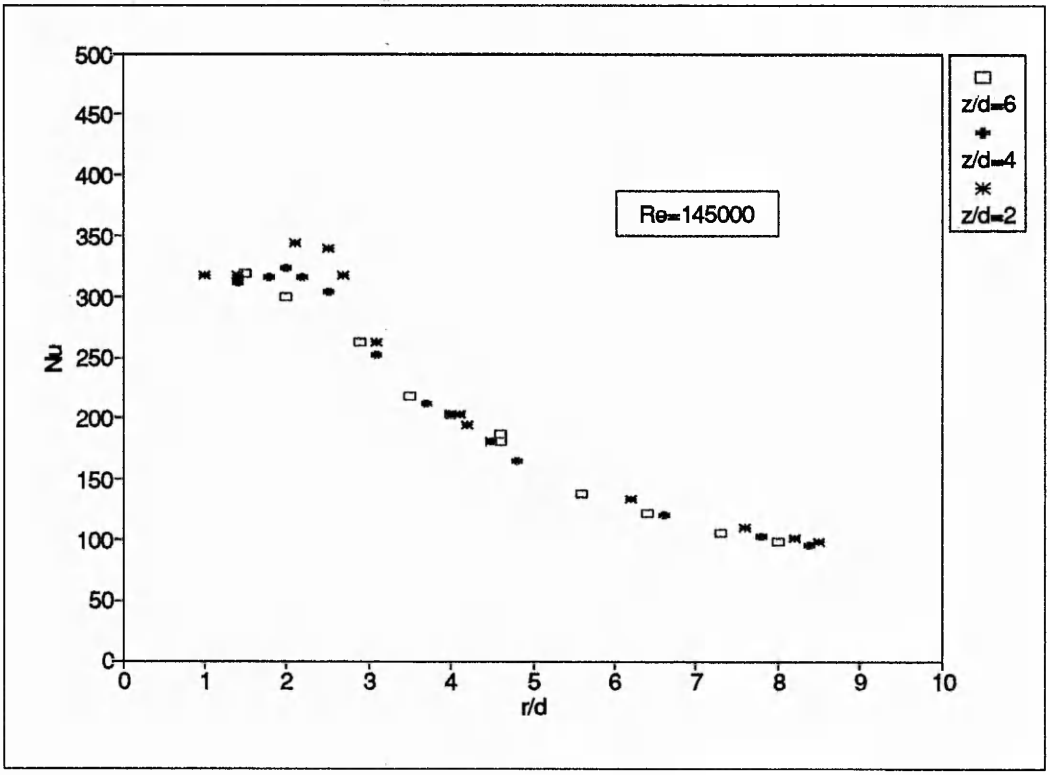

Fig 4.14 Repeatability test for unconfined jet. Re=39 000 and 70 000

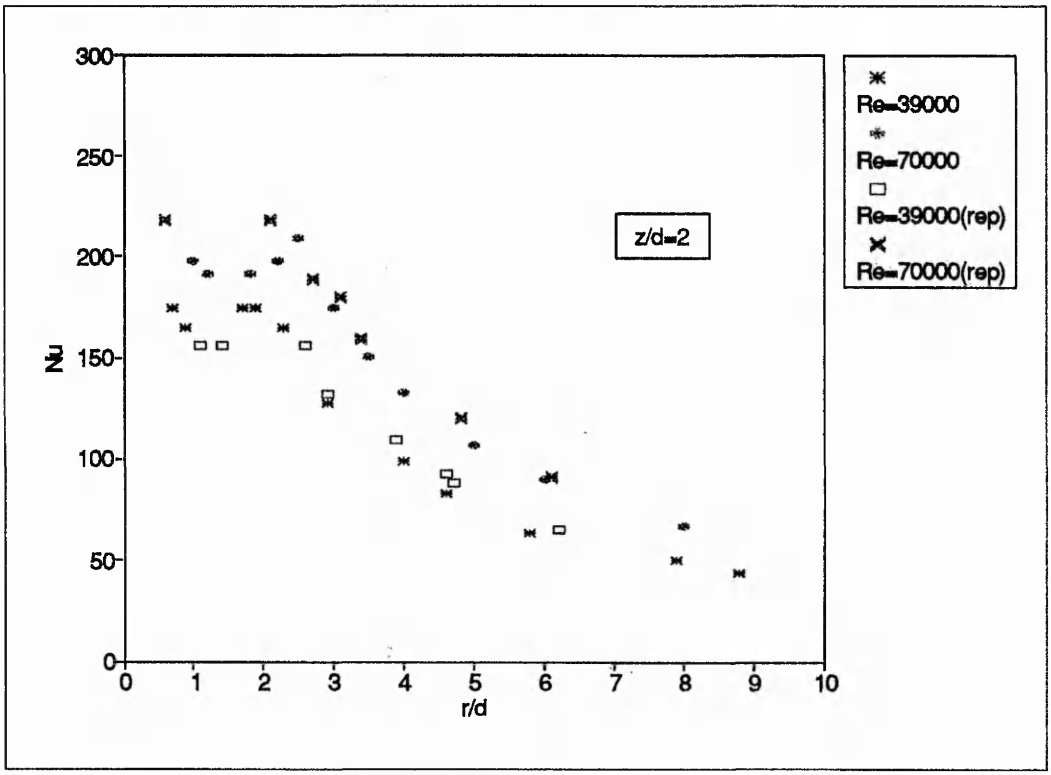

Fig 4.15 Repeatability test for unconfined jet. Re=39 000 and z/d=4,6

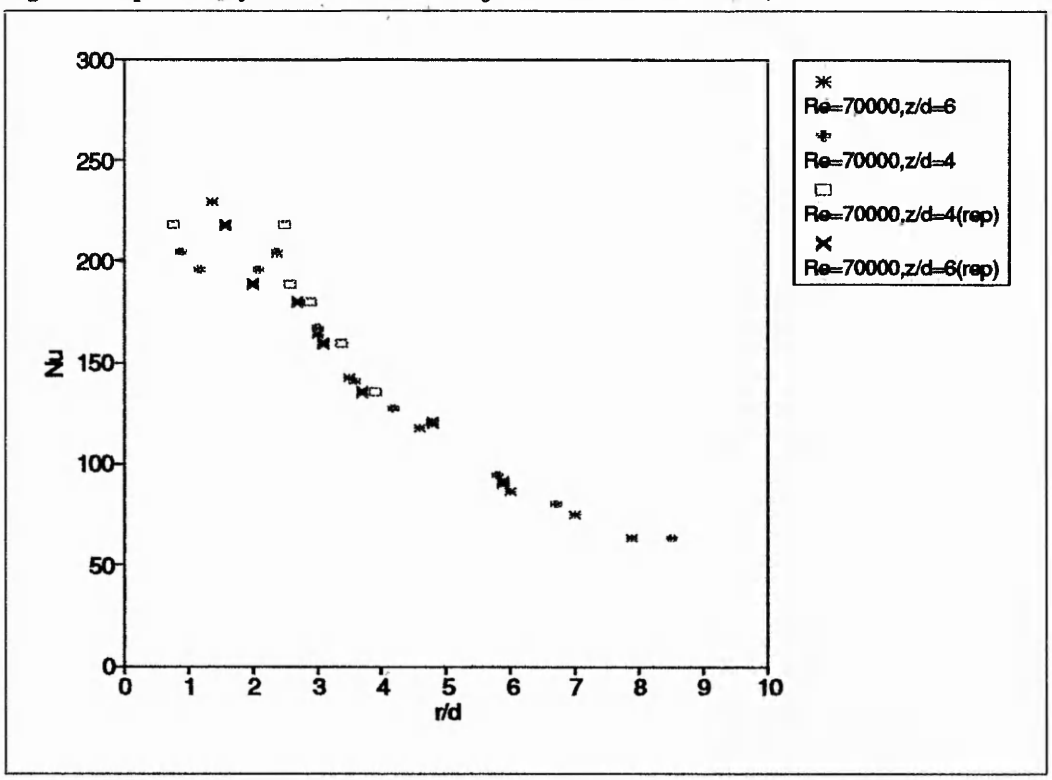

Fig 4.16 Nu versus r/d for Re=30 000→69 000 and z/d=2 for semi-confined jet

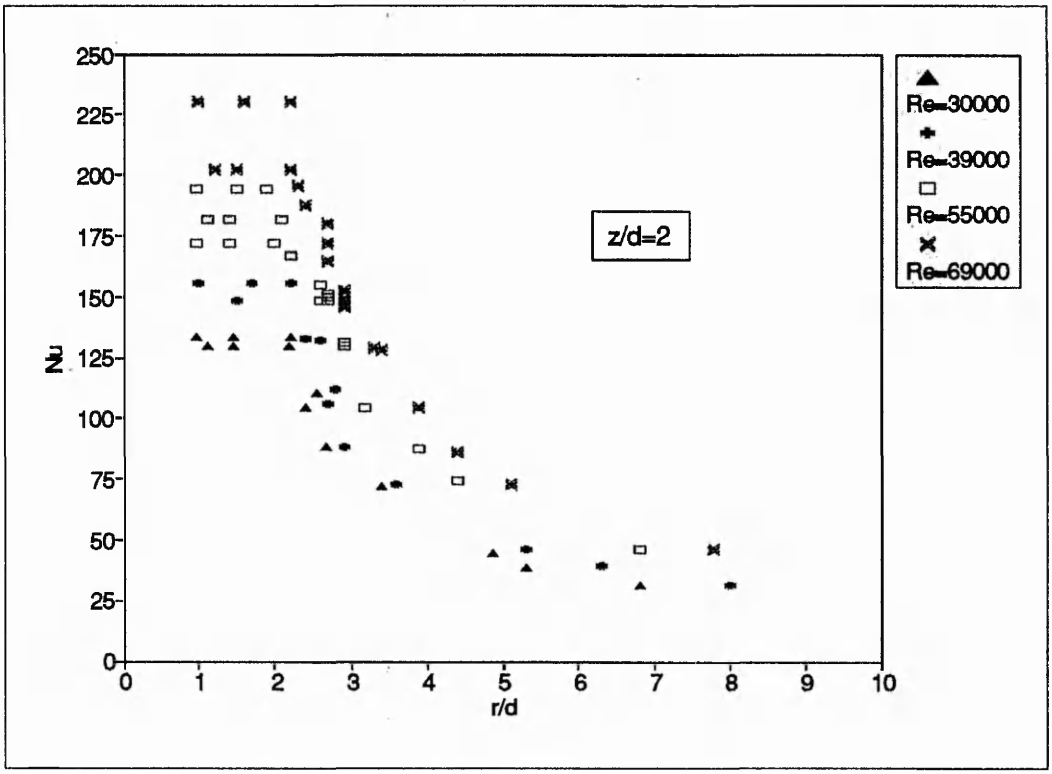

Fig 4.17 Nu versus r/d for Re=89 000→145 000 and z/d=2 for semi-confined jet

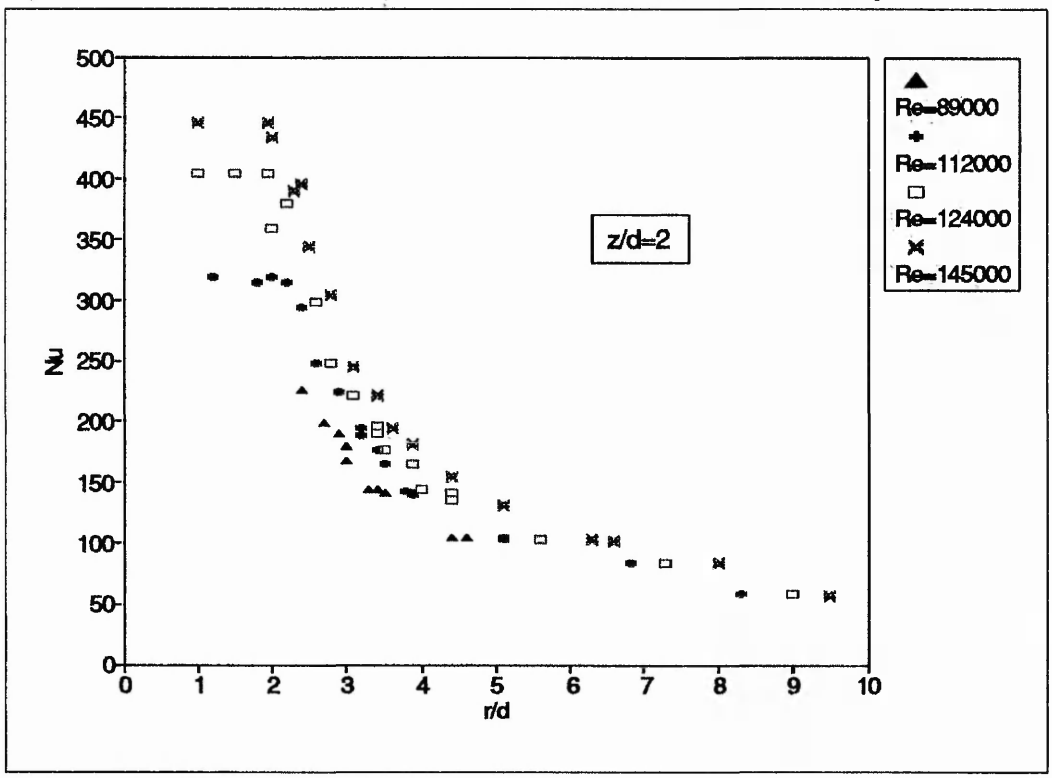

Fig 4.18 Nu versus r/d for Re=30 000→69000 and z/d=4 for semi-confined jet

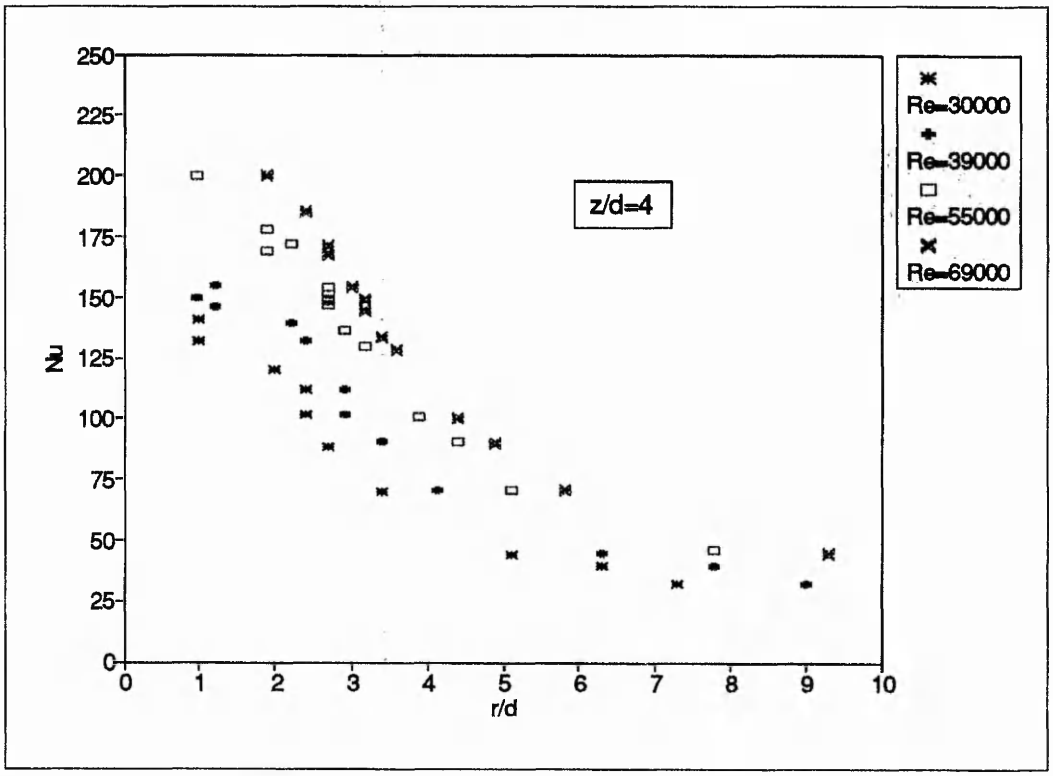

Fig 4.19 Nu versus r/d for Re=89 000→145 000 and z/d=4 for semi-confined jet

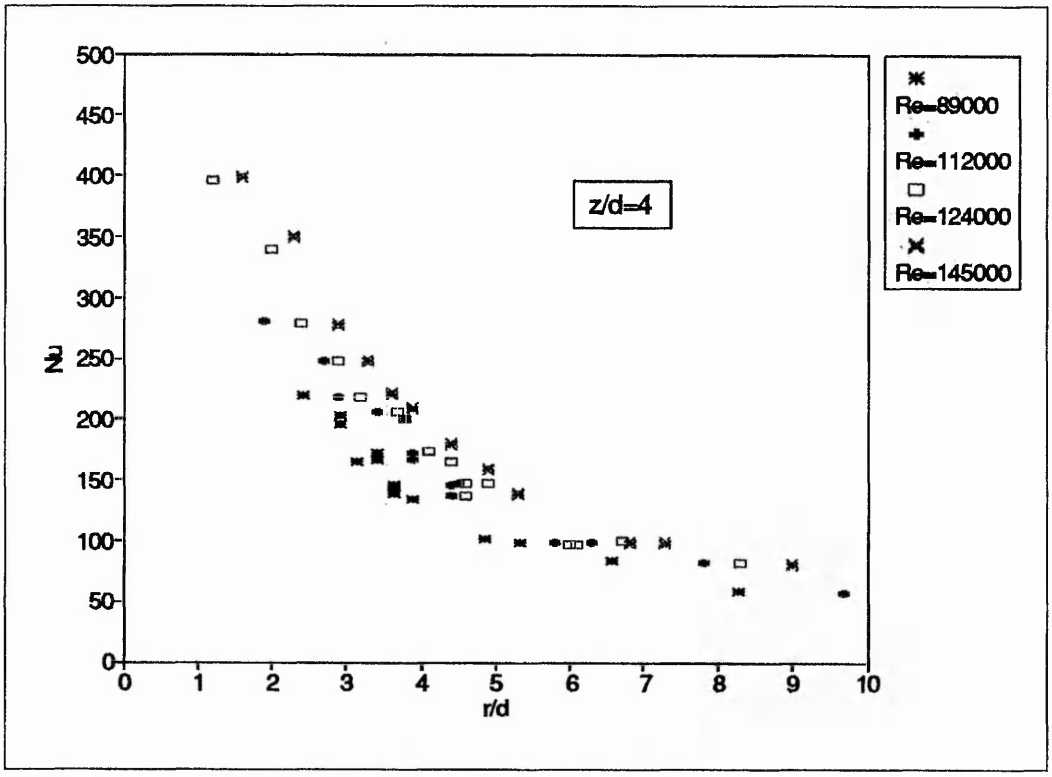

Fig 4.20 Nu versus r/d for Re=30 000→69000 and z/d=6 for semi-confined jet

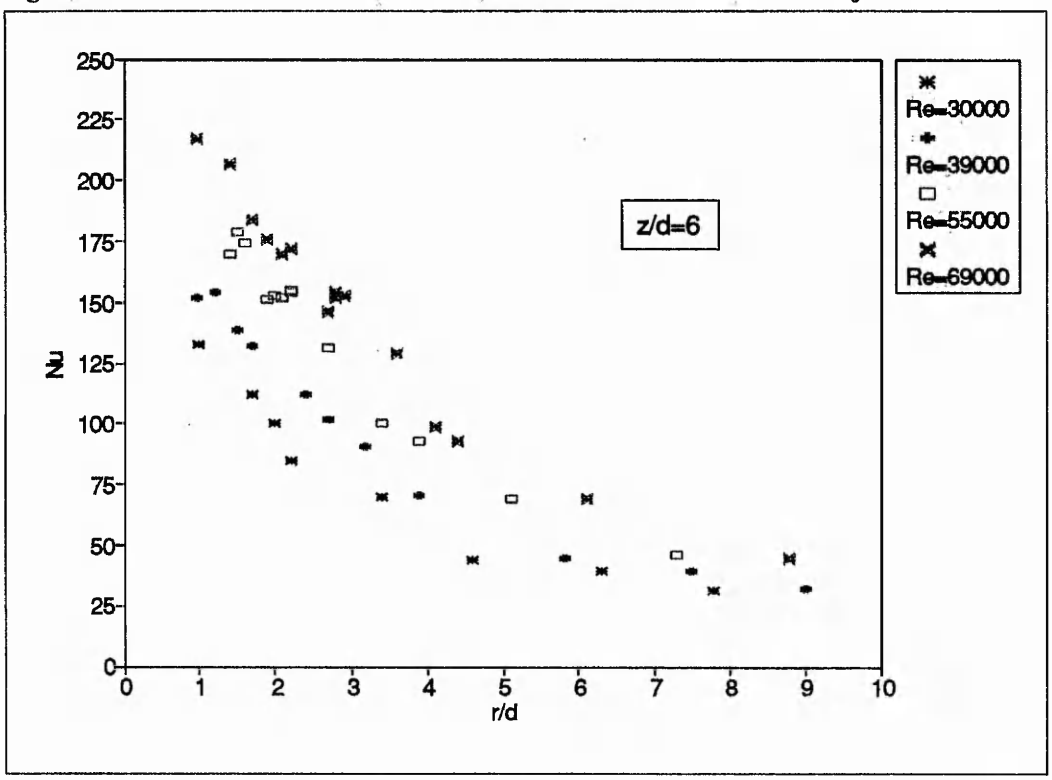

Fig 4.21 Nu versus r/d for Re=89 000→145 000 and z/d=6 for semi-confined jet

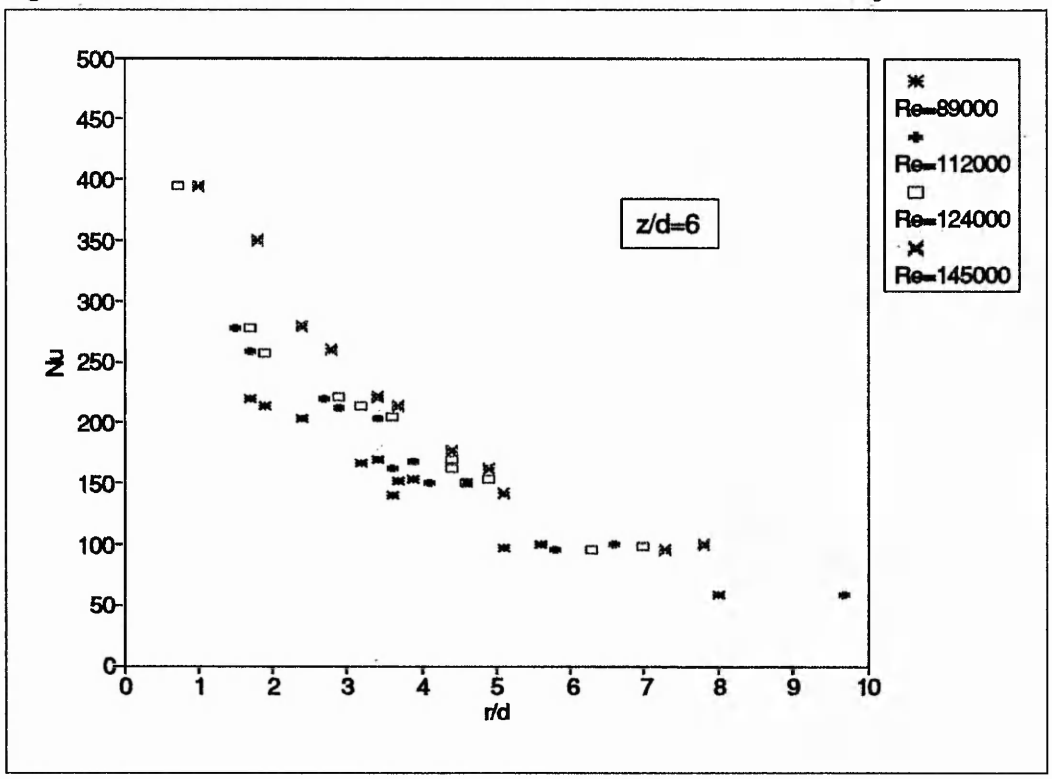

Fig 4.22 Nu versus r/d for z/d=2,4 and 6 and Re=30 000 for semi-confined jet

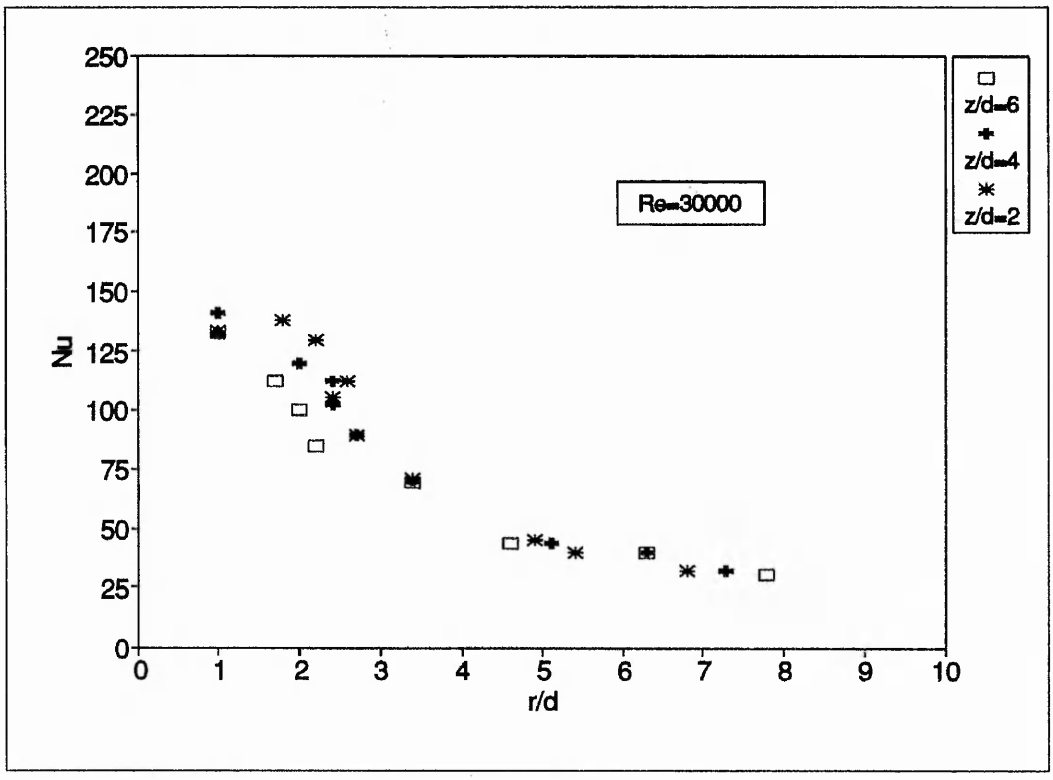

Fig 4.23 Nu versus r/d for z/d=2,4 and 6 and Re=39 000 for semi-confined jet

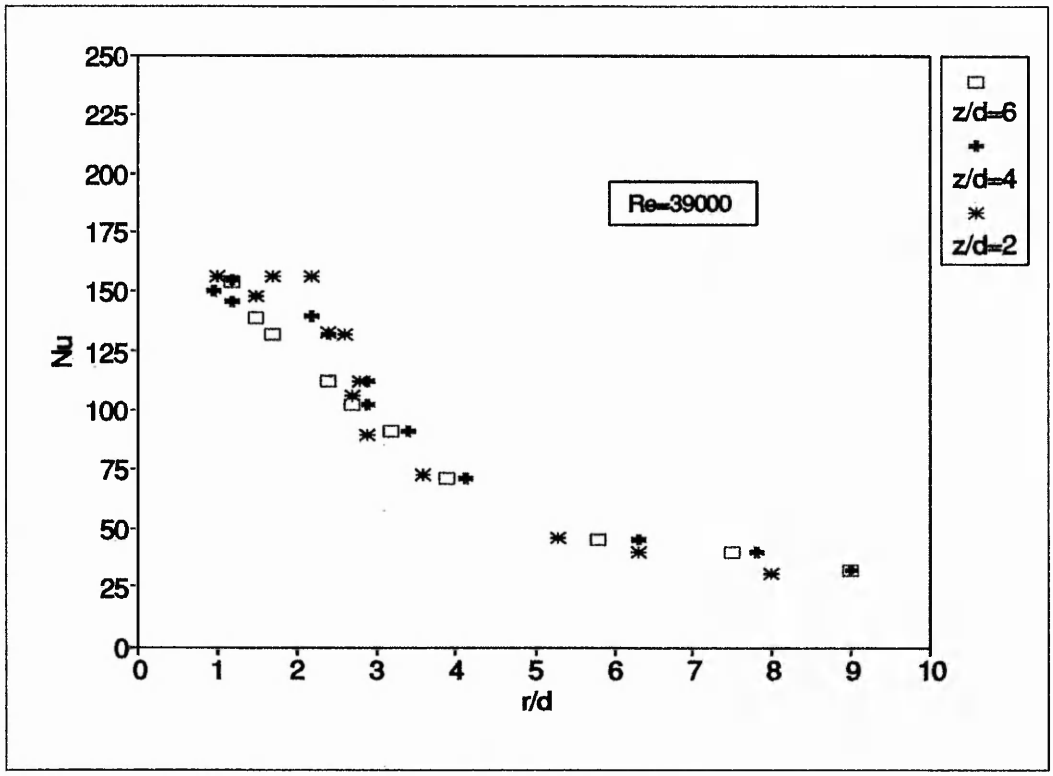

Fig 4.24 Nu versus r/d for z/d=2,4 and 6 and Re=55 000 for semi-confined jet

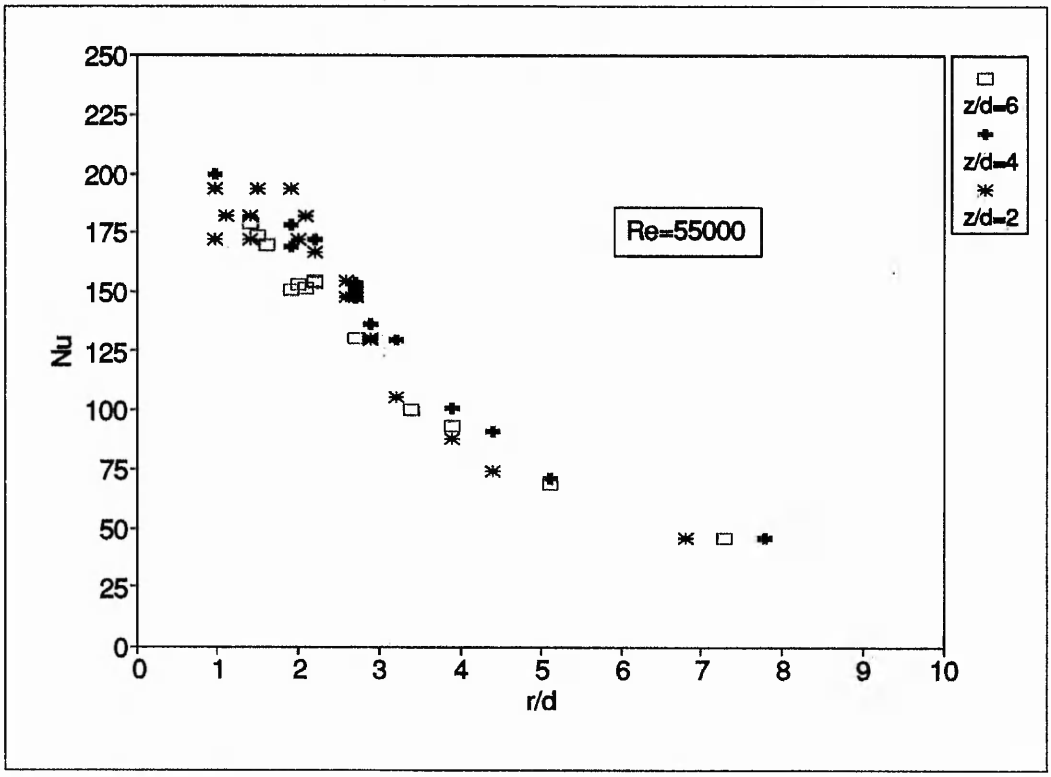

Fig 4.25 Nu versus r/d for z/d=2,4 and 6 and Re=69 000 for semi-confined jet

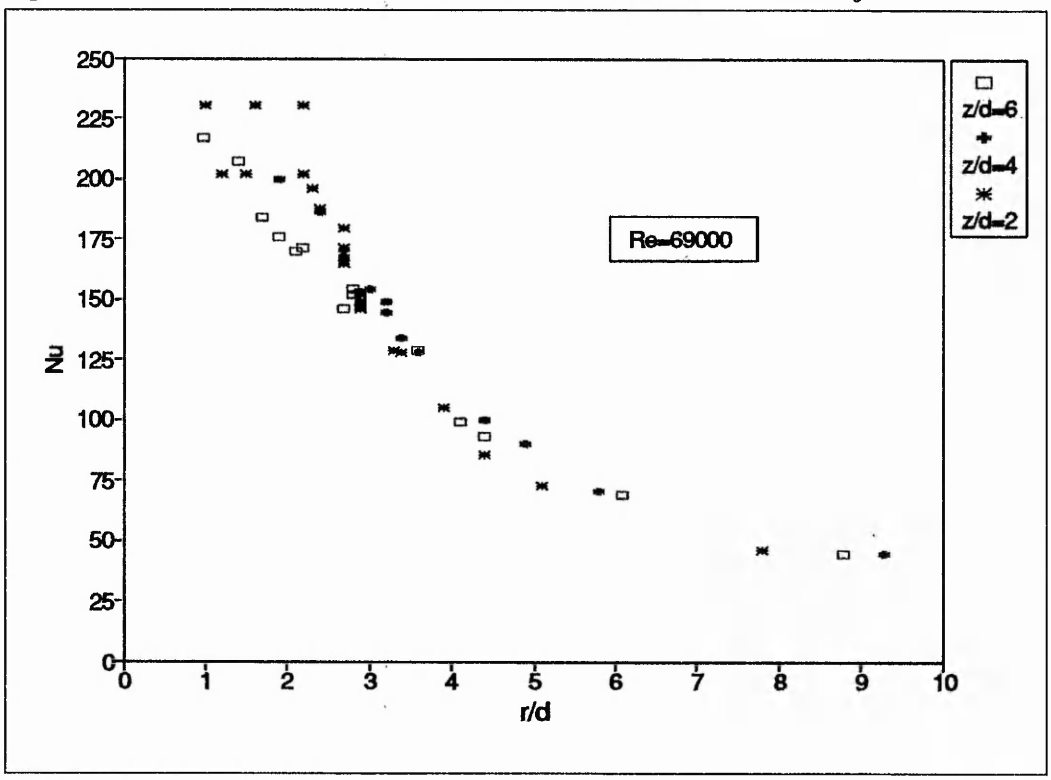

Fig 4.26 Nu versus r/d for z/d=2,4 and 6 and Re=89 000 for semi-confined jet

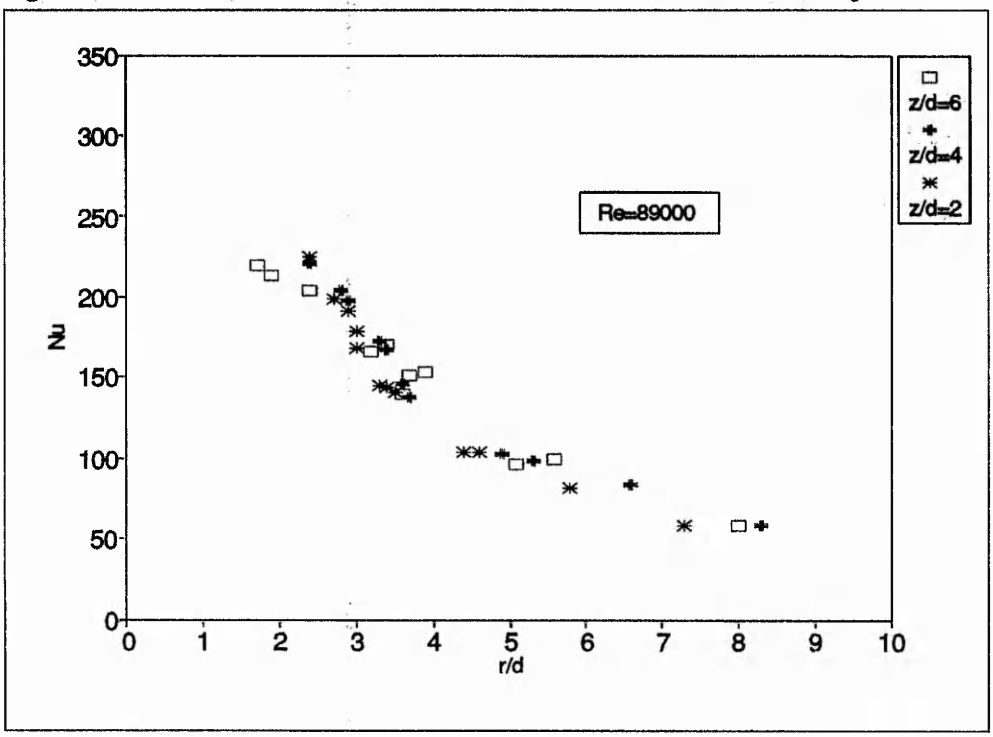

Fig 4.27 Nu versus r/d for z/d=2,4 and 6 and Re=112 000 for semi-confined jet

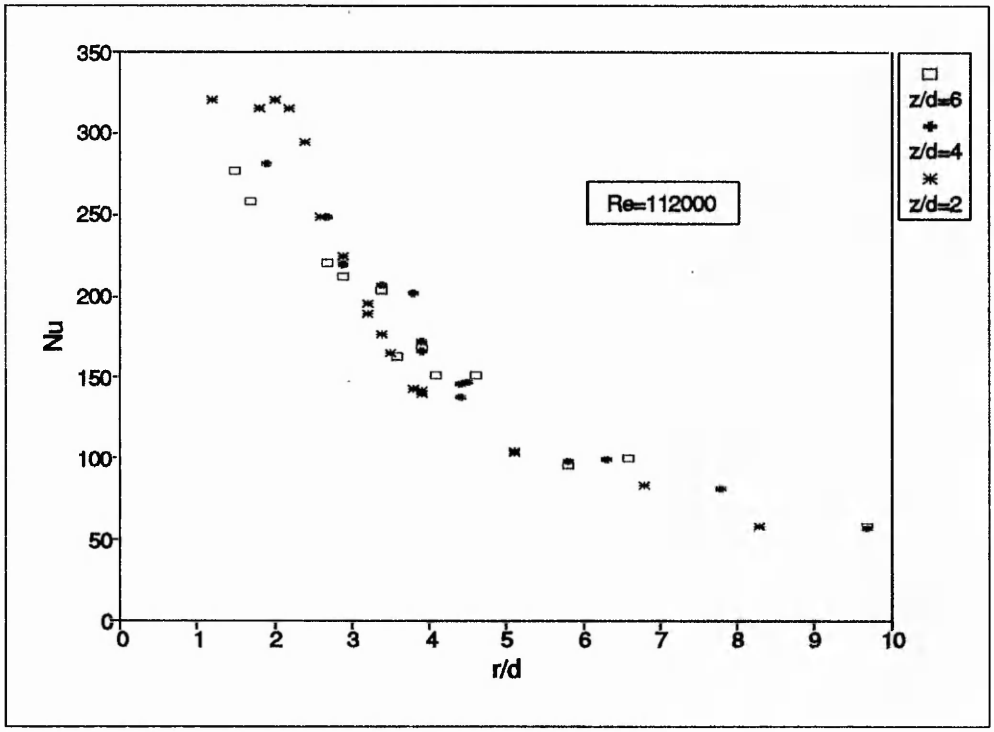

Fig 4.28 Nu versus r/d for z/d=2,4 and 6 and Re=124 000 for semi-confined jet

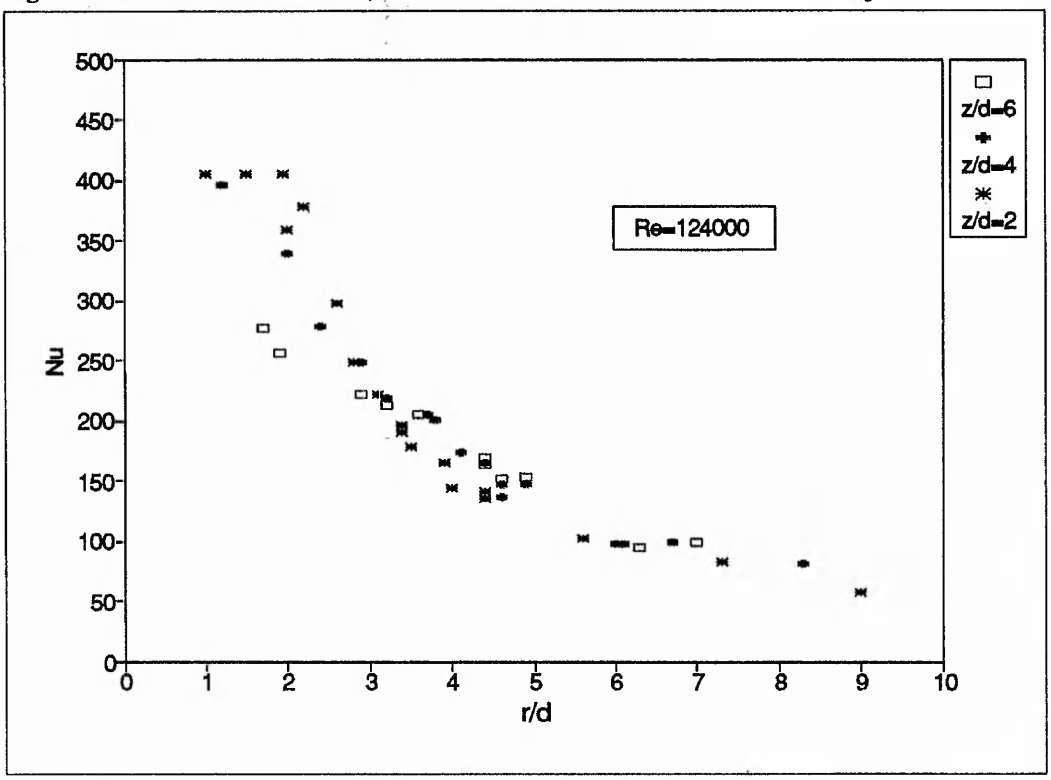

Fig 4.29 Nu versus r/d for z/d=2,4 and 6 and Re=145 000 for semi-confined jet

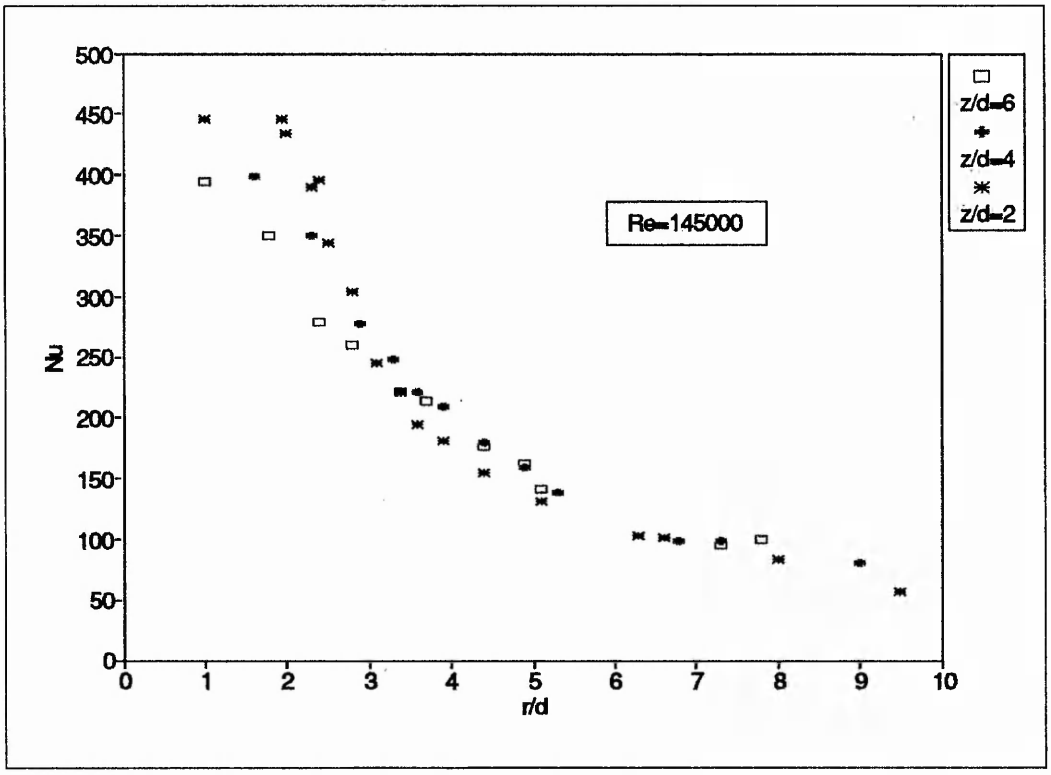

Fig 4.30 Repeatability test for semi-confined jet. Re=39 000 and 112 000. z/d=2

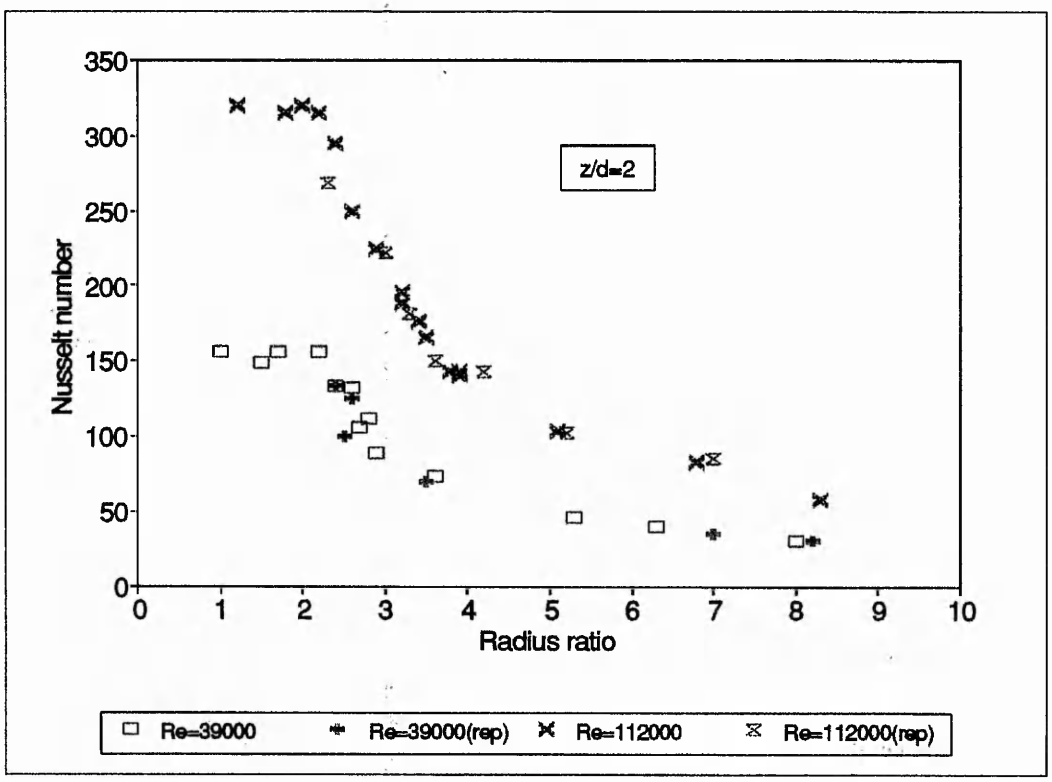

Fig 5.1 Standard residuals against fitted values for unconfined jet and 3<(r/d)<9

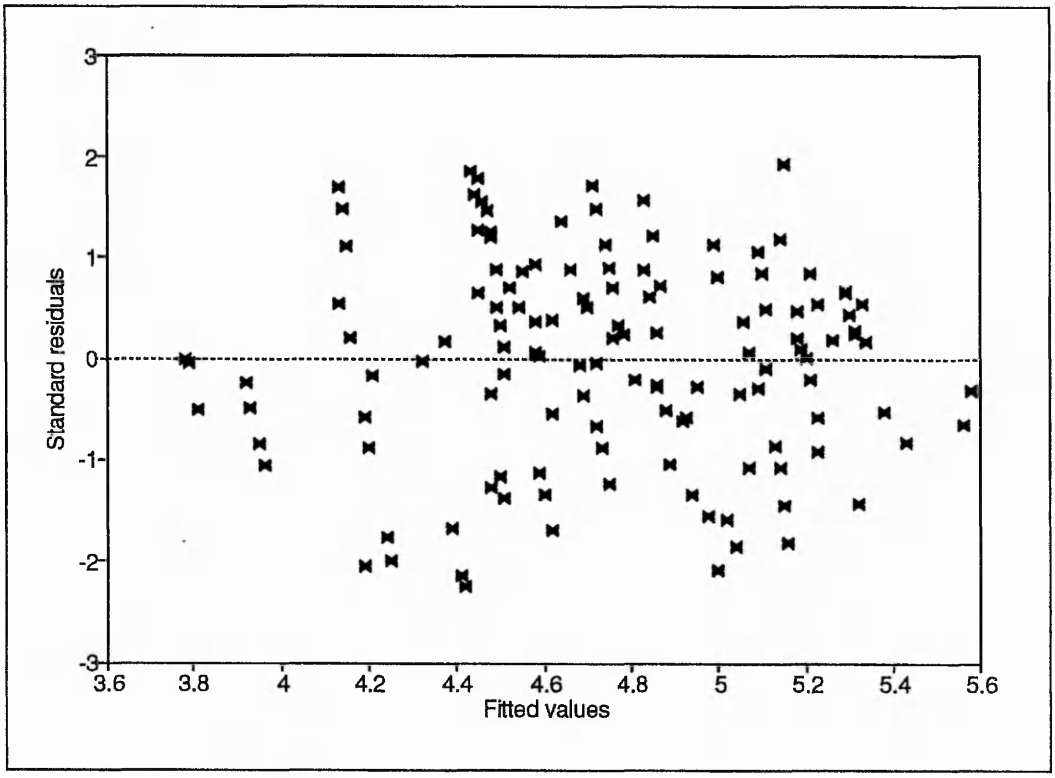

Fig 5.2 95 per cent prediction levels for unconfined jet and 3<(r/d)<9

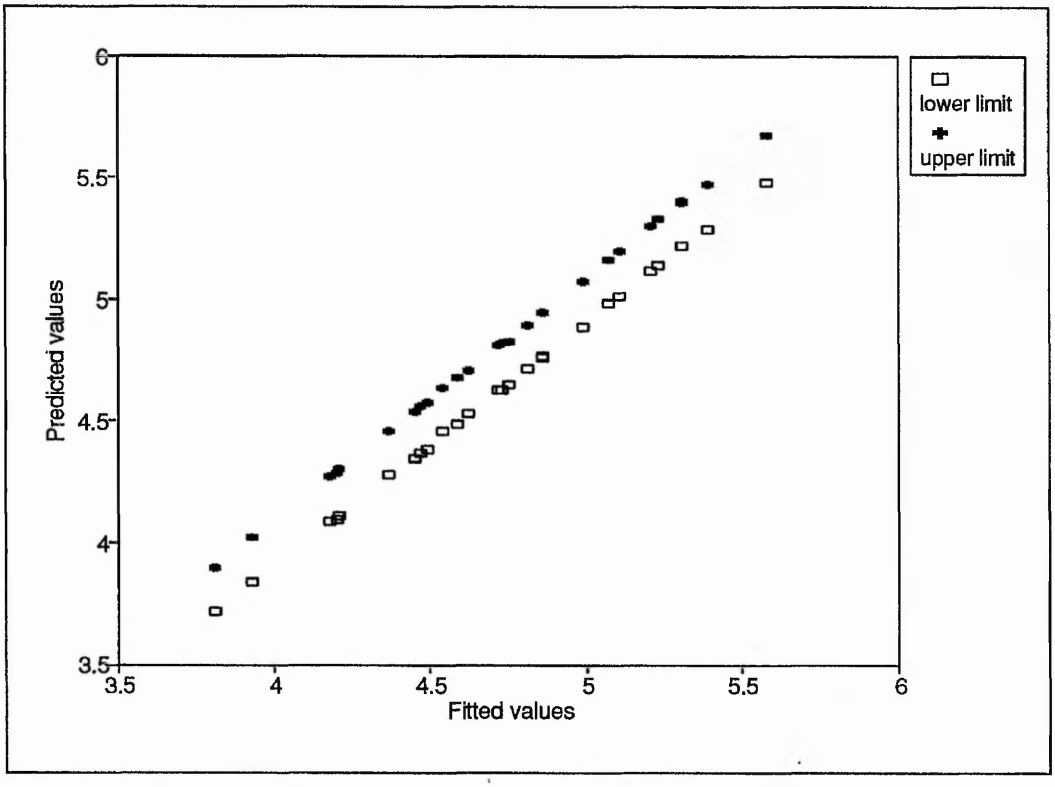

Fig 5.3 Fitted equation for unconfined jet and 3<(r/d)<9

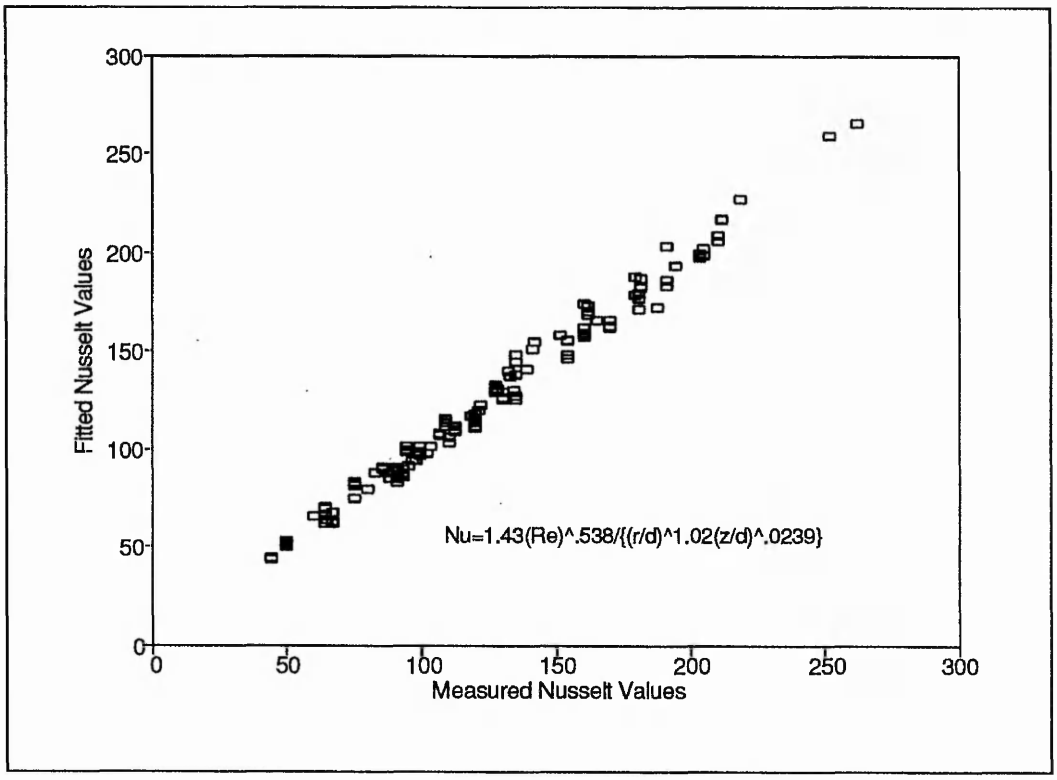

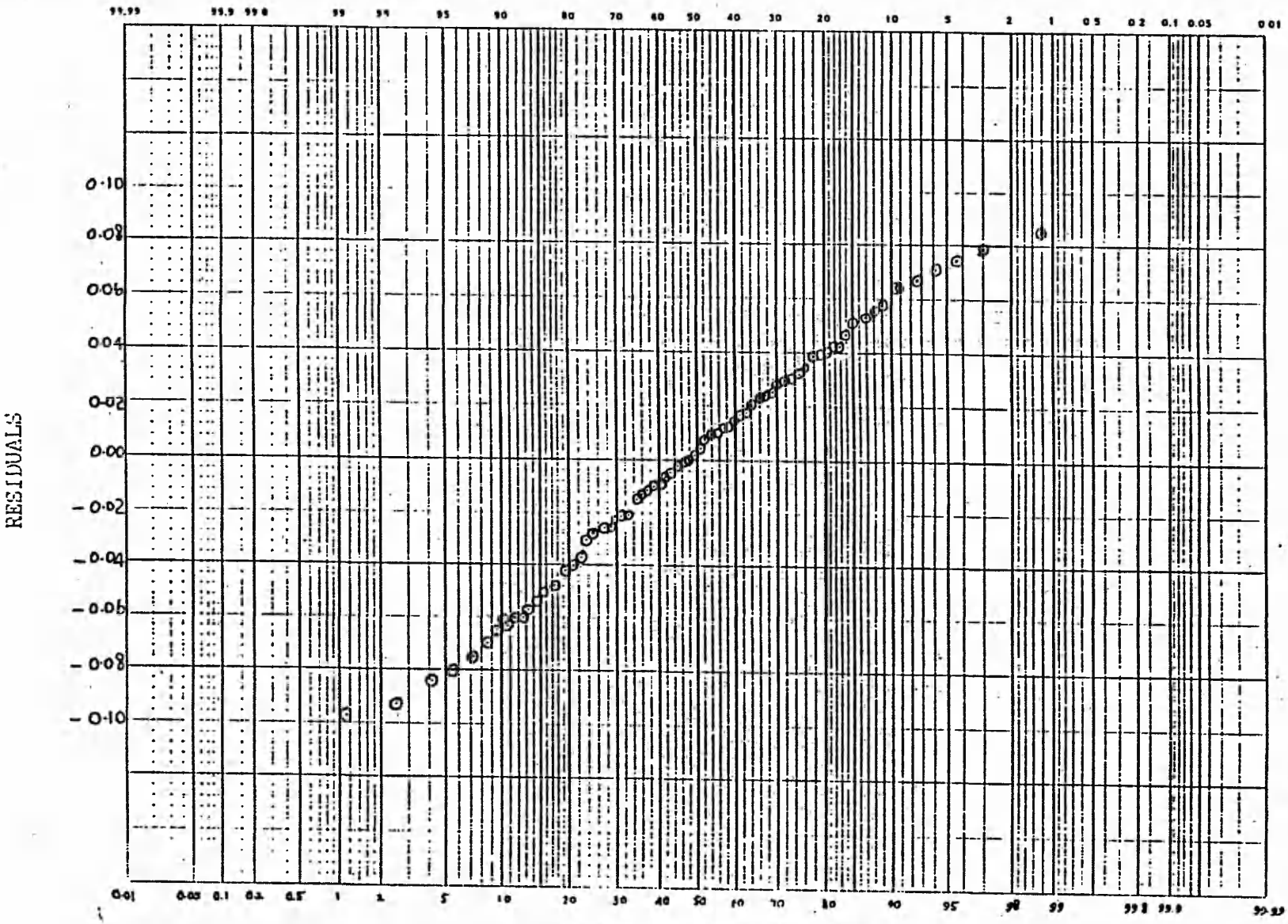

Fig 5.4 Distribution frequency of residuals for the unconfined jet, d_0/d_0

Fig 5.5 Standard residuals against fitted values for semi-confined jet and 2.5<(r/d)<9

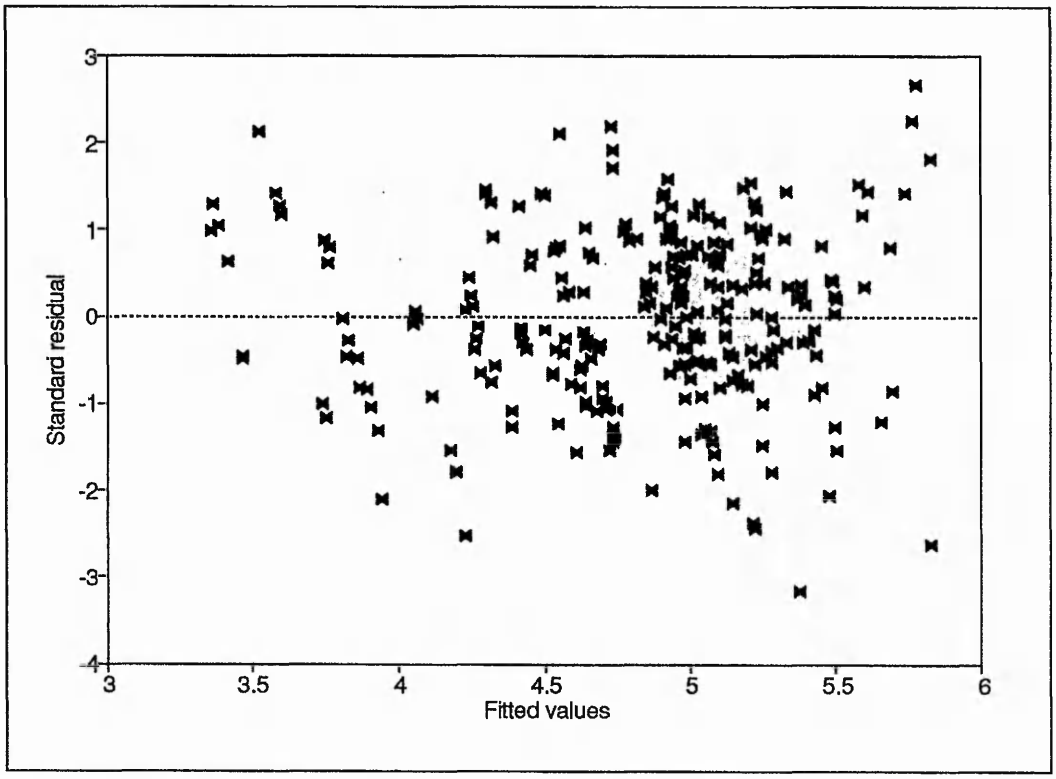

Fig 5.6 95 per cent prediction levels for semi-confined jet and 2.5<(r/d)<9

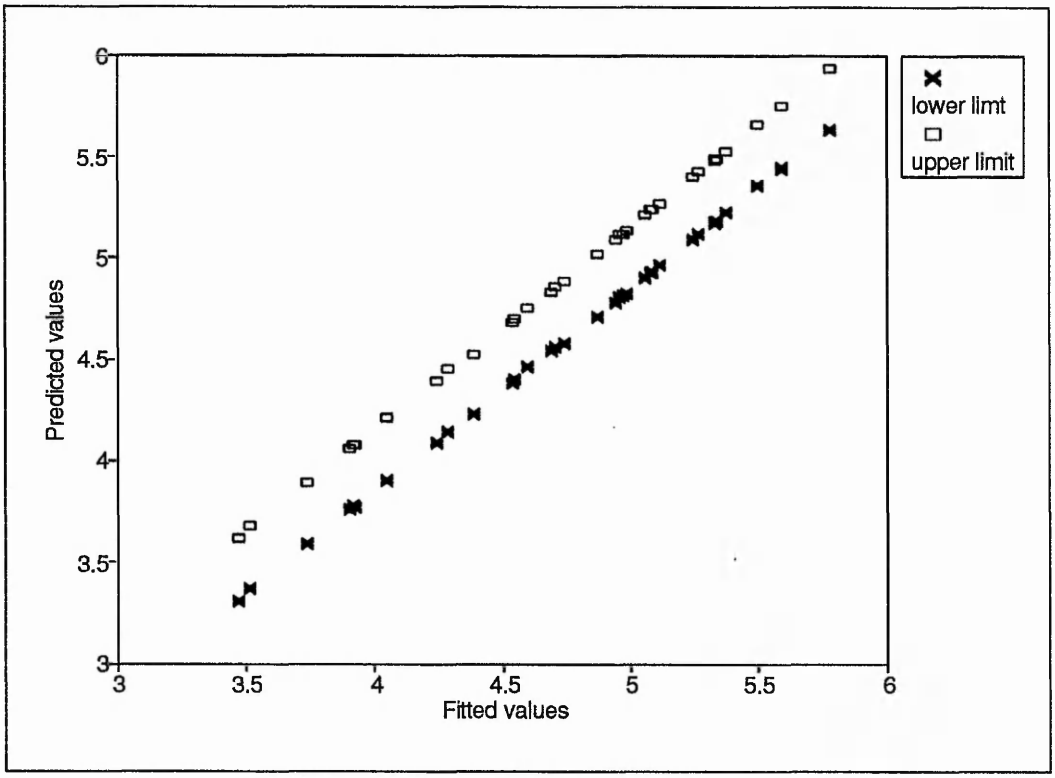

Fig. 5.7 Fitted equation for semi-confined jet and 2.5<(r/d)<9

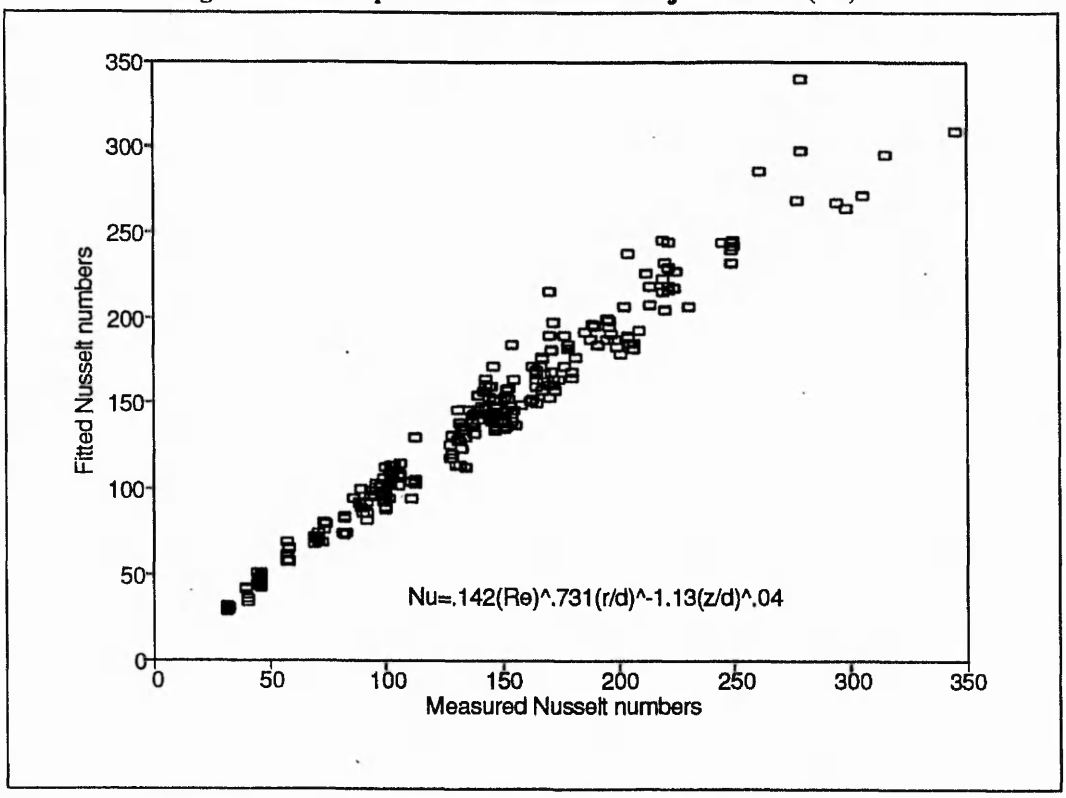

Fig 6.1 Non-dimensional heat transfer for z/d=2,4 and 6 and 3≤r/d≤9 for unconfined jet

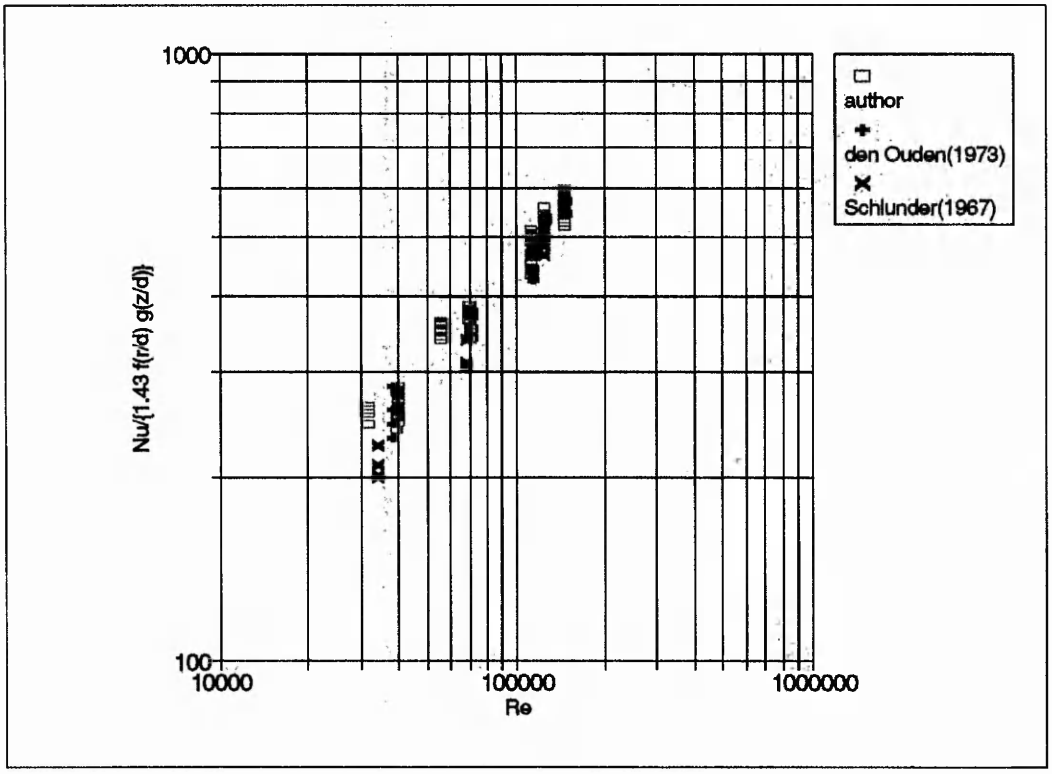

$$Nu=1.43(Re)^{0.538}(r/d)^{-1.02}(z/d)^{-0.0239}$$

Fig 6.2 Average Nu versus Re for the unconfined jet compared with Sclunder et al,1967

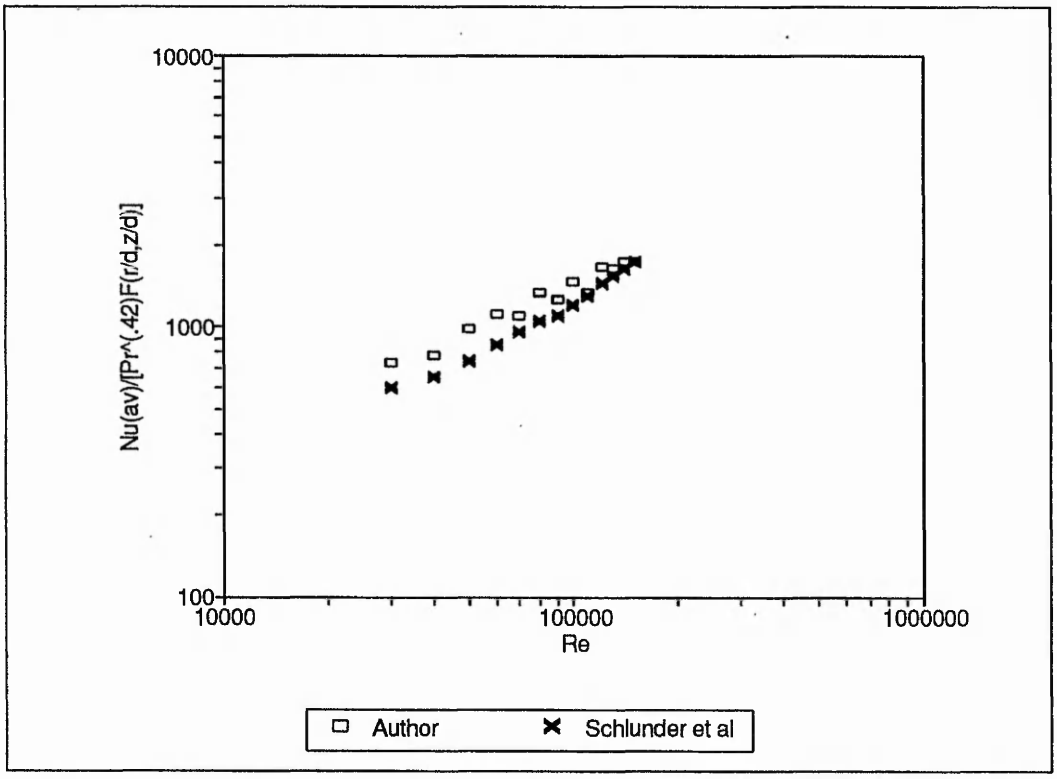

Fig 6.3 Nu versus r/d for z/d=2 and Re=30 000 compared with Obot(1981) for the semi-confined jet

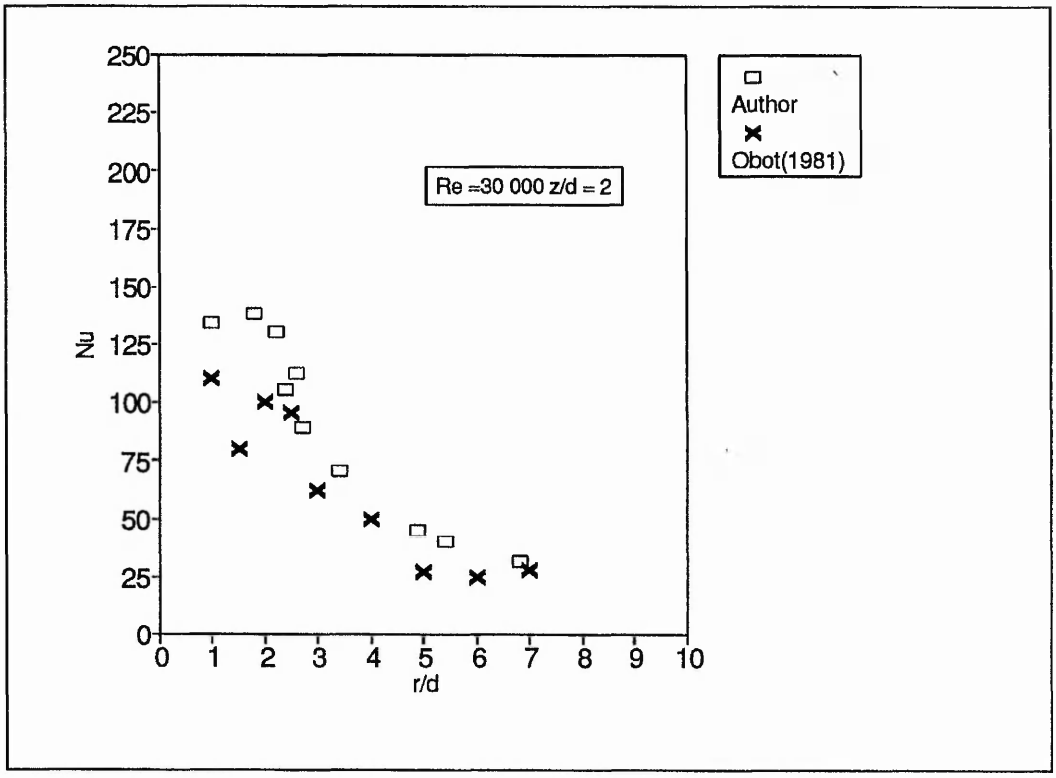

Fig 6.4 Nu versus r/d for z/d=2 and Re=39 000 compared with Obot(1981) for the semi-confined jet

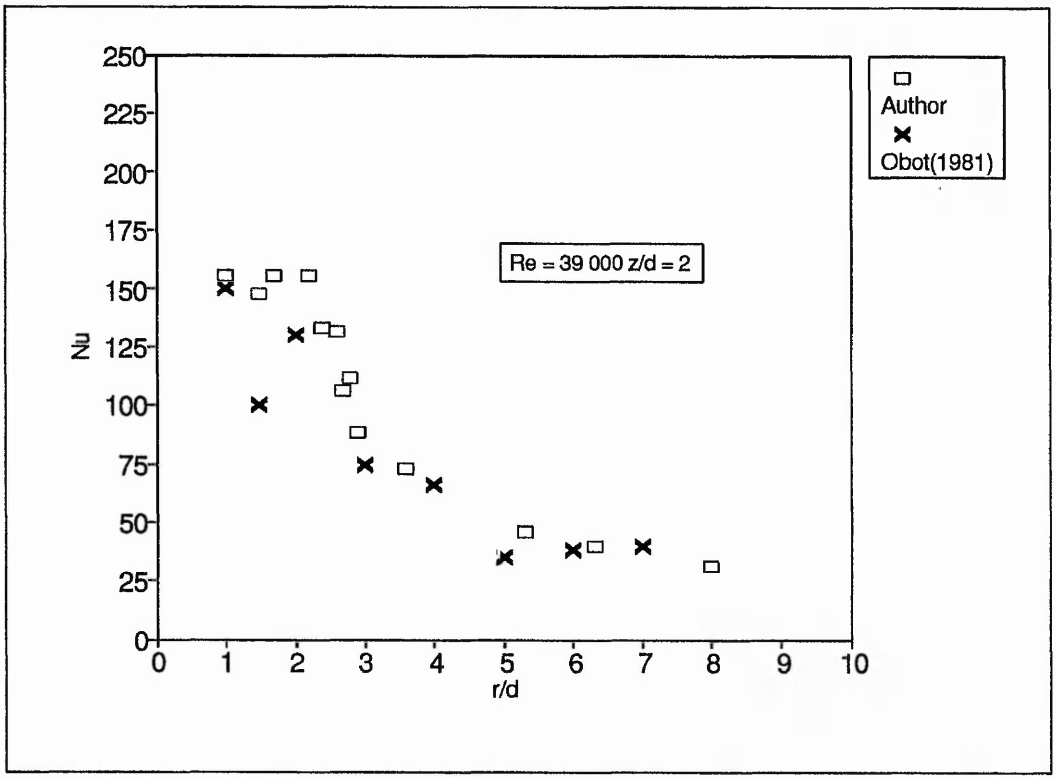

Fig 6.5 Nu versus r/d for z/d=2,4 and 6 and Re=39 000 for unconfined and semi-confined jets

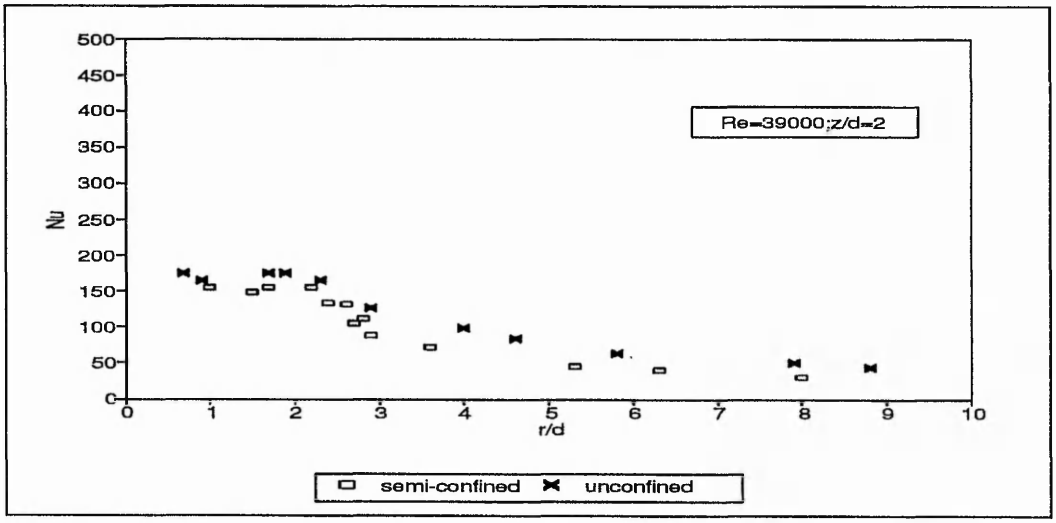

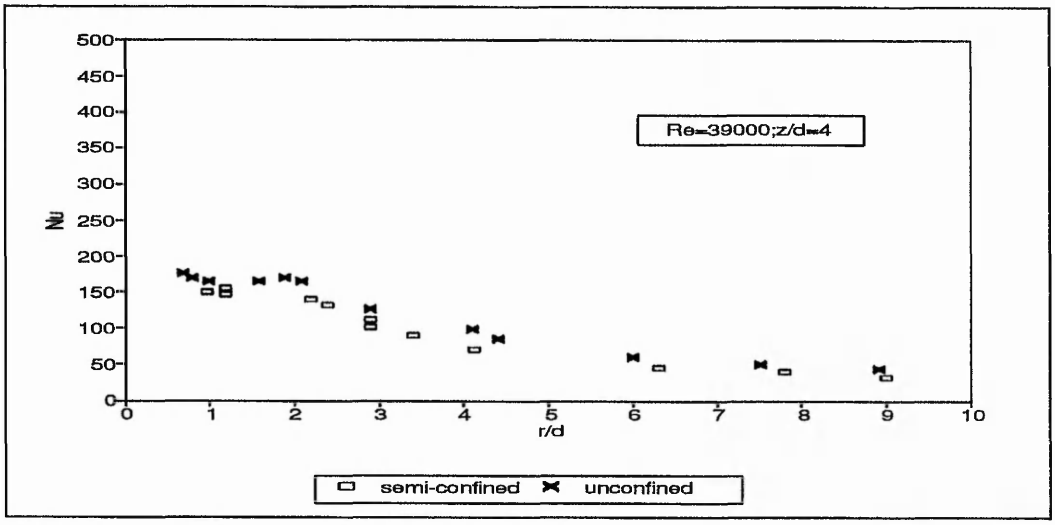

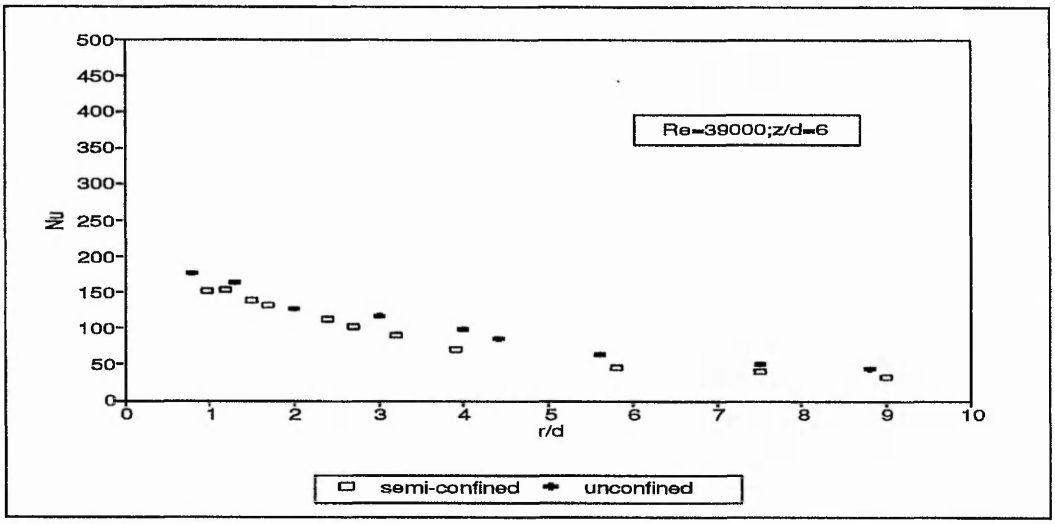

Fig 6.6 Nu versus r/d for z/d=2,4 and 6 and Re=55 000 for unconfined and semi-confined jets

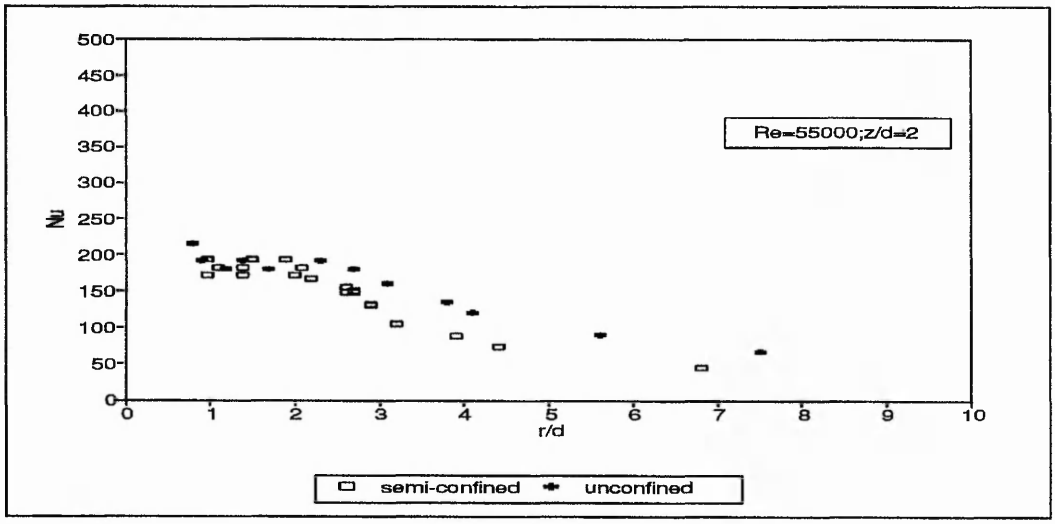

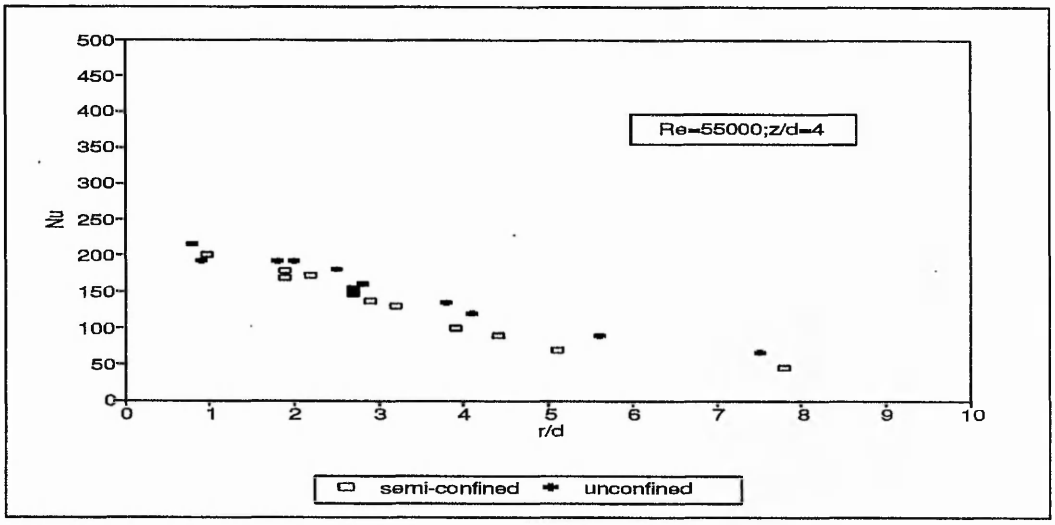

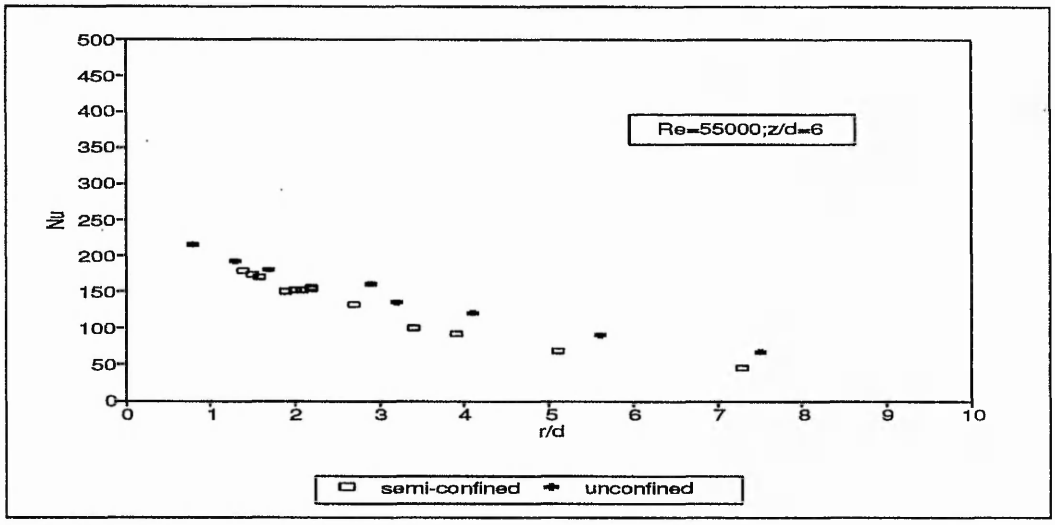

Fig 6.7 Nu versus r/d for z/d=2,4 and 6 and Re=69 000 for unconfined and semi-confined jets

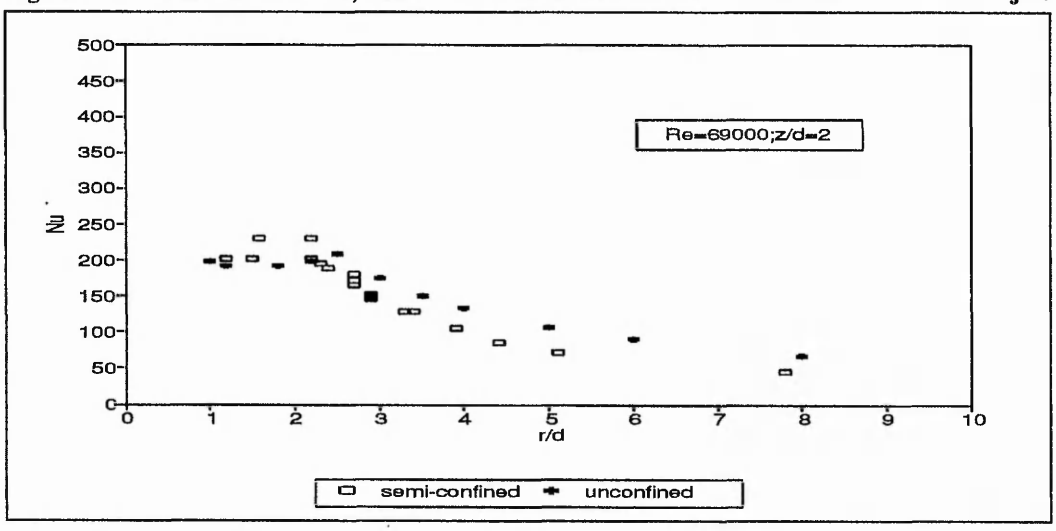

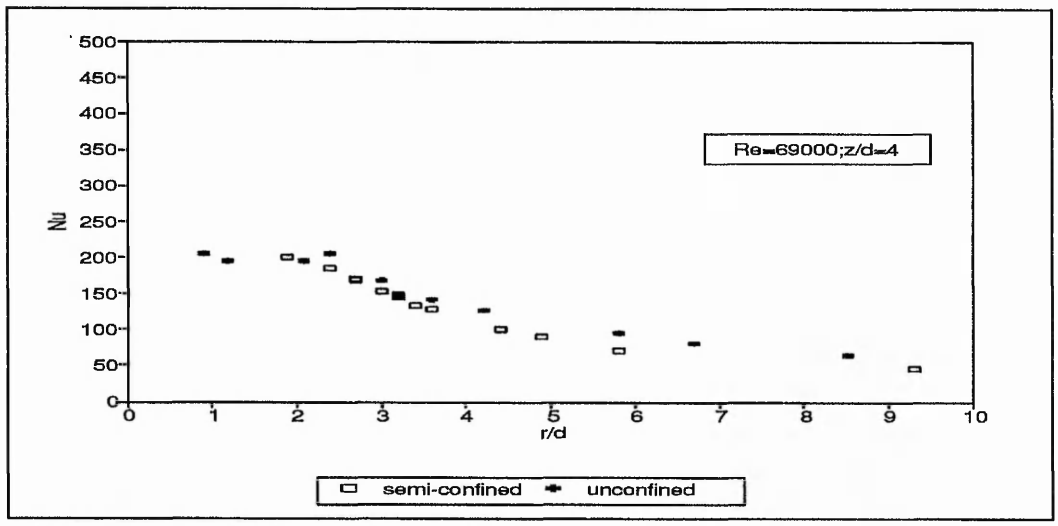

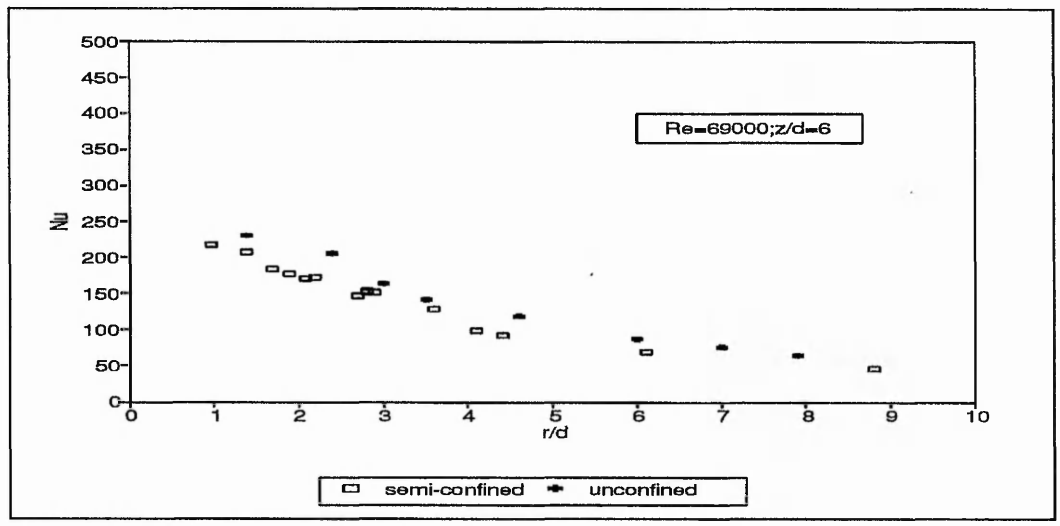

Fig 6.8 Nu versus r/d for z/d=2,4 and 6 and Re=112 000 for unconfined and semi-confined jets

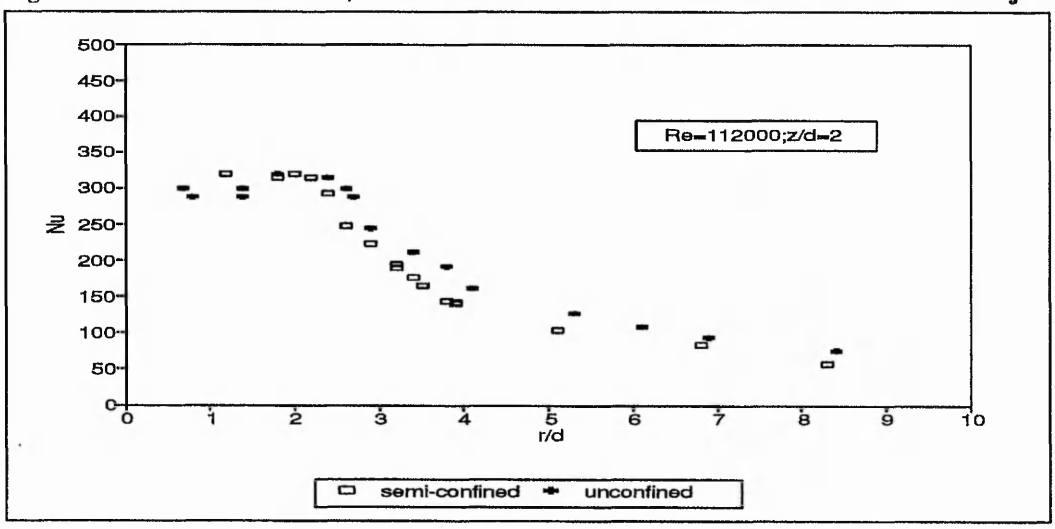

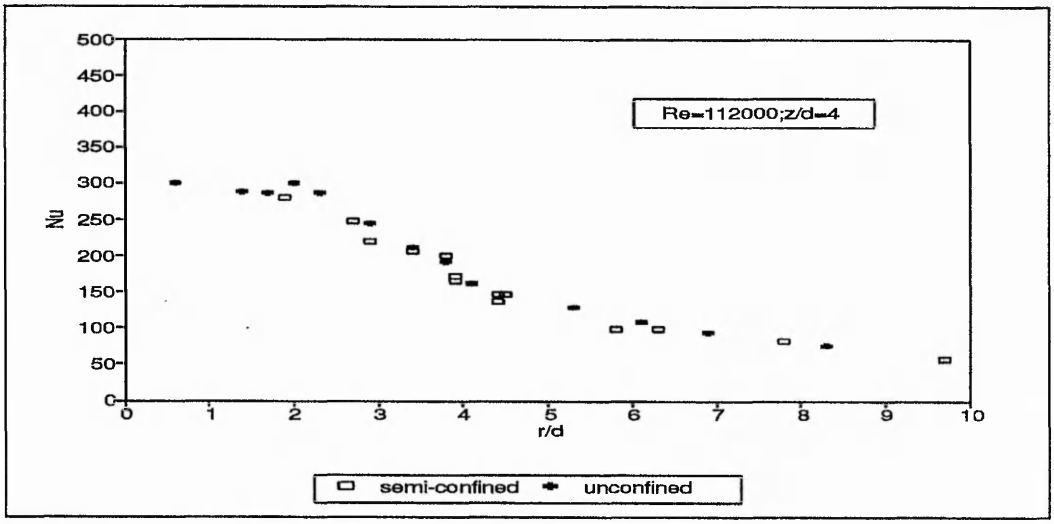

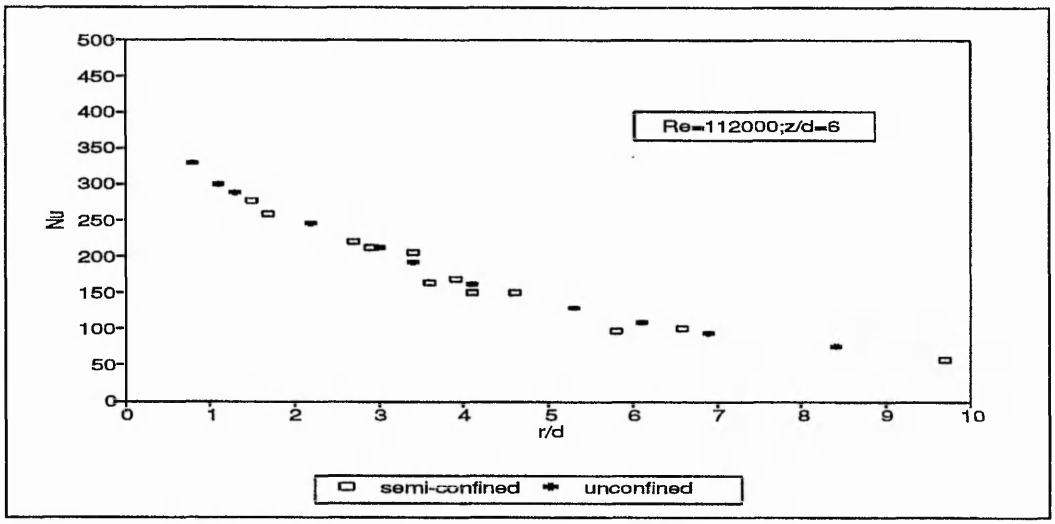

Fig 6.9 Nu versus r/d for z/d=2,4 and 6 and Re=145 000 for unconfined and semi-confined jets

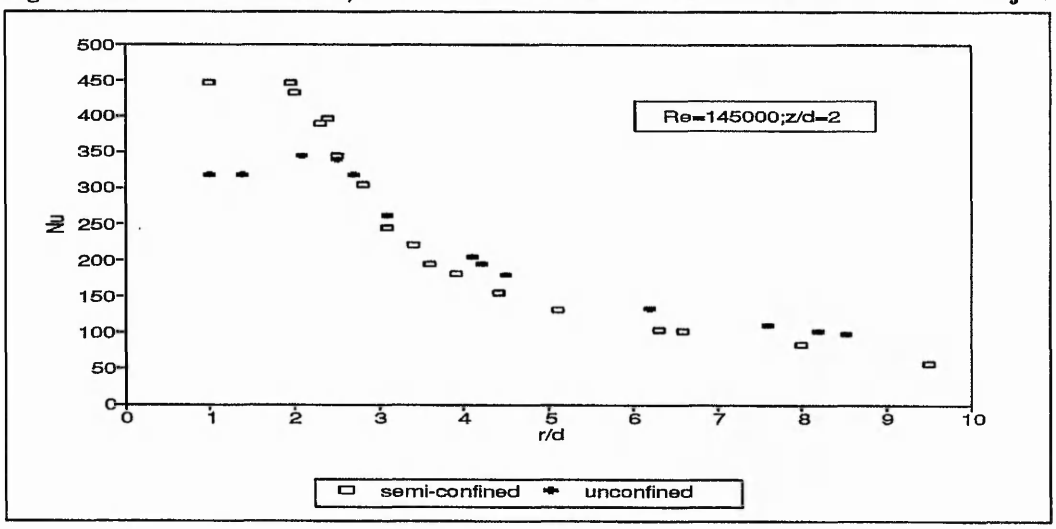

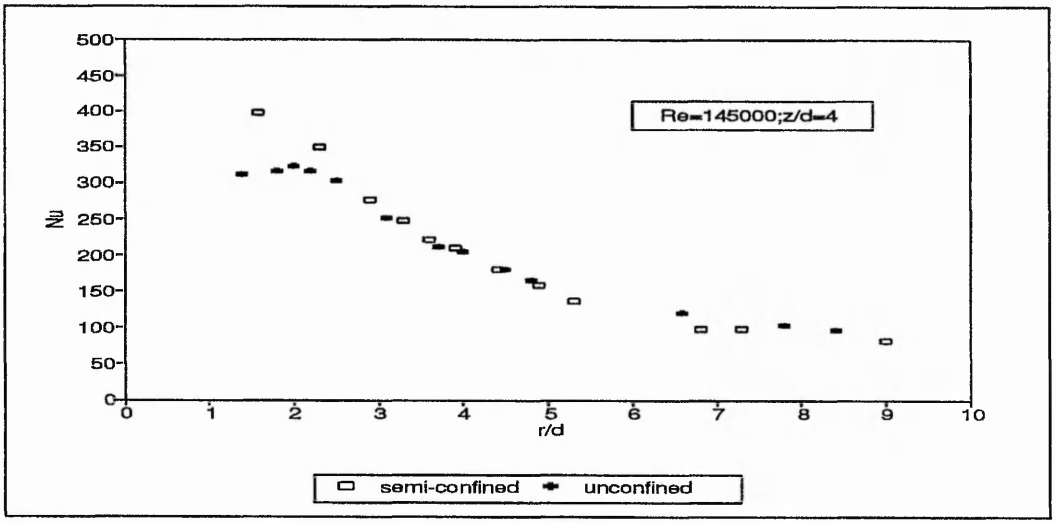

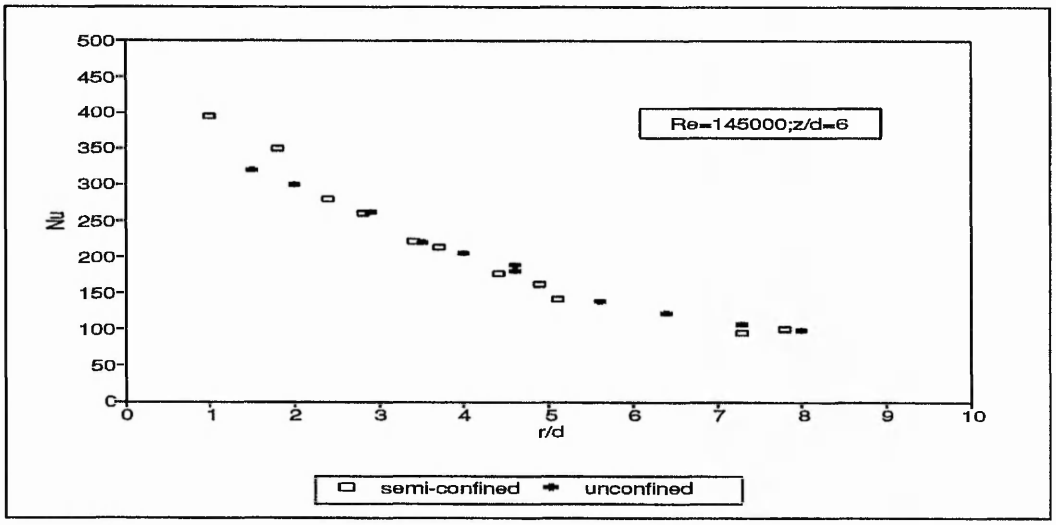

Fig 6.10 Mean Nu versus Re for 2.5≤r/d≤9 and z/d=2 for unconfined and semi-confined jets

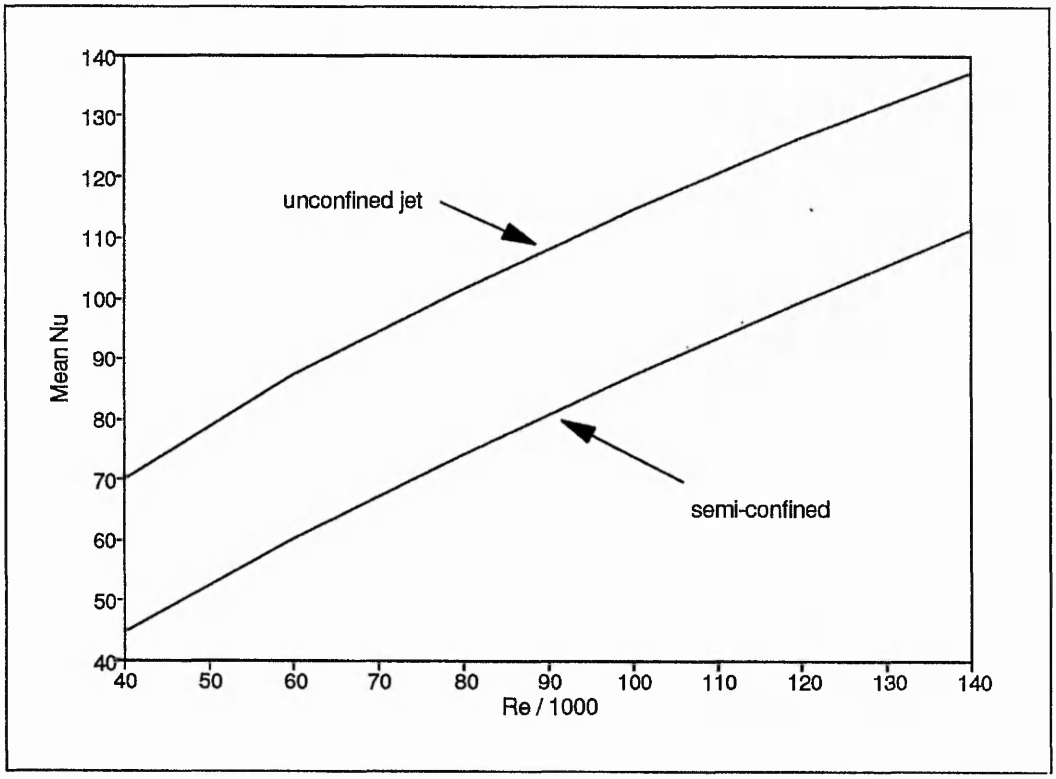

Fig 6.11 Nu differences versus Re for r/d=3 and z/d =2,4 and 6 for unconfined and semi-confined jets

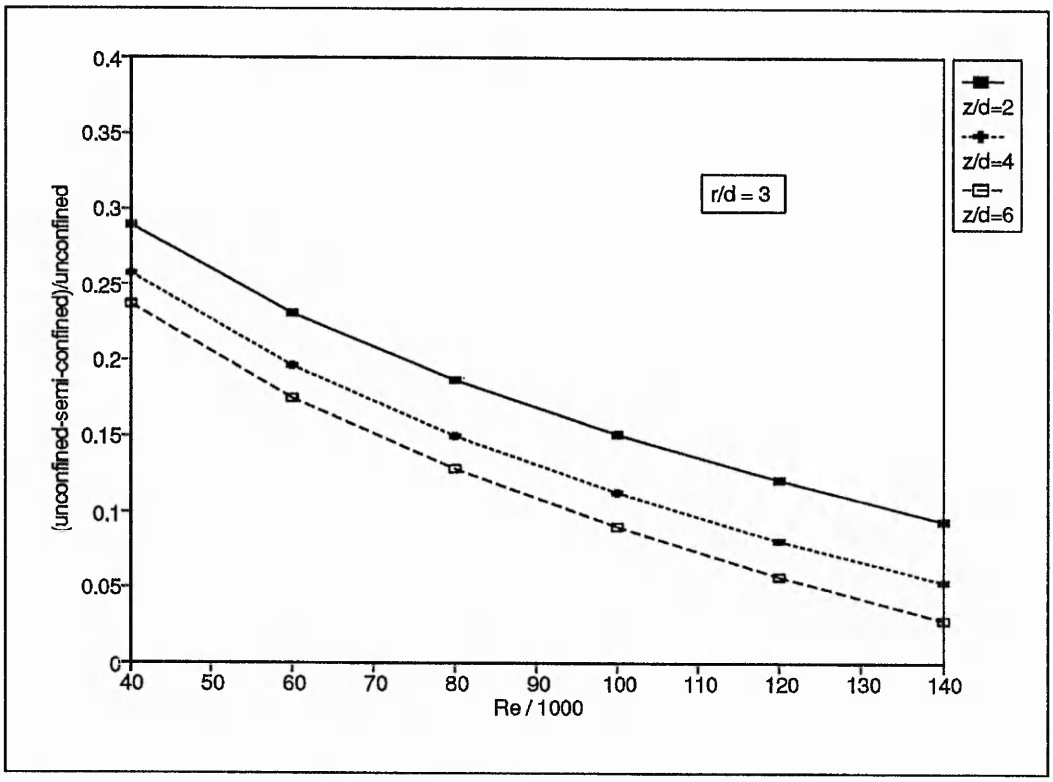

Fig 6.12 Nu differences versus Re for r/d=5 and z/d =2,4 and 6 for unconfined and semi-confined jets

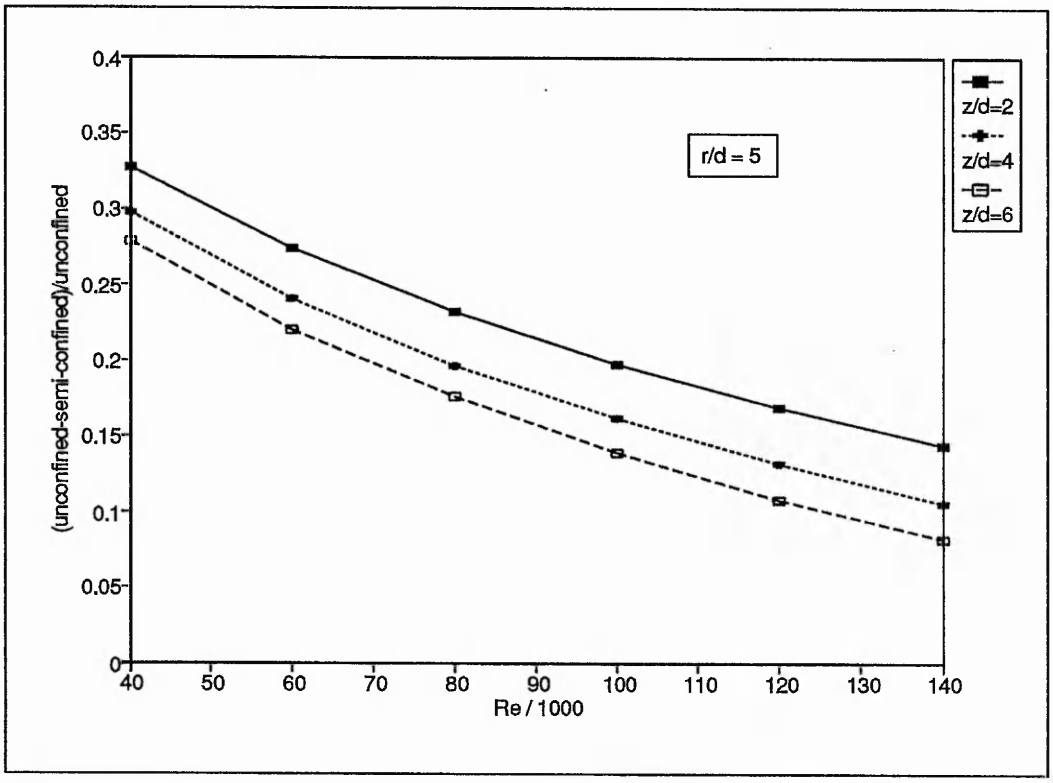

Fig 6.13 Nu differences versus Re for r/d=7 and z/d =2,4 and 6 for unconfined and semi-confined jets

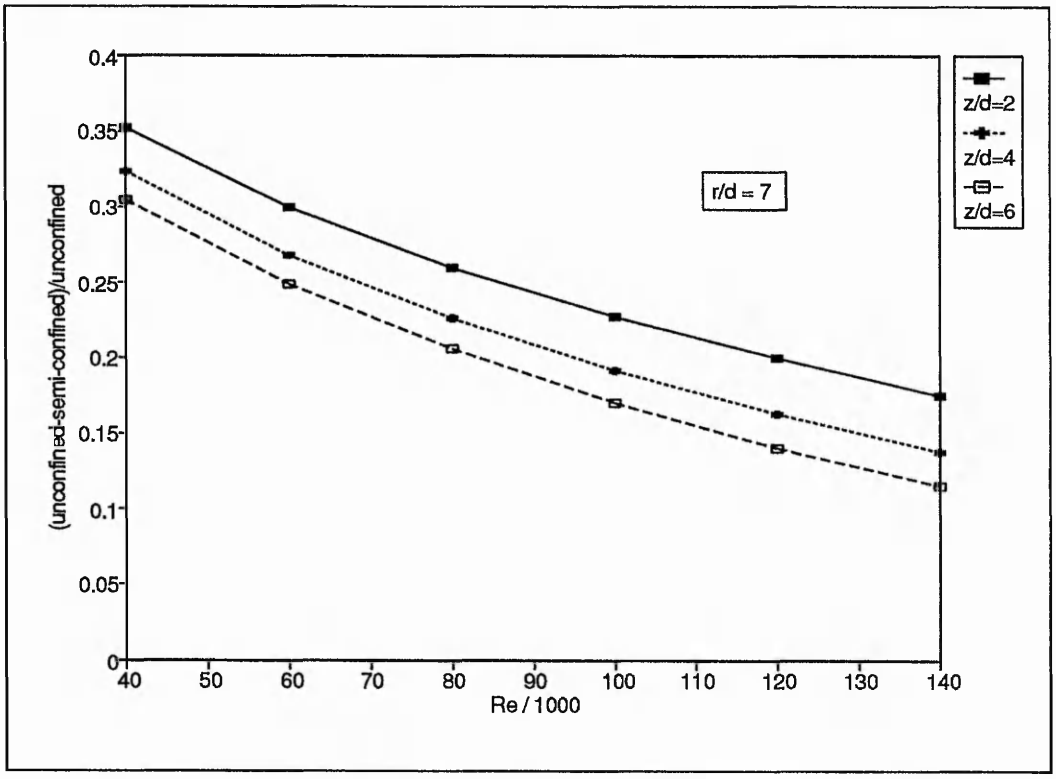

Fig 6.14 Nu differences versus Re for r/d=9 and z/d =2,4 and 6 for unconfined and semi-confined jets

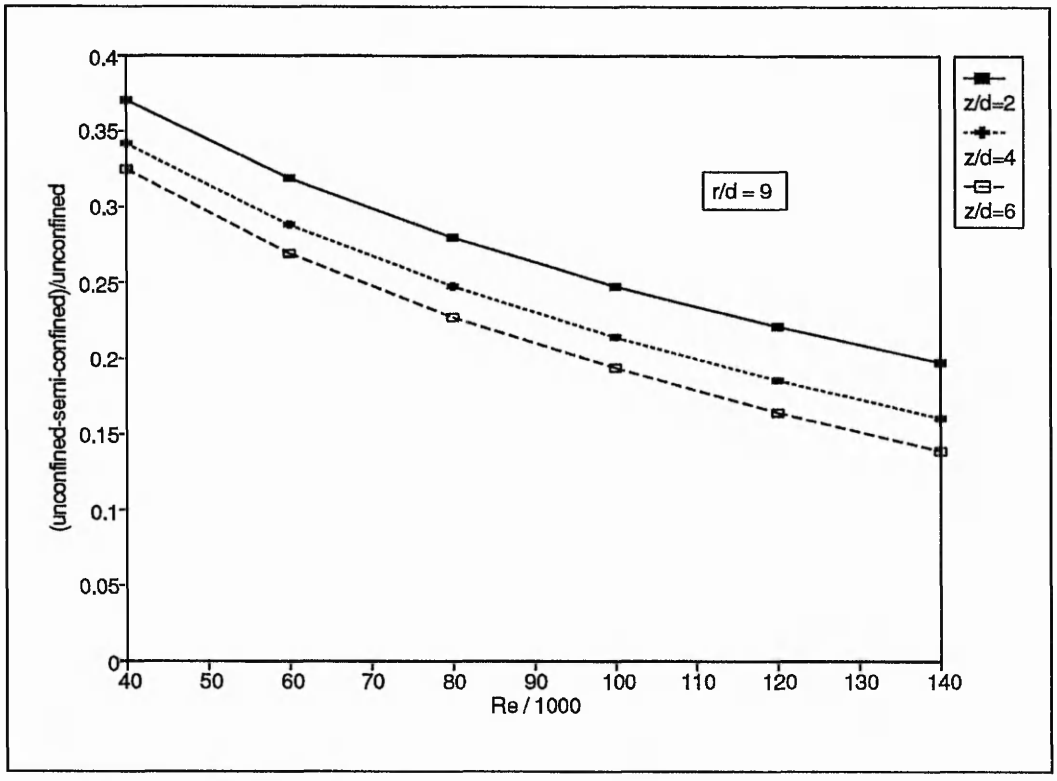

Fig 6.15 Nu differences versus r/d for z/d=2 and Re=40 000, 70 000, 110 000 and 140 000 for unconfined and semi-confined jets

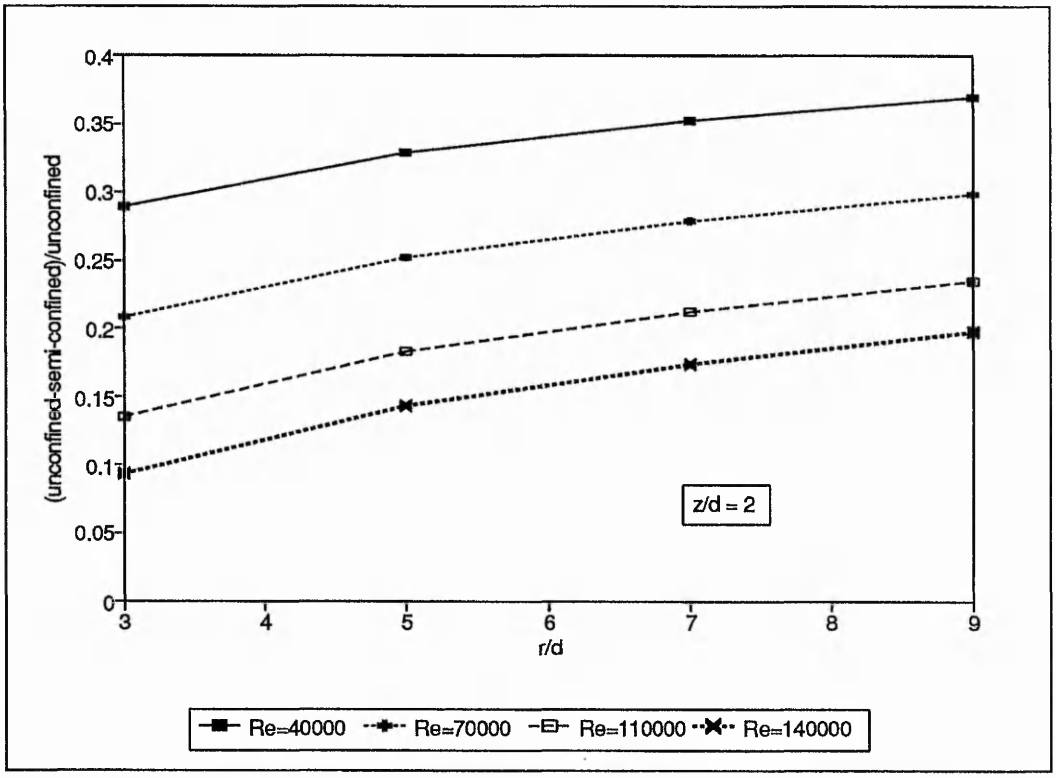

Fig 6.16 Nu differences versus r/d for z/d=4 and Re=40 000, 70 000, 110 000 and 140 000 for unconfined and semi-confined jets

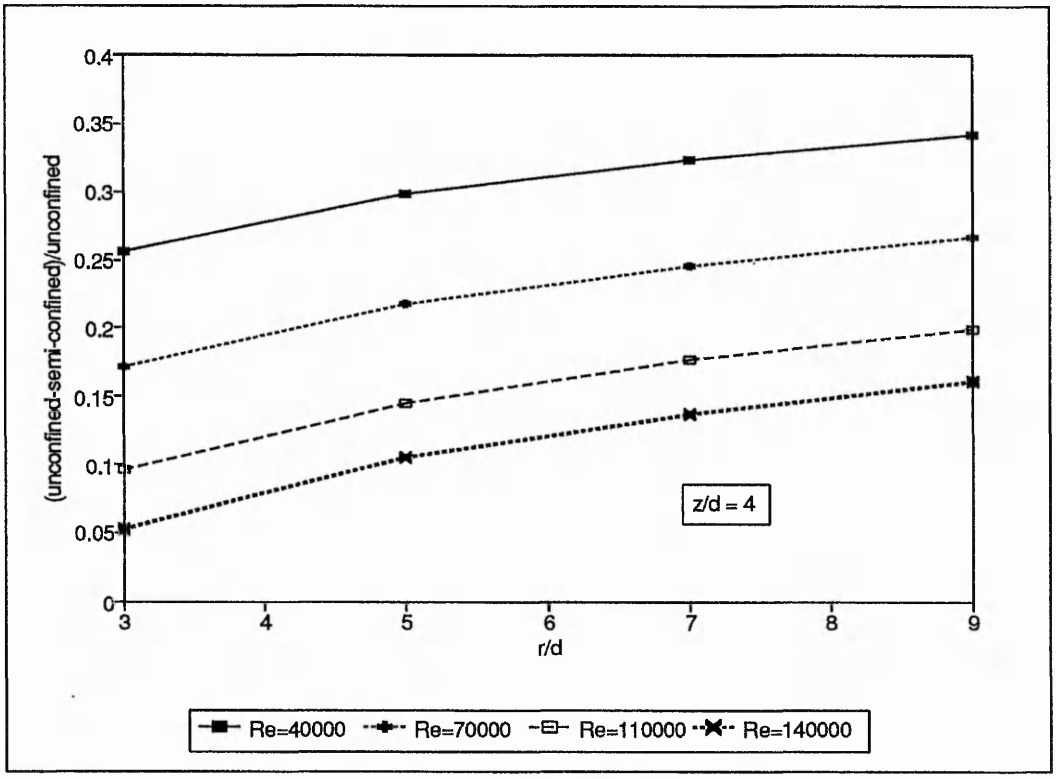

Fig 6.17 Nu differences versus r/d for z/d=6 and Re=40 000, 70 000, 110 000 and 140 000 for unconfined and semi-confined jets

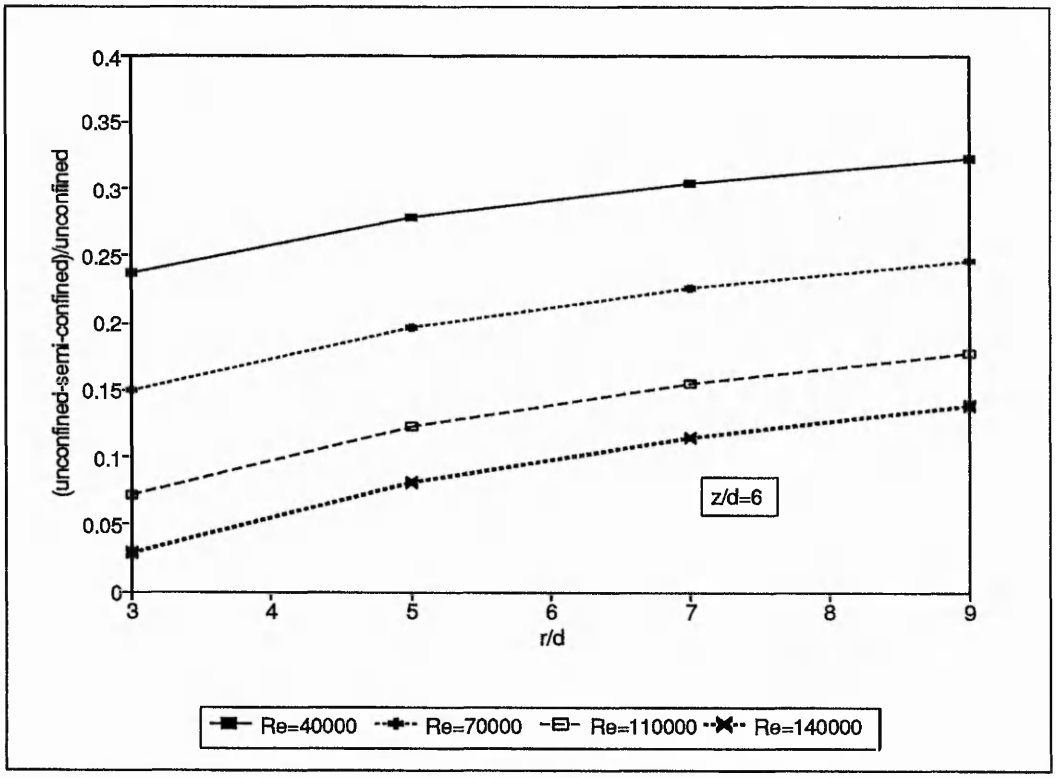

Fig 6.18 Nu ratios versus Re for r/d=3 and 9 for unconfined and semi-confined jets

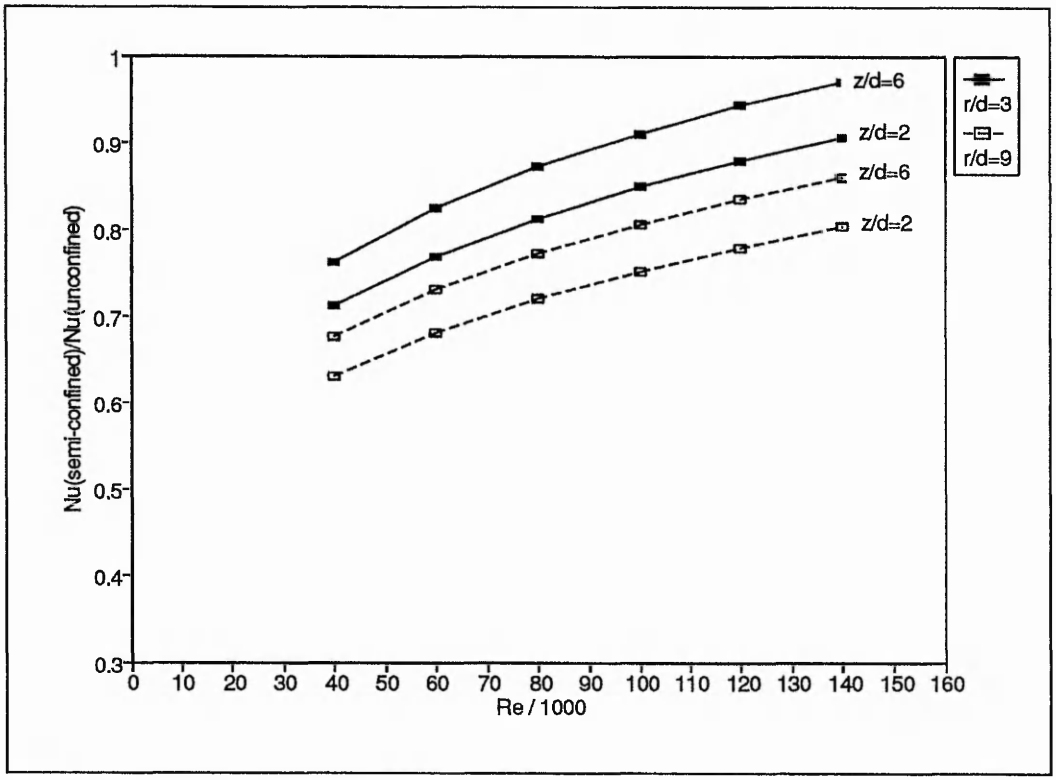

Fig 6.19 Re exponent versus r/d for z/d=2,4 and 6 for unconfined and semi-confined jets

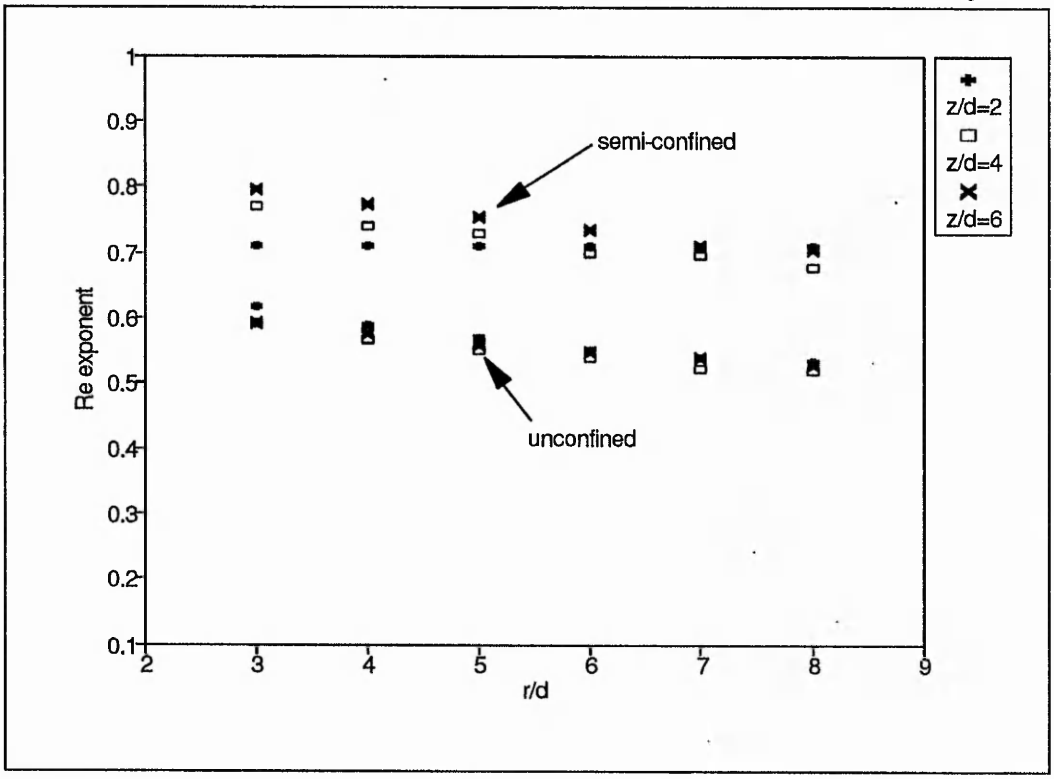

Table 1.1 **Uncertainty values for primary variables**

Variable/device	Units	Operating range	First order uncertainty	Nth Order uncertainty
Temperature:thermocouple	°C	20.0 - 80.0	±0.1	±0.1
thermometer	°C	30.0 - 90.0	±0.1	±0.1
thermometer	°C	15.0 - 20.0	±0.2	±.2
liquid crystal(1)	°C	31.0 - 31.5	±0.1	±0.15
(2)	°C	35.0 - 36.0	±0.1	±0.15
Pressure: Bourdon gauge	bar	0.40 - 3.60	±0.05	±0.05
Press diff: manometer	mm	50 - 330	±1	±1.5
Nozzle diameter	mm	10.28	±0.02	±0.02
Impingement plate:thickness	mm	3.92	±0.025	±0.025
Air thermal conductivity[1]	$W\ m^{-1}\ K^{-1}$	2.600×10^{-2}	$\pm 1 \times 10^{-4}$	$\pm 1 \times 10^{-4}$
Air dynamic viscosity[2]	$kg\ m^{-1}\ s^{-1}$	1.800×10^{-5}	$\pm 1 \times 10^{-7}$	$\pm 1 \times 10^{-7}$
Glass thermal conductivity	$W\ m^{-1}\ K^{-1}$	1.10	±0.04	±0.04
Orifice plate diameter	mm	15.045	±0.005	±0.005
Nozzle distance	mm	21 - 62	±1	±1.5
Radius	mm	20 - 80	±1	±2.5
Orifice coefficient		0.600	±0.018	±0.018
Orifice expansibility		1.000	±0.0002	±0.0002

Notes:(1)Rogers and Mayhew 1988. The uncertainties were estimated at the 0.5% level. (2)Uncertainties are as recommended in BS1042:Section 1.2:1984

Table 1.2 Significance of glass thermal conductivity uncertainties on Nu

Glass thermal conductivity uncertainty/per cent	Nusselt number uncertainty/per cent	
	low value of Nu	high value of Nu
1	± 2.6	± 1.6
2	± 3.1	± 2.2
3	± 5.2	± 4.7

Table 1.3 Significance of thermal radiation losses in the measurement of glass thermal conductivity

Energy transfer by conduction/W	Energy transfer by radiation/10^{-3}W	Radiation losses/per cent
11.8	6.6 (7.6)	0.06 (0.06)
26.0	14.2 (15.8)	0.05 (0.06)
38.8	18.3 (20.4)	0.04 (0.06)

Table 1.4 Paint thermal resistance and temperature differences for a thermal flux of 118 W m^{-2}

Film thermal resistance/(K W^{-1})	Temperature difference/K
8.4×10^{-5}	0.01
8.4×10^{-4}	0.1
1.7×10^{-3}	0.2

Table 1.5.1 Calibration of a liquid crystal (R35C1W)

Manufacturer's reference R35C1W.

Temp/°C	Colour(up)	Colour(down)	Manufacturer
34.40	colourless	colourless	
34.50	colourless	colourless	
34.54		red	
34.55	red		
34.60		brown/red	
34.65	red/brown		
34.75	brown		
34.80		brown	
34.90	brown/green		colourless
35.10		green/brown	red
35.14	green/brown		
35.28		green/yellow	
35.30	bright green		
35.32		bright green	
35.40			green/yellow
35.42	dark green		
35.50	green/blue		bright green
35.56		dark green	
36.04	blue		
36.10		blue/green	blue
36.70	blue	blue	
37.12		dark blue	

Calibration temperature = (35.3 ± 0.15) °C

Table 1.5.2. Calibration of a liquid crystal (R31C0.5W)

Manufacturer's reference: R31C0.5W

Temp/°C	Colour(up)	Colour(down)
30.80	colourless	colourless
30.90	colourless	
30.95		red
31.00		brown
31.02	red start	
31.10	brown/green	green/brown
31.20	bright green	
31.22		bright green
31.30	dark green	
31.35		dark green
31.45	green/blue	blue/green
31.48		blue
31.52	blue	
31.90	colourless	colourless

Calibration temperature =(31.20 ± 0.15) °C

Table 1.6 Uncertainty values for Nu, Re, z/d and r/d

Variables	high		low		
	value	uncertainty/per cent Nth order	value	uncertainty/per cent Nth order	1st order
Nu	475	4.1	122	5.1	4.5
Re	1.43×10^5	3.1	3×10^4	3.6	3.4
z/d	6	1.6	2	4.8	4.8
r/d	8	2.0	2	7.5	5.0

Table 2.1 Analysis of variance table for the unconfined jet and $3.0 \leq r/d \leq 9.0$

SOURCE	DF	SS	MS	F	R^2
Regression Residual	3 129	22.17 0.276	7.390 0.0021	3459	98.8
Lack of fit Pure error	113 16	0.240 0.0357	0.00212 0.00223	0.95	
Total	132	22.446			

Table 2.2 95 per cent confidence intervals for predictor coefficients,unconfined jet

Predictor coefficient	Interval
β_0	$0.176 \rightarrow 0.538$
β_1	$0.522 \rightarrow 0.554$
β_2	$-1.05 \rightarrow -0.998$
β_3	$-.041 \rightarrow -0.006$

Table 2.3 Analysis of variance table for the semi-confined jet and $2.5 \leq r/d \leq 9.0$

SOURCE	DF	SS	MS	F	R^2
Regression Residual	3 256	69.851 1.514	23.284 0.006	3938	97.8
Total	259	71.364			

Table 2.4 95 per cent confidence intervals for predictor coefficients, semi-confined jet

Predictor coefficient	Interval
β_0	$-2.17 \rightarrow -1.73$
β_1	$0.712 \rightarrow 0.751$
β_2	$-1.15 \rightarrow -1.10$
β_3	$0.018 \rightarrow 0.060$

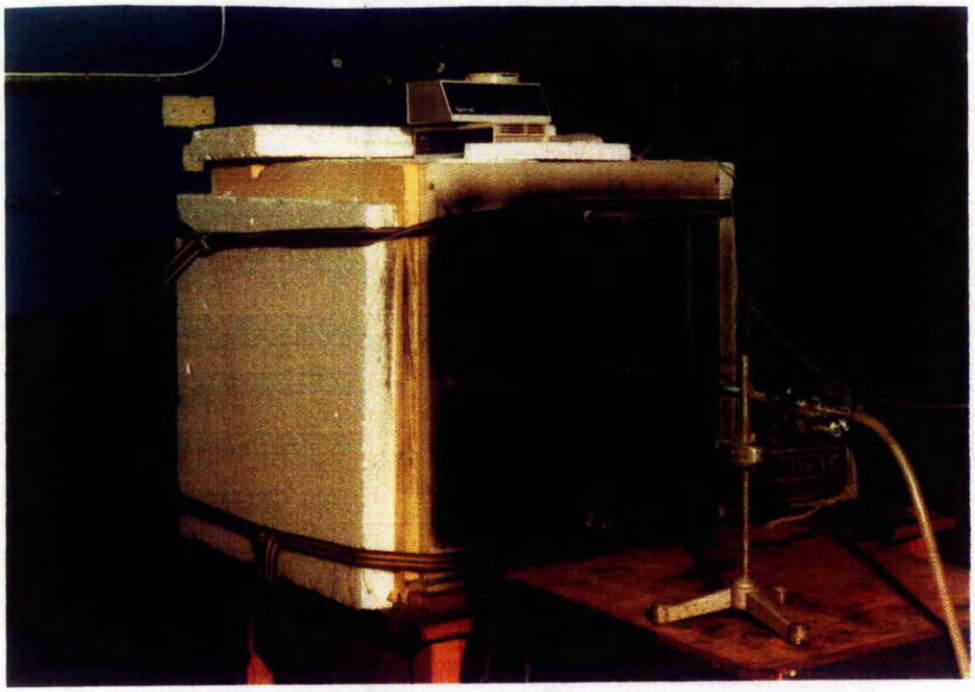

Plate 1.1 Rig arrangement for the unconfined jet.

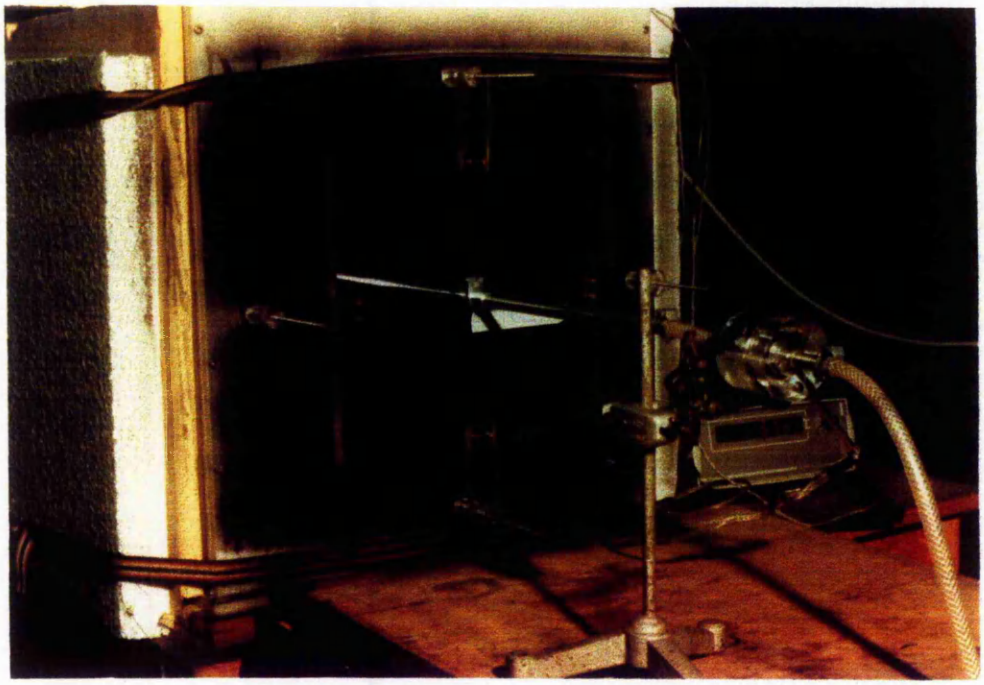

Plate 1.2 Rig arrangement for the semi–confined jet.

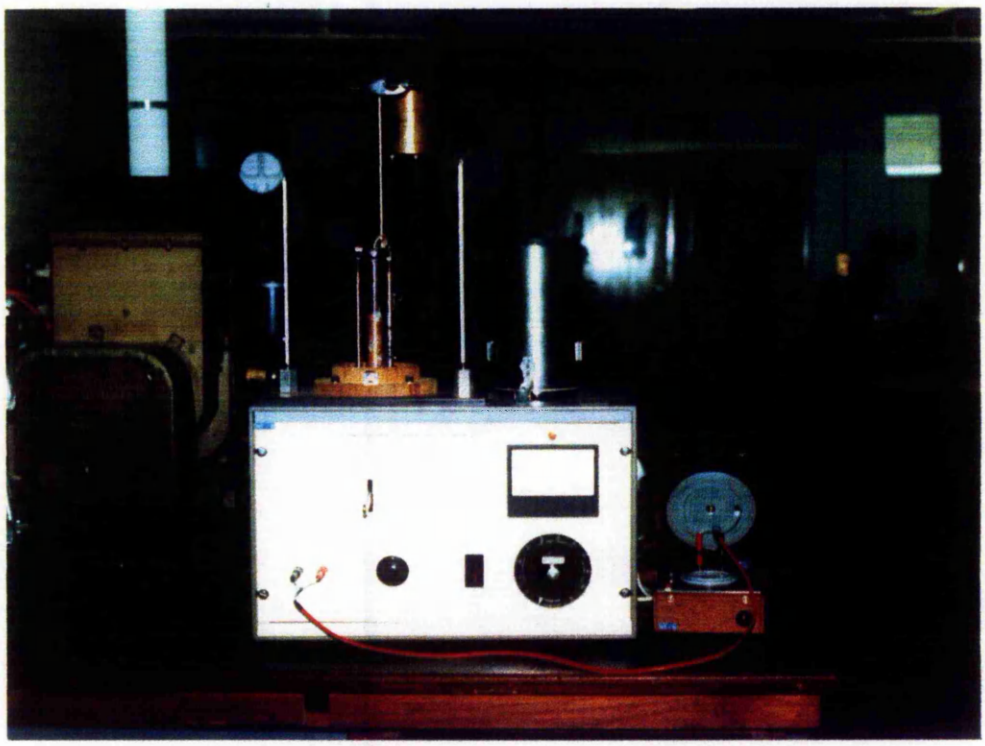

Plate 1.3 Thermal conductivity apparatus.

(i)

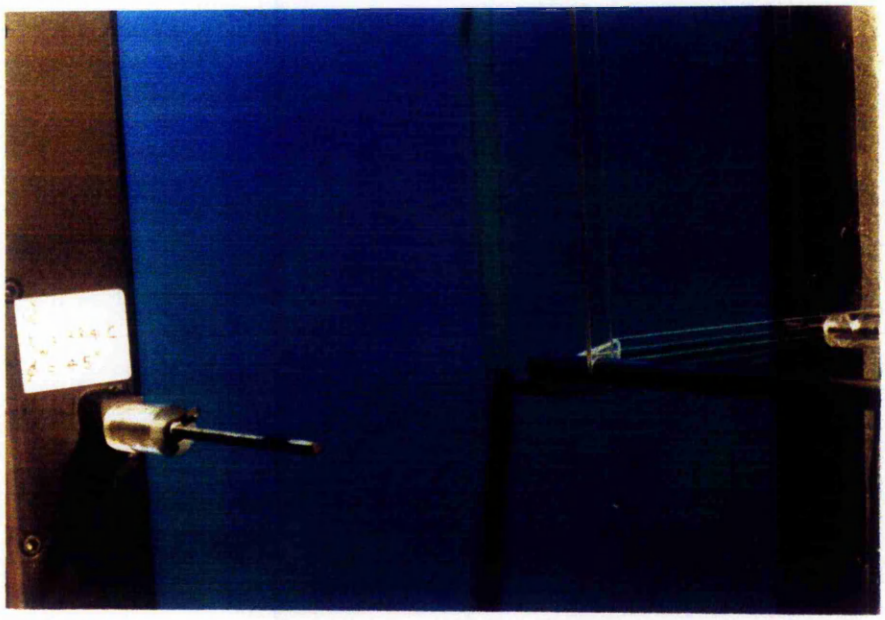

(ii)

Plate 2.1 Effect of viewing angle on the output display of a liquid crystal at a fixed temperature.

(i) angle = 90° (ii) angle = 45°

(i)

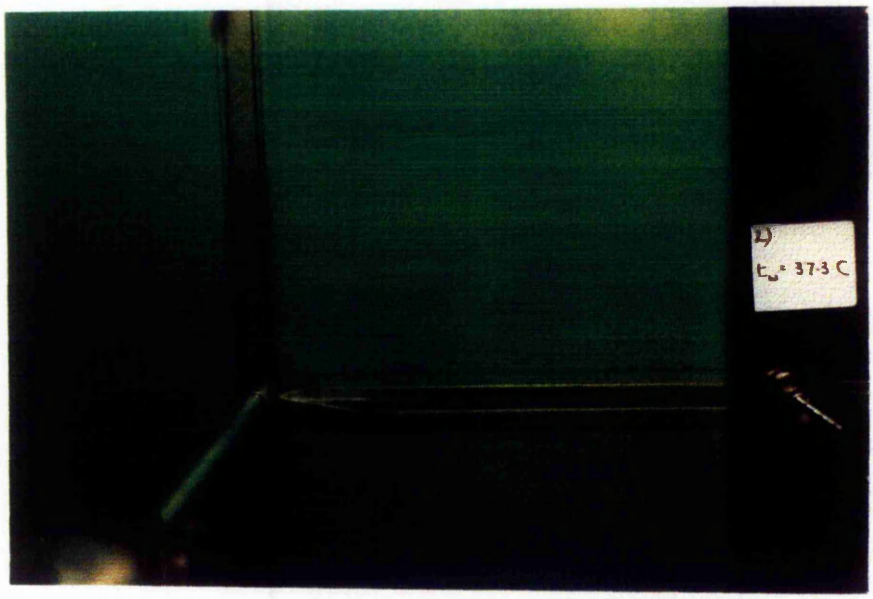

(ii)

Plate 2.2 The effect of exposure to floodlighting on a liquid crystal display.

(i) time = 0 (ii) time = 10s.

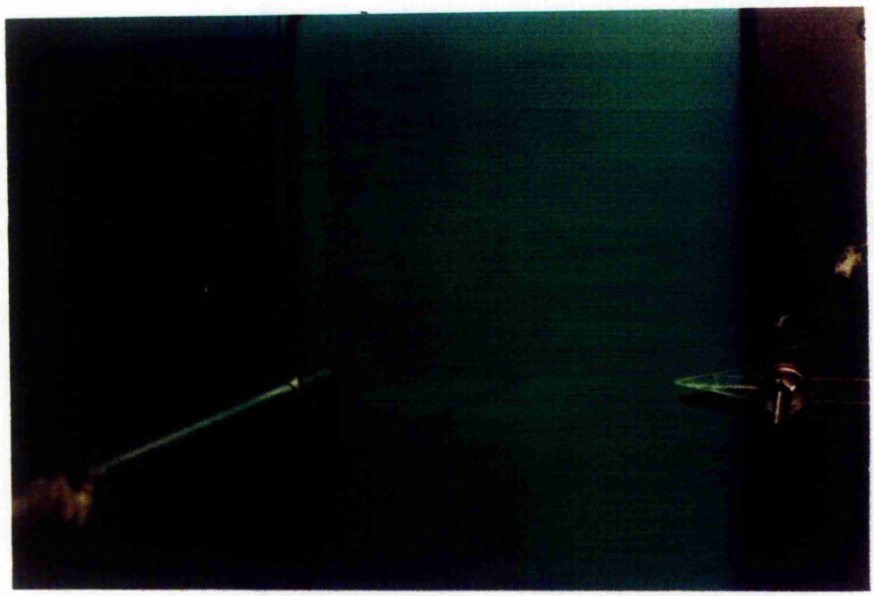

Plate 2.3 illustration of the permanent effect of light on the output display of a liquid crystal. The "ghost-like" outline of the measuring pointer represents a "protected" area.

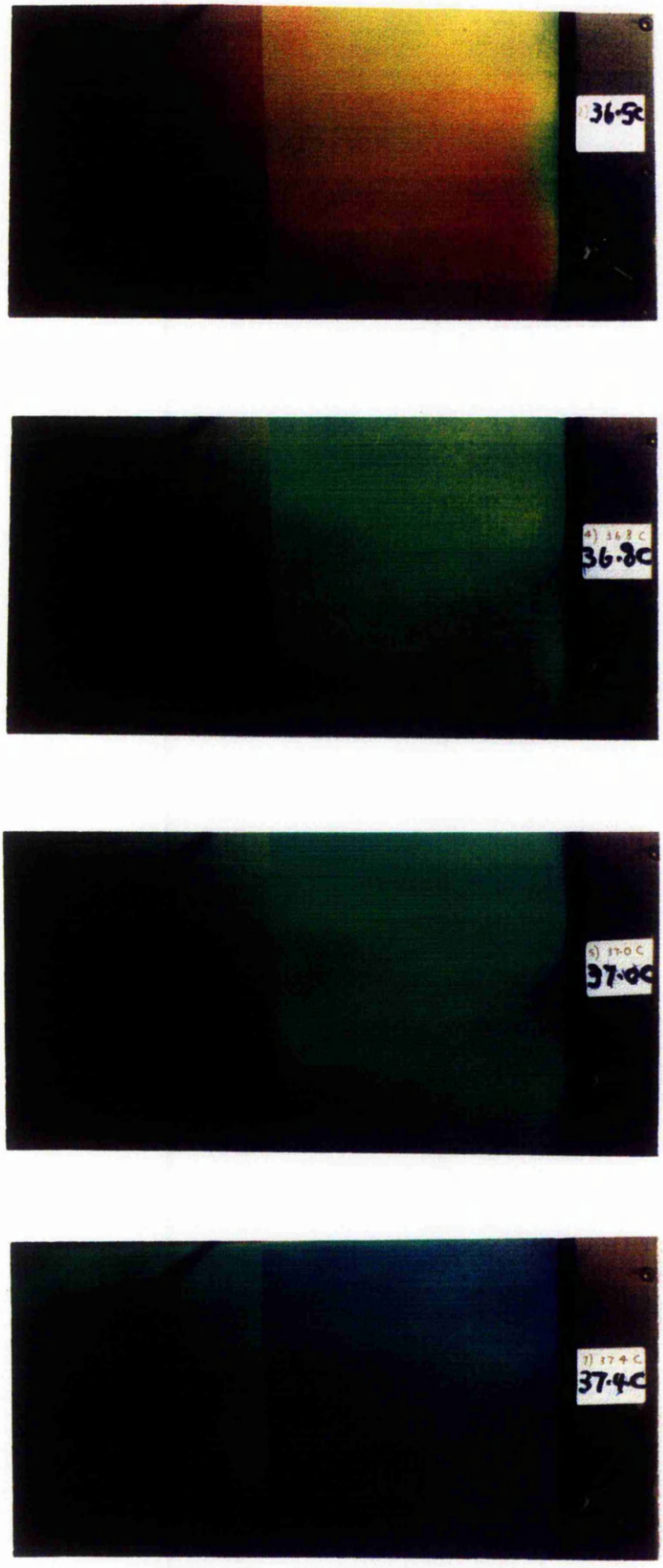

not painted painted

Plate 2.4 Effect of a sub–strata of black paint on a liquid crystal display. Illustration with increasing temperature.

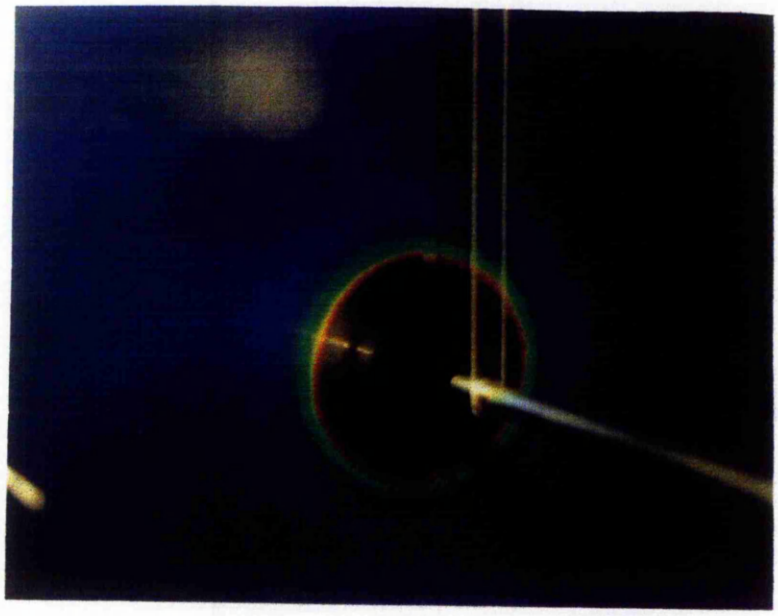

not painted painted

Nu = 70 Re = 112 000 z/d = 4

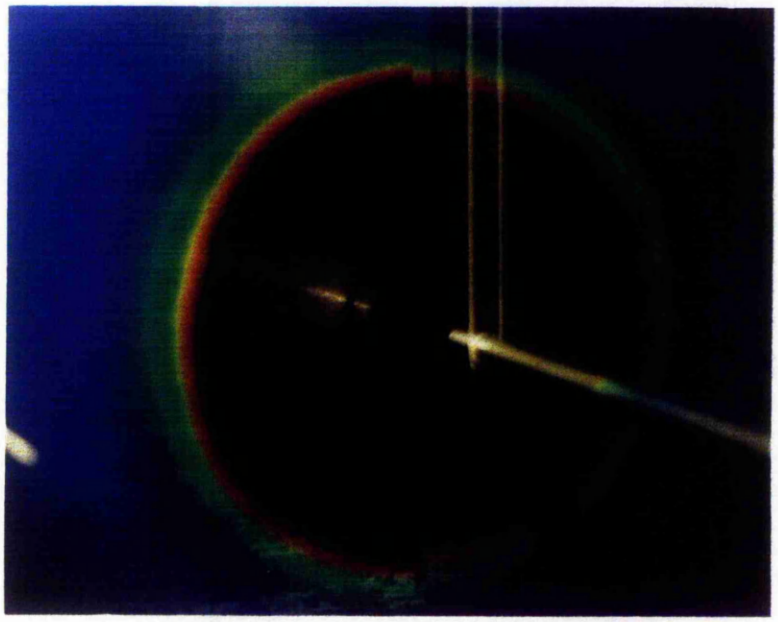

not painted painted

Nu = 70 Re = 31 500 z/d = 4

Plate 2.5 Effect of a sub–strata of black paint on a liquid crystal display. Illustration for the unconfined jet and two Reynolds numbers

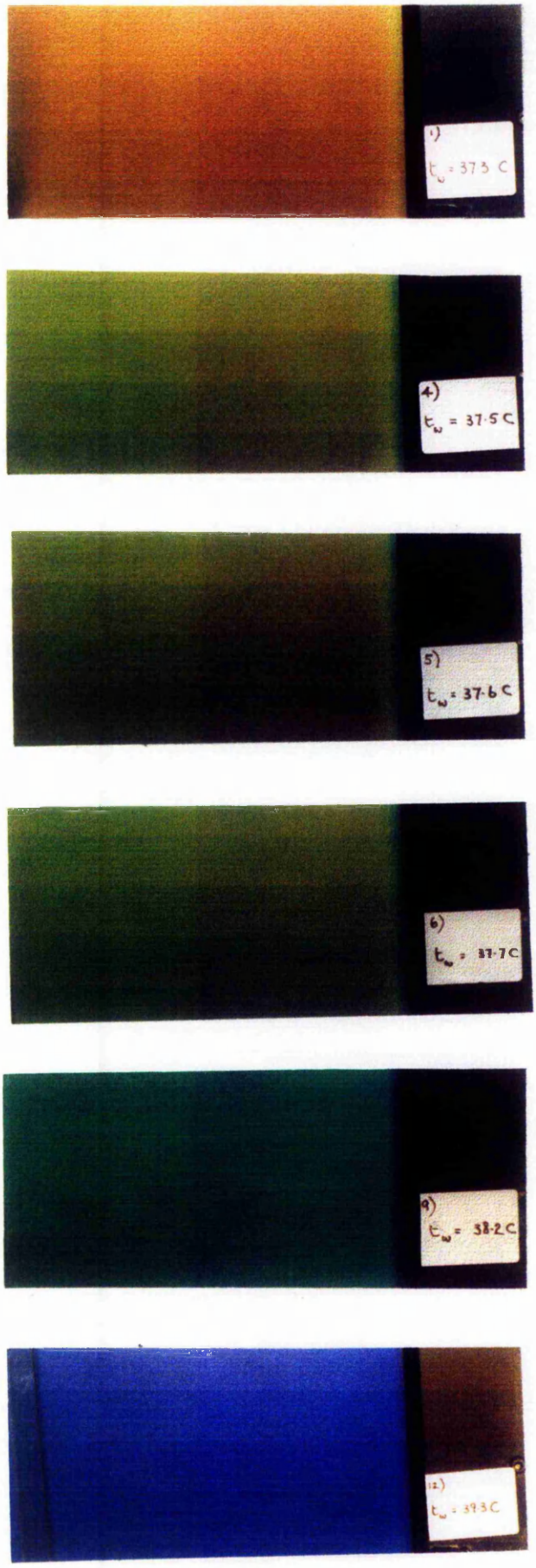

Plate 2.6 Sensitivity of a liquid crystal to changing temperatures.

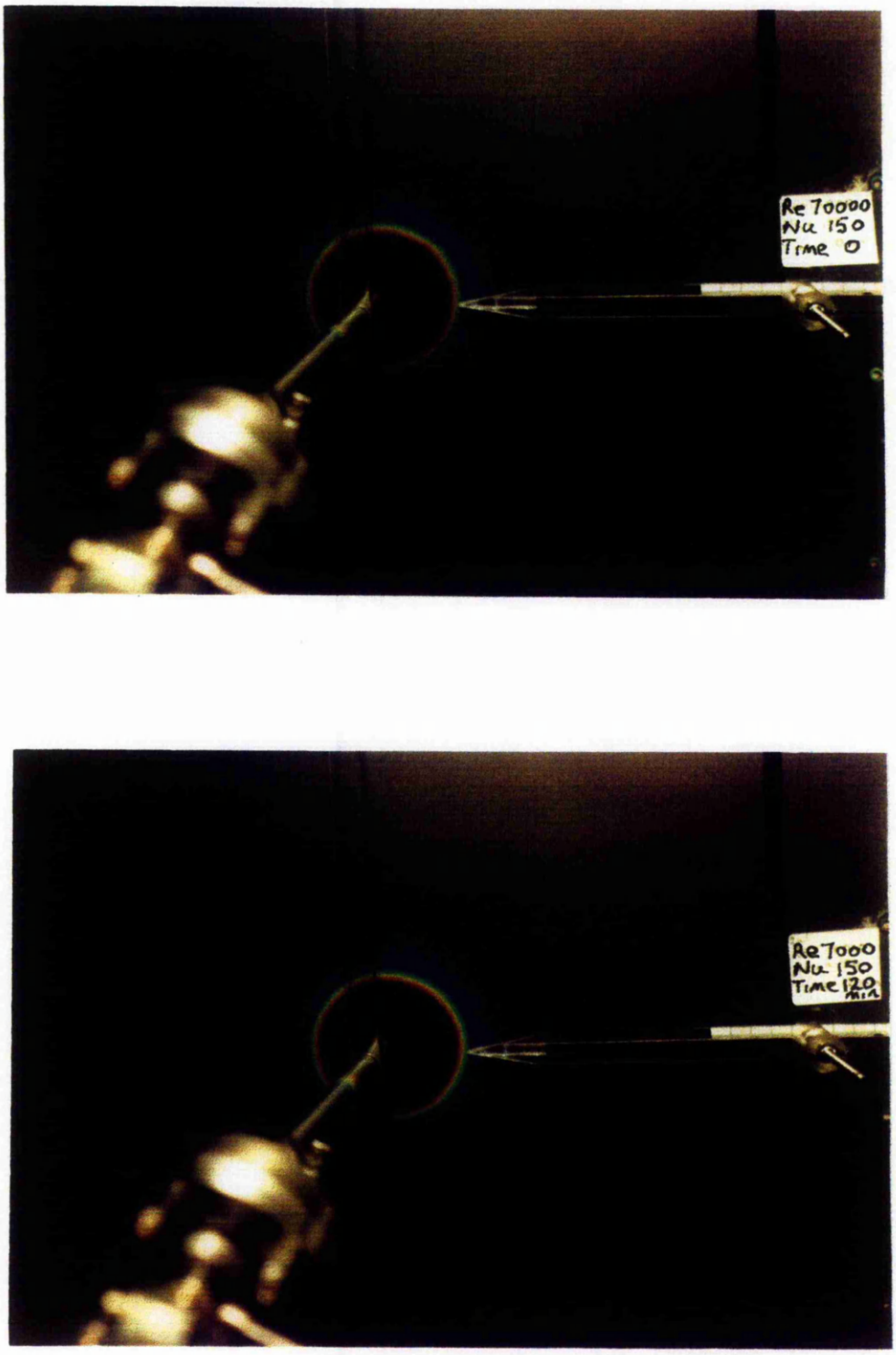

Plate 2.7 Durability of liquid crystals. Effect of the continuous impact for 120 minutes of an unconfined jet.

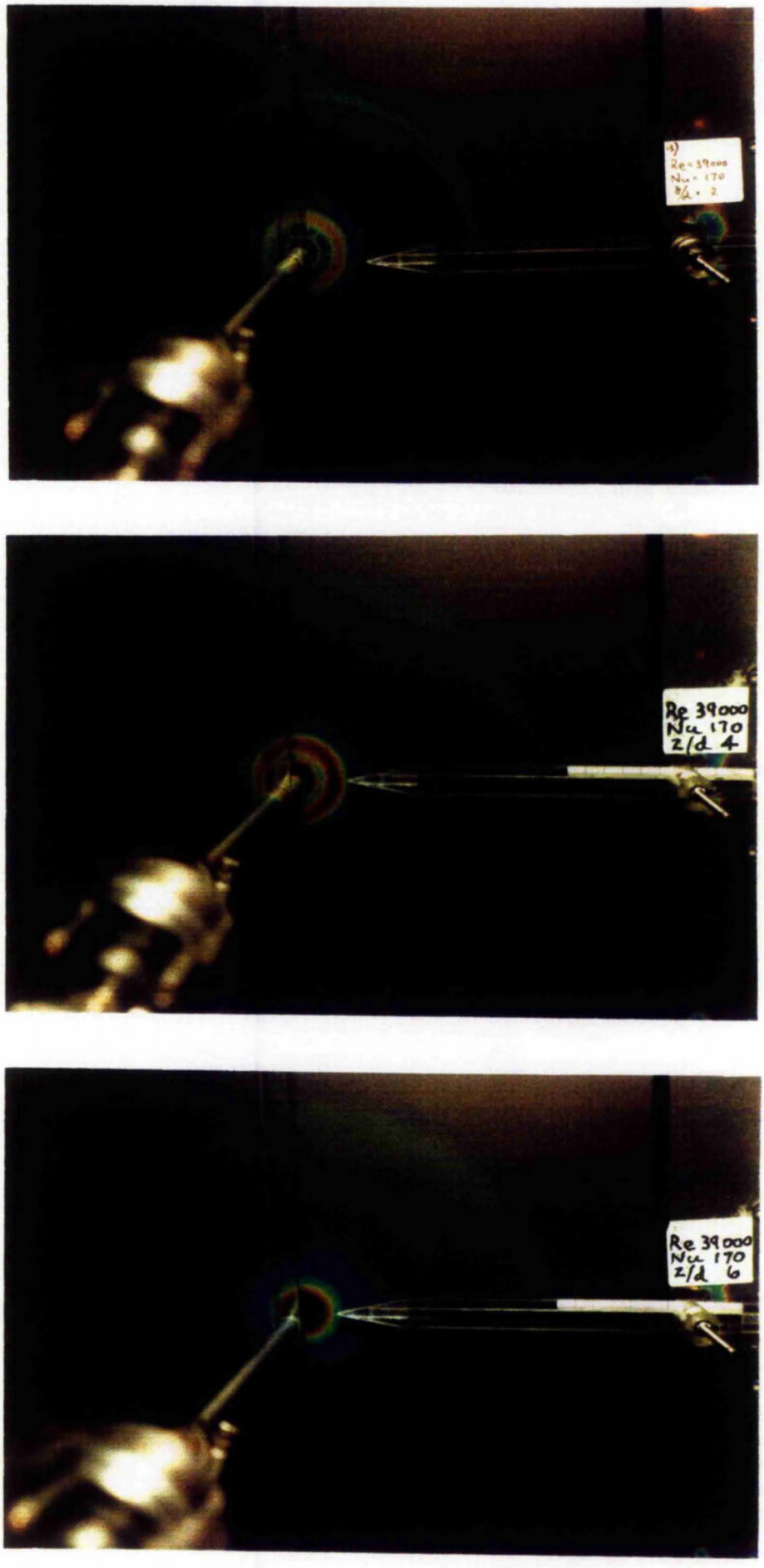

Plate 3.11 Liquid crystal displays with increasing z/d.

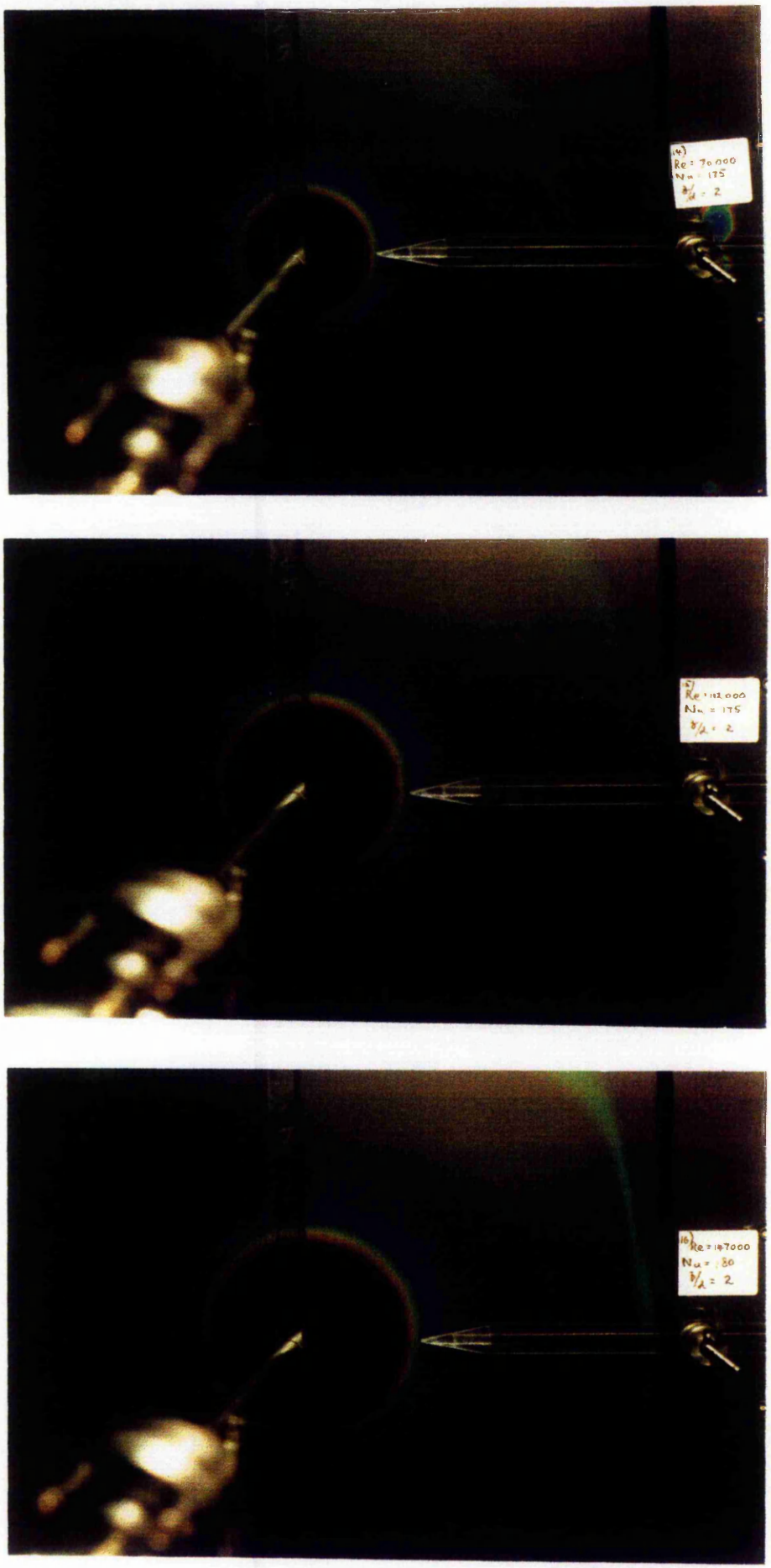

Plate 3.2 Liquid crystal displays with increasing Re.

Appendix A.1

A1.1 Uncertainty analysis in experimentation.

At the planning stage of any experimental programme, it is a requirement that estimates be made of the uncertainties associated with the measured data. The exercise serves to provide a final result with a known degree of uncertainty at specified odds. It also identifies those measurements which contribute strongly to he final uncertainty value. The analysis justifies the chosen method of experimentation and provides for comparisons between different procedures. As such it therefore plays an important part in reducing costs at the planning stage. It is to the work of Kline and McClintock 1953 that uncertainty analysis owes its origins. However, its full potential as an aid to the experiment has been further exploited by Moffat 1985.The analysis relies for its validity on each measurement

a) being an independent observation,

b) being from a normal or Gaussian population

c) having a known uncertainty interval, quoted at the same "odds".

The uncertainty interval can be based upon First-Order estimates, which reflect only the reading uncertainties or on Nth Order uncertainties. The latter estimates allow for additional calibration uncertainties and introduce the concept of "fixed errors" into the system.

First Order estimates are to be used for replication as they are relevant to measurements using the same instruments when associated "fixed errors" do not contribute to the general scatter of readings. Values of the estimates are obtained when practical from a sample of some 30 readings at equilibrium conditions

from which the figure of twice the standard deviation is calculated. The Nth order uncertainty is calculated from the root sum square of the First Order and the calibration uncertainties.

If ∇ is a calculated result of a series of experiments in which the independent variables x_1, x_2, x_3 .... x_n are measured, each with an uncertainty Ω_1, Ω_2, Ω_3 .... Ω_n then the uncertainty in the result is given by

$$\Omega = \left[\left(\frac{\partial \nabla}{\partial x_1} \Omega_1 \right)^2 + \left(\frac{\partial \nabla}{\partial x_2} \Omega_2 \right)^2 + \cdots + \left(\frac{\partial \nabla}{\partial x_n} \Omega_n \right)^2 \right]^{1/2} \quad \text{.....Eq A1.1}$$

It is a prerequisite that the uncertainties in the independent variables are all at the same odds.The computer programme for the evaluation of the partial derivatives and hence for the calculation of the uncertainty in the result Ω is listed in Appendix A1.3. The principle employed is one of successive perturbation of the variables x_1, x_2 ....x_n by the small steps Δx_1 Δx_2 .... Δx_n. For each variable the differences $\nabla_{(x + \Delta x)} - \nabla_x$ are calculated before returning (x + Δx) etc to its original value.

If Δx is sufficiently small then

$$\frac{\partial \nabla}{\partial x_1} \approx \frac{\nabla_{(x_1 + \Delta x_1)} - \nabla_{(x_1)}}{\Delta x_1} \quad \text{....Eq A1.2}$$

Likewise the partial differential coefficients for x_2,x_3.....x_n are obtained.

The programme concludes by evaluating $\left(\frac{\partial \nabla}{\partial x} \Omega \right)^2$ for each variable before

summing and taking the square root. The print out provides information on the calculated result ∇, its uncertainty Ω_R and on the significance level of each of the variable uncertainties as given by $(\frac{\partial \nabla}{\partial x}\Omega)^2$

The relative significance of each uncertainty can then be expressed in percentage terms.

A1.2 Working equations for the determination of the uncertainties in Nu, Re, z/d and r/d

$$q_{rad}/[Wm^{-2}] = 56.9x10^{-9}\epsilon[(t_s+273)^4-(t_a+273)^4] \quad ..Eq\ A1.3$$

$$Nu = \frac{d[(k_g/x_g)(t_w-t_s)-q_{rad}]}{k_a(t_s-t_a)} \quad ....Eq\ A1.4$$

$$m/[kg\ s^{-1}] = 6.78x10^{-5}Ced_o^2[\frac{(p_0)\Delta p}{t_0+273}]^{0.5} \quad .....Eq\ A1.5$$

Δp/[mmwater]=pressure difference across the orifice plate

$$Re = 1273\frac{m}{d\mu} \quad .....Eq\ A1.6$$

$$radius\ ratio = \frac{r}{d} \quad ...Eq\ A1.7$$

$$nozzle\ distance\ ratio = \frac{z}{d} \quad ....eq\ A1.8$$

A1.3 Computer program for error analysis

```
10 REM error analysis
12 PR"NT "list programme for instruction"
15 REM insert function at line100
16 REM function to be of the form; F=X(1),X(2) etc up to N terms
20 INPUT "Have you inserted your function at line 100?.Y/N";A$
25 IF A$="Y" THEN 200
30 STOP
100 F=X(1)*(X(2)-X(3))/(X(4)*(X(3)-X(5)))
110 RETURN
200 INPUT "number of measured values=";N
201 E=0
205 FOR I=1 TO N
210 PRINT "input values of measured values, uncertainty,increments"
220 INPUT X0(I),E(I),DX(I)
225 X(I)=X0(I)
227 NEXT I
230 GOSUB 100
250 F1=F
290 FOR I = 1 TO N
300 X(I)=X0(I)+DX(I):GOSUB 100
310 DF(I)=F
320 DIF(I)=(DF(I)-F1)/DX(I)
400 X(I)=X0(I)
420 EC(I)=(DIF(I)*E(I))^2
430 E=E+EC(I)
540 NEXT I
600 ER=E^.5
620 PRINT "RESULT IS           "F1
645 PRINT
646 PRINT
650 PRINT "UNCERTAINTY IN RESULT=",ER"-"ER*100/F1"%"
661 PRINT
662 PRINT
664 FOR I=1 TO N
665 PRINT "ERROR SIGNIFICANCE IN X"I"="TAB(40)(DIF(I)*E(I))^2
670 NEXT I
1000 END
```

A1.4 Computer program for the determination of Nu and Re

```
10 REM this programme is called "jetprog2"
20 D1=28!
30 INPUT "nozzle distance mm";Z
40 INPUT "nozzle diameter mm";DN
50 INPUT "orifice diameter mm";D2
60 IF D2<6 THEN 700
62 F=1
63 IF D2>.1*D1 THEN 65 ELSE 70
65 F=1.003
70 LPRINT "orifice diameter="D2"mm; nozzle diameter="DN"mm; nozzle
dist.="Z"mm"
80 LPRINT:LPRINT
90 LPRINT "Inlet press";TAB(14)"Press diff";TAB(25)"Air temp";TAB(34)"Noz
temp";TAB(43)"Mass rate";TAB(56)"Re(pipe)"TAB(65)"Water temp"
100 LPRINT TAB(3)"bar(gauge)";TAB(15)"mm
water";TAB(30)"C";TAB(37)"C";TAB(44)"kg/s";TAB(69)"C"
110 INPUT "surface temperature C";TS
120 INPUT "orifice differential mm water";PDIF
130 INPUT "gauge pressure upstream N/m^2";INPR
140 INPUT "atmos press mmHg";ATPR
145 INPUT "ambient temperature C";AMBTE
150 INPUT "air temperatureC";INTE
155 INPUT "Nozzle temperature C";TN
160 INPUT "water temperature C";TW
170 INPUT "readings for radius mm";R
180 BETA=D2/D1
190 IF BETA > .7 THEN 740
200 IF BETA < .23 THEN 740
210 E=(1-BETA^4)^(-.5)
220 PA=132.93*ATPR
230 P1=INPR+PA
240 T1=INTE+273.16
260 RHO1=P1/(T1*287.1)
265 DP=PDIF*.00981*(1000-RHO1)
270 ETA=1-(.41+.35*BETA^4)*DP/(1.4*P1)
280 GOSUB 800
290 C=.5959
300 RE=(C*E*ETA*D2^2*(2*DP*RHO1)^.5)/(MU*D1*1000)
310 C1=C
320
C2=.5959+.0312*BETA^2.1-.184*BETA^8+.0029*BETA^2.5*(10^6/RE)^.75+.0
39*BETA^4*(1-BETA^4)^-1-.0337*.47*BETA^3
330 DIF=C1-C2
340 IF ABS(DIF)<.0001 THEN 370
350 C=C+.0001
360 GOTO 300
```

```
370 IF C*E*BETA^2 < .032 THEN 720
380 IF C*E*BETA^2 > .35 THEN 720
390 IF RE < 1260*BETA^2*D1 THEN 760
400 P2=P1-DP
410 IF P2 < .75*P1 THEN 780
420 PRINT "Beta^2=";BETA^2
440 C=C*F
450 PRINT "C=";C
460 PRINT "E=";E
470 PRINT "eta=";ETA
480 PRINT "k=orifice coefficient=";C*E*ETA*10^(-6)*D2^2*.7854
490 PRINT "dp=(N/m^2)";DP
500 PRINT "rho1(kg/m^3)=";RHO1
510 PRINT "Re=";RE
520 MDOT=C*E*ETA*.7854*10^(-6)*D2^2*(2*DP*RHO1)^.5
530 REN= RE*D1/DN
540 LPRINT
TAB(4)INPR/100000!;TAB(18)PDIF;TAB(29)INTE;TAB(35)TN;TAB(40)MDO
T;TAB(54)RE;TAB(67)TW
550 LPRINT:LPRINT
560 REM Determination of Nusselt Number
570 REM glas thickness,XG=3.925E-3 m
580 XG=.003925
590 REM glass thermal conductivity KG=1.047+1.21E-3T-2.6E-6T^2 W m^-1
K^-1
600 T=(TW+TS)/2
610 KG=1.047+.00121*T-.0000026*T^2
615 T2=TN+273.16
620 TA=(T2+TS+273.16)/2
630 GOSUB 890
640 H=KG*(TW-TS)/(XG*(TS-TN))
650 NU=H*DN*10^-3/KA
651 QLOSS=56.7*10^-9*.9*((TS+273.2)^4-(AMBTE+273.2)^4)
652 H=H-QLOSS/(TS-TN)
653 NU=NU-(QLOSS*DN*10^-3)/((TS-TN)*KA)
654 LPRINT "Heat tr.coef."TAB(20)"Nusselt
No."TAB(40)"r/d"TAB(57)"z/d"TAB(70)"Re(noz)"
655 LPRINT "  W/m^2 K     "
660 LPRINT
TAB(3)H;TAB(19)NU;TAB(38)R/DN;TAB(55)Z/DN;TAB(68)REN
661 LPRINT:LPRINT
662
LPRINT"_____
      "
670 INPUT "if more readings type 1";Y
680 IF Y=1 THEN 90
690 GOTO 980
700 PRINT "Orifice diameter too small,programme terminated"
```

```
710 GOTO 980
720 PRINT "CEBeta^2 out of range, programme terminated"
730 GOTO 980
740 PRINT "ratio of diameters out of range,propramme terminated"
750 GOTO 980
760 PRINT "Re too small,programme terminated"
770 GOTO 980
780 PRINT "pressure ratio across orifice too small"
790 GOTO 980
800 IF T1>= 300 THEN 850
810 X=(T1-275)/25
820 MU=1.725+X*(1.846-1.725)
830 MU=MU*10^-5
840 RETURN
850 X=(T1-300)/25
860 MU=1.846+X*(1.962-1.846)
870 MU=MU*10^-5
880 RETURN
890 IF TA>=300 THEN 940
900 X=(TA-275)/25
910 KA=2.428+X*(2.624-2.428)
920 KA=KA*10^-2
930 RETURN
940 X=(TA-300)/25
950 KA=2.624+X*(2.816-2.624)
960 KA=KA*10^-2
970 RETURN
980 END
```

Appendix A1.5

Flow diagram for the determination of Re

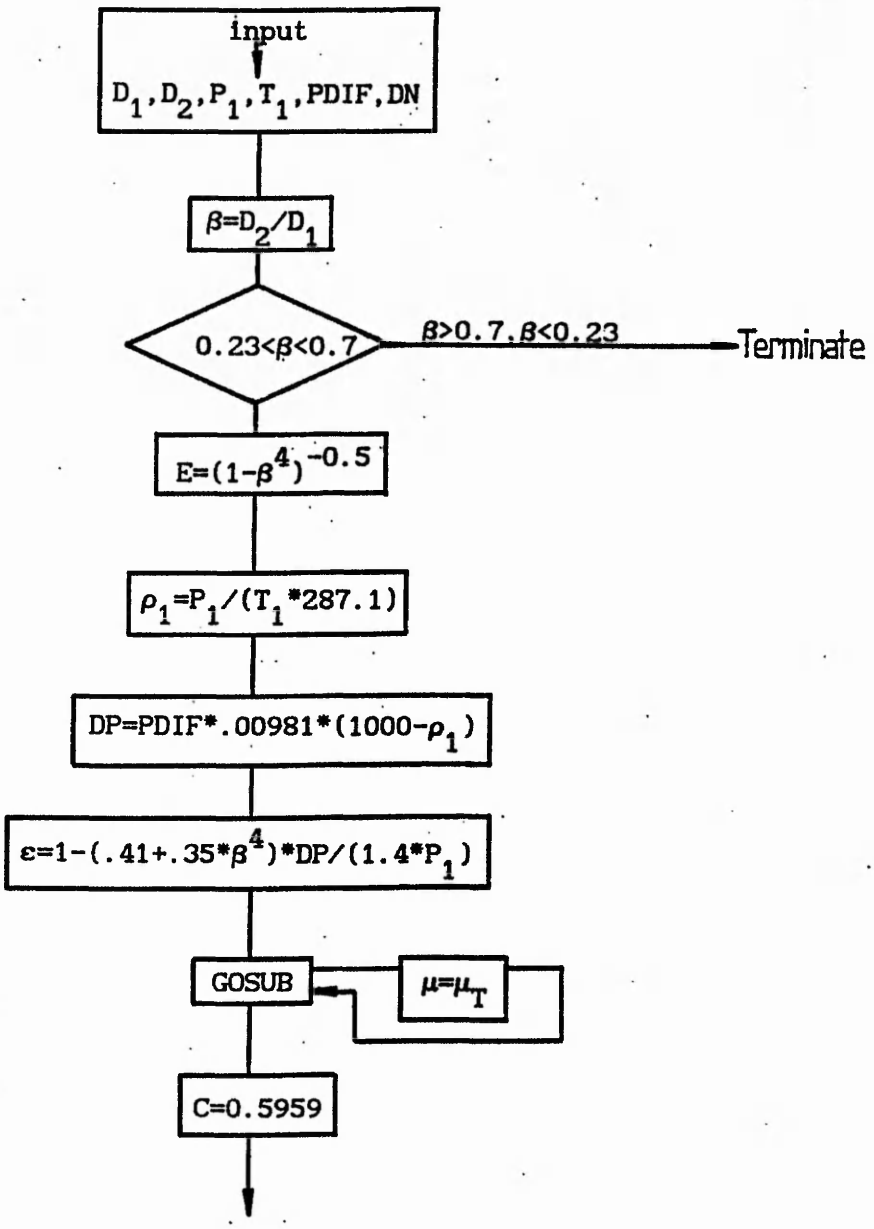

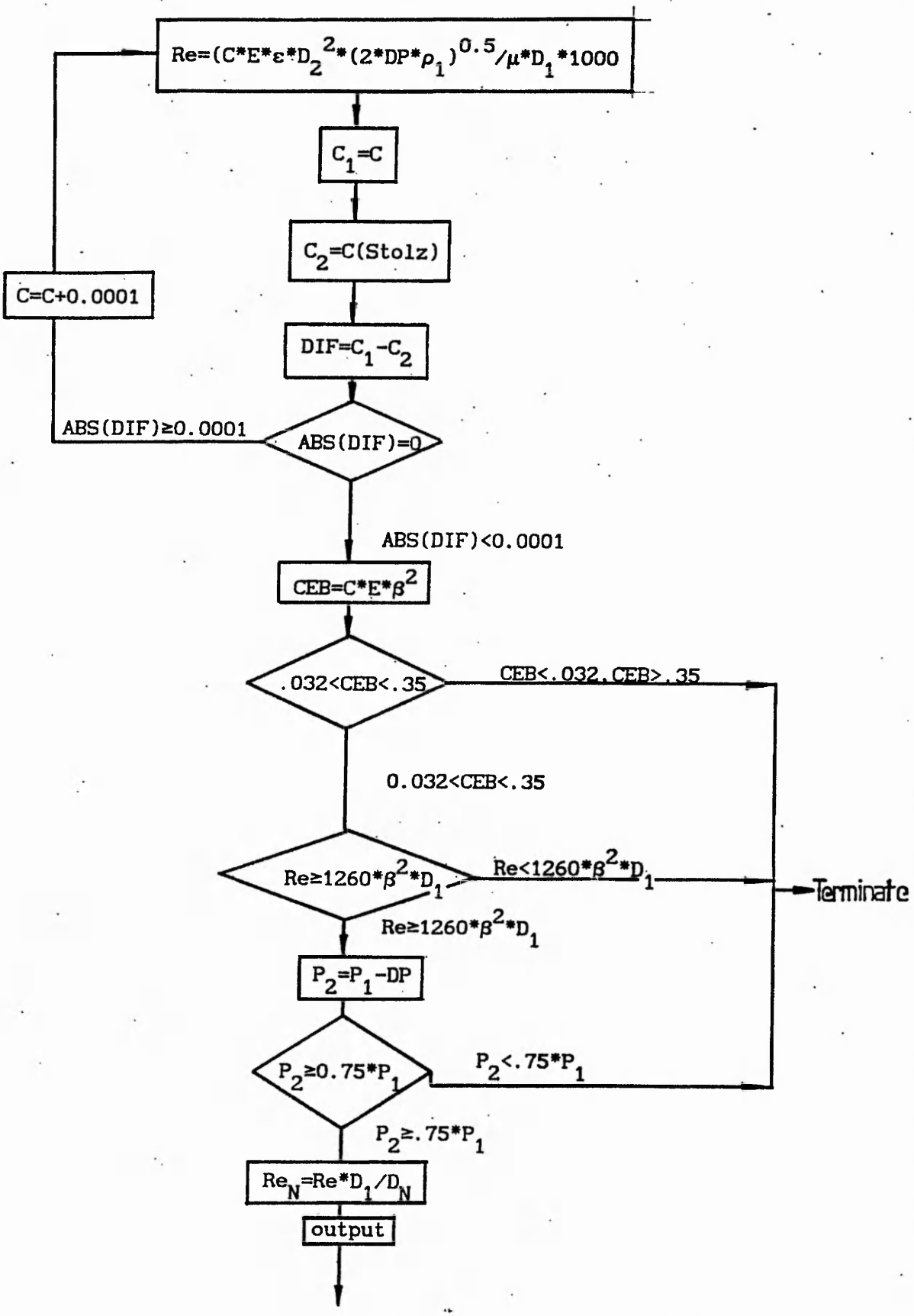
Re=(C*E*ε*D2^2*(2*DP*ρ1)^0.5/μ*D1*1000
C1=C
C2=C(Stolz)
C=C+0.0001
DIF=C1-C2
ABS(DIF)≥0.0001
ABS(DIF)=0
ABS(DIF)<0.0001
CEB=C*E*β^2
.032<CEB<.35
CEB<.032, CEB>.35
0.032<CEB<.35
Re≥1260*β^2*D1
Re<1260*β^2*D1
Terminate
Re≥1260*β^2*D1
P2=P1-DP
P2≥0.75*P1
P2<.75*P1
P2≥.75*P1
ReN=Re*D1/DN
output

Appendix A2

A2.1 Details of orifice plate installation compared with BS 1042

British Standard 1042	Operating Conditions
d ≮ 6 mm	d = 15.045 mm
$0.23 \leq \beta \leq 0.7$	$\beta = 0.537$
$0.032 \leq CE\beta^2 \leq 0.350$	$CE\beta^2 = 0.173$
$0.75 \leq (p_2/p_1) < 1$	$0.96 \leq (p_2/p_1) < 1$
$10^4 \leq Re_D \leq 10^8$)	$110000 < Re_D < 66000$

Suffixes 1 and 2 refer to upstream and downstream conditions. .

A2.2 Internal diameters of the pipe at sections upstream of the orifice plate

Distance from orifice plate /mm	Diameters /mm	Mean diameter /mm
28	28.01 28.00 28.00 28.00	28.00
35	28.00 28.00 28.00 28.00	28.00
42	28.00 28.00 28.00 28.00	28.00

Overall mean diameter = 28.00 ± 0.01 mm

A2.3 The circularity of the orifice plate bore

Bore diameter /mm	Difference from mean as per cent of mean
15.045	0.000
15.041	-0.027
15.048	0.019
15.047	0.011

Mean diameter = 15.045 ± 0.005 mm

DRG. No. 1061

DO NOT SCALE

6. HOLES DRILL ϕ 4
EQUI SPACED ON
55 PCD

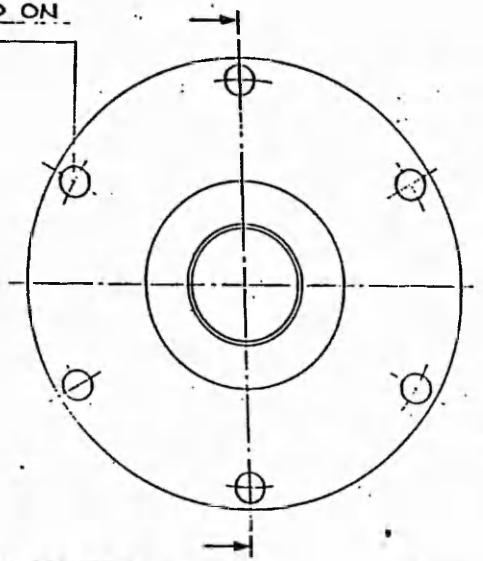

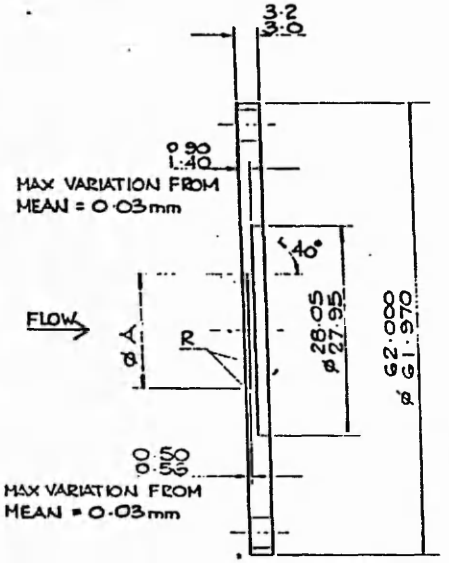

DIAMETER A	MAX DEVIATION FROM MEAN DIA	MAX RAD R
8·050 7·950	0·004 mm	0·003mm
15·050 14·950	0·007mm	0·006mm

THE ORIFICE SHALL BE CYLINDRICAL & PERPENDICULAR TO THE UPSTREAM FACE.

NOTE:- THE UPSTREAM FACE IS TO BE FLAT. I.E. THE SLOPE OF ANY LINE CONNECTING TWO POINTS SHOULD BE LESS THAN 1% FROM A PLANE PERPENDICULAR TO THE CENTRE LINE.
& SMOOTH :- IE. THE ARITHMETIC MEAN DEVIATION FROM THE MEAN LINE SHALL BE LESS THAN $10^{-4} \times A$

2		ORIFICE PLATE, ORIFICE ϕ 8	BRASS		
1		ORIFICE PLATE, ORIFICE ϕ 15	BRASS		
REV	PART No	NAME OF PART	MATERIAL	FINISH	No.
DRN	J.G.	SCALE 2:1	ORIFICE PLATE	DRG No	
APP'D		SHEET		1061	
DATE	14-6-78	SHEET No	TREIIT POLYTECHNIC		

Appendix A3

A3.1 Calculation of radiation losses in the determination of the thermal conductivity of glass

Referring to figure 2.7 the corrected energy transfer rate through the glass $\dot{Q}_{cor} = \dot{Q}_R + \dot{Q}$ where $\dot{Q}_R$ = measured radiation losses and $\dot{Q}$ = energy transfer rate to the water.

Treating the system as being analogous to an enclosed body with zero radiation end losses then

$$\dot{Q}_R = \frac{A_c(\dot{q}_{bc} - \dot{q}_{bf})}{\frac{1}{\epsilon_c} + \frac{A_c}{A_f}\left(\frac{1}{\epsilon_f} - 1\right)} \quad \ldots . EQ\ 2.3$$

suffixes c and f refer to the copper and shield and $\dot{q}_{bc} = \sigma(T_c)^4$ and $\dot{q}_{bf} = \sigma(T_f)^4$.

$A_c = 2.985 \times 10^{-3}$ m^2 and $A_c / A_f = 0.29$.

For $\epsilon_c = 0.1$ and $\epsilon_f = 0.2$ then

$$\dot{Q}_R / [W] = 1.52 \times 10^{-11}(T_c^4 - T_f^4)$$

Results

t_c /°C	t_f /°C	Q_R /10^{-3} W	Q /W	Q_R / Q /%
30	26	6.6(7.6)	11.8	0.06(0.06)
39	31	14.2(15.8)	26.0	0.05(0.06)
43	33	18.3(20.4)	38.8	0.04(0.06)

A3.2 Measurement of the surface contact resistance in the determination of the thermal conductivity of glass

t(1)/°C	t(2)/°C	t(3)/°C	t(4)/°C	ts(1)/°C	ts(2)/°C	contact res./°C
54	69	82	112	72.9	77.8	4.9
56	70	82	113	73.6	77.7	4.0
54	70	83	113	74.2	78.8	4.6
55	71	84	114	75.2	79.8	4.6
55	70	83	114	73.9	78.7	4.8

Mean contact resistance = 4.6 K

A3.3 Measurement of the thermal conductivity of glass

temperature							water					
glass/°C	t(1)/°C	t(2)/°C	t(3)/°C	t(4)/°C	$t(w_1)$/°C	$t(w_2)$/°C	vol/ml	time/s	$t(g_1)$	$t(g_2)$	$q/[10^4$ W $m^{-2}]$	$k_s/[W$ m^{-1} $K^{-1}]$
69	31	33	105	108	19.8	24.1	82.5	126.0	99.7	38.0	2.391	1.125
68	28	31	105	109	18.9	23.3	89.0	137.5	99.4	36.3	2.419	1.112
66	27	29	103	108	19.6	24.3	87.5	142.4	97.1	34.0	2.453	1.128
66	27	29	103	107	19.6	24.2	88.5	142.4	97.4	34.0	2.428	1.111
65	25	28	103	107	19.6	24.2	90.0	142.4	97.4	33.3	2.467	1.116
mean thermal conductivity at 67 °C = 1.118 W m^{-1} K^{-1}												
109	36	39	180	185	19.9	25.9	85.5	84.8	174.1	44.3	5.138	1.148
110	37	40	181	186	19.9	26.1	86.0	88.0	175.1	45.3	5.146	1.150
113	38	41	186	191	20.0	27.4	91.0	108.0	180.1	46.3	5.296	1.148
114	38	41	187	193	20.1	27.7	87.0	105.5	180.8	46.3	5.323	1.147
114	37	41	187	193	20.0	27.0	86.5	96.8	180.8	46.5	5.313	1.147
mean thermal conductivity at 112 °C = 1.147 W m^{-1} K^{-1}												
147	42	45	249	254	18.9	25.0	175	116.0	243.1	50.3	7.816	1.175
147	42	45	250	254	18.8	24.8	148	95.8	244.3	50.3	7.872	1.176
148	41	44	252	258	18.8	24.8	152	97.6	245.8	49.3	7.936	1.171
147	41	44	250	255	18.9	25.0	166	109.5	244.1	49.3	7.854	1.169
148	41	44	253	258	18.9	24.9	160	102.0	247.1	49.3	7.993	1.172
mean thermal conductivity at 150 °C = 1.172 W m^{-1} K^{-1}												

Appendix A4

A4.1 Calibration of thermocouples

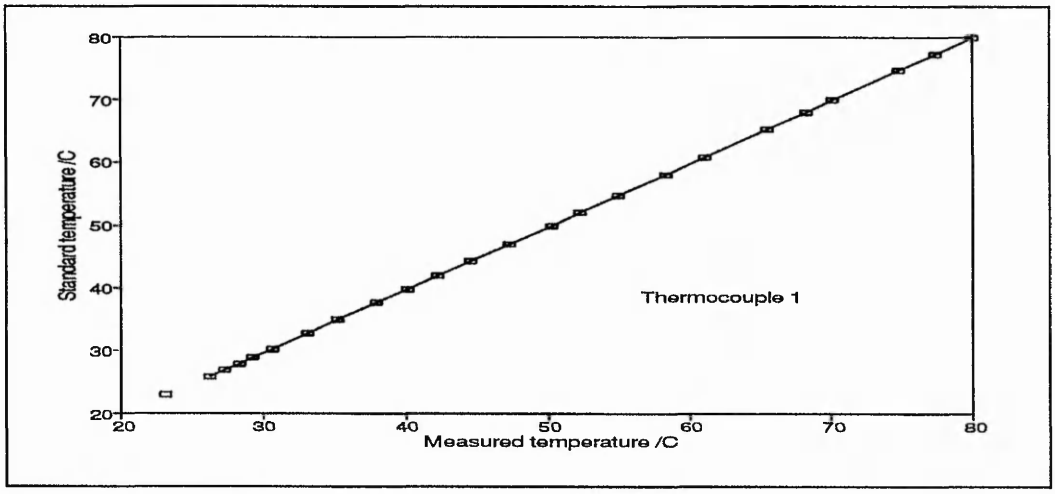

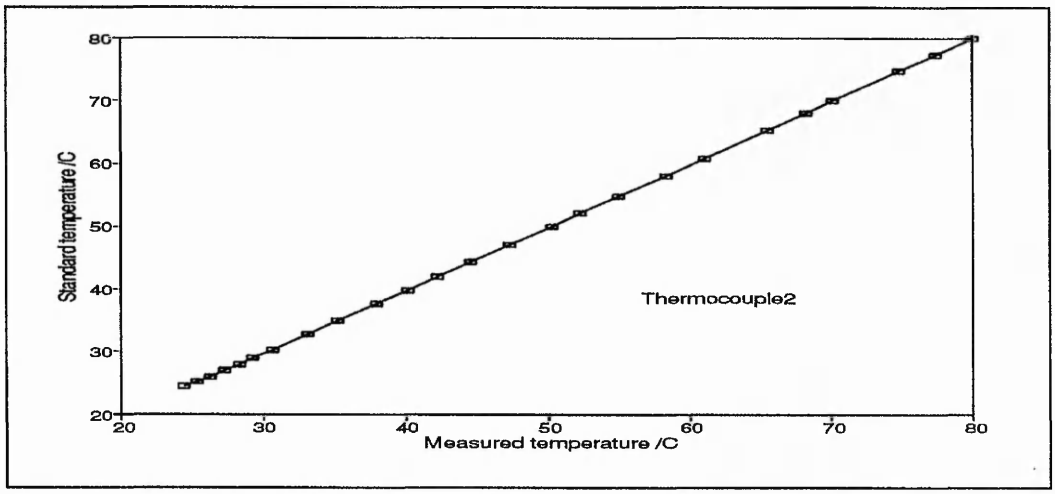

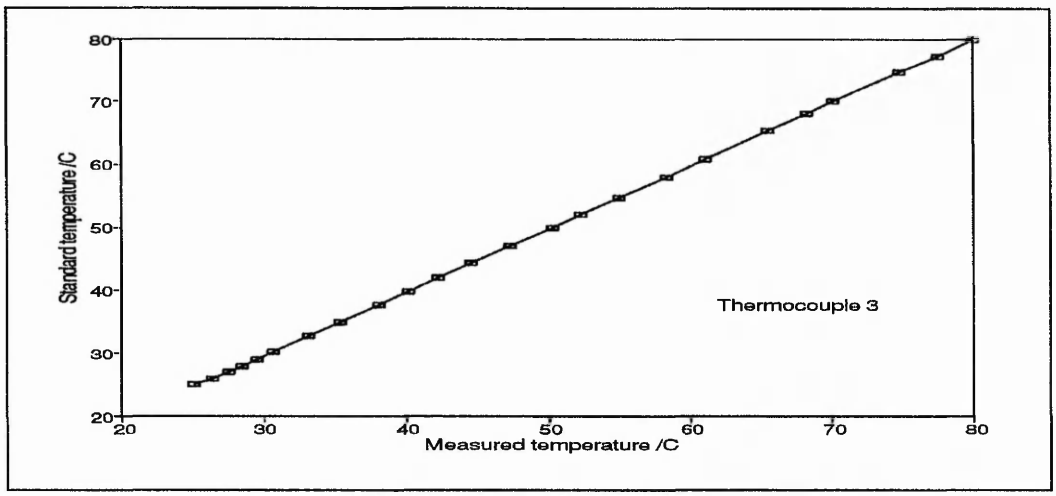

A4.1

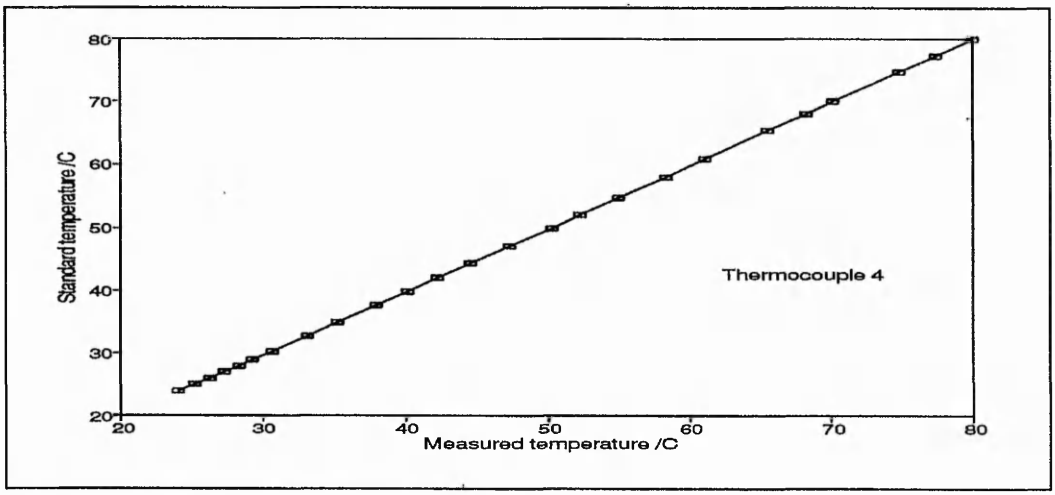

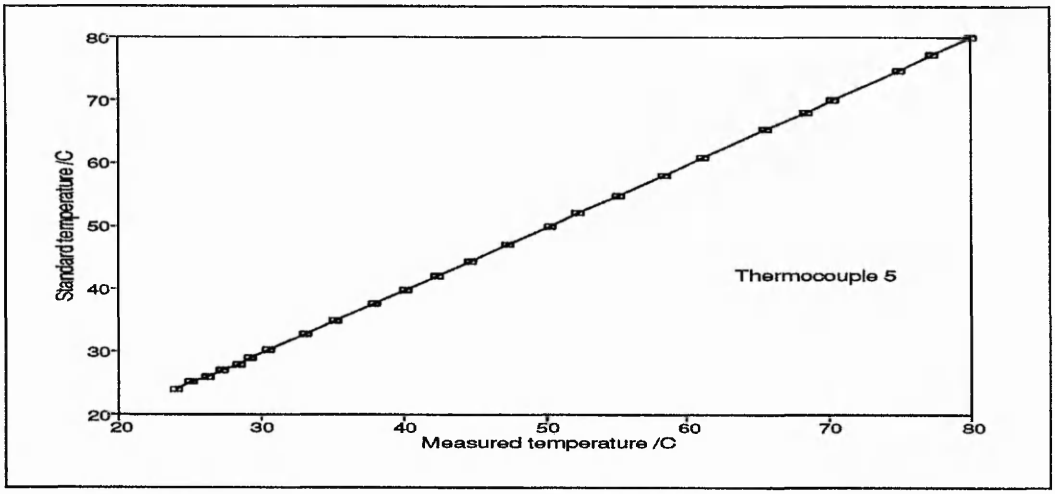

A4.2 Calibration of thermometers

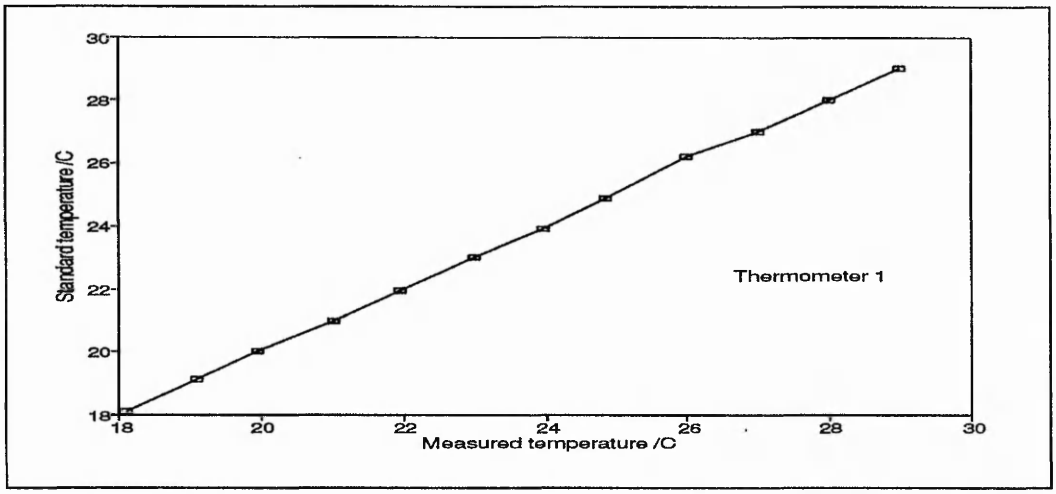

A4.2

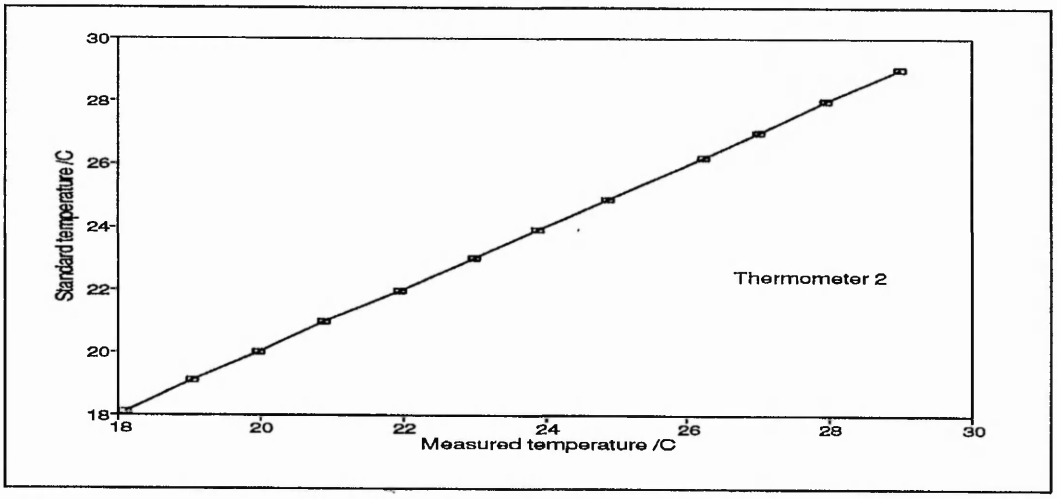

A4.3 Calibration of Bourdon pressure gauge

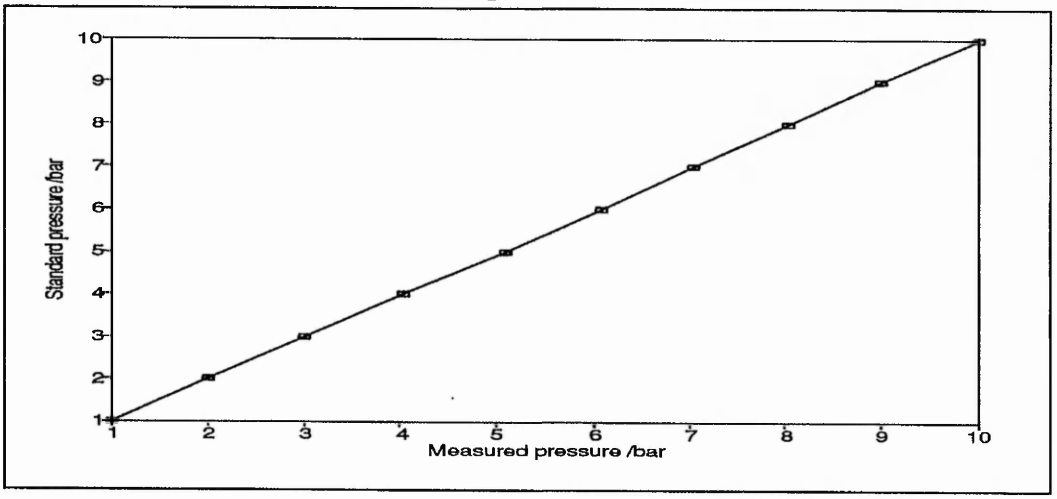

Appendix A5

A5.1 Measurement of the water bath thermal losses at the calibration temperature

Water temperature = 30.0 °C

Duration /s	Energy supplied /kWh	Mean temp /°C	Mean power /W	Thermal losses per unit temp diff. /W K^{-1}
8700	0.190	15.5	78	5.4
5900	0.130	15.7	79	5.5
5160	0.110	15.7	77	5.4
6300	0.140	14.1	80	5.0
6540	0.140	14.4	77	4.9
11280	0.250	14.6	80	5.2

The apparatus specific power loss = 5.2 W K^{-1}

A5.2 Measurement of the thermal flux for the painted calibration plate at the calibration temperature

Water temperature = 30.1 °C

Duration /s	Energy supplied /kW h	Mean air temp /°C	Mean power /W	Corrected power /W	Thermal flux /W m^{-2}
5170	0.130	16.4	90.5	19.3	121
3605	0.090	16.4	89.9	18.7	117
5935	0.150	16.4	91.0	19.8	124
3345	0.084	16.3	90.4	19.2	120
3950	0.098	16.4	89.3	18.1	113
4646	0.116	16.4	89.9	18.7	117

Corrected power = mean power-(specific power loss x temperature difference)
Mean thermal flux = 118 W m^{-2}

Appendix A6

Measurement of the thermal resistance for the sub strata of black paint.

Copper disc without painted face

temperature/°C						water vol/ml	water time/s	temperature/°C		q/ [10^4 W m^{-2}]	th res/ [10^{-5} K m^2 W]
t(1)	t(2)	t(3)	t(4)	t(w1)	t(w2)			t(s1)	t(s2)		
37.3	40.1	43.8	49.1	21.25	28.80	76	114.4	43.06	40.83	4.260	5.235
37.2	40.0	43.6	49.0	21.3	28.75	76	118.8	42.84	40.73	4.048	5.228
37.2	40.1	43.7	49.1	21.25	28.70	79	114.2	42.94	40.85	4.377	4.775
37.3	40.0	43.8	49.2	21.20	28.70	78	116.1	43.04	40.89	4.279	5.031
37.3	40.1	43.7	49.2	21.20	28.70	84	124.7	42.93	40.83	4.291	4.899
											5.033

Copper disc with one face painted.

temperature/°C						water vol/ml	water time/s	temperature/°C		q/ [10^4 W m^{-2}]	th res/ [10^{-5}K m^2 W]
t(1)	t(2)	t(3)	t(4)	t(w1)	t(w2)			t(s1)	t(s2)		
37.3	40.1	48.3	53.7	21.80	29.10	80	121.1	47.54	40.83	4.095	1.640
37.3	40.0	48.2	53.6	21.70	29.10	79	120.7	47.44	40.70	4.114	1.639
37.3	40.0	48.1	53.5	21.60	28.90	77	116.7	47.34	40.70	4.112	1.615
37.3	39.9	48.1	53.4	21.60	28.90	79	119.7	47.36	40.58	4.092	1.657
37.2	39.9	48.1	53.4	21.50	28.90	78	118.8	47.36	40.60	4.126	1.637
											1.638

For a cross sectional area of 1 m^2 the thermal resistance of the paint = 1.64E-4 - 5.03E-5 = 1.14E-4 K W^-1.
Film thickness =0.05 mm. Thermal conductivity of the film= 0.44 W m^-2 K^-1.

Appendix A7
Measured and derived values for a single unconfined jet

A7.1

Test No	Surf temp /°C	Water temp /°C	Air temp /°C	z/d	Orif press /bar	Orif diff /mmwater	Orif temp /°C	radius /mm	Nu	r/d	Re
1	35.3	43.3	17.9	2	0.40	49	20.7	71.0	50	6.9	31500
2	35.3	45.3	17.9	2	0.40	49	20.7	55.0	64	5.4	31500
3	35.3	48.1	20.7	2	0.40	49	20.7	41.0	93	4.0	31500
4	35.3	51.8	20.9	2	0.40	49	20.8	29.0	122	2.8	31500
5	35.3	54.3	20.9	2	0.40	49	20.9	13.0	141	1.3	31600
6	35.3	54.3	20.9	2	0.40	49	20.9	21.0	141	2.0	31600
7	35.3	54.3	20.9	2	0.40	49	20.9	25.0	141	2.4	31600
8	35.3	57.3	20.6	2	0.40	49	21.0	8.0	160	0.8	31600
9	35.3	43.3	17.9	2	0.40	49	20.7	71.0	50	6.9	31500
10	35.3	45.3	17.9	2	0.40	49	20.7	55.0	64	5.4	31500
11	35.3	48.1	20.7	4	0.40	49	20.7	41.0	93	4.0	31500
12	35.3	51.8	20.9	4	0.40	49	20.8	29.0	122	2.8	31500
13	35.3	54.3	20.9	4	0.40	49	20.9	11.0	141	1.1	31600
14	35.3	57.3	20.6	4	0.40	49	21.0	7.0	160	0.7	31700
15	35.3	48.1	20.7	6	0.40	49	20.7	41.0	93	4.0	31500
16	35.3	51.8	20.9	6	0.40	49	20.7	29.0	122	2.8	31500
17	35.3	48.1	20.7	6	0.40	49	20.7	41.0	93	4.0	31500
18	35.3	51.8	20.9	6	0.40	49	20.8	22.0	122	2.1	31500
19	35.3	54.3	20.9	6	0.40	49	20.9	12.0	141	1.2	31600
20	35.3	57.3	20.6	6	0.40	49	21.0	7.0	160	0.7	31600
21	35.3	41.7	18.0	2	0.56	68	18.2	90.5	44	8.8	39500
22	35.3	43.3	17.9	2	0.56	69	17.9	81.0	50	7.9	39900

A7.2

Test No	Surf temp /°C	Water temp /°C	Air temp /°C	z/d	Orif press /bar	Orif diff /mmwater	Orif temp /°C	radius /mm	Nu	r/d	Re
23	35.3	45.3	18.0	2	0.56	69	17.9	59.6	64	5.8	39900
24	35.3	48.5	17.9	2	0.56	69	18.0	47.0	83	4.6	39900
25	35.3	51.0	18.0	2	0.56	69	18.2	41.0	99	4.0	39900
26	35.3	55.5	17.9	2	0.56	69	18.2	30.0	127	2.9	39400
27	35.3	58.5	20.0	2	0.56	69	20.5	24.0	165	2.3	39000
28	35.3	58.5	20.0	2	0.56	69	20.5	9.0	165	0.9	39000
29	35.3	60.7	19.4	2	0.56	69	19.6	20.0	175	1.9	39200
30	35.3	60.7	19.4	2	0.56	69	19.6	17.0	175	1.7	39200
31	35.3	60.7	19.4	2	0.56	69	19.6	7.0	175	0.7	39200
32	35.3	45.7	18.0	2	1.00	110	20.5	77.0	67	7.5	55500
33	35.3	48.0	20.5	2	1.00	110	20.5	58.0	91	5.6	55500
34	35.3	51.8	20.7	2	1.00	110	21.0	42.0	120	4.1	55500
35	35.3	54.2	20.6	2	1.00	110	21.1	39.0	135	3.8	55500
36	35.3	57.3	20.6	2	1.00	110	21.2	32.0	160	3.1	55500
37	35.3	59.5	21.0	2	1.00	110	22.4	12.0	180	1.2	55500
38	35.3	59.5	21.0	2	1.00	110	22.4	17.0	180	1.7	55500
39	35.3	59.5	21.0	2	1.00	110	22.4	28.0	180	2.7	55500
40	35.3	61.5	20.6	2	1.00	110	21.2	9.0	192	0.9	55500
41	35.3	61.5	20.6	2	1.00	110	21.2	14.0	192	1.4	55500
42	35.3	61.5	20.6	2	1.00	110	21.2	24.0	192	2.3	55500
43	35.3	64.3	20.8	2	1.00	110	21.4	8.0	216	0.8	55500
44	35.3	45.7	18.0	4	1.00	110	20.5	77.0	67	7.5	55500

A7.3

Test No	Surf temp /°C	Water temp /°C	Air temp /°C	z/d	Orif press /bar	Orif diff /mmwater	Orif temp /°C	radius /mm	Nu	r/d	Re
45	35.3	48.0	20.5	4	1.00	110	20.5	58.0	91	5.6	55500
46	35.3	51.8	20.7	4	1.00	110	21.0	42.0	120	4.1	55500
47	35.3	54.2	20.6	4	1.00	110	21.1	39.0	135	3.8	55500
48	35.3	57.3	20.6	4	1.00	110	21.2	29.0	160	2.8	55500
49	35.3	59.5	21.0	4	1.00	110	22.4	26.0	180	2.5	55500
50	35.3	61.5	20.6	4	1.00	110	21.2	9.0	192	0.9	55500
51	35.3	61.5	20.6	4	1.00	110	21.2	18.0	192	1.8	55500
52	35.3	61.5	20.6	4	1.00	110	21.2	21.0	192	2.0	55500
53	35.3	64.3	20.8	4	1.00	110	21.4	8.0	216	0.8	55500
54	35.3	45.7	18.0	6	1.00	110	20.5	77.0	67	7.5	55500
55	35.3	48.0	20.5	6	1.00	110	20.5	58.0	91	5.6	55500
56	35.3	51.8	20.7	6	1.00	110	21.0	42.0	120	4.1	55500
57	35.3	54.2	20.6	6	1.00	110	21.1	33.0	135	3.2	55500
58	35.3	57.3	20.6	6	1.00	110	21.2	30.0	160	2.9	55500
59	35.3	59.5	21.0	6	1.00	110	22.4	17.0	180	1.7	55500
60	35.3	61.5	20.6	6	1.00	110	21.2	13.0	192	1.3	55500
61	35.3	64.3	20.8	6	1.00	110	21.4	8.0	216	0.8	55500
62	35.3	45.7	18.0	2	1.40	144	19.6	82.2	67	8.0	70000
63	35.3	49.2	18.0	2	1.40	144	19.7	61.7	90	6.0	70000
64	35.3	51.3	18.5	2	1.40	143	19.6	51.4	107	5.0	69500
65	35.3	55.2	18.5	2	1.40	143	19.5	41.1	133	4.0	69500
66	35.3	57.5	18.8	2	1.40	146	19.3	36.0	151	3.5	71000

A7.4

Test No	Surf temp °/C	Water temp /°C	Air temp /°C	z/d	Orif press /bar	Orif diff /mmwater	Orif temp /°C	radius /mm	Nu	r/d	Re
67	35.3	60.8	18.9	2	1.40	146	19.3	30.8	175	3.0	71000
68	35.3	65.6	19.0	2	1.40	145	19.3	25.7	209	2.5	70000
69	35.3	64.0	19.0	2	1.40	143	19.2	22.6	198	2.2	69000
70	35.3	64.0	19.0	2	1.40	143	19.3	10.3	198	1.0	70000
71	35.3	62.8	19.2	2	1.40	144	19.1	18.5	192	1.8	70000
72	35.3	63.0	19.1	2	1.40	144	19.3	12.3	192	1.2	70000
73	35.3	47.5	17.1	2	2.60	250	18.5	86.4	75	8.4	112800
74	35.3	50.9	17.1	2	2.60	250	18.5	71.0	94	6.9	112800
75	35.3	53.9	16.6	2	2.60	250	18.1	63.0	109	6.1	112900
76	35.3	56.9	16.7	2	2.60	250	18.2	54.0	127	5.3	112900
77	35.3	61.8	17.3	2	2.60	250	18.6	42.0	162	4.1	112700
78	35.3	65.9	17.7	2	2.60	250	19.2	39.0	191	3.8	112000
79	35.3	69.5	17.5	2	2.60	250	19.0	35.0	211	3.4	112500
80	35.3	74.0	17.9	2	2.60	250	19.5	30.0	245	2.9	112300
81	35.3	78.3	18.8	2	2.60	250	21.0	28.0	288	2.7	111900
82	35.3	78.3	18.8	2	2.60	250	21.0	14.5	288	1.4	111900
83	35.3	78.3	18.8	2	2.60	250	21.0	8.0	288	0.8	111900
84	35.3	80.3	18.9	2	2.60	250	20.3	26.5	300	2.6	112000
85	35.3	80.3	18.9	2	2.60	250	20.3	14.5	300	1.4	112000
86	35.3	80.3	18.9	2	2.60	250	20.3	7.0	300	0.7	112000
87	35.3	80.9	18.9	2	2.60	250	20.3	24.5	315	2.4	112300
88	35.3	81.6	18.9	2	2.60	250	20.2	18.5	320	1.8	112300

A7.5

Test No	Surf temp /°C	Water temp /°C	Air temp /°C	z/d	Orif press /bar	Orif diff /mmwater	Orif temp /°C	radius /mm	Nu	r/d	Re
89	35.3	51.7	19.6	2	3.00	280	19.7	70.0	112	6.8	125000
90	35.3	54.2	19.7	2	3.00	280	20.8	60.0	130	5.8	125500
91	35.3	57.3	19.9	2	3.00	280	21.0	52.0	154	5.1	125000
92	35.3	59.3	20.0	2	3.00	280	21.4	46.0	170	4.5	125000
93	35.3	61.4	19.8	2	3.00	280	21.3	41.0	182	4.0	124000
94	35.3	64.1	20.1	2	3.00	280	21.7	38.0	205	3.7	124000
95	35.3	72.5	19.3	2	3.00	280	21.3	39.0	262	3.8	124000
96	35.3	80.2	19.3	2	3.00	280	21.3	27.0	318	2.6	124000
97	35.3	80.2	19.3	2	3.00	280	21.3	16.0	318	1.6	124000
98	35.3	83.9	19.3	2	3.00	280	21.3	24.0	340	2.3	124000
99	35.3	83.8	19.6	4	3.00	280	19.7	67.0	112	6.5	125000
100	35.3	54.2	19.7	4	3.00	280	20.8	60.0	130	5.8	125500
101	35.3	57.3	19.9	4	3.00	280	21.0	48.0	154	4.7	125000
102	35.3	59.3	20.0	4	3.00	280	21.4	46.0	170	4.5	125000
103	35.3	61.4	19.8	4	3.00	280	21.3	41.0	182	4.0	124000
104	35.3	64.1	20.1	4	3.00	280	21.7	38.0	205	3.7	124000
105	35.3	72.1	18.8	4	3.00	280	21.7	29.0	252	2.8	125000
106	35.3	78.8	19.1	4	3.00	280	21.3	24.0	304	2.3	124500
107	35.3	78.8	19.1	4	3.00	280	21.9	21.0	304	2.0	124500
108	35.3	51.7	19.6	6	3.00	280	19.7	68.0	112	6.6	125000
109	35.3	54.2	19.7	6	3.00	280	20.8	60.0	130	5.8	125000
110	35.3	57.3	19.9	6	3.00	280	21.0	50.0	154	4.9	125000

A7.6

Test No	Surf temp /°C	Water temp /°C	Air temp /°C	z/d	Orif press /bar	Orif diff /mmwater	Orif temp /°C	Radius /mm	Nu	r/d	Re
111	35.3	59.3	20.2	6	3.00	280	21.4	46.0	170	4.5	125000
112	35.3	61.4	19.8	6	3.00	280	21.3	41.0	182	4.0	124000
113	35.3	64.1	20.1	6	3.00	280	21.9	37.0	205	3.6	124000
114	35.3	74.4	18.4	6	3.00	280	21.9	24.0	262	2.3	124500
115	35.3	80.5	18.2	6	3.00	280	21.9	14.0	300	1.4	124500
116	35.3	49.8	18.8	2	3.60	334	19.7	87.5	98	8.5	146000
117	35.3	50.3	18.9	2	3.60	333	19.5	84.5	102	8.2	146000
118	35.3	51.2	19.1	2	3.60	332	19.6	78.0	110	7.6	146000
119	35.3	54.7	19.1	2	3.60	331	19.6	64.0	134	6.2	145000
120	35.3	61.4	19.7	2	3.60	330	21.2	46.0	181	4.5	145000
121	35.3	63.4	19.1	2	3.60	331	19.6	43.0	195	4.2	145000
122	35.3	64.1	20.0	2	3.60	330	21.6	42.0	204	4.1	145000
123	35.3	72.5	19.3	2	3.60	338	19.6	32.0	262	3.1	147000
124	35.3	80.2	19.3	2	3.60	338	19.6	10.0	318	1.0	147000
125	35.3	80.2	19.3	2	3.60	338	19.6	14.5	318	1.4	147000
126	35.3	80.2	19.3	2	3.60	338	19.6	28.0	318	2.7	147000
127	35.3	83.8	19.1	2	3.60	333	19.5	25.5	340	2.5	146000
128	35.3	84.5	19.1	2	3.60	333	19.4	21.5	345	2.1	145000
129	35.3	42.2	17.9	4	0.56	69	17.9	91.5	44	8.9	39900
130	35.3	43.3	17.9	4	0.56	69	17.9	77.0	50	7.5	39900
131	35.3	44.5	18.1	4	0.56	69	17.8	61.7	60	6.0	39900
132	35.3	48.7	18.0	4	0.56	69	18.1	45.0	85	4.4	39900

A7.7

Test No	Surf temp /°C	Water temp /°C	Air temp /°C	z/d	Orif press /bar	Orif diff /mmwater	Orif temp /°C	radius mm	Nu	r/d	Re
133	35.3	51.0	18.0	4	0.56	69	18.1	42.0	99	4.1	39900
134	35.3	55.5	17.8	4	0.56	69	17.9	30.0	126	2.9	39500
135	35.3	58.5	19.9	4	0.56	69	20.3	10.0	165	1.0	39100
136	35.3	58.5	19.9	4	0.56	69	20.3	16.5	165	1.6	39100
137	35.3	58.5	19.9	4	0.56	69	20.3	21.5	165	2.1	39100
138	35.3	61.4	18.0	4	0.56	69	20.1	19.5	170	1.9	39200
139	35.3	61.4	18.0	4	0.56	69	20.1	8.0	170	0.8	39200
140	35.3	62.3	18.0	4	0.56	69	20.0	7.0	176	0.7	39200
141	35.3	44.5	19.2	4	1.40	143	19.6	87.0	64	8.5	70000
142	35.3	46.7	19.4	4	1.40	142	19.5	69.0	80	6.7	69500
143	35.3	48.8	19.4	4	1.40	142	19.5	60.0	95	5.8	69500
144	35.3	53.7	19.1	4	1.40	143	19.6	43.0	127	4.2	70000
145	35.3	55.6	19.2	4	1.40	145	19.4	37.0	141	3.6	71000
146	35.3	59.7	19.0	4	1.40	142	19.3	31.0	168	3.0	70000
147	35.3	63.7	19.0	4	1.40	142	19.3	21.5	196	2.1	70000
148	35.3	63.5	19.1	4	1.40	142	19.3	12.5	196	1.2	69500
149	35.3	64.8	19.1	4	1.40	142	19.3	24.5	205	2.4	69500
150	35.3	64.5	19.3	4	1.40	143	19.5	9.3	205	0.9	70000
151	35.3	46.4	18.8	4	2.62	250	21.0	85.5	75	8.3	112800
152	35.3	94.0	17.1	4	2.62	250	18.5	71.0	94	6.9	112800
153	35.3	53.9	16.6	4	2.62	250	18.1	63.0	109	6.1	113000
154	35.3	56.9	16.7	4	2.62	250	18.2	54.0	128	5.3	113000

A7.8

Test No	Surf temp /°C	Water temp /°C	Air temp /°C	z/d	Orif press /bar	Orif diff /mmwater	Orif temp /°C	radius /mm	Nu	r/d	Re
155	35.3	61.8	17.3	4	2.62	250	18.6	42.0	162	4.1	112700
156	35.3	65.9	17.7	4	2.62	250	19.2	39.0	191	3.8	112500
157	35.3	69.5	17.5	4	2.62	250	19.0	35.0	211	3.4	112500
158	35.3	74.0	17.9	4	2.62	250	19.5	30.0	245	2.9	112300
159	35.3	78.3	18.8	4	2.62	250	19.5	24.0	287	2.3	112000
160	35.3	78.3	18.8	4	2.62	250	19.4	17.5	287	1.7	112000
161	35.3	78.3	18.8	4	2.62	250	19.4	14.5	288	1.4	112000
162	35.3	78.7	18.9	4	2.62	250	20.3	20.5	300	2.0	112000
163	35.3	80.3	18.9	4	2.62	250	20.3	6.0	300	0.6	112000
164	35.3	49.4	18.9	4	3.60	333	19.9	86.5	96	8.4	146000
165	35.3	50.4	18.9	4	3.60	333	20.0	80.0	103	7.8	146000
166	35.3	53.3	18.6	4	3.60	331	20.0	68.0	121	6.6	145000
167	35.3	59.8	18.6	4	3.60	334	19.9	49.5	165	4.8	145000
168	35.3	61.4	19.7	4	3.60	330	21.2	46.0	181	4.5	145000
169	35.3	64.1	20.0	4	3.60	330	21.6	41.0	204	4.0	145000
170	35.3	66.3	18.8	4	3.60	335	19.9	38.0	212	3.7	146000
171	35.3	72.1	18.8	4	3.60	333	19.8	32.0	252	3.1	145000
172	35.3	78.8	19.1	4	3.60	333	19.8	25.5	304	2.5	146000
173	35.3	79.9	19.1	4	3.60	331	19.9	14.5	312	1.4	145000
174	35.3	80.5	19.1	4	3.60	333	19.7	22.5	316	2.2	146000
175	35.3	80.5	19.1	4	3.60	333	19.7	18.5	316	1.8	146000
176	35.3	82.7	18.7	4	3.60	336	19.8	20.5	324	2.0	146000

A7.9

Test No	Surf temp /°C	Water temp /°C	Air temp /°C	z/d	Orif press /bar	Orif diff /mmwater	Orif temp /°C	radius /mm	Nu	r/d	Re
177	35.3	42.2	17.9	6	0.56	69	17.9	90.5	44	8.8	39900
178	35.3	43.3	17.9	6	0.56	69	17.9	77.0	50	7.5	39900
179	35.3	45.3	17.9	6	0.56	69	17.9	57.6	64	5.6	39900
180	35.3	48.7	18.1	6	0.56	69	18.2	45.0	85	4.4	39900
181	35.3	51.0	17.9	6	0.56	69	18.0	41.0	99	4.0	39900
182	35.3	53.4	18.4	6	0.56	69	18.8	31.0	117	3.0	39300
183	35.3	55.5	17.7	6	0.56	69	17.9	21.0	126	2.0	39500
184	35.3	58.5	19.8	6	0.56	69	19.1	13.0	163	1.3	39300
185	35.3	60.8	19.6	6	0.56	69	19.9	8.0	177	0.8	39100
186	35.3	45.1	18.1	6	1.40	142	18.5	81.2	64	7.9	70000
187	35.3	46.8	18.1	6	1.40	140	18.5	72.0	75	7.0	69500
188	35.3	48.6	18.2	6	1.40	145	18.6	62.0	87	6.0	70100
189	35.3	53.3	18.2	6	1.40	146	18.8	47.0	118	4.6	71000
190	35.3	56.9	18.2	6	1.40	146	18.8	36.0	142	3.5	71000
191	35.3	60.6	17.9	6	1.40	142	18.7	30.8	164	3.0	70000
192	35.3	66.7	17.9	6	1.40	140	18.7	24.7	204	2.4	69500
193	35.3	70.1	18.2	6	1.40	142	18.7	14.4	230	1.4	70000
194	35.3	47.5	17.1	6	2.62	250	18.5	86.4	75	8.4	112900
195	35.3	50.9	17.1	6	2.62	250	18.5	71.0	94	6.9	112800
196	35.3	53.9	16.6	6	2.62	250	18.1	63.0	109	6.1	113000
197	35.3	56.9	16.7	6	2.62	250	18.2	54.0	128	5.3	112900
198	35.3	61.8	17.3	6	2.62	250	18.6	42.0	162	4.1	112700

A7.10

Test No	Surf temp /°C	Water temp /°C	Air temp /°C	z/d	Orif press /bar	Orif diff /mmwater	Orif temp /°C	radius /mm	Nu	r/d	Re
199	35.3	65.9	17.7	6	2.62	250	19.2	35.0	191	3.4	112400
200	35.3	68.5	17.5	6	2.62	250	19.2	30.8	211	3.0	112500
201	35.3	74.0	17.9	6	2.62	250	19.5	22.5	245	2.2	112300
202	35.3	78.3	18.8	6	2.62	250	21.0	13.0	288	1.3	111900
203	35.3	80.3	18.9	6	2.62	250	20.3	11.0	300	1.1	112000
204	35.3	83.0	18.9	6	2.62	250	20.3	8.2	330	0.8	112400
205	35.3	49.5	19.1	6	3.60	333	19.8	82.2	98	8.0	146000
206	35.3	50.9	19.0	6	3.60	334	19.7	75.0	107	7.3	146000
207	35.3	53.1	19.0	6	3.60	336	19.7	65.8	122	6.4	147000
208	35.3	55.9	18.7	6	3.60	334	19.5	57.6	139	5.6	146000
209	35.3	61.4	19.7	6	3.60	330	21.2	47.0	181	4.6	145000
210	35.3	63.2	18.6	6	3.60	333	19.4	47.3	188	4.6	146000
211	35.3	64.1	20.0	6	3.60	330	21.6	41.0	204	4.0	145000
212	35.3	67.7	18.6	6	3.60	331	19.4	36.0	219	3.5	145500
213	35.3	74.4	18.4	6	3.60	333	19.5	29.8	262	2.9	146000
214	35.3	80.5	18.2	6	3.60	335	19.6	20.6	300	2.0	147000
215	35.3	83.4	18.2	6	3.60	332	19.2	15.4	320	1.5	146000
216	35.3	45.2	19.3	2	0.56	69	20.5	64.0	65	6.2	39400
217	35.3	48.3	19.6	2	0.56	69	19.6	48.0	88	4.7	39400
218	35.3	51.4	19.7	2	0.56	69	19.9	40.0	110	3.9	39400
219	35.3	54.5	19.8	2	0.56	69	20.0	30.0	132	2.9	39400
220	35.3	54.5	20.0	2	0.56	69	20.0	11.0	156	1.1	39400

A7.11

Test No	Surf temp /°C	Water temp /°C	Air temp /°C	z/d	Orif press /bar	Orif diff /mmwater	Orif temp /°C	Radius (r) mm	Nu	r/d	Re
221	35.3	54.5	20.0	2	0.56	69	20.0	14.0	156	1.4	39400
222	35.3	54.5	20.0	2	0.56	69	20.0	27.0	156	2.6	39400
223	35.3	48.1	20.7	2	0.60	70	20.7	47.0	93	4.6	40000
224	35.3	48.1	20.7	4	0.60	70	20.7	47.0	93	4.6	40000
225	35.3	48.1	20.7	6	0.60	70	20.7	47.0	93	4.6	40000
226	35.3	48.0	20.2	2	1.40	144	20.5	63.0	91	6.1	69700
227	35.3	51.8	20.7	2	1.40	144	21.0	49.0	120	4.8	70000
228	35.3	57.3	20.6	2	1.40	144	21.2	35.0	160	3.4	70000
229	35.3	59.4	20.9	2	1.40	144	21.5	32.0	180	3.1	70000
230	35.3	61.4	20.4	2	1.40	144	21.3	28.0	189	2.7	69500
231	35.3	64.2	21.0	2	1.40	144	21.9	6.0	218	0.6	69500
232	35.3	64.2	21.0	2	1.40	144	21.9	22.0	218	2.1	69500
233	35.3	48.0	20.2	4	1.40	144	20.5	61.0	91	5.9	69700
234	35.3	51.8	20.7	4	1.40	144	21.0	49.0	120	4.8	70000
235	35.3	54.2	20.6	4	1.40	144	21.0	40.0	135	3.9	70000
236	35.3	57.3	20.6	4	1.40	144	21.2	35.0	160	3.4	70000
237	35.3	59.4	20.9	4	1.40	144	21.5	30.0	180	2.9	70000
238	35.3	61.4	20.4	4	1.40	144	21.3	27.0	189	2.6	69500
239	35.3	64.2	21.0	4	1.40	144	21.9	8.0	218	0.8	69500
240	35.3	64.2	21.0	4	1.40	144	21.9	26.0	218	2.5	69500
241	35.3	48.0	20.2	6	1.40	144	20.5	61.0	91	5.9	69700
242	35.3	51.8	20.7	6	1.40	144	21.0	49.0	120	4.8	70000

A7.12

Test No	Surf temp /°C	Water temp /°C	Air temp /°C	z/d	Orif press /bar	Orif diff /mmwater	Orif temp /°C	Radius (r) mm	Nu	r/d	Re
243	35.3	54.2	20.6	6	1.40	144	21.0	38.0	135	3.7	70000
244	35.3	57.3	20.6	6	1.40	144	21.2	32.0	160	3.1	70000
245	35.3	59.4	20.9	6	1.40	144	21.5	28.0	180	2.7	70000
246	35.3	61.4	20.4	6	1.40	144	21.3	21.0	189	2.0	69500
247	35.3	64.2	21.0	6	1.40	144	21.9	16.0	218	1.6	69500

Appendix A8
Measured and derived values for a single semi-confined jet

A8.1

Test No	Surf temp /°C	Water temp /°C	Air temp /°C	z/d	Orif press /bar	Orif diff /mmwater	Orif temp /°C	radius /mm	Nu	r/d	Re
1	31.2	35.5	17.7	2	0.4	49	20.7	70.0	31	6.8	31000
2	31.2	36.7	17.2	2	0.4	49	20.7	54.5	39	5.3	31000
3	31.2	35.5	21.6	2	0.4	49	20.8	50.0	45	4.9	31000
4	31.2	37.6	22.0	2	0.4	49	20.5	35.0	72	3.4	31000
5	31.2	39.5	21.5	2	0.4	49	21.0	27.4	89	2.7	30500
6	31.2	44.6	18.5	2	0.4	49	20.0	26.2	111	2.6	31100
7	31.2	41.5	21.0	2	0.4	49	21.0	24.7	105	2.4	30500
8	31.2	43.5	21.6	2	0.4	49	21.0	22.6	134	2.2	30700
9	31.2	47.6	17.8	2	0.4	49	19.0	22.5	130	2.2	31500
10	31.2	47.6	17.8	2	0.4	49	19.0	15.0	130	1.5	31500
11	31.2	43.5	21.6	2	0.4	49	21.0	15.0	134	1.5	30500
12	31.2	47.6	17.8	2	0.4	49	19.0	11.5	130	1.1	31600
13	31.2	43.5	21.6	2	0.4	49	21.0	10.0	134	1.0	30400
14	31.2	35.5	17.5	2	0.56	69	18.0	82.2	31	8.0	39200
15	31.2	36.7	17.2	2	0.56	69	19.0	65.0	39	6.3	39100
16	31.2	35.5	21.9	2	0.56	69	21.0	54.9	46	5.3	38800
17	31.2	37.6	22.2	2	0.56	69	21.0	37.5	73	3.7	38800
18	31.2	39.5	21.5	2	0.56	69	21.0	30.0	89	2.9	38800
19	31.2	44.6	18.5	2	0.56	69	19.0	28.8	111	2.8	39100
20	31.2	41.5	21.1	2	0.56	69	21.0	27.4	106	2.7	38800
21	31.2	47.6	18.0	2	0.56	69	19.0	26.4	132	2.6	39100
22	31.2	43.5	21.5	2	0.56	69	21.0	25.0	133	2.4	38800

A8.2

Test No	Surf temp /°C	Water temp /°C	Air temp /°C	z/d	Orif press /bar	Orif diff /mmwater	Orif temp /°C	radius /mm	Nu	r/d	Re
23	31.2	50.7	17.9	2	0.56	69	18.0	22.4	156	2.2	39300
24	31.2	50.7	17.9	2	0.56	69	18.0	17.5	156	1.7	39300
25	31.2	45.5	21.0	2	0.56	69	21.0	15.0	148	1.5	38800
26	31.2	50.7	17.9	2	0.56	69	18.0	10.3	156	1.0	39300
27	31.2	35.5	22.0	2	1.00	110	20.5	70.0	46	6.8	54700
28	31.2	37.6	22.4	2	1.00	110	21.0	45.2	74	4.4	54500
29	31.2	39.5	21.4	2	1.00	110	21.0	40.0	88	3.9	55000
30	31.2	41.5	21.0	2	1.00	110	21.0	32.5	106	3.2	54500
31	31.2	43.5	21.3	2	1.00	110	21.5	30.0	131	2.9	54350
32	31.2	47.6	17.9	2	1.00	110	19.0	30.0	131	2.9	55000
33	31.2	50.7	17.1	2	1.00	110	17.0	28.0	148	2.7	55000
34	31.2	45.5	21.2	2	1.00	110	21.0	27.4	151	2.7	54500
35	31.2	47.5	19.7	2	1.00	110	20.0	27.4	151	2.7	54700
36	31.2	54.6	14.1	2	1.00	110	16.0	26.5	147	2.6	55370
37	31.2	50.7	17.8	2	1.00	110	18.0	26.4	155	2.6	55200
38	31.2	57.8	15.4	2	1.00	110	16.0	22.5	182	2.2	55370
39	31.2	50.1	19.1	2	1.00	110	20.0	22.5	167	2.2	54700
40	31.2	52.9	17.7	2	1.00	110	18.0	19.9	173	1.9	54750
41	31.2	61.0	14.5	2	1.00	110	16.0	19.5	194	1.9	55300
42	31.2	61.0	14.5	2	1.00	110	16.0	15.4	194	1.5	55300
43	31.2	52.9	17.7	2	1.00	110	18.0	15.0	173	1.5	54750
44	31.2	57.8	15.4	2	1.00	110	16.0	15.0	182	1.5	55370

A8.3

Test No	Surf temp /°C	Water temp /°C	Air temp /°C	z/d	Orif press /bar	Orif diff /mmwater	Orif temp /°C	radius /mm	Nu	r/d	Re
45	31.2	57.8	15.4	2	1.00	110	16.0	12.3	182	1.2	55370
46	31.2	61.0	14.5	2	1.00	110	16.0	10.3	194	1.0	55300
47	31.2	52.9	17.7	2	1.00	110	18.0	10.0	173	1.0	54750
48	31.2	35.5	22.0	2	1.40	144	21.0	80.2	46	7.8	69000
49	31.2	37.6	22.3	2	1.40	144	21.0	52.4	73	5.1	69500
50	31.2	39.5	21.2	2	1.40	142	21.0	44.9	86	4.4	69000
51	31.2	41.5	21.0	2	1.40	146	21.0	40.1	105	3.9	69000
52	31.2	43.5	21.1	2	1.40	144	21.5	35.0	128	3.4	69400
53	31.2	47.6	17.7	2	1.40	144	19.0	33.4	129	3.3	69500
54	31.2	45.5	21.1	2	1.40	145	21.0	30.0	149	2.9	69500
55	31.2	50.7	16.9	2	1.40	144	18.0	30.0	146	2.9	69500
56	31.2	50.7	17.6	2	1.40	146	18.0	30.0	153	2.9	69800
57	31.2	47.5	19.6	2	1.40	146	20.0	30.0	149	2.9	69800
58	31.2	54.6	14.0	2	1.40	144	18.0	30.0	147	2.9	69000
59	31.2	50.1	19.0	2	1.40	144	20.0	27.4	165	2.7	69800
60	31.2	57.8	16.3	2	1.40	145	18.0	27.4	180	2.7	69000
61	31.2	52.9	17.7	2	1.40	145	17.7	27.4	172	2.7	69300
62	31.2	53.3	18.6	2	1.40	145	19.0	25.0	188	2.4	69200
63	31.2	61.0	14.7	2	1.40	144	16.0	23.6	196	2.3	70000
64	31.2	55.8	18.1	2	1.40	144	19.0	22.5	202	2.2	69200
65	31.2	58.2	18.6	2	1.40	143	19.0	22.5	231	2.2	69200
66	31.2	58.2	18.6	2	1.40	146	19.0	16.4	231	1.6	69200

A8.4

Test No	Surf temp /°C	Water temp /°C	Air temp /°C	z/d	Orif press /bar	Orif diff /mmwater	Orif temp /°C	radius /mm	Nu	r/d	Re
67	31.2	55.8	18.1	2	1.40	145	19.0	15.0	202	1.5	69200
68	31.2	55.8	18.1	2	1.40	146	19.0	12.3	202	1.2	69200
69	31.2	58.2	18.6	2	1.40	146	19.0	10.3	231	1.0	69200
70	31.2	41.6	17.8	2	2.00	195	18.0	59.6	82	5.8	89300
71	31.2	44.4	17.7	2	2.00	196	20.0	47.5	103	4.6	89000
72	31.2	41.6	20.7	2	2.00	196	20.0	44.9	103	4.4	88500
73	31.2	47.3	19.1	2	2.00	195	20.0	36.0	141	3.5	89000
74	31.2	50.7	16.7	2	2.00	197	17.0	35.0	144	3.4	89500
75	31.2	54.6	13.8	2	2.00	197	16.0	33.9	145	3.3	90000
76	31.2	52.9	17.3	2	2.00	195	18.0	30.9	167	3.0	89120
77	31.2	57.8	15.1	2	2.00	197	16.0	30.0	178	2.9	90000
78	31.2	55.8	17.9	2	2.00	195	19.0	30.0	199	2.9	89000
79	31.2	61.0	14.2	2	2.00	197	16.0	29.8	191	2.9	90000
80	31.2	58.2	18.3	2	2.00	195	19.0	25.0	225	2.4	89000
81	31.2	38.5	18.2	2	2.50	248	19.0	85.0	58	8.3	111600
82	31.2	41.6	17.9	2	2.50	250	18.0	70.0	82	6.8	112000
83	31.2	41.6	20.7	2	2.50	245	20.0	52.4	104	5.1	111100
84	31.2	44.4	17.7	2	2.50	248	20.0	52.4	103	5.1	111300
85	31.2	50.7	16.5	2	2.50	250	17.0	40.0	142	3.9	113000
86	31.2	47.5	19.2	2	2.50	250	20.0	40.0	144	3.9	112500
87	31.2	47.3	19.0	2	2.50	248	20.0	40.0	140	3.9	111300
88	31.2	54.1	13.6	2	2.50	250	16.0	39.0	143	3.8	113000

A8.5

Test No	Surf temp /°C	Water temp /°C	Air temp /°C	z/d	Orif press /bar	Orif diff /mmwater	Orif temp /°C	radius /mm	Nu	r/d	Re
89	31.2	52.9	17.1	2	2.50	248	18.0	36.5	165	3.6	111800
90	31.2	57.8	15.0	2	2.50	250	16.0	35.0	178	3.4	113000
91	31.2	55.8	17.6	2	2.50	248	19.0	33.5	195	3.3	111600
92	31.2	61.0	14.1	2	2.50	250	16.0	32.9	190	3.2	113000
93	31.2	58.2	18.2	2	2.50	248	18.0	30.0	224	2.9	112000
94	31.2	63.1	17.3	2	2.50	248	18.0	27.0	250	2.6	112000
95	31.2	66.1	18.3	2	2.50	248	19.0	25.0	294	2.4	111600
96	31.2	67	19	2	2.50	248	19.0	22.6	315	2.2	111500
97	31.2	68	19	2	2.50	248	18.8	20.6	320	2	111600
98	31.2	67	19	2	2.50	248	19.0	18.5	315	1.8	111600
99	31.2	68	19	2	2.50	249	19.0	12.3	320	1.2	111700
100	31.2	38.3	18.1	2	3.00	280	19.0	92.5	58	9.0	123500
101	31.2	41.6	17.9	2	3.00	285	18.0	74.9	82	7.3	124100
102	31.2	44.4	17.7	2	3.00	284	19.0	57.5	103	5.6	124000
103	31.2	41.6	20.7	2	3.00	283	20.0	57.5	103	5.6	123000
104	31.2	50.7	16.5	2	3.00	284	17.0	44.9	143	4.4	124400
105	31.2	47.3	18.6	2	3.00	284	20.0	44.9	136	4.4	123500
106	31.2	54.6	13.6	2	3.00	284	16.0	41.0	143	4.0	125100
107	31.2	52.9	17.1	2	3.00	283	18.0	40.0	165	3.9	124100
108	31.2	57.8	15.0	2	3.00	286	16.0	36.0	177	3.5	125100
109	31.2	61.0	14.1	2	3.00	286	17.0	35.0	189	3.4	124600
110	31.2	55.8	17.7	2	3.00	286	19.0	35.0	196	3.4	124000

A8.6

Test No	Surf temp /°C	Water temp /°C	Air temp /°C	z/d	Orif press /bar	Orif diff /mmwater	Orif temp /°C	radius /mm	Nu	r/d	Re
111	31.2	58.2	18.1	2	3.00	284	18.5	31.5	222	3.1	124000
112	31.2	63.1	17.3	2	3.00	284	17.3	29.0	249	2.8	124400
113	31.2	66.1	18.5	2	3.00	286	19.0	26.5	298	2.6	124000
114	31.2	69.0	20.4	2	3.00	284	21.0	22.5	379	2.2	123500
115	31.2	68.6	21.2	2	3.00	282	21.0	19.9	405	1.9	124000
116	31.2	66.9	20.4	2	3.00	285	21.0	19.5	358	1.9	122700
117	31.2	69.0	20.4	2	3.00	285	21.0	15.0	379	1.5	123500
118	31.2	68.6	21.2	2	3.00	285	21.0	15.0	405	1.5	124000
119	31.2	68.6	21.2	2	3.00	284	21.0	10.3	405	1.0	124000
120	31.2	38.5	18.0	2	3.60	334	19.0	97.5	57	9.5	144700
121	31.2	41.6	17.9	2	3.60	336	18.0	82.2	82	8.0	145400
122	31.2	41.6	20.5	2	3.60	333	20.0	67.4	101	6.6	144300
123	31.2	44.4	17.6	2	3.60	336	19.0	65.0	102	6.3	145000
124	31.2	47.3	18.2	2	3.60	334	20.0	52.4	132	5.1	144400
125	31.2	50.6	17.8	2	3.60	335	18.0	44.9	155	4.4	145600
126	31.2	55.8	17.6	2	3.60	337	18.0	37.5	195	3.7	145500
127	31.2	58.2	18.1	2	3.60	336	18.5	35.0	222	3.4	145000
128	31.2	63.1	17.1	2	3.60	336	18.0	32.0	245	3.1	145400
129	31.2	53.3	18.2	2	3.60	332	19.0	29.7	182	2.9	145000
130	31.2	66.1	18.8	2	3.60	334	19.0	29.0	305	2.8	144800
131	31.2	66.9	20.0	2	3.60	336	21.0	25.7	345	2.5	144300
132	31.2	69.0	20.9	2	3.60	334	20.0	25.0	397	2.4	144200

A8.7

Test No	Surf temp /°C	Water temp /°C	Air temp /°C	z/d	Orif press /bar	Orif diff /mmwater	Orif temp /°C	radius /mm	Nu	r/d	Re
133	31.2	68.6	20.8	2	3.60	332	21.0	23.5	390	2.3	144000
134	31.2	72.0	21.0	2	3.60	332	21.0	21.0	434	2.0	144400
135	31.2	75.0	20.5	2	3.60	332	21.0	19.9	445	1.9	144500
136	31.2	75.0	20.5	2	3.60	332	21.0	10.3	445	1.0	144500
137	31.2	35.5	17.8	4	0.39	49	17.0	74.9	32	7.3	30500
138	31.2	36.7	17.3	4	0.39	49	18.0	65.0	40	6.3	30400
139	31.2	35.5	21.5	4	0.39	49	20.0	52.4	44	5.1	30400
140	31.2	37.6	21.8	4	0.39	49	21.0	35.0	70	3.4	30000
141	31.2	39.5	21.5	4	0.39	49	21.0	27.4	88	2.7	30000
142	31.2	41.5	20.7	4	0.39	49	20.5	25.0	102	2.4	30100
143	31.2	44.6	18.6	4	0.39	49	19.0	24.7	112	2.4	30300
144	31.2	43.5	22.1	4	0.39	49	21.0	10.0	141	1.0	30000
145	31.2	47.6	18.0	4	0.39	49	19.0	10.0	132	1.0	30310
146	31.2	35.5	17.8	4	0.56	69	18.0	92.5	32	9.0	39300
147	31.2	36.7	17.3	4	0.56	69	18.0	80.0	40	7.8	39280
148	31.2	35.5	21.8	4	0.56	69	21.0	65.0	45	6.3	38800
149	31.2	37.6	22.0	4	0.56	69	21.0	42.1	71	4.1	38800
150	31.2	39.5	21.8	4	0.56	69	21.0	35.0	91	3.4	38800
151	31.2	44.6	18.6	4	0.56	69	19.0	30.0	112	2.9	39100
152	31.2	41.5	20.7	4	0.56	69	20.0	30.0	102	2.9	38930
153	31.2	47.6	18.0	4	0.56	69	19.0	25.0	132	2.4	39100
154	31.2	43.5	22.0	4	0.56	69	20.0	22.5	140	2.2	39000

A8.8

Test No	Surf temp /°C	Water temp /°C	Air temp /°C	z/d	Orif press /bar	Orif diff /mmwater	Orif temp /°C	radius /mm	Nu	r/d	Re
155	31.2	50.7	17.8	4	0.56	69	19.0	12.4	155	1.2	39000
156	31.2	45.5	20.9	4	0.56	69	21.0	12.4	147	1.2	39000
157	31.2	47.5	19.7	4	0.56	69	20.0	10.0	151	1.0	39000
158	31.2	35.5	21.9	4	1.00	110	21.0	80.0	46	7.8	54500
159	31.2	37.6	22.0	4	1.00	110	21.0	52.4	71	5.1	55000
160	31.2	39.5	21.8	4	1.00	110	21.0	44.9	91	4.4	54500
161	31.2	41.5	20.6	4	1.00	110	20.0	40.0	101	3.9	54700
162	31.2	47.6	17.7	4	1.00	110	19.0	32.5	129	3.2	54900
163	31.2	43.5	21.8	4	1.00	110	21.0	29.8	138	2.9	54500
164	31.2	50.7	17.7	4	1.00	110	19.0	27.4	154	2.7	55000
165	31.2	54.5	14.3	4	1.00	110	15.0	27.4	148	2.7	55600
166	31.2	50.7	17.1	4	1.00	110	17.0	27.4	148	2.7	55000
167	31.2	45.5	20.9	4	1.00	110	21.0	27.4	146	2.7	54500
168	31.2	47.5	19.7	4	1.00	110	20.0	27.4	151	2.7	54700
169	31.2	52.8	17.7	4	1.00	110	17.0	22.4	171	2.2	55000
170	31.2	57.7	15.1	4	1.00	110	15.0	20.0	178	2.0	55600
171	31.2	50.0	19.2	4	1.00	110	20.0	20.0	169	2.0	54700
172	31.2	60.9	15.1	4	1.00	110	16.0	10.0	200	1.0	55300
173	31.2	35.5	21.8	4	1.40	145	21.0	94.9	45	9.2	68500
174	31.2	37.6	22.0	4	1.40	145	21.0	59.9	71	5.8	68700
175	31.2	39.5	21.7	4	1.40	145	21.0	50.4	90	4.9	68000
176	31.2	41.5	20.5	4	1.40	145	20.0	45.2	100	4.4	68800

A8.9

Test No	Surf temp /°C	Water temp /°C	Air temp /°C	z/d	Orif press /bar	Orif diff /mmwater	Orif temp /°C	radius /mm	Nu	r/d	Re
177	31.2	47.6	17.6	4	1.40	145	19.0	37.5	128	3.7	68500
178	31.2	43.5	21.6	4	1.40	145	21.0	35.0	134	3.4	68500
179	31.2	50.7	17.7	4	1.40	145	19.0	32.5	154	3.2	68500
180	31.2	45.5	20.8	4	1.40	145	21.0	32.5	146	3.2	68500
181	31.2	47.5	19.6	4	1.40	145	20.0	32.5	149	3.2	68400
182	31.2	50.2	19.1	4	1.40	145	20.0	27.4	168	2.7	68400
183	31.2	52.8	17.7	4	1.40	145	17.5	27.4	171	2.7	68700
184	31.2	53.3	18.5	4	1.40	145	19.0	25.0	186	2.4	68200
185	31.2	60.9	15.1	4	1.40	145	16.0	20.0	200	2.0	69000
186	31.2	38.5	18.1	4	2.00	196	19.0	85.0	58	8.3	89500
187	31.2	41.6	18.1	4	2.00	196	19.0	67.4	83	6.6	89500
188	31.2	44.4	17.0	4	2.00	196	18.0	54.9	98	5.3	89700
189	31.2	41.6	19.9	4	2.00	196	20.0	50.0	102	4.9	89000
190	31.2	45.5	19.9	4	2.00	196	21.0	40.0	134	3.9	88900
191	31.2	47.5	19.3	4	2.00	196	20.0	37.5	145	3.7	89000
192	31.2	47.3	20.8	4	2.00	196	18.0	37.5	138	3.7	89500
193	31.2	50.7	16.9	4	2.00	196	17.0	37.5	146	3.7	89900
194	31.2	57.5	14.7	4	2.00	196	18.0	35.0	173	3.4	89300
195	31.2	52.8	17.3	4	2.00	196	17.5	35.0	167	3.4	89600
196	31.2	50.2	18.9	4	2.00	196	20.0	32.5	165	3.2	89000
197	31.2	60.9	14.9	4	2.00	196	17.0	30.0	197	2.9	90400
198	31.2	55.7	18.3	4	2.00	196	18.5	30.0	204	2.9	89600

A8.10

Test No	Surf temp /°C	Water temp /°C	Air temp /°C	z/d	Orif press /bar	Orif diff /mmwater	Orif temp /°C	radius /mm	Nu	r/d	Re
199	31.2	58.2	18.0	4	2.00	196	19.0	25.0	220	2.4	89000
200	31.2	38.5	18.0	4	2.60	250	18.0	100.0	57	9.7	112000
201	31.2	41.6	17.8	4	2.60	250	18.0	80.2	82	7.8	112000
202	31.2	44.4	17.1	4	2.60	250	18.0	65.0	99	6.3	112300
203	31.2	41.6	20.1	4	2.60	250	19.0	59.9	98	5.8	112000
204	31.2	54.5	14.1	4	2.60	250	15.0	46.0	147	4.5	113000
205	31.2	50.7	16.8	4	2.60	248	17.0	44.9	145	4.4	112300
206	31.2	47.3	18.7	4	2.60	250	19.0	44.9	137	4.4	111800
207	31.2	57.7	14.5	4	2.60	250	15.0	40.0	172	3.9	113000
208	31.2	52.8	17.2	4	2.60	250	17.5	40.0	165	3.9	112100
209	31.2	60.9	14.9	4	2.60	252	15.0	35.0	198	3.4	113000
210	31.2	55.7	18.4	4	2.60	250	19.0	35.0	206	3.4	111500
211	31.2	58.2	17.9	4	2.60	250	18.0	30.0	219	2.9	112000
212	31.2	63.1	17.3	4	2.60	250	18.0	27.4	250	2.7	112000
213	31.2	66.1	17.7	4	2.60	249	18.0	20.0	282	2.0	112000
214	31.2	41.6	17.8	4	3.00	280	18.0	84.9	82	8.3	124000
215	31.2	44.4	17.2	4	3.00	280	18.0	68.5	100	6.7	124000
216	31.2	41.6	19.9	4	3.00	280	19.0	62.4	96	6.1	123500
217	31.2	54.5	14.1	4	3.00	280	15.0	50.0	147	4.9	125700
218	31.2	47.3	18.7	4	3.00	280	19.0	47.5	137	4.6	124000
219	31.2	50.7	17.0	4	3.00	280	17.0	47.5	147	4.6	124400
220	31.2	52.8	17.1	4	3.00	280	17.5	44.9	165	4.4	124100

A8.11

Test No	Surf temp /°C	Water temp /°C	Air temp /°C	z/d	Orif press /bar	Orif diff /mmwater	Orif temp /°C	radius /mm	Nu	r/d	Re
221	31.2	57.7	14.7	4	3.00	280	15.0	42.5	174	4.1	125600
222	31.2	60.9	15.2	4	3.00	280	15.0	39.5	201	3.8	125700
223	31.2	55.7	18.4	4	3.00	280	19.0	37.5	206	3.7	124000
224	31.2	58.2	17.9	4	3.00	280	18.8	32.9	219	3.2	124000
225	31.2	63.1	17.3	4	3.00	280	18.0	29.8	249	2.9	124100
226	31.2	66.1	17.6	4	3.00	280	19.0	24.7	279	2.4	124000
227	31.2	68.3	21.1	4	3.00	280	21.0	12.3	397	1.2	123000
228	31.2	41.6	17.7	4	3.60	335	18.0	92.5	81	9.0	145300
229	31.2	44.4	17.1	4	3.60	334	18.0	75.0	99	7.3	145600
230	31.2	47.3	18.8	4	3.60	336	19.0	54.5	138	5.3	145000
231	31.2	50.6	18.1	4	3.60	335	19.0	50.4	158	4.9	145000
232	31.2	53.3	18.0	4	3.60	335	19.0	45.2	180	4.4	145000
233	31.2	55.7	18.6	4	3.60	335	19.0	40.1	209	3.9	144900
234	31.2	58.2	18.0	4	3.60	332	18.5	38.0	220	3.7	145200
235	31.2	63.1	17.3	4	3.60	336	18.0	33.9	249	3.3	145400
236	31.2	66.1	17.5	4	3.60	332	19.0	29.8	277	2.9	144900
237	31.2	68.3	21.1	4	3.60	332	21.0	16.4	397	1.6	144800
238	31.2	35.5	17.5	6	0.40	49	17.0	80.2	31	7.8	30500
239	31.2	36.7	17.3	6	0.40	49	17.0	64.8	40	6.3	30500
240	31.2	35.5	21.5	6	0.40	49	21.0	47.3	44	4.6	30050
241	31.2	37.6	21.8	6	0.40	49	21.0	35.0	69	3.4	30000
242	31.2	41.5	20.5	6	0.40	49	20.0	20.6	100	2.0	30100

A8.12

Test No	Surf temp /°C	Water temp /°C	Air temp /°C	z/d	Orif press /bar	Orif diff /mmwater	Orif temp /°C	radius /mm	Nu	r/d	Re
243	31.2	39.5	21.1	6	0.40	49	21.0	22.6	85	2.2	30000
244	31.2	44.6	18.6	6	0.40	49	19.0	17.5	112	1.7	30300
245	31.2	47.6	18.1	6	0.40	49	19.0	10.3	133	1.0	30300
246	31.2	35.5	17.7	6	0.56	69	17.0	92.5	32	9.0	39500
247	31.2	36.7	17.3	6	0.14	69	17.0	77.4	40	7.5	39500
248	31.2	35.5	21.8	6	0.14	69	21.0	59.9	45	5.8	38800
249	31.2	37.6	22.0	6	0.14	69	21.0	40.0	71	3.9	39000
250	31.2	39.5	21.8	6	0.14	69	21.0	32.5	91	3.2	38800
251	31.2	41.5	20.7	6	0.14	69	20.0	27.4	102	2.7	39000
252	31.2	44.6	18.6	6	0.14	69	19.0	25.0	112	2.4	39100
253	31.2	47.6	18.0	6	0.14	69	19.0	17.5	132	1.7	39100
254	31.2	43.5	22.9	6	0.14	69	20.0	12.4	154	1.2	39000
255	31.2	45.5	20.3	6	0.14	69	20.0	15.4	138	1.5	38900
256	31.2	50.7	17.7	6	0.14	69	19.0	12.4	155	1.2	39100
257	31.2	47.5	19.8	6	0.14	69	20.0	10.0	152	1.0	39000
258	31.2	52.6	17.7	6	0.14	69	18.0	5.0	170	0.5	39000
259	31.2	35.5	21.8	6	1.00	110	21.0	75.0	46	7.3	55000
260	31.2	37.6	21.7	6	1.00	110	21.0	52.4	69	5.1	54500
261	31.2	39.5	22.0	6	1.00	110	21.0	40.0	93	3.9	54500
262	31.2	41.5	20.5	6	1.00	110	20.0	35.0	100	3.4	54700
263	31.2	47.6	17.9	6	1.00	110	19.0	27.4	131	2.7	54900
264	31.2	50.7	17.7	6	1.00	110	19.0	22.5	154	2.2	55000

A8.13

Test No	Surf temp /°C	Water temp /°C	Air temp /°C	z/d	Orif press /bar	Orif diff /mmwater	Orif temp /°C	radius /mm	Nu	r/d	Re
265	31.2	54.5	14.9	6	1.00	110	16.0	22.4	154	2.2	55300
266	31.2	50.7	17.5	6	1.00	110	18.0	21.0	152	2.0	54700
267	31.2	47.5	19.9	6	1.00	110	20.0	20.0	153	2.0	54700
268	31.2	43.5	22.7	6	1.00	110	21.0	17.5	151	1.7	54500
269	31.2	57.7	14.7	6	1.00	110	16.0	15.0	174	1.5	55300
270	31.2	50.2	19.9	6	1.00	110	20.0	15.0	179	1.5	54700
271	31.2	52.6	17.7	6	1.00	110	18.0	14.9	171	1.5	54700
272	31.2	35.5	21.7	6	1.40	145	21.0	90.0	45	8.8	68500
273	31.2	37.6	21.7	6	1.40	145	21.0	62.4	69	6.1	68500
274	31.2	39.5	22.0	6	1.40	145	21.0	44.9	93	4.4	68500
275	31.2	41.5	20.3	6	1.40	145	20.5	42.5	99	4.1	68900
276	31.2	47.6	17.7	6	1.40	145	19.0	37.5	129	3.7	69000
277	31.2	50.7	17.5	6	1.40	146	18.0	30.0	152	2.9	69200
278	31.2	54.5	14.8	6	1.40	145	16.0	30.0	153	2.9	69300
279	31.2	50.7	17.5	6	1.40	145	19.0	30.0	152	2.9	69000
280	31.2	43.5	22.4	6	1.40	145	21.0	27.8	146	2.7	68500
281	31.2	57.5	14.5	6	1.40	144	16.0	25.0	172	2.4	69400
282	31.2	52.6	17.7	6	1.40	145	18.0	22.4	170	2.2	68900
283	31.2	50.2	19.7	6	1.40	145	20.0	19.9	176	1.9	69000
284	31.2	53.3	18.3	6	1.40	145	19.0	17.5	184	1.7	69000
285	31.2	60.7	15.7	6	1.40	145	16.0	14.9	206	1.5	69300
286	31.2	55.7	19.1	6	1.40	144	19.5	10.0	218	1.0	68500

A8.14

Test No	Surf temp /°C	Water temp /°C	Air temp /°C	z/d	Orif press /bar	Orif diff /mmwater	Orif temp /°C	radius /mm	Nu	r/d	Re
287	31.2	38.5	18.1	6	2.00	196	18.5	82.5	57	8.0	89000
288	31.2	41.6	19.9	6	2.00	196	20.0	52.4	97	5.1	88900
289	31.2	45.5	19.9	6	2.00	194	18.0	40.0	133	3.9	89200
290	31.2	47.3	19.0	6	2.00	196	19.0	37.5	140	3.7	89100
291	31.2	50.7	17.5	6	2.00	196	18.0	37.5	152	3.7	89400
292	31.2	57.7	14.3	6	2.00	196	16.0	35.0	170	3.4	90000
293	31.2	52.6	17.4	6	2.00	196	18.0	32.5	166	3.2	89400
294	31.2	50.2	19.3	6	2.00	196	20.0	30.0	170	2.9	88800
295	31.2	60.7	15.5	6	2.00	198	17.0	25.0	204	2.4	89500
296	31.2	55.7	18.9	6	2.00	196	19.0	20.0	214	2.0	89000
297	31.2	58.3	17.9	6	2.00	194	18.0	17.5	220	1.7	89500
298	31.2	38.5	18.1	6	2.60	250	18.5	99.7	58	9.7	111800
299	31.2	44.4	17.2	6	2.60	252	19.0	67.4	100	6.6	112000
300	31.2	41.6	19.8	6	2.60	250	20.0	59.9	96	5.8	111100
301	31.2	54.5	14.6	6	2.60	250	16.0	47.5	151	4.6	113000
302	31.2	50.7	17.4	6	2.60	250	18.0	42.5	151	4.1	112000
303	31.2	57.7	14.1	6	2.60	255	16.0	40.0	168	3.9	113000
304	31.2	52.6	17.1	6	2.60	250	18.0	37.5	163	3.7	111900
305	31.2	60.7	15.5	6	2.60	250	17.0	35.0	204	3.4	112500
306	31.2	55.7	18.8	6	2.60	250	19.0	30.0	212	2.9	112000
307	31.2	58.3	17.9	6	2.60	250	18.0	27.8	219	2.7	112000
308	31.2	63.1	17.8	6	2.60	250	18.0	17.6	258	1.7	112000

A8.15

Test No	Surf temp /°C	Water temp /°C	Air temp /°C	z/d	Orif press /bar	Orif diff /mmwater	Orif temp /°C	radius /mm	Nu	r/d	Re
309	31.2	65.9	17.6	6	2.60	250	18.0	15.0	277	1.5	112100
310	31.2	44.4	17.1	6	3.00	280	19.0	72.5	99	7.1	124500
311	31.2	41.6	19.8	6	3.00	280	19.0	64.8	96	6.3	124500
312	31.2	54.5	14.7	6	3.00	280	16.0	50.0	152	4.9	125100
313	31.2	50.7	17.4	6	3.00	280	18.0	47.5	151	4.6	124400
314	31.2	57.7	20.0	6	3.00	280	16.0	44.9	170	4.4	125100
315	31.2	52.6	17.1	6	3.00	280	18.0	44.9	163	4.4	124000
316	31.2	60.7	15.6	6	3.00	280	17.0	37.5	205	3.7	124600
317	31.2	55.7	18.9	6	3.00	280	19.0	32.9	214	3.2	124000
318	31.2	58.3	18.0	6	3.00	280	19.0	30.0	222	2.9	124000
319	31.2	63.1	17.7	6	3.00	280	18.0	20.0	256	2.0	124500
320	31.2	65.9	17.6	6	3.00	280	18.0	17.5	278	1.7	124500
321	31.2	68.3	21.0	6	3.00	280	21.0	7.5	395	0.7	124000
322	31.2	44.4	17.2	6	3.60	338	19.0	80.0	100	7.8	145000
323	31.2	41.6	19.7	6	3.60	335	19.0	75.0	95	7.3	144700
324	31.2	47.3	19.1	6	3.60	336	20.0	52.4	141	5.1	144400
325	31.2	50.6	18.4	6	3.60	338	18.5	50.0	162	4.9	145300
326	31.2	53.3	17.8	6	3.60	334	18.0	44.9	177	4.4	145500
327	31.2	55.7	18.9	6	3.60	335	19.0	37.5	214	3.7	145000
328	31.2	58.3	18.0	6	3.60	335	18.5	35.0	222	3.4	145300
329	31.2	63.1	17.9	6	3.60	335	18.0	29.0	261	2.8	145400
330	31.2	65.9	17.7	6	3.60	334	18.0	25.0	279	2.4	145400

A8.16

Test No	Surf temp /°C	Water temp /°C	Air temp /°C	z/d	Orif press /bar	Orif diff /mmwater	Orif temp /°C	radius /mm	Nu	r/d	Re
331	31.2	66.5	17.8	6	3.60	338	18.0	18.5	350	1.8	145300
332	31.2	68.3	21.0	6	3.60	338	21.0	10.0	394	1.0	144000
333	31.2	34.7	18.0	2	0.56	69	18.5	84.3	31	8.2	39000
334	31.2	35.2	18.0	2	0.56	69	18.5	72.0	35	7.0	39100
335	31.2	38.6	19.0	2	0.56	69	19.0	36.0	70	3.5	39110
336	31.2	41.3	19.5	2	0.56	69	20.0	25.7	100	2.5	39050
337	31.2	44.3	19.0	2	0.56	69	19.0	26.7	125	2.6	39100
338	31.2	44.0	20.1	2	0.56	69	20.0	24.7	133	2.4	39105
339	31.2	41.0	18.1	2	2.6	250	20.0	72.0	85	7.0	112000
340	31.2	41.9	19.0	2	2.6	248	20.0	53.5	102	5.2	111800
341	31.2	44.6	20.0	2	2.6	249	20.8	43.2	142	4.2	111900
342	31.2	45.4	20.2	2	2.6	250	20.7	37.0	150	3.6	112000
343	31.2	49.5	19.5	2	2.6	248	20.8	33.9	181	3.3	111800
344	31.2	53.5	19.5	2	2.6	249	21.0	30.8	221	3.0	111950
345	31.2	58.2	19.6	2	2.6	250	21.0	23.6	270	2.3	112000

Appendix A9

Lack of fit test for the unconfined jet. 3≤r/d≤9

Y values are the logarithmic transformations of the measured Nusselt numbers.

Test no	j	Y	$\sum_{u=1}^{n_j} (Y_{ju}-\overline{Y_j})^2/10^{-3}$	ν
24	1	4.419		
217	1	4.477	6.5	2
223	1	4.533		
25	2	4.595	5.51	1
218	2	4.700		
26	3	4.844	0.761	1
219	3	4.883		
63	4	4.500	0.0605	1
226	4	4.511		
64	5	4.673	6.613	1
227	5	4.788		
66	6	5.017	1.666	1
228	6	5.075		
67	7	5.165	0.392	1
229	7	5.193		
132	8	4.443	4.05	1
224	8	4.533		
143	9	4.554	0.9245	1
233	9	4.511		
146	10	5.124	2.381	1
237	10	5.193		
180	11	4.443	4.05	1
225	11	4.533		
188	12	4.466	1.012	1
241	12	4.511		
189	13	4.711	0.1445	1
242	13	4.788		
190	14	4.956	1.3	1
243	14	4.905		
191	15	5.100	0.392	1
244	15	5.075	Σ = 35.7	Σ=16

Appendix A10

Lack of fit test for the semi-confined jet. 2.5≤r/d≤9

Y values are the logarithmic transformations of the measured Nusselt numbers.

Test no	j	Y	$\sum_{u=1}^{n_j} (Y_{ju}-\overline{Y_j})^2/10^{-3}$	ν
263	1	4.796	2.000	2
10	1	4.804		
8	1	4.745		
264	2	3.932	4.325	1
15	2	4.025		
265	3	4.511	2.045	1
18	3	4.575		
267	4	4.719	1.000	2
33	4	4.736		
34	4	4.779		
268	5	5.094	6.845	1
35	5	4.977		
270	6	5.283	4.705	1
45	6	5.380		
271	7	5.513	4.232	1
47	7	5.421		
272	8	4.663	1.568	1
54	8	4.719		
273	9	5.247	3.698	1
58	9	5.333		
274	10	5.580	4.901	1
60	10	5.481		
275	11	4.691	1.105	1
67	11	4.644		
276	12	5.273	0.882	1
70	12	5.231		
277	13	5.790	0.181	1
75	13	5.771		
282	14	5.429	4.608	1
165	14	5.333		
283	15	4.654	0.041	1
232	15	4.663		
284	16	5.094	0.072	1
233	16	5.106		
			Σ = 42.2	Σ =18